U.S. DEPARTMENT OF COMMERCE PB80-169675

Computer Modeling of Simulated Photochemical Smog

SRI International
Menlo Park, CA

Prepared for

Environmental Sciences Research Lab.
Research Triangle Park, NC

Feb 80

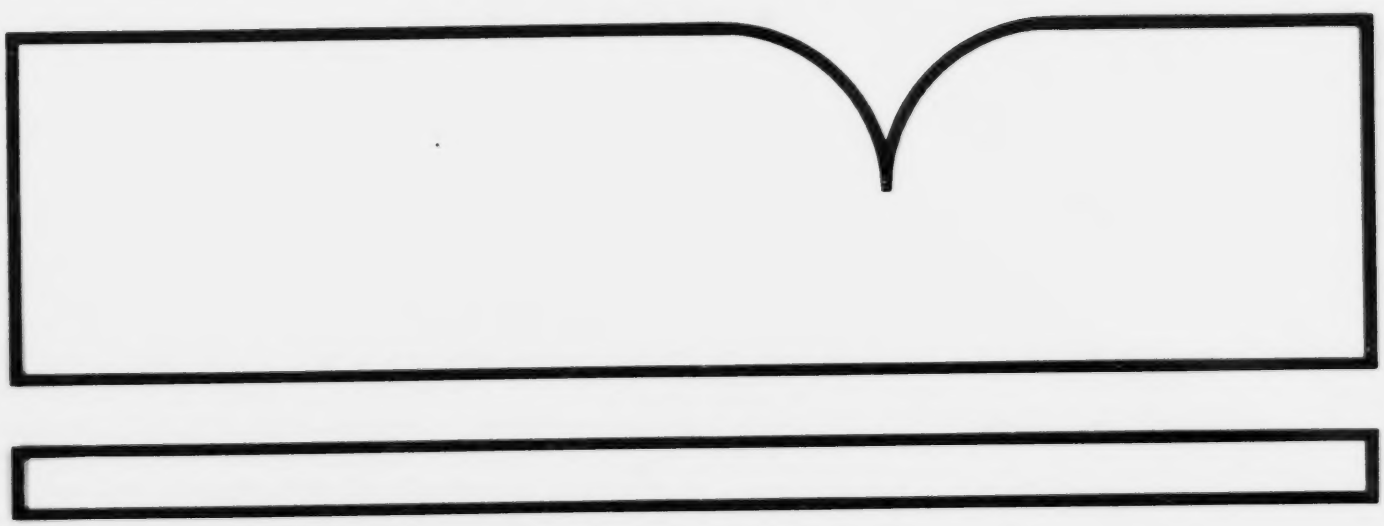

U.S. Department of Commerce
National Technical Information Service
NTIS

United States
Environmental Protection
Agency

Environmental Sciences Research
Laboratory
Research Triangle Park NC 27711

EPA-600/3-80-029
February 1980

Research and Development

PB80-169675

EPA

Computer Modeling of Simulated Photochemical Smog

Final Report

REPRODUCED BY
NATIONAL TECHNICAL
INFORMATION SERVICE
U.S. DEPARTMENT OF COMMERCE
SPRINGFIELD, VA. 22161

RESEARCH REPORTING SERIES

Research reports of the Office of Research and Development, U.S. Environmental Protection Agency, have been grouped into nine series. These nine broad categories were established to facilitate further development and application of environmental technology. Elimination of traditional grouping was consciously planned to foster technology transfer and a maximum interface in related fields. The nine series are:

1. Environmental Health Effects Research
2. Environmental Protection Technology
3. Ecological Research
4. Environmental Monitoring
5. Socioeconomic Environmental Studies
6. Scientific and Technical Assessment Reports (STAR)
7. Interagency Energy-Environment Research and Development
8. "Special" Reports
9. Miscellaneous Reports

This report has been assigned to the ECOLOGICAL RESEARCH series. This series describes research on the effects of pollution on humans, plant and animal species, and materials. Problems are assessed for their long- and short-term influences. Investigations include formation, transport, and pathway studies to determine the fate of pollutants and their effects. This work provides the technical basis for setting standards to minimize undesirable changes in living organisms in the aquatic, terrestrial, and atmospheric environments.

This document is available to the public through the National Technical Information Service, Springfield, Virginia 22161.

TECHNICAL REPORT DATA
(Please read Instructions on the reverse before completing)

1. REPORT NO.	2.	3. RECIPIENT'S ACCESSION NO.
EPA-600/3-80-029		PB 80 169675

4. TITLE AND SUBTITLE	5. REPORT DATE
COMPUTER MODELING OF SIMULATED PHOTOCHEMICAL SMOG Final Report	February 1980 6. PERFORMING ORGANIZATION CODE
7. AUTHOR(S)	**8. PERFORMING ORGANIZATION REPORT NO.**
D. G. Hendry, A.C. Baldwin, and D. M. Golden	
9. PERFORMING ORGANIZATION NAME AND ADDRESS	**10. PROGRAM ELEMENT NO.**
SRI International 333 Ravenswood Avenue Menlo Park, California 94025	1AA603 AC-27 (FY-79) **11. CONTRACT/GRANT NO.** Contract No. 68-02-2427
12. SPONSORING AGENCY NAME AND ADDRESS	**13. TYPE OF REPORT AND PERIOD COVERED**
Environmental Sciences Research Laboratory-RTP, NC Office of Research and Development U.S. Environmental Protection Agency Research Triangle Park, North Carolina 27711	Final 9/77 - 8/79 **14. SPONSORING AGENCY CODE** EPA/600/09

15. SUPPLEMENTARY NOTES

16. ABSTRACT

Efforts to develop chemical kinetic mechanisms to describe the formation of photochemical smog are discussed. Detailed mechanisms for the atmospheric reactions of toluene, m-xylene, propene, ethene, formaldehyde and acetaldehyde were constructed from available experimental and chemical kinetic data. These mechanisms were used to simulate smog chamber data from the Statewide Air Pollution Research Center at the University of California, Riverside and the outdoor facility of the University of North Carolina.

17. KEY WORDS AND DOCUMENT ANALYSIS

a. DESCRIPTORS	b. IDENTIFIERS/OPEN ENDED TERMS	c. COSATI Field/Group
* Air pollution		13B
* Reaction kinetics		07D
* Photochemical reactions		07E
* Mathematical models		12A
* Computerized simulation		14B

18. DISTRIBUTION STATEMENT	19. SECURITY CLASS *(This Report)*	21. NO. OF PAGES
RELEASE TO PUBLIC	UNCLASSIFIED	---
	20. SECURITY CLASS *(This page)* UNCLASSIFIED	22. PRICE

EPA Form 2220-1 (9-73)

EPA-600/3-80-029
February 1980

COMPUTER MODELING OF SIMULATED PHOTOCHEMICAL SMOG

Final Report

by

D. G. Hendry, A. C. Baldwin, and D. M. Golden

SRI International
333 Ravenswood Avenue
Menlo Park, California 94025

Contract No. 68-02-2427

Project Officer

Marcia C. Dodge
Atmospheric Chemistry and Physics Division
Environmental Sciences Research Laboratory
Research Triangle Park, North Carolina 27711

ENVIRONMENTAL SCIENCES RESEARCH LABORATORY
OFFICE OF RESEARCH AND DEVELOPMENT
U.S. ENVIRONMENTAL PROTECTION AGENCY
RESEARCH TRIANGLE PARK, NORTH CAROLINA 27711

DISCLAIMER

This report has been reviewed by the Environmental Sciences Research Laboratory, U.S. Environmental Protection Agency, and approved for publication. Approval does not signify that the contents necessarily reflect the views and policies of the U.S. Environmental Protection Agency, nor does mention of trade names or commercial products constitute endorsement or recommendation for use.

ABSTRACT

The chemistry by which hydrocarbons affect photochemical smog formation has been investigated using computer modeling techniques. Detailed chemical kinetic mechanisms for the atmospheric reactions of toluene, m-xylene, propene, ethene, formaldehyde, and acetaldehyde were constructed from available experimental and chemical kinetic data. These mechanisms were used to simulate smog chamber data from both the Statewide Air Pollution Research Center at the University of California at Riverside and the outdoor facility at the University of North Carolina at Chapel Hill.

In general, the simulations predict the experimentally observed time-concentration for NO, NO_2, and hydrocarbons quite well. The rate of buildup of ozone is also well predicted, although the maximum concentrations of ozone as well as the time to reach the maxima are overpredicted 30%-50% in many cases.

This report was submitted in fulfillment of contract number 68-02-2427 by SRI International under the sponsorship of the U.S. Environmental Protection Agency. This report covers a period from 1 September 1977 to 31 August 1979, and work was completed as of 30 November 1979.

CONTENTS

Abstract iii
Figures vi
Tables vii

1. Introduction 1
2. Conclusions and Recommendations 5
3. Approach 8
   Smog Chambers 8
   Light Intensity Calculations 9
   Chamber Characteristics 9
   Modeling Technique 10
4. Aromatic Hydrocarbons 11
   Contribution of Aromatics to Total Atmospheric Hydrocarbons 11
   Reactions of Aromatic Hydrocarbons 12
   Products of Reaction of Aromatic Hydrocarbons 14
   Toluene-OH Reactions 20
   Reactions of Cresol 26
   NO Oxidation and NO_x Consumption in Toluene Reaction . 26
   Mechanism for Modeling Toluene Smog Chamber Data . . . 29
   Toluene Simulation Results 34
   Mechanism for Modeling m-Xylene Smog Chamber Experiments 42
   m-Xylene Simulation Results 45
5. Alkenes 51
   Mechanism 51
   SAPRC Data Set 52
   UNC Data Set 62
6. Alkanes 65
   Mechanism 65
   SAPRC Data Set 65
   UNC Data Set 65
7. Aldehydes 74
   Mechanism 74
   SAPRC Data Set 74
   UNC Data Set 74

References 80

Appendices
A. Simulation of Aromatic Hydrocarbon Chamber Runs 85
B. Simulation of Alkene Chamber Runs 139
C. Simulation of n-Butane and Aldehyde Chamber Runs 185

FIGURES

Number		Page
1	Simulation of SAPRC Toluene Run EC-266	41
2	Simulation of UNC Toluene Run 8.16.78 Red	43
3	Simulation of UNC Toluene Run 9.14.78 Red	44
4	Simulation of SAPRC m-Xylene Run EC-344	48
5	Simulation of SAPRC Propene Run EC-277	56
6	Simulation of SAPRC Ethene Run EC-156	57
7	Simulation of UNC Propene Run 6.16.78 Blue	63
8	Simulation of UNC Ethene Run 11.19.78 Red	64
9	Simulation of SAPRC Butane Run EC-309	69
10	Simulation of UNC Butane Run 2.27.78 Red	73
11	Simulation of SAPRC Acetaldehyde Run EC-253	76
12	Simulation of SAPRC Formaldehyde Run EC-252	77
13	Simulation of UNC Acetaldehyde Run 8.08.78 Red	78
14	Simulation of UNC Formaldehyde Run 9.14.77 Red	79

TABLES

Number		Page
1	Atmospheric Reactions of Toluene	13
2	Reported Rate Constants for Reaction of OH Plus Aromatic Hydrocarbons	14
3	Observed Products from SAPRC Chamber Run EC-273	15
4	Fraction Methyl Attack by OH for Several Aromatic Hydrocarbons	18
5	Atmospheric Reactions of Cresols	27
6	Analysis of Selected SAPRC Smog Chamber Experiments	28
7	Toluene Mechanism	36
8	Inorganic Reactions	38
9	Summary of Initial Conditions for Smog Chamber Experiments for Toluene and m-Xylene	39
10	Comparison of Experimental and Simulation Results for Toluene and m-Xylene Chamber Experiments	40
11	m-Xylene Mechanism	46
12	Propene Mechanism	53
13	Ethene Mechanism	55
14	Summary of Initial Conditions for Smog Chamber Experiments for Propene	58
15	Comparison of Experimental and Simulation Results for Propene Chamber Experiments	59
16	Summary of Initial Conditions for Smog Chamber Experiment for Ethene	60
17	Comparison of Experimental and Simulation Results for Ethene Chamber Experiments	61
18	n-Butane Mechanism	66

19 Summary of Initial Conditions of Miscellaneous Smog Chamber Experiments 70

20 Comparison of Experimental and Simulation Results for Miscellaneous Chamber Experiments 71

21 Aldehyde Mechanism 75

SECTION 1

INTRODUCTION

To assist the United States Environmental Protection Agency in developing models to describe the chemistry of photochemical smog formation, SRI International has continued to develop explicit mechanisms describing the chemistry of individual hydrocarbons.[1] This report discusses our efforts during the past two years to develop mechanisms describing the chemistry of aromatic hydrocarbons and simple alkenes and alkanes. EPA-supported smog chamber data from the Statewide Air Pollution Research Center (SAPRC) at the University of California,[2] Riverside, and the outdoor facility at the University of North Carolina[3] have been used to test and verify these models.

Considerable effort has been made to develop detailed models to describe the photochemical smog chemistry of individual hydrocarbons. Demerjian, Kerr, and Calvert[4] and Niki, Daby, and Weinstock[5] were the first to work on problems of developing detailed mechanisms. Hecht, Seinfeld, and Dodge[6] investigated constructing a more compact mechanism while maintaining important details generalizing certain reactions. Whitten et al.[7] have also worked on developing detailed mechanisms, but with the goal of developing a method to generalize the reactivity of a wide variety of hydrocarbons. The most recent effort to update the complex chemistry of propene and n-butane, besides our own effort, is the work of Carter et al.[8] who have applied the mechanisms to modeling SAPRC data.

Our general approach to developing the kinetic models has been to use critically evaluated kinetic data for each of the reactions wherever possible. Where data on specific reactions were not available or not at the appropriate temperature and pressures, we have used thermochemical techniques to estimate the desired rate constants. Whenever thermochemical data were used to predict rate constants, error bounds

were determined for both the thermochemical estimates and the resulting rate constants. If needed, we varied the estimated rate constants within these error limits to optimize the agreement between computed and experimental concentration-time profiles. This type of procedure can artificially compensate for other inaccuracies in the model and reduce the reliability of the model for application to conditions at atmospheric concentrations of reactants. When rate constants were varied to optimize agreement between simulated and experimental results, the mechanisms for different hydrocarbons were considered together and the rate constants of concern were adjusted as a group. In this way we used the maximum possible data base to guard against fortuitous compensations obscuring deficiencies in the mechanisms.

The major effort in model development during the last two years has been on the toluene mechanism. The experimental data base has been enlarged since our report two years ago,[1] but the product balances in chamber experiments still account for less than 30% of the carbon for the most complete product analyses. The major changes in the toluene mechanism have been made based on the following new experimental data.

(1) A smog chamber study of o-xylene has shown that one reaction channel, accounting for 18% of the reaction of OH with o-xylene, gives biacetyl as a product.[9] A similar type of ring cleavage reaction has been assumed for toluene where glyoxal and methylglyoxal are formed. There are no data from smog chamber experiments that these compounds form, but they would readily polymerize and react with hydroxylic compounds and may be extremely difficult to quantitatively measure or even detect using direct gas chromatography techniques.

(2) New laboratory data on the reaction of benzaldehyde plus OH indicate that only the following reaction is important

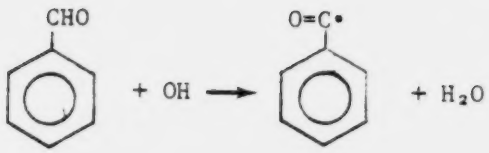

with no evidence of ring addition of the type observed for alkyl-substituted aromatic hydrocarbons.[10]

(3) Laboratory data have been reported for the chemistry of peroxybenzoyl nitrate (PBzN).[11] The reactions that have been evaluated are

$$PhC(O)O_2\bullet + NO_2 \longrightarrow PhC(O)O_2NO_2$$

$$PhC(O)O_2NO_2 \longrightarrow PhC(O)O_2\bullet + NO_2$$

$$PhC(O)O_2\bullet + NO \longrightarrow PhC(O)O\bullet + NO_2$$

$$PhC(O)O\bullet \longrightarrow Ph\bullet + CO_2$$

These data fix the role of PBzN in the toluene mechanism and, together with data on the reaction of OH and benzaldehyde, clarify the role of benzaldehyde in the overall toluene mechamism, although the fate of Ph• is still unknown.

The major change in the mechanisms for alkenes is the observation of Herron and Huie[12] that the reaction of alkene plus ozone does not form free radicals as readily as was originally thought. For ethene, the reported reactions are

$$CH_2{=}CH_2 + O_3 \longrightarrow CH_2O + CH_2O_2$$

$$CH_2O_2 \xrightarrow{20\%} H_2 + CO_2$$

$$CH_2O_2 \xrightarrow{70\%} H_2O + CO$$

$$CH_2O_2 \xrightarrow{10\%} 2H\bullet + CO_2$$

Thus the interaction of ethene and O_3 gives a pair of radicals only 10% of the time rather than the 100% that had been assumed earlier by most modelers.

SECTION 2

CONCLUSIONS AND RECOMMENDATIONS

Models have been developed to describe the participation of toluene, m-xylene, ethene, propene, and n-butane in the formation of photochemical smog. Each model uses the best kinetic data available and is chemically consistent with the others. Some adjustment of unknown rate constants was necessary to give good agreement between the smog chamber experiments and the simulations. Although this has been especially true for the models for the aromatic hydrocarbons, it was also necessary to a lesser extent for ethene, propene, and n-butane. The amount of adjusting of parameters has been kept to a minimum, and although better overall agreement could undoubtedly be obtained by further fitting, it would not necessarily improve the predictability of the model under atmospheric conditions and would certainly obscure the deficiencies of the models.

A toluene mechanism has been developed that reflects the chamber data observation that approximately three NO are oxidized and one NO_x is consumed for each toluene molecule reacted. The mechanism has been applied to 31 SAPRC and 2 UNC toluene runs. In the simulation of the SAPRC data, the average time to NO_2 maximum was 4(±26)% greater than observed, and the NO_2 maximum concentration was 8(±6)% higher. The simulated ozone maximum came 32(±28)% later than observed, and the maximum concentration was 47(±39)% larger. The data for ozone reflect the tendency to predict the correct initial ozone formation rate but not to predict the leveling off in the ozone formation at the maximum. This phenomena is not unique to toluene and appears to be related to an overprediction of $HO_2\bullet$ once the NO_x is essentially totally consumed.

A model for the reaction of m-xylene was constructed based on the toluene model and taking into account both the higher reactivity of m-xylene and the additional methyl group in the parent hydrocarbon.

Using the four SAPRC m-xylene runs to test the model, we found the simulated time to the ozone maximum 36(± 44)% high and the maximum ozone concentration 17(± 16)% high.

With minor changes in kinetic models describing the photochemical smog chemistry of ethene, propene, and n-butane, proposed earlier,[1] both new SAPRC and UNC smog chamber experiments for these hydrocarbons have been simulated with relatively good results. The modeling of the outdoor UNC chamber requires no modification of the homogeneous mechanisms used for SAPRC data, although some changes in heterogeneous processes were made as would be expected. It is only necessary to account for diurnal and seasonal effects on light intensity at each wavelength as well as the random variation of temperature and cloud cover. In all cases it was necessary to use initial nitrous acid as an adjustible parameter. In the case of the propene experiments, where there is the best data base, the ozone maxima are overestimated by 31(±37)% in the SAPRC experiments (13 runs) and 18(±35)% in the UNC experiments (17 runs). The ethene and n-butane mechanism overestimates ozone similarly.

To improve our ability to model photochemical smog and increase the accuracy of our current mechanisms, we recommend that the following information be obtained:

(1) Analyze the loss mechanisms of relevant species at the point of experimental ozone maximum to determine what reactions and rate constants can cause the observed discrepancies in the ozone maximum and the time to ozone maximum.

(2) Obtain complete product analysis for the toluene smog chamber experiments as well as product analyses for other aromatic hydrocarbons.

(3) Determine rates and pathways for photolysis of the critical photoactive intermediates that are proposed in the toluene mechanisms.

(4) Determine mechanisms of the reactions of alkenes with ozone.

(5) Determine alternative decomposition pathways for peroxynitrates.

(6) Determine effect of beta-OH-substituents on rates and products of cleavage of alkoxy radicals.

SECTION 3

APPROACH

SMOG CHAMBERS

In this report explicit chemical mechanisms for the formation of photochemical smog in the photooxidation of hydrocarbon-NO_x mixtures are validated against smog chamber experiments. Two sets of data are used: one from the Statewide Air Pollution Research Center (SAPRC)[2] at the University of California-Riverside and another from the University of North Carolina (UNC).[3] Both data bases consist of concentration-time profiles from the irradiation of static mixtures of a hydrocarbon and NO_x. Data are available for a number of hydrocarbons, at various hydrocarbon/NO_x and NO/NO_2 ratios.

The SAPRC data are obtained under conditions of constant temperature (mostly at $\sim$ 300 K), constant light intensity, and constant spectral distribution. The data are thus relatively easy to simulate, but somewhat different from real atmospheric conditions. The UNC data, on the other hand, are obtained using solar irradiation. Therefore, during the experiments, the temperature and the solar intensity and spectral distribution change as the sun rises and sets. In addition, meteorological variables such as cloud cover produce an additional variation on each run. These data are more difficult to simulate because of these added variables, but are more representative of the real atmospheric conditions. The UNC chamber also has a much lower surface-to-volume ratio than the SAPRC chamber, which should minimize heterogeneous effects.

In simulation of the SAPRC data, once the temperature and light intensity dependent rate constants are calculated for a particular run, they remain constant throughout that run. The necessary experimental parameters are reported by SAPRC and there is little doubt that these processes are well represented in the model. In simulation of the UNC

data, many rate constants vary with time during the run because of the changes in temperature and light intensity. This makes the simulations more complex and is a possible source of error. In general, however, we feel that the variations of temperature and light are well represented in the model, within the limits of the reported experimental parameters, and that this is not a significant source of error.

LIGHT INTENSITY CALCULATIONS

For the SAPRC runs, the light intensity distribution is computed from the relative light intensity at 12 wavelengths between 300 and 500 nm and from the experimentally determined value of the NO_2 photolysis. Photo rates for compounds are then computed from the reported cross section and quantum yields plus the computed light intensity spectrum.

For the UNC experiments, which rely on solar radiation, the photo rates are computed hourly using the procedure of Schere and Demerjian.[13] These calculations correct for location and difference in distribution during the day. To correct for cloud cover, hourly averaged total solar radiations were compared with clear day values, and the ratio was used to reduce all photo rates accordingly. The UNC chamber has an aluminum floor that reflects the solar radiation and enhances the light intensity, primarily from 3 to 6 PM. To correct for this effect, we increased the computed photo rates by a factor of 1.125 during this interval.

CHAMBER CHARACTERISTICS

In addition to light intensity differences, both facilities were characterized with regard to ozone decay. A decay constant of 1×10^{-3} min^{-1} was used for the SAPRC runs and a value of 4×10^{-4} min^{-1} was used for the UNC chambers.

Dilution rates for the chambers also vary. For the SAPRC chamber the value is approximately 3×10^{-4} min^{-1} and for the UNC chamber the value is 1×10^{-4} min^{-1}.

Our earlier analysis[1] of the SAPRC data concluded that there is a source of either OH or $HO_2\bullet$ radicals from the chamber walls equal to a rate of 2.0×10^{-4} ppm min^{-1}. We have continued to include this source of radicals in the simulation of all SAPRC data. There is no evidence for such a source of radicals in the UNC experiments.

MODELING TECHNIQUE

The simulations of the concentration-time profiles of various species were obtained from the given mechanism and the appropriate starting concentrations using the computer program CHEMK of Whitten and Meyer.[14] This program constructs the differentials describing the rate of change in concentration of each species of the input mechanism. The actual numerical integration of these differentials is then performed by the Hindmarsh[15] version of the Gear[16] integration method.

SECTION 4

AROMATIC HYDROCARBONS

CONTRIBUTION OF AROMATICS TO TOTAL ATMOSPHERIC HYDROCARBONS

Single-ring aromatic hydrocarbons make up a substantial fraction of the hydrocarbons found in urban and nonurban atmospheres. Calvert[17] reported that in Los Angeles, California (1973) 23% of the carbon present as hydrocarbons, excluding methane, is in the form of aromatic compounds. A report for Manhattan, New York (1969), indicates that 32% of the organic carbon is from aromatic compounds.[18] Measurements of hydrocarbons in various non-urban areas of sourthern Florida (1976) indicate that 20% to 30% of the carbon is found in aromatic compounds.[19] Based on the Los Angeles data,[17] the aromatic hydrocarbons are composed of about one-third toluene and one-third xylene isomers, with the remaining third composed of, in decreasing order, benzene, sec-butylbenzene, ethylbenzene, and n-propylbenzene. The Florida study indicated this same general distribution of compounds but identified additional minor amounts of di- and tri-alkylbenzene.[19]

Calvert[17] analyzed the distribution of hydrocarbons based on their reactivity toward OH and showed that, in the Los Angeles case, aromatic hydrocarbons contribute up to about 20% of the total reactions of OH with hydrocarbaron. The xylene isomers contribute 12.5% to the total OH-hydrocarbon reactions, more than any other compound detected in the atmosphere. Toluene, the second most important aromatic compound, is the sixth most important compound overall and accounts for 5.1% of all OH-hydrocarbon reactions. The only compounds contributing more than toluene are propene (6.3%), isobutene (8.1%), isopentane (8.4%), 1-heptene (7.5%), and the xylenes (12.5%).

The aromatic compounds found in the urban atmosphere are considered to come largely from gasoline in which they are used to increase the octane rating. Gasoline in the Los angeles basin is composed largely

of aromatic hydrocarbons (30%-40%) and includes 6% to 8% toluene. Therefore, it is not surprising that aromatics make up a large fraction of the hydrocarbons in the urban atmosphere. In recent years the aromatic component of gasoline has been increased so as to maintain the octane rating because the use of tetraalkyl lead compounds has been restricted. Since additives to enhance the octane rating are not likely to be developed and produced in sufficient quantitites to significantly affect the use of aromatics in gasoline, aromatics will continue to be a major component of the atmosphere for some time.

REACTIONS OF AROMATIC HYDROCARBONS

Table 1 summarizes the atmospheric reactants that we believe could react with aromatic hydrocarbons, along with approximate concentrations of these reactive species and the best estimates of rate constants for their reaction with toluene. From these data, only the reaction with OH is expected to be important. Collision with aerosol particles is considerably faster, but adsorption is expected to be very inefficient ($< 10^{-6}$ per collision) and thus should not compete with the reaction of OH.

Reaction with $O(^3P)$ could account for 0.1% as much reaction as OH; even under conditions favoring $O(^3P)$ this percentage would not be greater than 1%. The limit for the photolysis rate is about the same as the $O(^3P)$ rate. The photo rate is a limit because we do not know the cross sections in the solar region or the quantum yields; we have used liberal estimates in both cases to define an upper limit.

For aromatic hydrocarbons besides toluene, we expect the reaction rates with the various atmospheric species to parallel those for toluene. Therefore, only their reactions with OH are of interest. Table 2 summarizes the rate constants for OH reactions for a variety of aromatic hydrocarbons as reported by four sources. The values reported by Davis et al.,[20,21] Perry et al.,[22] and Hansen et al.[23] were obtained using resonance fluorescence to monitor OH decays, and in the case of Doyle et al.[28] the values were obtained by measuring the rate of disappearance in smog

TABLE 1. ATMOSPHERIC REACTIONS OF TOLUENE

Species	Conc, ppm	k, $ppm^{-1}\ min^{-1}$	(Reference)	τ_{tol}, min
$O(^3P)$	10^{-8}	1.1×10^{2}	(24)	9.0×10^{5}
OH	10^{-7}	9.4×10^{3}	(20, 22, 23)	1.1×10^{3}
$HO_2\bullet(RO_2\bullet)$	10^{-3}	2.5×10^{-7}	(25)	4.0×10^{11}
O_3	0.1	5.0×10^{-7}	(26)	2.0×10^{7}
NO_2	0.1	1.0×10^{-8}	(a)	1.0×10^{9}
NO_2^*	$< 10^{-4}$	4×10^{-5}	(a)	2.5×10^{8}
NO_3	10^{-6}	$< 3 \times 10^{-2}$	(27)	$> 3.3 \times 10^{7}$
$O_2(^1\Delta)$	$\sim 10^{-5}$	$< 2 \times 10^{-3}$	(a)	5.0×10^{7}
$h\nu$	--	$<< 7 \times 10^{-5}$	(b)	$>> 1.4 \times 10^{4}$
Particulate	$\sim 10^{3}$[c]	$\sim 10^{-6}$[d]		~ 0.2

[a]Estimated.
[b]Assumes $\sigma < 2 \times 10^{-22}$ $molec^{-1}$ cm^{-2} from 290-400 nm and a quantum yield of unity.
[c]Particles cm^{-3} average particle of 0.1-μm diameter.
[d]Collisions s^{-1}.

chamber experiments relative to the disappearance of n-butane, which is known to react solely with OH. The agreement between the two methods is as good as the agreement between the reported values obtained by resonance fluorescence, about ± 15%. The exception is that, for toluene, the average of the three resonance fluorescence values agrees within 5% while the second method gives a value about 30% less than the mean of these values.

TABLE 2. REPORTED RATE CONSTANTS FOR REACTION OF OH PLUS AROMATIC HYDROCARBONS

Compound	Perry (Ref. 22)	Hansen (Ref. 23)	Doyle (Ref. 28)	Davis (Ref. 20, 21)
Benzene	1.20	1.24	≤ 3.8	1.59
Toluene	6.40	5.78	4.2	6.11
o-Xylene	14.3	15.3	12.8	12.4
m-Xylene	24.0	23.6	23.2	20.5
p-Xylene	15.3	12.2	12.3	10.5
1,2,3-Mesitylene	33.3	26.4	23.0	--
1,2,4-Mesitylene	40.0	33.5	33.0	--
1,3,5-Mesitylene	62.4	47.2	52.0	--

PRODUCTS OF REACTION OF AROMATIC HYDROCARBON

All attempts to determine the toluene reaction products in controlled smog chamber experiments have failed to account for large fractions of the reacted hydrocarbon. Table 3 summarizes data for a typical experiment reported from the SAPRC facility.[2] Early in the experiment, less than 20% of the carbon from the consumed toluene is accounted for. PAN, CO, and benzaldehyde account for most of the detected products. The cresol isomers account for only a small portion of the consumed toluene. They form early in the reaction and the amount detected stays constant until late in the reaction when it decreases slightly. Later in the reaction, the carbon accounted for increases to 22%, but most of the increase is due to CO, which accounts for 67% of the found carbon. Some of the CO may result from wall decomposition of products that are present from previous runs. In this case the observed CO values would be considerably larger than they should be.

O'Brien and coworkers[29] of Portland State University have investigated the reaction of toluene at concentrations of toluene and NO_x about 10 times higher than those at SAPRC. They observed low yields of benzaldehyde

TABLE 3. OBSERVED PRODUCTS FROM SAPRC CHAMBER RUN EC-273

	Time, min						
	0	60	120	180	240	300	360
Toluene, ppm	0.587	0.423	0.383	0.334	0.309	0.284	0.255
Δ Toluene, ppm	--	0.155	0.197	0.247	0.272	0.298	0.327
PAN	0.000	0.024	0.032	0.031	0.029	0.028	0.028
CH_2O	0.002	0.006	0.004	0.009	0.009	0.013	0.017
AcH	0.001	0.002	0.004	0.006	0.007	0.007	0.008
CO	0.33	0.38	0.37	0.47	0.57	0.63	0.67
o-Cresol	0.0005	0.0027	0.0026	0.0024	0.0027	0.0018	0.0014
m-Cresol	0.0003	0.0001	0.0001	0.0002	0.0001	0.0001	0.0001
p-Cresol	0.0047	0.0053	0.0056	0.0052	0.0054	0.0040	0.0048
Benzaldehyde (+ trace of benzylnitrate)	0.0009	0.0097	0.0111	0.0118	0.0158	0.0123	0.0116
Nitrotoluenes	0.0000	0.0010	0.0008	0.0008	0.0010	0.0008	0.0009
Consumed toluene accounted for as products, % carbon	--	17.6	15.1	18.2	23.5	22.4	22.1
As CO, % carbon	--	4.6	2.9	8.1	12.6	14.4	14.8
As products,[a] % CH_3	--	2.39	24.8	20.2	20.2	15.8	14.7

[a]Includes PAN and AcH but not CH_2O, which only in part is from the CH_3-group.

(~ 4%) and o-cresol (6%) and several nitrogen-containing compounds: benzylnitrate (1.6%), m-nitrotoluene (3.8%), and p-nitrotoluene (1.65%). Including these nitrogen-containing products, which are expected to be more prevalent in these experiments because of the higher concentration of NO_x, and CO, 27% of the consumed toluene is accounted for. A limit of less than 1% is set on the amount of ring cleavage products in the early stages by these workers. At very long reaction times significant CO formation occurs, a result supporting the high CO data in the SAPRC run summarized in Table 3.

Jefferies, Fox, and Kamen of University of North Carolina have carried out some runs with toluene in their outdoor smog chamber.[3] Although they have not yet made an extensive study of the products, it is clear that CO formation occurs in the reaction. At 60% conversion of the toluene, about 9% of the consumed carbon is converted to CO.

To summarize these smog chamber studies of toluene, one must conclude that gas phase products account for about 20%-26% of the carbon consumed. After the NO_2 maximum, much of the carbon found is of low molecular weight products CO, PAN, CH_2O, which can be formed only by ring cleavage. Because it is impossible to use these data to construct a clear picture of the toluene mechanism for modeling purposes, it is important to consider other studies beside the smog chamber data.

In their determination of the rate constants of OH with aromatic hydrocarbons, Perry et al.[22] found an unusual temperature dependence for the OH decay with all aromatic compounds. They concluded that two reaction paths are important, one of which is reversible at elevated temperatures. The two pathways are

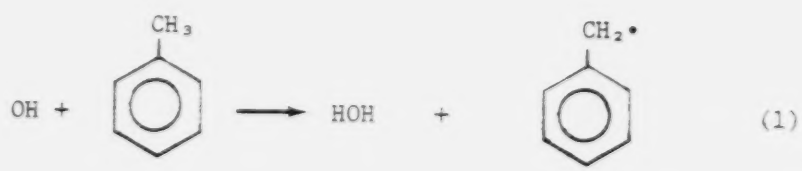

(1)

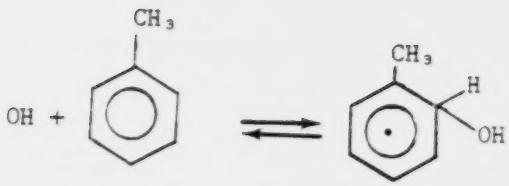

(2)

At high temperatures (85° to 200°C) where reaction (2) was readily reversibly, the decay of OH was governed by reaction (1). They found for this reaction log (k_1/cm^3 molec^{-1} sec^{-1}) = -11.3 (± 0.05) - 900(± 1000)/RT; thus at 30°C $k_1 = 1.1 \times 10^{-12}$ cm^3 molec^{-1} s^{-1}. Because of the extrapolation, k_1 may range from 0.65 to 1.9×10^{-12}. At 30°C they found a much faster decay constant, which is $k_1 + k_2$ and equals $6.4(\pm 0.64) \times 10^{-12}$. Therefore, $k_2 = 5.3 \times 10^{-12}$ cm^3 molec^{-1} s^{-1} and $k_1/(k_1 + k_2) = 0.16$ (range:0.11 to 0.20). Thus, attack at the methyl group under atmospheric conditions accounts for about 16% of the OH reaction, with the large uncertainty due to the value range of k_1. The possibility that the reversibility of reaction (2) is important at atmospheric conditions is ruled out by the lack of a pressure effect on the observed decay content at 30°C. Values of $k_1/(k_1 + k_2)$ for several aromatic hydrocarbons are listed in Table 4.

To determine the stable products from reactions (1) and (2) under atmospheric conditions and thereby evaluate the ratio $k_1/(k_1 + k_2)$ by a more direct method, we investigated the OH-aromatic reaction in our own laboratory.[10] A low pressure flow system is used to generate OH, which is then allowed to react with various aromatic hydrocarbons. The products are determined by sampling the gas stream with solid phase absorbance and by condensing the organics, followed by gas chromatography and/or field ionization mass spectroscopy. These results indicate that, at the high ratios of O_2/NO_2 found in the atmosphere, the benzyl radical formed in reaction (1) gives benzaldehyde by the proposed mechanism

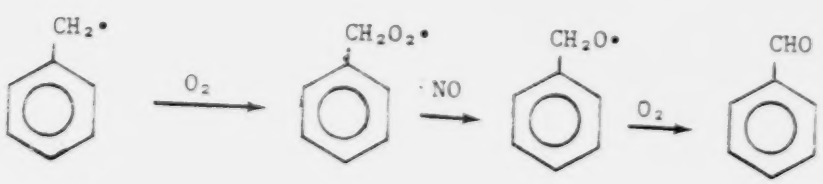

(3)

TABLE 4. FRACTION METHYL ATTACK BY OH FOR SEVERAL AROMATIC HYDROCARBONS

Hydrocarbon	$k_1/(k_1 + k_2)$	
	Perry et al.(23)	Hendry et al.(10)
Benzene[a]	0.05 (0.01-0.13)	< 0.05
Toluene	0.16 (0.11-0.23)	0.15 ± 0.02
o-Xylene	0.20 (0.10-0.35)	
m-Xylene	0.04 (0.02-0.04)	
p-Xylene	0.07 (0.04-0.14)	0.15 ± 0.02
1,2,3-Trimethyl benzene	0.035 (0.02-0.12)	
1,2,4-Trimethyl benzene	0.03 (0.02-0.06)	
1,3,5-Trimethyl benzene	0.02 (0.02-0.04)	0.021 ± 0.006

[a]Rate constant k_1 includes abstraction of aromatic ring hydrogens in this case. In other cases this added process is relatively unimportant because of the much larger values of k_1 and k_2.

and the adduct formed in reaction (2) gives o-, m-, and p-cresols by the reaction

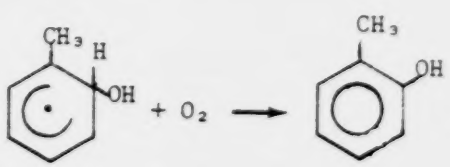

(4)

From the ratio of products, it is possible to estimate the ratio $k_1/(k_1 + k_2)$. These values are also included in Table 4. Comparison of these values with those reported by Perry et al., shows that they are in excellent agreement.

These results suggest that the initial products from the reaction of toluene should be ~ 15% benzaldehyde and 85% cresol. This conclusion contrasts strongly with the smog chamber results discussed above where, at best, about 6% benzaldehyde and about 5% total cresol isomers are observed early in the run (see Table 3). Other laboratory results complicate the issue even further. Heuss and Glasson[30] found, in their smog chamber study of toluene, that benzaldehyde accounted for 19% of the products, a value agreeing well with laboratory measurements mentioned above. However, the only other products reported were 3% formaldehyde and 4% PAN. Kopczynski et al.[31] conducted experiments on mixtures of aromatics including toluene and reported no evidence of benzaldehyde, although toluene was a relatively small fraction of the mixture.

Hoshino et al.[32] attempted to determine the atmospheric products of OH plus toluene by photolyzing HONO and a large excess of toluene in air. These results indicate that 70% of the detected products are cresol or products that would have been expected to give cresol if the OH-toluene adduct were not partially trapped by the high concentration of NO_2; 30% of the products are benzaldehyde or benzylnitrate, which would have given benzaldehyde in the absence of high NO_2.

Akimoto et al.[33] determined the toluene products from photolysis of NO_2-toluene mixtures under conditions where they suggest $O(^3P)$ is the reactive species. However, because of the high NO_2 concentration (11-174 ppm), a very high fraction of $O(^3P)$ reacts with NO_2 by the reaction

$$O + NO_2 \longrightarrow NO + O_2 \qquad (5)$$

Thus it is possible that OH is the dominating reactant species in these reactions. The ratio of products resulting from methyl attack versus the sum of methyl attack and ring attack (corresponding to $k_1/(k_1 + k_2)$ ranges

from 0.16 to 0.30, overlapping the value expected for OH reactions from the laboratory experiments.

Nojima et al.[34] investigated the products resulting from photolyzing toluene (2000 ppm) in the presence of air containing 50-1000 ppm NO. The reaction mechanism could involve OH, although the conditions may favor wall reactions. They found only 11% of the consumed toluene as benzaldehyde, cresol, m-nitrotoluene, p-nitrotoluene, and nitrated cresols. With 50 ppm NO and after one hour, they found ~ 0.5% glyoxol and 3% methylglyoxol, which are indicative of ring cleavage. Because of the severity of the reaction conditions, it is not possible to tell if these last two products are formed directly or by secondary reaction of the benzaldehyde and cresols products.

Strong evidence for direct ring cleavage of aromatic rings by OH comes from recent SAPRC chamber data for o-xylene reported by Darnall et al.[9] They found that biacetyl formation occurs very early in these runs, consistent with 18 ± 2% of the xylene-OH reaction giving this product directly. They found that the biacetyl photolyzes rapidly, generating acetyl radicals, which are converted to PAN. Complete product analyses are not given and these two products account for only about 12% of the carbon from the consumed xylene. However, based on this data, the reaction of toluene would be expected to give methyl glyoxal (pyruvaldehyde) to approximately the same extent as biacetyl in the o-xylene experiment.

TOLUENE-OH REACTIONS

From the data of Perry et al.[22] and Kenley et al.,[10,35] the first step of the OH toluene reaction is

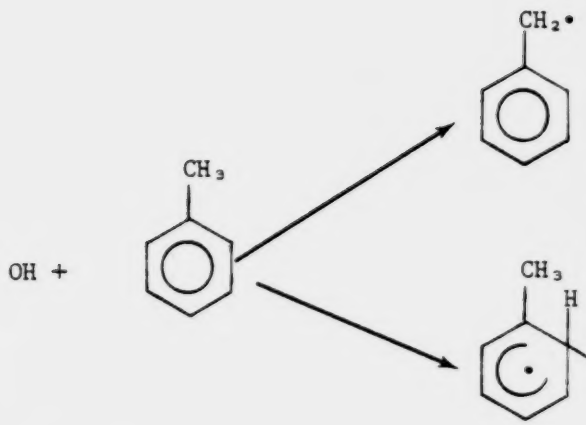

(6)

(7)

The isomer distribution of the last product is 81% ortho, 14% para, and 5% meta.[10] The benzyl reacts by the following series of reactions

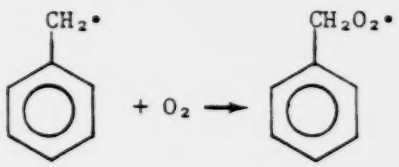

(8)

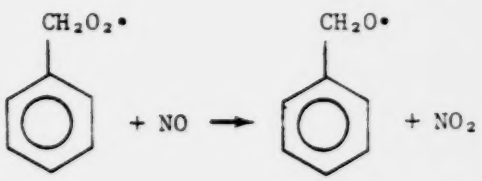

(9)

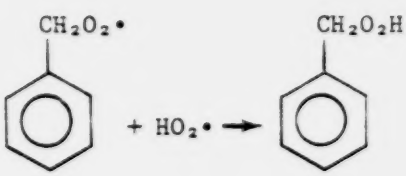

(10)

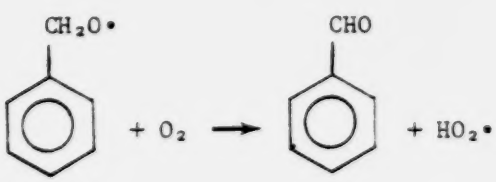

(11)

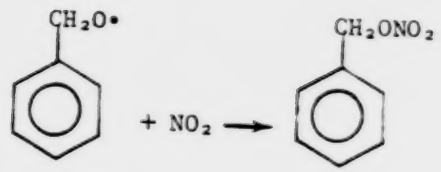

(12)

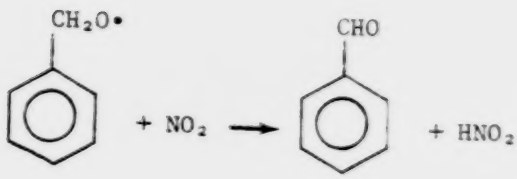

(13)

Under normal atmospheric conditions, reaction (11) dominates the other reactions involving $PhCH_2O\bullet$. The chemistry of the OH adduct formed in reaction (7) is as follows

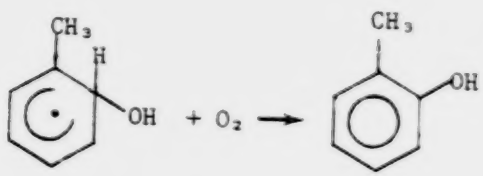

(14)

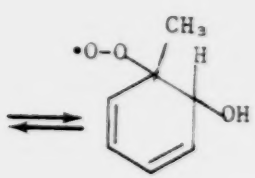

(+ 8 kcal/mol) (15)

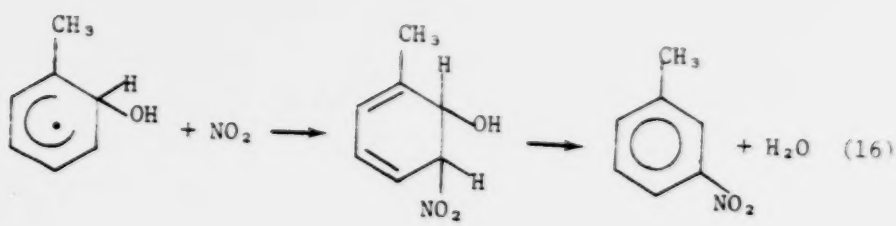

(16)

From the data of Kenley et al.,[35] the ratio of rate constants for reaction (14) and reaction (16) is 2.3×10^{-4}. Since k_{NO_2} is expected to approximate $3 \times 10^9\ M^{-1}\ s^{-1}$, k_{O_2} must be approximately $1.0 \times 10^5\ M^{-1}$

s^{-1}. This value compares with 3.9×10^5 M^{-1} s^{-1} for the similar reaction[36] of methoxy plus O_2

$$CH_3O\bullet + O_2 \longrightarrow CH_2O + HO_2\bullet \qquad (17)$$

The second reaction with oxygen [reaction (15)] to form the organic peroxy radical is expected to be just $\sim 1 \times 10^9$ M^{-1} s^{-1}. The heat of reaction is estimated to be 8 kcal/mol; thus the back reaction may be approximated by the expression

$$\log k_{-15} = 15.0 - 8{,}000/RT$$

$$k_{300} = 1.5 \times 10^9 \ s^{-1}$$

The fate of this peroxy radical is determined by what can compete with its decay back to carbon radical and oxygen. Possible competing reactions are

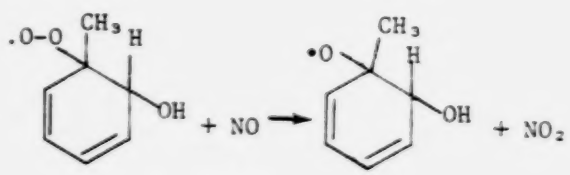

(18)

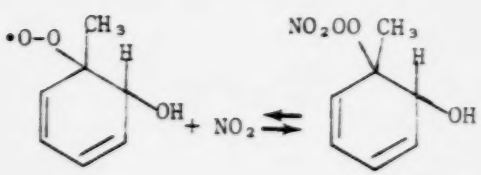

(19)

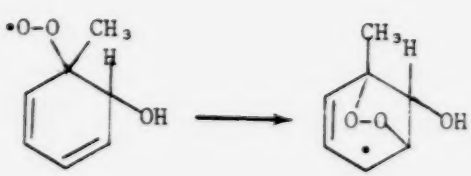

(20)

The reaction with NO is expected to proceed rapidly with a rate constant of $k = 1 \times 10^9\ M^{-1}\ s^{-1}$. Thus at even NO = 0.1 ppm (4×10^{-9} M), $k[NO] = 4s^{-1}$. The reaction with NO_2 is expected to proceed at a rate similar to reaction (18); however, in this case the product is expected to decompose back with a rate constant of $10^{-2}\ s^{-1}$ such that further reaction is unlikely.[37]

Reaction (20) has been suggested by Darnall et al.[9] as the major reaction leading to ring cleavage in the reaction of o-xylene. However, the addition of peroxy radicals to conjugated dienes has an activation energy of 10 kcal/mol.[25] Thus the activation energy for reaction (20) is expected to be 10 plus the increase in strain energy, which is another 5-10 kcal/mol. Thus assigning an A factor reflecting the large loss of entropy gives the maximum rate constant for reaction (20) as

$$\log k < 12 - 15000/RT$$

$$k_{(300)} < 10\ s^{-1}$$

Thus none of three reactions of the organic peroxy radical that we can visualize is fast enough to compete with its decomposition back to OH-toluene adduct and oxygen [reaction (-15)]. This leads us to the conclusion that the only reaction the toluene-OH adduct should undergo in the atmosphere is reaction (14) to the corresponding cresol. This conclusion is consistent with our laboratory data,[10] except that only traces of cresols are found in smog chamber experiment. Thus either we have not anticipated all the possible homogeneous reactions of the toluene-OH system or very rapid reactions of the cresols and possibly benzaldehyde account for the large degree of ring cleavage observed in smog chamber runs.

If we assume that the reactions of cresol and benzaldehyde are only with OH, a simple consecutive model may be assumed where the OH radical concentration is constant. The concentrations of toluene, cresol, and benzaldehyde as function of time may be approximated by the expressions[38]

$$[Tol] = [Tol]_o e^{-k_{Tol}[OH]t}$$

$$[Cresol] = \frac{f_c k_{Tol}[Tol]_o}{k_{Cres} - k_{Tol}}(e^{-k_{Tol}[OH]t} - e^{-k_{Cres}[OH]t})$$

$$[Benzaldehyde] = \frac{f_B k_{Tol}[Tol]_o}{k_{Benz} - k_{Tol}}(e^{-k_{Tol}[OH]t} - e^{-k_{Benz}[OH]t})$$

where k's are rate constants for reaction of OH with toluene (9.0×10^3 ppm^{-1} min^{-1})[22] cresol (6.9×10^4 ppm^{-1} min^{-1}),[39] and benzaldehyde (2.0×10^4 ppm^{-1} min^{-1}),[40] and f_c and f_b are the fractions of reaction of toluene plus OH to give cresol (0.85) and benzaldehyde (0.15). Assuming an OH concentration of 2×10^{-7} ppm^{-1}, 1 ppm toluene will be reacted to the extent of 0.103 ppm after 60 min, and the concentration of cresol and benzaldehyde would be 0.057 and 0.014 ppm, respectively, or 55% and 13% of the consumed toluene. The remaining 32% would be cresol and benzaldehyde reaction products. After 300 min these expressions indicate 0.417 ppm toluene reacted ($\sim$ 42%) and concentrations of cresol and benzaldehyde of 0.067 and 0.034 ppm or 16% and 8% of the consumed toluene, respectively.

The data in Table 3 indicate much lower concentrations of cresol and benzaldehyde, especially early in the reaction. Thus we must again conclude that there are alternative pathways by which toluene reacts or alternative pathways by which the cresols and possibly benzaldehyde react. In the case of the cresols, the rates of the alternative pathways would have to be 10 times faster than the cresol plus OH reaction. The reported rate constant for the OH-cresol reaction is close to diffusion control so it is impossible for it to be 10 times faster. It is important for us to consider what cresol reactions might compete favorably with the OH reaction and whether or not they can account for the cleavage of the aromatic ring and thereby formation of PAN and other low molecular weight products.

REACTIONS OF CRESOL

Since cresol isomers are anticipated based on thermochemical and kinetic reasoning but are not found, it is important to consider what reactions of cresol can be important. Table 5 lists typical concentrations of various atmospheric species, their rate constant with cresol, and their lifetimes. From the table we see that the reactive species $O(^3P)$, $HO_2\bullet$ ($RO_2\bullet$), and O_3 are considerably less important than the reaction with OH. We know less about NO_2, NO_3, and $O_2(^1\Delta)$, but from our estimates it does not appear that any of these species will account for the observed discrepancy. Similarly, direct photolysis appears to be unimportant because of the weak adsorption in the solar spectrum.

The only process that is faster than reaction with OH is collision of cresol molecules with particulate. Collision with walls in a chamber will proceed at an even faster rate. If the cresol has no affinity for absorption to the surface, there should be no effect. However, because cresols are highly polar, they would be expected to be readily absorbed and because they are susceptible to oxidation, further reaction may occur. Thus it appears that if toluene is converted largely to cresols, then cresols at least must be rapidly reacting on the chamber walls. This possibility should be carefully investigated.

ANALYSIS OF NO OXIDATION AND NO_x CONSUMPTION IN TOLUENE REACTIONS

We analyzed several toluene runs reported by SAPRC to determine both the amount of NO being oxidized per toluene consumed and the amount of NO_x disappearing per toluene consumed during the time leading up to the NO_x maximum and for the comparable length of time following the NO_x maximum. Table 6 gives these results.

During the time required to reach the NO_2 maximum, an average of 2.7 net NO molecules are oxidized to form NO_2 and O_3 for each consumed toluene. After the NO_x maximum, the value falls to 1.8. Conversion of toluene to benzaldehyde is expected to require 2 NO per toluene, whereas conversion to cresol requires only 1 NO per toluene. Thus the additional oxidation of NO must occur upon cleavage of the ring and/or

TABLE 5. ATMOSPHERIC REACTIONS OF CRESOLS

Species	Conc., ppm	k, ppm^{-1} min^{-1} (Ref)	$\tau = 1/k[conc]$, min
$O(^3P)$	10^{-8}	8.6×10^{2} (41)	1.2×10^{5}
OH	10^{-7}	6.9×10^{4} (39)	1.4×10^{2}
$HO_2\cdot(RO_2\cdot)$	10^{-3}	2.5×10^{-2} (42)	4.0×10^{6}
O_3	0.1	8.8×10^{-4} (39,43)	1.1×10^{4}
NO_2	0.1	1.0×10^{-8} (a)	1×10^{9}
NO_2^*	$< 10^{-4}$	10 (a)	$> 1.0 \times 10^{5}$
$O_2(^1\Delta)$	10^{-3}	$< 1 \times 10^{2}$ (a)	$> 1.0 \times 10^{3}$
$h\nu$	--	10^{-5} (b)	1.0×10^{5}
Particulate	10^{3}[c]	10^{-6}[d]	0.2

[a] Estimated.
[b] Assumes $\alpha = > 2 \times 10^{-22}$ $molec^{-1}$ cm^{-2} from 290-400 nm and a unit quantum yield and average summer light intensity.[44]
[c] Particles cm^{-3}; average particle of 0.1-μm diameter.
[d] Collisions s^{-1}.

upon further reaction of the products. The proposed mechanism must take this into consideration.

The consumption of NO_x averages about 1.0 NO_x per toluene reacted up to the NO_x maximum and about 1.2 after. Much of this loss of NO_x is due to the reaction

$$OH + NO_2 \longrightarrow HNO_3 \qquad (21)$$

The data in Table 6 indicate that 20%-40% of the loss is due to this reaction in the interval up to the NO_2 maximum in most cases. After the NO_2 maximum, about 45% of the NO_x is lost by this reaction. PAN accounts for only a small fraction of the NO_x loss: about 8% up to the

TABLE 6. ANALYSIS OF SELECTED SAPRC SMOG CHAMBER EXPERIMENTS

	EC-327	EC-340	EC-266	EC-78	EC-85	EC-344	EC-314
Hydrocarbon	Toluene	Toluene	Toluene	Toluene	Toluene	m-Xylene	Propene
Hydrocarbon, ppm	0.573	0.537	1.196	0.210	1.92	0.486	1.046
NO, ppm	0.357	0.333	0.432	0.069	0.431	0.520	0.684
NO_2, ppm	0.096	0.096	0.060	0.032	0.092	0.154	0.246
HC/NO_x	1.26	1.25	2.40	2.95	3.67	0.72	1.12
k_1	0.40	0.39	0.35	0.16	0.16	0.39	0.48
$(\Delta NO + \Delta O_3)/\Delta HC$							
$t_o - t_{max}^{NO_2}$	2.58	2.86	2.21	3.73	1.96	2.67	1.37
$t_{max}^{NO_2} - 2t_{max}^{NO_2}$	2.27	3.05	1.69	1.40	0.72	2.88	0.88
$\Delta NO_x/\Delta HC$							
$t_o - t_{max}^{NO_2}$	0.85	0.78	1.28	1.09	1.15	0.94	0.32
$t_{max}^{NO_2} - 2t_{max}^{NO_2}$	1.67	1.86	0.91	0.85	0.81	2.18	0.81
$\Delta HNO_3/\Delta HC$(from OH + NO_2)[a]							
$t_o - t_{max}^{NO_2}$	0.83	0.51	0.28	0.41	0.20	0.42	0.24
$t_{max}^{NO_2} - 2t_{max}^{NO_2}$	0.98	0.96	0.37	0.41	0.23	0.53	0.44
$\Delta PAN/\Delta HC$							
$t_o - t_{max}^{NO_2}$	0.06	0.04	0.07	0.14	0.09	0.22	0.03
$t_{max}^{NO_2} - 2t_{max}^{NO_2}$	0.17	0.17	0.21	0.22	0.09	0.61	0.24
Difference (%)[b]							
$t_o - t_{max}^{NO_2}$	~ 0(0)	0.23(29)	0.93(52)	0.54(49)	0.86(75)	0.30(32)	0.05(16)
$t_{max}^{NO_2} - 2t_{max}^{NO_2}$	0.52(31)	0.73(39)	0.33(36)	0.22(26)	0.49(60)	1.04(48)	0.13(16)

[a] Rate of formation of $HONO_2$ estimated from average $[NO_2]$ and [OH]; the latter concentration was estimated from the hydrocarbon disappearance.
[b] Difference = $(\Delta NO_x/\Delta HC) - \Delta HNO_3/\Delta HC - \Delta PAN/\Delta HC$; % = 100 x Difference/$(\Delta NO_x/\Delta HC)$.

NO_x maximum and about 16% after the NO_2 maximum. This leaves 50%-70% of the NO_x loss before the NO_2 maximum and 40% after the maximum that is unexplained and must be taken into consideration by the mechanism.

MECHANISM FOR MODELING TOLUENE SMOG CHAMBER DATA

Although uncertainty remains as to what initial products are formed from the direct addition of OH to toluene, the chamber data clearly indicate that at least 25% and possibly as much as 90% of the consumed toluene cleaves during or shortly after reaction by some mechanism. Thus any attempt to model the data must recognize this fact as well as the observation made above regarding molecules of NO oxidized and NO_x consumed per reacted toluene. However, any proposed mechanism will at best be a simplification of what may be a much more complex process.

For our current modeling effort we have assumed that 15% of the toluene-OH reaction is described by methyl abstraction, reactions (6), and (8)-(13). The remaining 85% is assumed to react by the following reactions

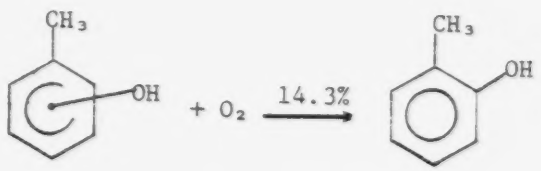

(22)

$$\xrightarrow{14.3\%} CH_3C(O)CHO + C_4H_4O_3 + HO_2\bullet \quad (23)$$

$$\xrightarrow{14.3\%} CH_3C(O)CHO + C_4H_3O_6\bullet + H_2O \quad (24)$$

$$\xrightarrow{28.6\%} HC(O)CHO + C_3H_6O_3 + HO_2\bullet \quad (25)$$

$$\xrightarrow{28.6\%} HC(O)CHO + C_3H_3O_6\bullet + H_2O \quad (26)$$

The fraction of the first pathway was assigned based on the observation of cresol. The remaining reactions were divided to give glyoxal 2/3 of the time and methylglyoxal 1/3 of the time. This ratio represents statistical cleavage of the ring.

In each of reactions (23) through (26), a fragment is proposed that we have no experimental evidence for, but is included to balance the C, H, and O. Obviously in reality each fragment could be composed of several compounds. For simplicity we assume fragments $C_4H_4O_3$ and $C_5H_6O_3$ in reactions (23) and (25) to be

$$HC(O)CH=CHC(O)OH \text{ and } HC(O)C(CH_3)=CHC(O)OH$$

The fragments $C_4H_3O_6\bullet$ and $C_5H_5O_6\bullet$ in reactions (24) and (26) are assumed to be complex acyl peroxy radicals

$$HO_2C(O)CH=CHC(O)O_2\bullet \text{ and } HO_2C(O)C(CH_3)=CHC(O)O_2\bullet$$

We have proposed that these reactions occur without oxidation of NO to NO_2; however, variations could be written for reactions (23) and (25) where NO is oxidized to NO_2 without change in the overall modeling results if OH were formed in place of $HO_2\bullet$. There would be no change in the overall conversion of NO to NO_2 because the fate of $HO_2\bullet$ is to oxidize NO except when NO_x is extremely low.

The peroxy radicals formed in reactions (24) and (26) are assumed to react further. However, for simplication $C_5H_5O_6\bullet$ has been assumed to be identical to $C_4H_3O_6\bullet$, which reacts as follows

$$C_4H_3O_6\bullet + NO \longrightarrow NO_2 + HC(O)CHO + CO + CO_2 + HO_2\bullet \qquad (27)$$

$$C_4H_3O_6\bullet + NO_2 \rightleftharpoons C_4H_3O_6NO_2 \qquad (28,-28)$$

$$C_4H_3O_6NO_2 \longrightarrow \text{to wall} \qquad (29)$$

Reaction (29) thus becomes a mechanism by which NO_x is removed from the system. The rate of NO_x loss depends on the NO/NO_2 ratio. Initially when the NO/NO_2 ratio is high, little NO_x is lost, but by the time the NO_x maximum is reached, this process is a major NO_x loss process.

Reactions of Glyoxal

Reactions (25) and (26) generate glyoxal. The glyoxal reactions used in the simulation are hydrogen abstraction by OH

$$HC(O)CHO + OH \longrightarrow HCO\bullet + CO + HOH \qquad (30)$$

and photolysis[45]

$$HC(O)CHO + h\nu \longrightarrow H_2CO + CO \qquad (31)$$

The rate constant used for reaction (30) is 2×10^4 ppm^{-1} min^{-1}, which is the same as for simple aldehydes.[40] The rate constant for reaction (31) has been adjusted to optimize the prediction of formaldehyde; this has led to a value of 0.01 times the NO_2 photolysis rate.

Reactions of Methylglyoxal

Reactions (23) and (24) form methylglyoxal. As for glyoxal we have assumed reactions with OH and solar radiation, although radical formation is assumed to result from photolysis

$$CH_3C(O)CHO + OH \xrightarrow{O_2} CH_3C(O)O_2\bullet + CO + HOH \qquad (32)$$

$$CH_3C(O)CHO + h\nu \xrightarrow{O_2} CH_3C(O)O_2\bullet + CO + HO_2\bullet \qquad (33)$$

The assumed value of k_{32} is 2×10^4 ppm^{-1} min^{-1}.[40] The value of k_{33} has been adjusted to optimize both total radicals entering the system and PAN formation; this value is about 0.04 times that for NO_2 photolysis. A minor alternative photo reaction is possibly

$$CH_3C(O)C(O)H + h\nu \longrightarrow CH_3C(O)H + CO\bullet \qquad (34)$$

and may be responsible for the small amount of acetaldehyde that is often reported in the SAPRC data. We have not included this reaction in our mechanism because of its very minor role and the uncertainties surrounding it.

Reactions of Benzaldehyde

Both photolysis and reactions with OH have been considered for the reaction of benzaldehyde. For the reaction with OH, we have assumed the following mechanism.

$$PhCHO + OH \longrightarrow PhC(O)\bullet + HOH \qquad (35)$$

$$PhC(O)\bullet + O_2 \longrightarrow PhC(O)O_2\bullet \qquad (36)$$

$$PhC(O)O_2\bullet + NO_2 \rightleftharpoons PhC(O)O_2NO_2 \qquad (37)$$

$$PhC(O)O_2\bullet + NO \longrightarrow PhCO_2\bullet + NO_2 \qquad (38)$$

$$PhCO_2\bullet \longrightarrow Ph\bullet + CO_2 \qquad (39)$$

$$Ph\bullet + O_2 \longrightarrow PhO_2\bullet \qquad (40)$$

$$PhO_2\bullet + NO \longrightarrow PhO\bullet + NO_2 \qquad (41)$$

$$PhO\bullet + NO_2 \longrightarrow NO_2\text{-}PhOH \text{ or } PhONO_2 \qquad (42)$$

$$PhO\bullet + O_2 \longrightarrow 2HC(O)C(O)H + CO + CO_2 + HO_2\bullet \qquad (43)$$

The reaction with OH is assumed to abstract only the aldehydic hydrogen. Addition to the aromatic has been shown to be unimportant (< 10% of total reaction) in low pressure reaction product studies.[10] Reaction (42) is based on the observation of Niki[46] who observed formation

of nitro phenol in controlled experiments when benzoyl radicals were generated in the presence of O_2 and NO_2. Reaction (43) is included to account for ring cleavage, which is expected to be important and may include participation of NO.

To estimate the importance of benzaldehyde photolysis, we have made use of the two SAPRC experiments with added benzaldehyde (EC-337 and -339). Simulation of these runs with our mechanism suggests that benzaldehyde photolysis is not an important source of radicals in the system and further that the disappearance of benzaldehyde is due largely to reaction with OH. To slightly improve the simulation of the benzaldehyde decay curve, we have included the reaction

$$PhCHO \longrightarrow \text{Benzene} + CO \qquad (44)$$

Using a rate constant of 2×10^4 ppm^{-1} min^{-1} for reaction (35), we determined the best value for k_{44} to be 4×10^{-3} min^{-1}.

Reactions of Cresol

The important reaction of cresol is with OH (see Table 5). The mechanism assumed in the simulation is

$$CH_3PhOH + OH \xrightarrow{O_2} CH_3C_6H_3(OH)_2 + HO_2\bullet \qquad (45)$$

$$CH_3PhOH + OH \longrightarrow CH_3PhO\bullet + H_2O \qquad (46)$$

$$CH_3PhO\bullet + O_2 \longrightarrow CH_3C_6H_4(O)O_2\bullet \qquad (47)$$

$$CH_3C_6H_4(O)O_2\bullet + NO \longrightarrow CH_3C_6H_4(O)O\bullet + NO_2 \qquad (48)$$

$$CH_3C_6H_4(O)O\bullet \xrightarrow{O_2} CH_3C(O)O_2\bullet + HC(O)CHO + \text{stable products} \qquad (49)$$

Reaction (45) has been substantiated by product analysis of OH + o-cresol at low pressure.[47] The rate constant for the sum of reactions (45) and

(46) was obtained from Atkinson et al.[39] for o-cresol and the relative values from Perry et al.[48]

Reactions of $C_4H_4O_3$

The species $C_4H_4O_3$ and $C_5H_6O_3$ formed in reactions (23) and (25) are assumed to be aldehydes and therefore reactive like other aldehydes. For simplicity $C_5H_6O_3$ is assumed to be identical to $C_4H_4O_3$. The reactions with OH are

$$C_4H_4O_3 + OH \xrightarrow{O_2} C_4H_3O_5\cdot + HOH \qquad (50)$$

The rate constant for reaction (50) was assumed to be 2.0×10^4 ppm^{-1} min, the same as other aldehydes. The following photolysis reaction was assumed.

$$C_4H_4O_3 + h\nu \longrightarrow C_4H_3O_5\cdot + HO_2\cdot \qquad (51)$$

The reaction was assigned a rate constant 0.03 times the value for NO_2 photolysis.

To simplify the mechanism, the $C_4H_3O_5\cdot$ formed in reactions (50) and (51) was assumed to be identical to $C_4H_3O_6\cdot$ formed in reaction (24).

TOLUENE SIMULATION RESULTS

SAPRC Data

The toluene mechanism, which is summarized in Table 7, was applied to the complete set of SAPRC toluene smog chamber runs. The list of the necessary inorganic reactions is given in Table 8. The data for peroxynitric acid has been undated from our last report in accord with new data of Baldwin and Golden.[51] Initial concentrations for each experiment are given in Table 9, and NO_2 and O_3 maxima and times to maxima are given in Table 10. Ozone decay rates, radical flux rates, and dilution rates were as discussed earlier. Plots showing comparisons of simulation and experimental data for the species monitored in each run are given in

Appendix A. Figure 1 compares the simulation ceoncentrations of NO, NO_2, O_3, and toluene as well as the products PAN, formaldehyde, benzaldehyde, and cresol for EC-266. Qualitatively the general agreement between the simulation and experiment is quite good in the initial stages. The agreement is much improved over previous attempts, which were made with a much smaller data base, especially less product information.

Looking more carefully at figure 1, we see that the simulation slightly overpredicts the rate of NO oxidation before the NO_2 maximum and that the amount of the NO_2 at maximum is slightly larger ($\sim$ 10%) than observed. The toluene and NO_2 decay is too slow after the NO_2 maximum, indicating insufficient OH radical concentration. Despite these differences, the simulation of ozone formation agrees well in the first part of run but does not level off as early as experimentally observed and the final value is overpredicted by 50%. The fact that the ozone agrees early in the run with insufficient reaction of toluene means that each consumed toluene eventually oxidizes too many molecules of NO. This may mean that more of the toluene fragments are less reactive than the model assumes or are trapped on the walls of the chamber. With regard to the products, the formaldehyde is overestimated and the PAN is underestimated. Benzaldehyde and cresol are slightly overestimated.

From the data in Table 10, the average of all runs indicates that the NO_2 maximum averages 8% high and comes 4% later than experimentally observed. The average ozone maximum is 47% high and comes 32% later than observed. The initial stages of ozone formation generally match the experimental very well, but the formation fails to level off at the proper point. This effect is not unique to toluene but is observed in many runs for other hydrocarbon and in principal could be due to a wide variety of factors.

UNC Data

Two toluene runs were made in the outdoor UNC chamber. The data are included at the bottom of Tables 9 and 10. Figures 2 and 3 are plots showing the comparison of simulation and measured concentrations of NO,

TABLE 7 TOLUENE MECHANISM

No.			A Factor[a]	Activation Energy K
1	$PhCH_3 + OH \xrightarrow{O_2}$	$PhCH_2O_2\cdot + H_2O$	1.6×10^3	
2	$PhCH_3 + OH \rightarrow$	$CH_3C_6H_5OH$	7.4×10^3	
3	$CH_3C_6H_5OH \xrightarrow{O_2}$	$CH_3C_6H_4OH + HO_2\cdot$	$^*1.5 \times 10^5$	
4	$CH_3C_6H_5OH \xrightarrow{O_2}$	$CH_3C(O)CHO + C_4H_4O_2 + HO_2\cdot$	$^*1.5 \times 10^5$	
5	$CH_3C_6H_5OH \xrightarrow{O_2}$	$CH_3C(O)CHO + C_4H_3O_3\cdot$	$^*1.5 \times 10^5$	
6	$CH_3C_6H_5OH \xrightarrow{O_2}$	$HC(O)CHO + C_5H_4O_2 + HO_2\cdot$	$^*3.0 \times 10^5$	
7	$CH_3C_6H_5OH \xrightarrow{O_2}$	$HC(O)CHO + C_5H_4O_2\cdot$	$^*3.0 \times 10^5$	
8	$CH_3C_6H_5OH + NO_2 \rightarrow$	$CH_3C_6H_4NO_2 + H_2O$	2.0×10^4	
9	$PhCH_2O_2\cdot + NO \rightarrow$	$PhCH_2O\cdot + NO_2$	1.0×10^4	
10	$PhCH_2O_2\cdot + NO_2 \rightarrow$	$PhCH_2O_2NO_2$	7.8×10^3	
11	$PhCH_2O_2NO_2 \rightarrow$	$PhCH_2O_2\cdot + NO_2$	$^*1.25 \times 10^{16}$	1.16×10^4
12	$PhCH_2O\cdot \xrightarrow{O_2}$	$PhCHO + HO_2\cdot$	$^*1.3 \times 10^5$	
13	$PhCH_2O\cdot + NO_2 \rightarrow$	$PhCHO + HNO_2$	1.5×10^4	
14	$PhCH_2O\cdot + NO_2 \rightarrow$	$PhCH_2ONO_2$	3.0×10^3	
15	$PhCHO + OH \xrightarrow{O_2}$	$PhC(O)O_2\cdot + H_2O$	2.0×10^4	
16	$PhCHO + h\nu \rightarrow$	$PhH + CO$	- - - - -	
17	$PhC(O)O_2\cdot + NO \rightarrow$	$PhC(O)O\cdot + NO_2$	3.7×10^4	
18	$PhC(O)O_2\cdot + NO_2 \rightarrow$	$PhC(O)O_2NO_2$	2.5×10^4	
19	$PhC(O)O_2NO_2 \rightarrow$	$PhC(O)O_2\cdot + NO_2$	$^*9.5 \times 10^{16}$	1.3×10^4
20	$PhC(O)O\cdot \rightarrow$	$PhO_2\cdot + CO_2$	$^*5.2 \times 10^7$	
21	$PhO_2\cdot + NO \rightarrow$	$PhO\cdot + NO_2$	1.0×10^4	
22	$PhO\cdot + NO_2 \rightarrow$	$PhONO_2$ (or NO_2-C_6H_4OH)	6.0×10^3	
23	$PhO\cdot \rightarrow$	$2HC(O)CHO + CO + HO_2\cdot$	$^*1.0 \times 10^8$	
24	$CH_3C_6H_4OH + OH \rightarrow$	$CH_3C_6H_3(OH)_2 + HO_2\cdot$	6.9×10^4	
25	$CH_3C_6H_4OH + OH \rightarrow$	$CH_3C_6H_4O\cdot + H_2O$	6.9×10^3	
26	$CH_3C_6H_4O_2\cdot + NO \xrightarrow{O_2}$	$NO_2 + CH_3C(O)O_2\cdot + HC(O)CHO + H_2O + 2\,CO + CO_2$	1.0×10^4	
27	$C_4H_3O_4\cdot + NO \rightarrow$	$NO_2 + HC(O)CHO + CO + CO_2 + HO_2\cdot$	7.5×10^3	
28	$C_5H_3O_4\cdot + NO \rightarrow$	$NO_2 + HC(O)CHO + CO + CO_2 + HO_2\cdot$	7.5×10^3	
29	$C_4H_4O_3 + OH \xrightarrow{O_2}$	$C_4H_3O_4\cdot$	2.0×10^4	
30	$C_5H_4O_3 + OH \xrightarrow{O_2}$	$C_5H_3O_4\cdot$	2.0×10^4	
31	$C_4H_4O_3 + h\nu \xrightarrow{O_2}$	$C_4H_3O_4\cdot + HO_2\cdot$	- -	
32	$C_5H_4O_3 + h\nu \xrightarrow{O_2}$	$C_5H_3O_4\cdot + HO$	- -	
33	$C_4H_3O_4\cdot + NO_2 \rightarrow$	$C_4H_3O_2NO_2$	2.5×10^3	
34	$C_5H_3O_4\cdot + NO_2 \rightarrow$	$C_5H_3O_4NO_2$	2.5×10^3	
35	$C_4H_3O_2NO_2 \rightarrow$	$C_4H_3O_4\cdot + NO_2$	$^*1.02 \times 10^{16}$	1.35×10^4
36	$C_4H_3O_2NO_2 \rightarrow$	wall	$^*3.0 \times 10^{-26}$	
37	$C_5H_3O_4NO_2 \rightarrow$	$C_5H_3O_4\cdot + NO_2$	$^*1.02 \times 10^{16}$	1.35×10^4
38	$C_5H_3O_4NO_2 \rightarrow$	wall	$^*3.0 \times 10^{-26}$	
39	$CH_3C(O)CHO + OH \xrightarrow{O_2}$	$CH_3C(O)O_2\cdot + CO + H_2O$	2.0×10^4	
40	$CH_3C(O)CHO + h\nu \xrightarrow{O_2}$	$CH_3C(O)O_2\cdot + CO + HO_2\cdot$	- -	

continued . . . .

Table 7 Toluene Mechanism (concluded)

No.			A Factor[a]	Activation Energy K
41	$CH_3C(O)O_2\cdot + NO \xrightarrow{O_2}$	$NO_2 + CH_3O_2\cdot + CO_2$	7.5×10^3	
42	$CH_3C(O)O_2\cdot + NO_2 \rightarrow$	$CH_3C(O)O_2NO_2$	2.5×10^3	
43	$CH_3C(O)O_2NO_2 \rightarrow$	$CH_3C(O)O_2\cdot + NO_2$	$^*1.02 \times 10^{18}$	1.35×10^4
44	$CH_3O_2\cdot + NO \rightarrow$	$CH_3O\cdot + NO_2$	1.0×10^4	
45	$CH_3O\cdot + O_2 \rightarrow$	$CH_2O + HO_2\cdot$	2.0×10^5	
46	$CH_3O\cdot + NO_2 \rightarrow$	$CH_2O + HNO_2$	2.2×10^3	
47	$CH_3O\cdot + NO_2 \rightarrow$	CH_3ONO_2	2.0×10^4	
48	$CH_2O + OH \rightarrow$	$HO_2\cdot + CO + H_2O$	2.0×10^4	
49	$CH_2O + h\nu \rightarrow$	$H_2 + CO$	- -	
50	$CH_2O + h\nu \rightarrow$	$2HO_2\cdot + CO$	- -	
51	$HC(O)CHO + OH \rightarrow$	$HO_2\cdot + CO + CO + H_2O$	2.0×10^4	
52	$HC(O)CHO + h\nu \rightarrow$	$2HO_2\cdot + 2CO$	- -	
53	$CH_3CHO + OH \xrightarrow{O_2}$	$CH_3C(O)O_2\cdot + H_2O$	2.0×10^4	
54	$CH_3CHO + h\nu \rightarrow$	$CH_3C(O)O_2\cdot + HO_2\cdot$	- -	
55	$PhCH_2O_2\cdot + HO_2\cdot \rightarrow$		2.0×10^3	
56	$PhCH_2O\cdot + HO_2 \rightarrow$		2.0×10^3	
57	$PhO_2\cdot + HO_2\cdot \rightarrow$		2.0×10^3	
58	$PhO\cdot + HO_2\cdot \rightarrow$		2.0×10^3	
59	$PhC(O)O_2\cdot + HO_2\cdot \rightarrow$		2.0×10^3	
60	$PhC(O)O\cdot + HO_2\cdot \rightarrow$		2.0×10^3	
61	$CH_3O_2\cdot + HO_2\cdot \rightarrow$		2.0×10^3	
62	$CH_3C(O)O_2\cdot + HO_2\cdot \rightarrow$		2.0×10^3	
63	$2CH_3C(O)O_2\cdot \xrightarrow{O_2}$	$2CH_3O_2\cdot + 2CO_2$	2.0×10^2	
64	$2CH_3O_2\cdot \rightarrow$	$CH_2O + CH_3OH$	2.0×10^2	
65	$CH_3C_6H_4OH + O_3 \rightarrow$	OH	1.0×10^3	

[a] Units are ppm^{-1} min^{-1} except those marked * are min^{-1}.

[b] In UNC chamber run, rate constant for reactions 36 and 38 is 7×10^{-3} min^{-1}.

TABLE 8. INORGANIC REACTIONS

No.	Reaction	A Factor	Activation Energy
1	$O(^3P) + O_2 + M \rightarrow O_3 + M$	$^{**}2.0 \times 10^{-5}$	
2	$O(^3P) + NO_2 \rightarrow NO + O_2$	1.3×10^4	
3	$O_3 + NO \rightarrow NO_2 + O_2$	1.33×10^3	1.20×10^3
4	$O(^1D) + M \rightarrow O(^3P) + M$	8.6×10^4	
5	$O(^1D) + H_2O \rightarrow 2OH$	5.1×10^5	
6	$O_3 + OH \rightarrow HO_2 + O_2$	2.22×10^3	1.00×10^3
7	$O_3 + HO_2 \rightarrow OH + 2O_2$	1.08	1.275×10^3
8	$O_3 + NO_2 \rightarrow NO_3 + O_2$	1.98×10^2	2.47×10^3
9	$O_3 \rightarrow$ wall	$^{*}1.0 \times 10^{-3}$	
10	$NO_3 + NO \rightarrow 2NO_2$	2.187×10^2	-8.16×10^2
11	$NO_3 + NO_2(+ M) \rightarrow N_2O_5(+ M)$	5.6×10^3	
12	$N_2O_5 + H_2O \rightarrow 2HNO_3$	5.0×10^{-6}	
13	$N_2O_5(+ M) \rightarrow NO_2 + NO_3(+ M)$	$^{*}7.44 \times 10^{15}$	1.03×10^4
14	$NO + NO_2 + H_2O \rightarrow 2HONO$	$^{**}2.2 \times 10^{-9}$	
15	$2HNO_2 \rightarrow NO + NO_2 + H_2O$	1.3×10^{-3}	
16	$NO_2 + OH(+ M) \rightarrow HNO_3(+ M)$	1.5×10^4	
17	$NO + OH(+ M) \rightarrow HONO (+ M)$	1.0×10^4	
18	$NO + HO_2 \rightarrow NO_2 + OH$	1.2×10^4	
19	$NO_2 + HO_2 \rightarrow HO_2NO_2$	2.0×10^3	
20	$HO_2NO_2 \rightarrow HO_2 + NO_2$	7.8×10^{15}	1.04×10^4
21	$HO_2 + HO_2 \rightarrow H_2O_2 + O_2$	4.0×10^3	
22	$CO + OH \rightarrow HO + CO$	2.1×10^2	
23	$NO + h\nu \rightarrow NO + O(^3P)$	b	
24	$O_3 + h\nu \rightarrow O(^1D) + O_2$	b	
25	$O_3 + h\nu \rightarrow O(^3P) + O_2$	b	
26	$HONO + h\nu \rightarrow OH + NO$	b	
27	$H_2O_2 + h\nu \rightarrow 2OH$	b	

[a]Units in ppm^{-1} min^{-1} except those marked * are min^{-1} and those marked ** are ppm^{-2} min^{-1}.

[b]Rates calculated from light intensity data for each run.

TABLE 9. SUMMARY OF INITIAL CONDITIONS FOR SMOG CHAMBER EXPERIMENTS FOR TOLUENE AND m-XYLENE[a]

EC No.	Toluene	NO	NO_2	H_2CO	AcH	BAL	HONO[b]	Tol/NO_x	k_{NO_2}
83	5.63	1.36	0.66	0.00	0.00	0.016	0.000	0.80	0.16
82	1.88	0.68	0.34	0.001	0.00	0.00	0.01	1.85	0.16
85	1.92	0.43	0.099	0.00	0.00	0.005	0.001	3.67	0.16
81	1.96	0.41	0.094	0.00	0.00	0.00	0.02	3.90	0.16
285	1.07	0.44	0.048	0.012	0.00	0.00	- -	2.22	0.35
286	1.20	0.43	0.060	0.010	0.00	0.00	0.001	2.43	0.35
284	1.16	0.42	0.056	0.008	0.00	0.00	- -	2.42	0.35
80	1.02	0.40	0.095	0.00	0.00	0.00	0.02	2.05	0.16
84	0.97	0.39	0.080	0.007	0.00	0.032	0.001	2.06	0.16
271	1.15	0.19	0.029	0.004	0.00	0.00	0.00	5.33	0.37
79	0.98	0.08	0.019	0.011	0.00	0.00	- -	9.86	
269	0.57	0.40	0.074	0.003	0.00	0.00	0.000	1.20	0.35
327	0.57	0.36	0.096	0.00	0.00	0.000	0.000	1.26	0.40
340	0.54	0.33	0.096	0.005	0.00	0.00	0.003	1.25	0.39
273	0.59	0.096	0.014	0.002	0.001	0.00	0.000	5.34	0.37
77	0.28	0.52	0.058	0.003	0.00	0.00	0.001	0.48	0.16
78	0.21	0.069	0.032	0.00	0.00	0.00	0.001	2.07	0.16
335	1.00	0.35	0.092	0.010	0.30	0.002	0.000	2.24	0.39
272	0.58	0.40	0.080	0.017	0.00	0.009	0.001	1.21	0.35
86	1.09	0.41	0.08	0.161	0.00	0.00	0.001	2.24	0.16
336	1.01	0.34	0.10	0.303	0.00	0.00	0.000	2.30	0.39
270	0.58	0.41	0.05	0.178	0.00	0.003	0.000	1.24	0.35
337	0.96	0.32	0.12	0.009	0.00	0.172	0.000	2.15	0.39
339	0.54	0.34	0.10	0.002	0.00	0.187	0.000	1.21	0.39
331[d]	1.99[d]	0.35	0.112	0.006	0.001	0.00	0.01	4.27	0.40
338[d]	0.95[d]	0.35	0.100	0.008	0.001	0.001	0.003	2.14	0.39
328	0.57[d]	0.36	0.096	0.015	0.001	0.00	0.003	1.25	0.40
334	0.99[e]	0.35	0.10	0.015	0.001	0.00	0.006	2.22	0.39
329	0.56[e]	0.35	0.10	0.001	0.002	0.00	0.002	1.22	0.40
330	0.57[e]	0.20	0.09	0.009	0.002	0.00	0.006	1.94	0.40
UNC 8.16.78R	0.56	0.60	0.088	0.00	0.00	0.00	0.010		- -
UNC 9.14.78R	0.32	0.24	0.057	0.00	0.00	0.00	0.004		- -
344[f]	0.49[f]	0.52	0.15	0.00	0.001	0.000[g]	0.000	0.73	0.39
343[f]	0.49[f]	0.21	0.066	0.009	0.001	0.002[g]	0.000	1.77	0.38
345[f]	0.48[f]	0.22	0.059	0.002	0.00	0.000[g]	0.000	1.71	0.39
346[f]	0.49[f]	0.20	0.059	0.006	0.001	0.000[g]	0.000	1.89	0.39

[a] Units are ppm. Standard conditions include in addition: ~ 2 x 10^4 ppm H_2O except for EC-83 where only 1.8 x 10^3 ppm H_2O was used; chamber temperature 302 K.
[b] Amount of HONO used in simulation.
[c] Units are min^{-1}.
[d] Plus 2.04 ppm n-butane.
[e] Plus 0.096 ppm propene.
[f] m-Xylene run, no toluene present.
[g] Methylbenzaldehyde.

TABLE 10. COMPARISON OF EXPERIMENTAL AND SIMULATION RESULTS FOR TOLUENE AND m-XYLENE CHAMBER EXPERIMENTS

EC No.	EXPERIMENTAL				SIMULATION			
	O_3-max		NO_2-max		O_3-max		NO_2-max	
	ppm	min	ppm	min	ppm	min	ppm	min
83	> 0.42	> 360	1.37	270	> 0.42	> 360	1.40	200
82	> 0.36	> 360	0.61	180	> 0.25	> 360	0.67	190
85	0.27	240	0.35	120	0.46	300	0.36	95
81	0.26	180	0.34	75	0.48	250	0.36	60
265	0.39	220	0.30	90				
266	0.40	220	0.30	90	0.60	310	0.33	90
264	0.42	220	0.29	90				
80	0.34	255	0.31	105	> 0.35	> 360	0.33	100
84	0.23	360	0.27	140	0.33	> 360	0.30	130
271	0.30	90	0.14	30	0.40	150	0.144	50
79	0.096	120	0.063	30	- -	- -	- -	- -
269	0.30	> 360	0.26	140	0.30	> 360	0.29	160
327	0.38	360	0.26	135	0.39	> 360	0.27	140
340	0.35	360	0.25	120	> 0.40	> 400	0.26	135
273	0.22	80	0.064	30	0.25	110	0.07	35
77	> 0.01	> 360	0.24	300	> 0.01	> 360	0.26	300
78	0.092	195	0.066	45	0.16	250	0.064	60
335	0.40	225	0.27	75	0.69	330	0.30	55
272	0.41	340	0.30	100	0.68	> 400	0.33	80
86	0.30	330	0.34	120	0.48	> 400	0.34	100
336	0.39	165	0.27	60	0.65	210	0.29	40
270	0.37	330	0.27	100	0.52	> 360	0.29	100
337	0.32	255	0.26	105	0.58	360	0.29	115
339	0.22	> 360	0.24	195	> 0.38	> 400	0.29	150
331	0.52	120	0.33	45	0.98	270	0.36	55
338	0.48	240	0.30	75	0.98	380	0.34	100
328	0.52	360	0.30	105	> 0.96	> 400	0.34	110
334	0.41	180	0.29	60	0.73	330	0.31	80
329	0.40	310	0.28	100	> 0.56	> 400	0.30	125
330	0.34	180	0.19	60	0.57	330	0.20	70
UNC 8.16.78B	> 0.27	> 750	0.40	490	> 0.30	> 720	0.38	540
UNC 9.14.78R	> 0.31	> 770	0.18	490	> 0.18	> 720	0.16	520
344	0.59	180	0.45	45	0.70	180	0.45	45
343	0.28	75	0.19	30	0.40	100	0.19	25
345	0.40	75	0.19	25	0.40	85	0.20	30
348	0.38	60	0.12	35	0.41	120	0.17	30

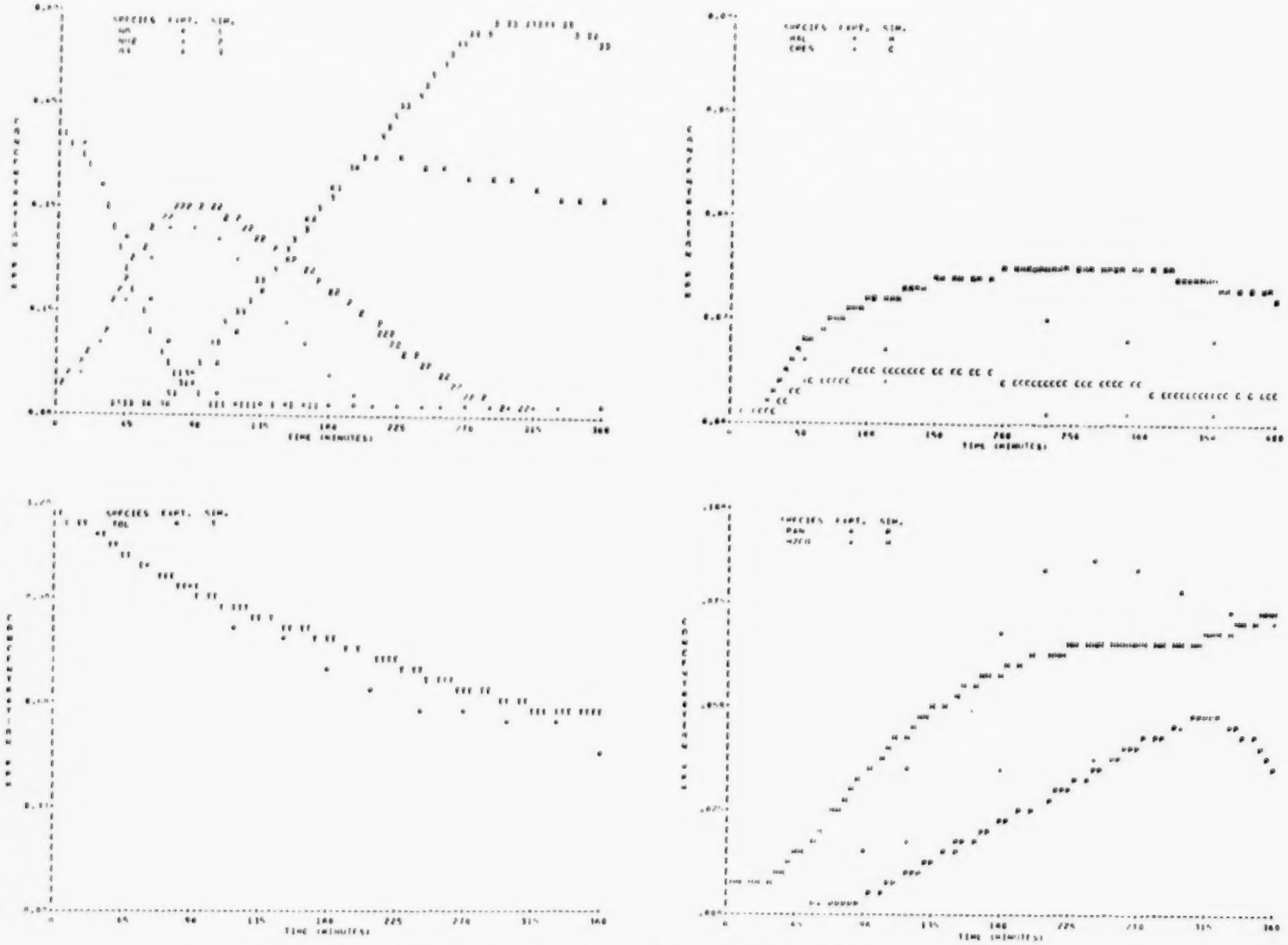

Figure 1. Simulation of SAPRC Toluene Run EC-266.

Reproduced from
best available copy.

NO_2, O_3, toluene, and CO for these runs. In both cases the agreement between simulation and experiment is quite good. In these runs the initial HNO_2 was varied to obtain the desired initial NO decay. In both cases after the NO_2 maximum, the decay of NO_2 is slightly slower than observed as was often also observed in the SAPRC runs. The ozone buildup is low in one case and high in the other. Unfortunately, it is not possible to make any generalization regarding the source of this discrepancy with just these two experiments.

MECHANISM FOR MODELING m-XYLENE SMOG CHAMBER EXPERIMENTS

The m-xylene mechanism was based on the toluene mechanism with the following changes:

- The total rate constant for the reaction of OH with m-xylene is 3.6×10^4 ppm^{-1} min^{-1} (see Table 2).
- The ratio of methyl attack to total reaction for OH + m-xylene is 0.083 (see Table 4).
- The xylene-OH adduct was assumed to react by reactions parallel to reactions (22) through (26), the same as for toluene; however the proportions assumed were 14.3:28.6:28.6:14.3:14.3, respectively, to account for the additional methyl group in xylene. The reactions for xylene are:

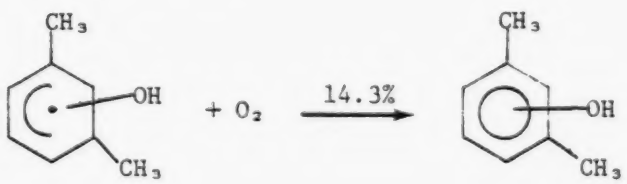

(22′)

$$\longrightarrow CH_3C(O)CHO + C_5H_6O_3 + HO_2\bullet \qquad (23')$$

$$\longrightarrow CH_3C(O)CHO + C_5H_5O_6\bullet + H_2O \qquad (24')$$

$$\longrightarrow HC(O)CHO + C_6H_8O_3 + HO_2\bullet \qquad (25')$$

$$\longrightarrow HC(O)CHO + C_6H_7O_6\bullet + H_2O \qquad (26')$$

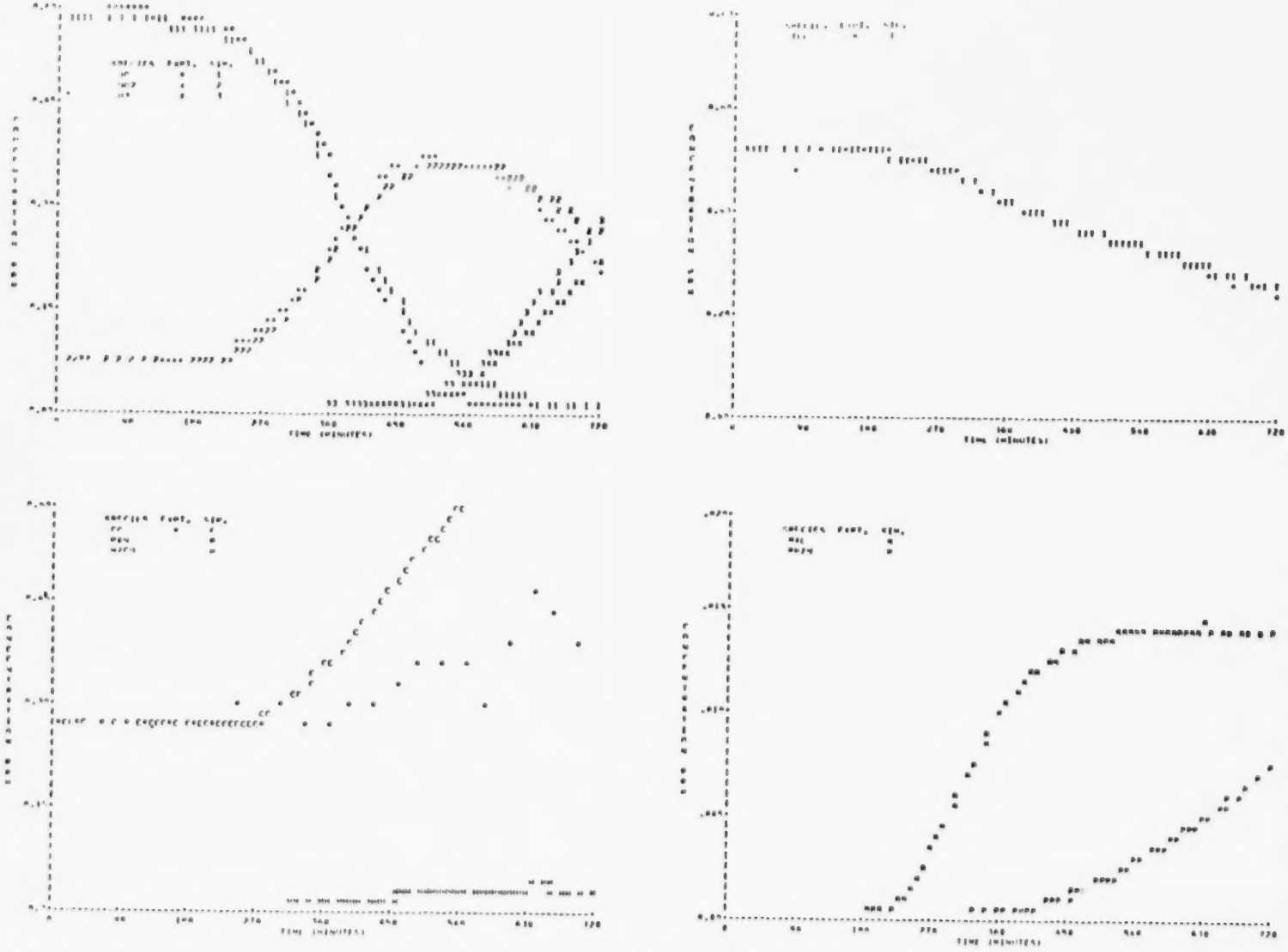

Figure 2. Simulation of UNC Toluene Run 8.16.78 Red.

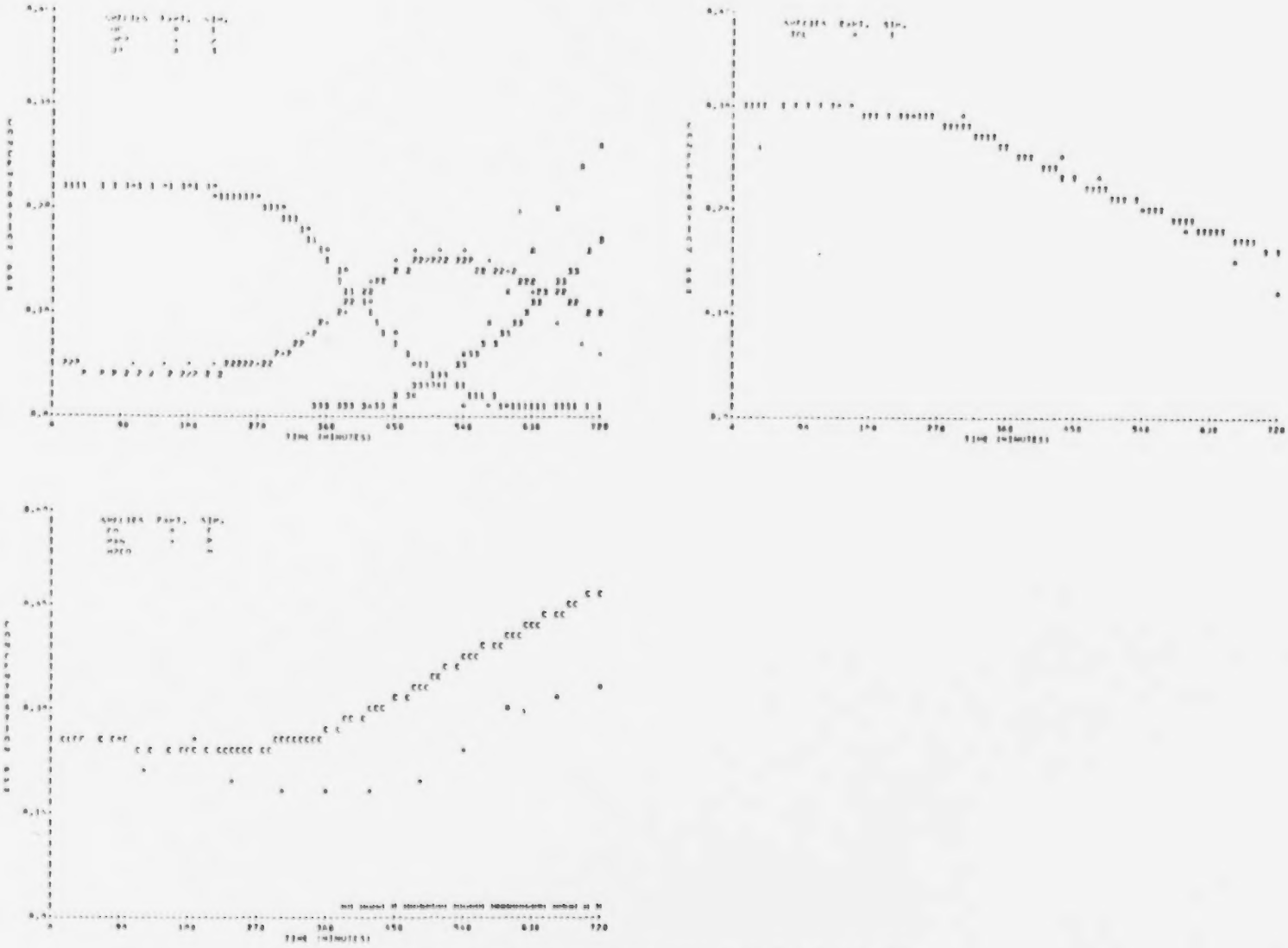

Figure 3. Simulation of UNC Toluene Run 9.14.78 Red.

- Since the fragments in reactions (23′)-(26′) have an additional CH_3, reactions (27)-(29), (50), and (51) are changed accordingly

$$C_5H_5O_6\bullet + NO \longrightarrow NO_2 + CH_3C(O)C(O)H + CO + CO_2 + HO_2\bullet \qquad (27')$$

$$C_5H_5O_6\bullet + NO_2 \rightleftharpoons C_5H_5O_6NO_2 \qquad (28')$$

$$C_5H_5O_6NO_2 \longrightarrow \text{wall} \qquad (29')$$

$$C_5H_6O_3 + OH \longrightarrow C_5H_5O_5\bullet + HOH \qquad (50')$$

$$C_5H_6O_3 + h\nu \longrightarrow C_5H_5O_5\bullet + HO_2\bullet \qquad (51')$$

The intermediates $C_6H_8O_3$ and $C_5H_6O_3$ are assumed to be identical, and $C_6H_7O_6\bullet$ and $C_5H_5O_5\bullet$ are the same as $C_5H_5O_6\bullet$.

The data in Table 6 calculated for xylene run EC-344 indicate that 32%-48% of the NO_x loss is due to reactions between the organic fragments and NO_x. This percentage is similar to that observed for toluene, so no changes were made in reactions (27) through (29).

The reactions of methyl benzaldehyde and dimethylphenol were assumed to be identical to those of benzaldehyde and cresol, which are formed in the toluene mechanism. The complete m-xylene mechanism is given in Table 11.

m-XYLENE SIMULATION RESULTS

The results from four SAPRC runs are available to develop and test the m-xylene mechanism (Table 11). Three of these runs are under nearly identical conditions. The concentration data for these experiments are included in Table 9; NO_2 and O_3 maxima and times to maxima are given in Table 10. Figure 4 plots the simulated and observed concentrations for EC-345 as an example. Plots of all four experiments are given in Appendix A.

Table 11 m-XYLENE MECHANISM

No.		A-Factor	Activation Energy K
1	$CH_3PhCH_3 + OH \xrightarrow{O_2} CH_3PhCH_2O_2\cdot + H_2O$	3.0×10^3	
2	$CH_3PhCH_3 + OH \xrightarrow{O_2} (CH_3)_2C_6H_4OH$	3.3×10^4	
3	$(CH_3)_2C_6H_4OH \xrightarrow{O_2} (CH_3)_2C_6H_3OH + HO_2\cdot$	$*1.5 \times 10^5$	
4	$(CH_3)_2C_6H_4OH \xrightarrow{O_2} CH_3C(O)CHO + C_3H_4O_3 + HO_2\cdot$	$*3.0 \times 10^5$	
5	$(CH_3)_2C_6H_4OH \xrightarrow{O_2} CH_3C(O)CHO + C_3H_3O_4\cdot$	$*3.0 \times 10^5$	
6	$(CH_3)_2C_6H_4OH \xrightarrow{O_2} HC(O)CHO + C_4H_4O_3 (=C_5H_4O_3)$	$*1.5 \times 10^5$	
7	$(CH_3)_2C_6H_4OH \xrightarrow{O_2} HC(O)CHO + C_4H_3O_4\cdot (=C_5H_5O_4\cdot)$	$*1.5 \times 10^5$	
8	$(CH_3)_2C_6H_4OH + NO_2 \rightarrow (CH_3)_2C_6H_3NO_2 + H_2O$	2.0×10^4	
9	$CH_3PhCH_2O_2\cdot + NO \rightarrow CH_3PhCH_2O\cdot + NO_2$	1.0×10^4	
10	$CH_3PhCH_2O_2 + NO_2 \rightarrow CH_3PhCH_2O_2NO_2$	7.8×10^3	
11	$CH_3PhCH_2O_2NO_2 \rightarrow CH_3PhCH_2O_2\cdot + NO_2$	$*1.25 \times 10^{16}$	1.16×10^4
12	$CH_3PhCH_2O\cdot \xrightarrow{O_2} CH_3PhCHO + HO_2$	$*1.3 \times 10^5$	
13	$CH_3PhCH_2O\cdot + NO_2 \rightarrow CH_3PhCHO + HNO_2$	1.5×10^4	
14	$CH_3PhCH_2O\cdot + NO_2 \rightarrow CH_3PhCH_2ONO_2$	3.0×10^3	
15	$CH_3PhCHO + OH \xrightarrow{O_2} CH_3PhC(O)O_2\cdot + H_2O$	2.0×10^4	
16	$CH_3PhCHO + h\nu \rightarrow CH_3PhH + CO$	- -	
17	$CH_3PhC(O)O_2\cdot + NO \rightarrow CH_3PhC(O)O\cdot + NO_2$	3.7×10^4	
18	$CH_3PhC(O)O_2\cdot + NO_2 \rightarrow CH_3PhC(O)O_2NO_2$	2.5×10^4	
19	$CH_3PhC(O)O_2NO_2 \rightarrow CH_3PhC(O)O_2\cdot + NO_2$	$*9.5 \times 10^{16}$	1.3×10^4
20	$CH_3PhC(O)O\cdot \xrightarrow{O_2} CH_3PhO_2\cdot + CO_2$	$*5.2 \times 10^7$	
21	$CH_3PhO_2\cdot + NO \rightarrow CH_3PhO\cdot + NO_2$	1.0×10^4	
22	$CH_3PhO\cdot + NO_2 \rightarrow CH_3PhONO_2 (or\ NO_2(CH_3)C_6H_3OH)$	6.0×10^3	
23	$CH_3PhO\cdot \xrightarrow{O_2} 2HC(O)CHO + CO + HO_2\cdot$	$*1.0 \times 10^8$	
24	$(CH_3)_2C_6H_3OH + OH \xrightarrow{O_2} (CH_3)_2C_6H_2(OH)_2 + HO_2\cdot$	6.9×10^4	
25	$(CH_3)_2C_6H_3OH + OH \rightarrow CH_3C_6H_4O\cdot + H_2O$	6.9×10^3	
26	$(CH_3)_2C_6H_3O\cdot + NO \xrightarrow{O_2} NO_2 + CH_3C(O)O_2\cdot + HC(O)CHO + CO + CO_2$	1.0×10^4	
27	$C_5H_5O_4\cdot + NO \rightarrow NO_2 + CH_3C(O)CHO + CO + CO_2 + HO_2\cdot$	7.5×10^3	
28	$C_5H_4O_3 + OH \xrightarrow{O_2} C_5H_3O_4\cdot$	2.0×10^4	
29	$C_5H_4O_3 + h\nu \xrightarrow{O_2} C_5H_5O_4$	- -	
30	$C_5H_5O_4\cdot + NO_2 \rightarrow C_5H_5O_4NO_2$	2.5×10^3	
31	$C_5H_5O_4NO_2 \rightarrow C_5H_5O_4\cdot + NO_2$	$*1.02 \times 10^{18}$	1.35×10^4
32	$C_5H_5O_4NO_2 \rightarrow wall$	$*3.0 \times 10^{-2}$	
33	$CH_3C(O)CHO + OH \xrightarrow{O_2} CH_3C(O)O_2\cdot + CO + H_2O$	2.0×10^4	
34	$CH_3C(O)CHO + h\nu \rightarrow CH_3C(O)O_2\cdot + CO + HO_2\cdot$	- -	
35	$CH_3C(O)O_2\cdot + NO \xrightarrow{O_2} NO_2 + CH_3O_2\cdot + CO_2$	7.5×10^3	
36	$CH_3C(O)O_2\cdot + NO_2 \rightarrow CH_3C(O)O_2NO_2$	2.5×10^3	
37	$CH_3C(O)O_2NO_2 \rightarrow CH_3C(O)O_2\cdot + NO_2$	$*1.02 \times 10^{18}$	1.35×10^4
38	$CH_3O_2\cdot + NO \rightarrow CH_3O\cdot + NO_2$	1.0×10^4	
39	$CH_3O\cdot + O_2 \rightarrow CH_2O + HO_2\cdot$	2.0×10^3	
40	$CH_3O\cdot + NO_2 \rightarrow CH_2O + HNO_2$	2.2×10^3	

continued . . .

Table 11 m-Xylene Mechanism (concluded)

No.		A-Factor[a]	Activation Energy K
41	$CH_3O\cdot + NO_2 \rightarrow CH_3ONO_2$	2.0×10^4	
42	$CH_2O + OH \rightarrow HO_2\cdot + CO + H_2O$	2.0×10^4	
43	$CH_2O + h\nu \rightarrow H_2 + CO$	- -	
44	$CH_2O + h\nu \rightarrow 2HO_2\cdot + CO$	- -	
45	$HC(O)CHO + OH \rightarrow HO_2\cdot + CO + CO + H_2O$	2.0×10^4	
46	$HC(O)CHO + h\nu \rightarrow 2HO_2\cdot + 2CO$	- -	
47	$CH_3CHO + OH \xrightarrow{O_2} CH_3C(O)O_2\cdot + H_2O$	2.0×10^4	
48	$CH_3CHO + h\nu \rightarrow CH_3C(O)O_2\cdot + HO_2\cdot$	- -	
49	$CH_3PhCH_2O_2\cdot + HO_2\cdot \rightarrow$	2.0×10^3	
50	$CH_3PhCH_2O\cdot + HO_2\cdot \rightarrow$	2.0×10^3	
51	$CH_3PhO_2\cdot + HO_2\cdot \rightarrow$	2.0×10^3	
52	$CH_3PhO\cdot + HO_2\cdot \rightarrow$	2.0×10^3	
53	$CH_3PhC(O)O_2\cdot + HO_2\cdot \rightarrow$	2.0×10^3	
54	$CH_3PhC(O)O\cdot + HO_2\cdot \rightarrow$	2.0×10^3	
55	$CH_3O_2\cdot + HO_2\cdot \rightarrow$	2.0×10^3	
56	$CH_3C(O)O_2\cdot + HO_2\cdot \rightarrow$	2.0×10^3	
57	$2CH_3C(O)O_2\cdot \rightarrow 2CH_3O_2\cdot + 2CO_2$	2.0×10^3	
58	$2CH_3O_2\cdot \rightarrow CH_2O + CH_3OH$	2.0×10^3	
59	$(CH_3)_2C_6H_4OH + O_3 \rightarrow OH$	1.0×10^3	

[a] Units are ppm^{-1} min^{-1} except those marked * are min^{-1}.

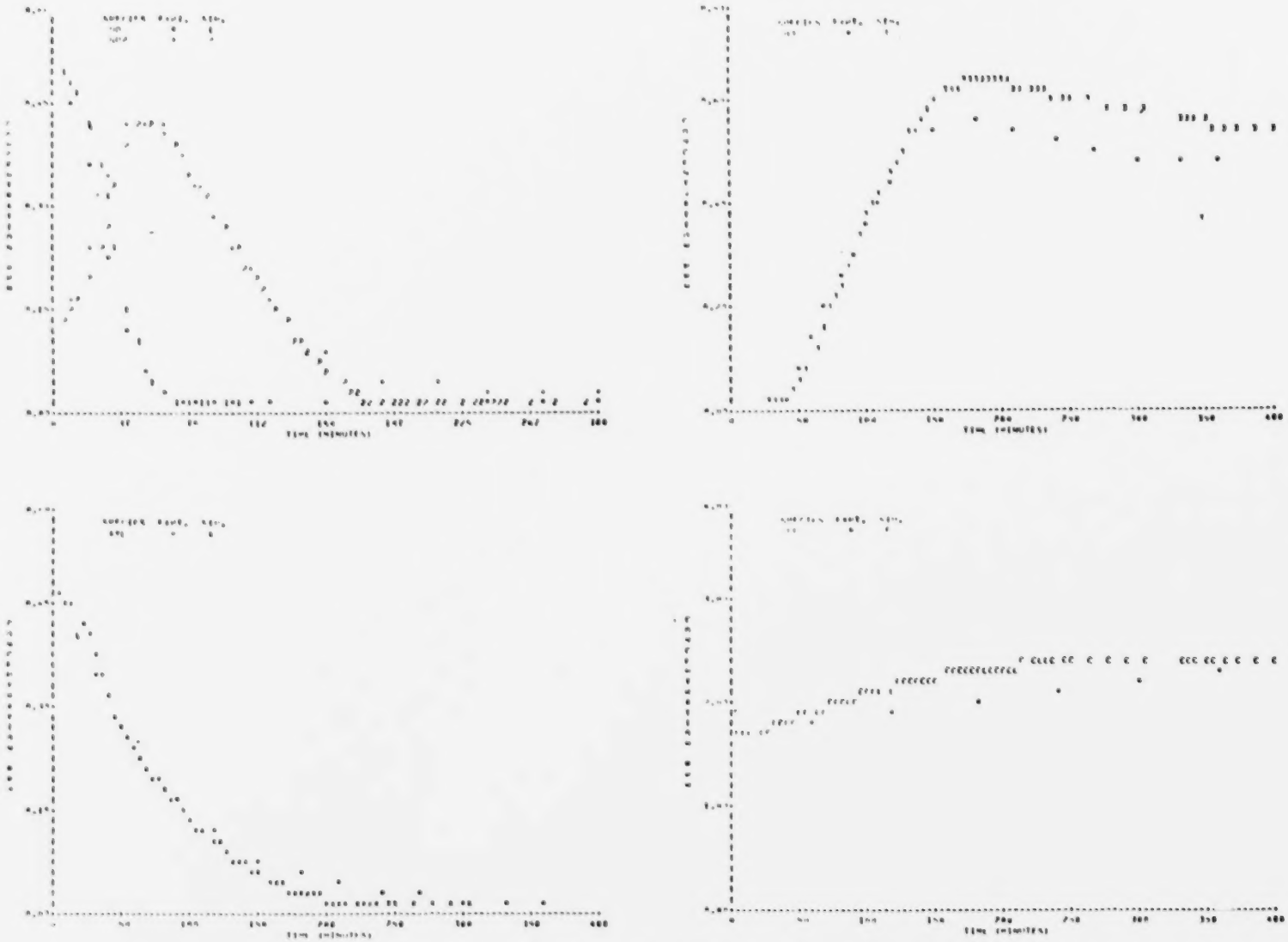

Figure 4. Simulation of SAPRC m-Xylene Run EC-344.

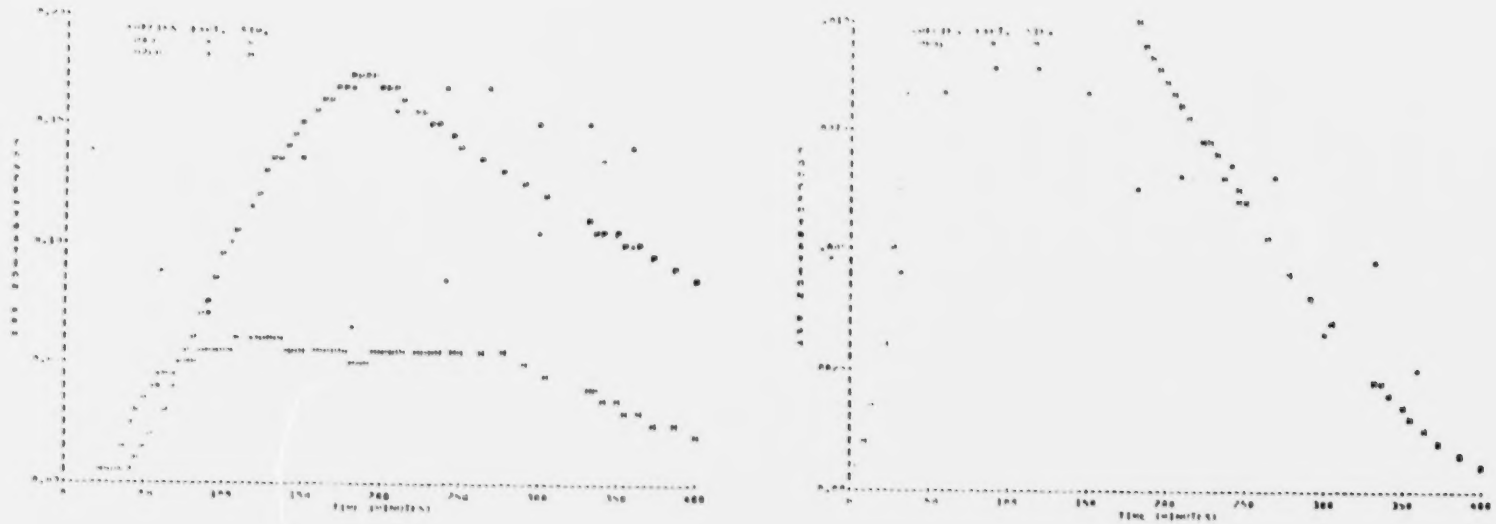

Figure 4. Simulation of SAPRC m-Xylene Run EC-344 (concluded).

All the simulated and observed concentration profiles agree very well. The experimental ozone for run EC-343 does not agree with parallel runs EC-345 and EC-346, and this is reflected in the simulated values. The model greatly overpredicts the PAN decay after the maxima. This effect appears to be due to overpredicting the peroxy radical-radical interactions, which in turn, may be due to errors in the computed NO and NO_2 values.

The success in applying the toluene mechanism to the xylene reaction, with only the changes indicated, confirms the general nature of the toluene and xylene mechanism. The basic assumption that cleavage of the aromatic ring does occur to give α-dicarbonyl forces one to expect more methylglyoxal instead of glyoxal in the xylene experiments than in the toluene experiments. Since methylglyoxal is a radical source and glyoxal is not, m-xylene is expected to be more reactive in oxidizing NO than toluene, not only because of the larger OH rate constant, but also because of the larger radical input from the increased amount of methylglyoxal. This dual effect is apparent in the modeling results.

SECTION 5

ALKENES

MECHANISM

In our previous report we modeled data reported by SAPRC for the hydrocarbons propene, ethene, 1-butene, and trans-2-butene. In this report the mechanisms have been slightly updated and the temperature dependence of reactions having a significant activation energy has been included. Using the revised mechanisms we have modeled SAPRC data for propene and ethene, including one propene run at higher and one run at lower than the standard (300 K) temperature. We also modeled UNC data for ethene and propene, using the temperature-dependent mechanism to simulate the experimentally observed temperature changes.

The complete mechanisms for ethene and propene are given in Tables 12 and 13, respectively. The only significant changes from our previously reported mechanisms are as follows:

- The ozone-alkene mechanism has been modified to be consistent with the experimental results of Herron and Huie.[12] They found that the ozonolysis of ethene formed formaldehyde and Criegee biradical, which decomposed to give 20% radical products. Thus we represent this reaction as:

$$CH_2{=}CH_2 + O_3 \longrightarrow CH_2O + 0.2HO_2\bullet$$

Similarly for propene:

$$CH_3CH{=}CH_2 + O_3 \longrightarrow 0.5CH_2O + 0.5CH_3CHO + 0.2HO_2\bullet$$

Although in this case the production of radicals may be higher,[49] this mechanism assumes that the two possible Criegee biradicals formed in the propene case are equally likely to be formed and

that the two carbon biradical decomposes to radical products in the same ratio as the one carbon biradical.

- The temperature dependence of the critical rate constants have been added. This includes the decomposition of peroxyacyl nitrates[50] and peroxyalkyl nitrates,[51] the reactions of alkoxy radical,[52] and the reactions of $O(^3P)$, OH, and O_3 (Table 8).

In accordance with the experimental results of Niki et al.,[54] the OH-substituted alkoxy radicals formed by OH addition to propene and ethene are assumed to decompose faster than they react with oxygen. Earlier, based on thermochemical estimates[1,8,52] we assumed that for the ethene case the reaction with oxygen was nearly identical with decomposition. The reason for this inconsistency is an unresolved question at present. Thus the reactions of the OH-substituted alkoxy radicals may be more complex than the present mechanism indicates.

SAPRC DATA SET

Simulations are presented for 13 propene and 6 ethene chamber runs performed at the SAPRC facility (see Appendix B); typical propene and ethene results are shown in Figures 5 and 6. Initial conditions are given for the propene runs in Table 14, and O_3 and NO_2 maxima and time to each maxima are given in Table 15. Similar data for the ethene results are given in Tables 16 and 17. In all the simulations a standard heterogeneous input of 2×10^{-4} ppm min^{-1} of HO_2 radicals is used, although input of OH at the same level gives the same results in cases tested. In general the simulations reproduce the experimental results with reasonable accuracy. The only discernible systematic trend is that the maximum ozone concentration is overpredicted 31(±18) % on the average for propene and 23(±21)% for ethene.

Two propene experiments were reported at other than the standard temperature. The increase in the reactivity observed at higher temperature (312 K, EC-316) is well simulated by the homogeneous mechanism. The run at lower than standard temperature (289.5 K, EC-215) shows a much decreased reactivity, which is not predicted by the model. It is difficult to draw meaningful conclusions based on one experiment, but the

TABLE 12 PROPENE MECHANISM

No.		A Factor[a]	Activation Energy K
1	$CH_2{=}CHCH_3 + OH \xrightarrow{O_2} HOCH_2CH_2(\dot{O}_2)CH_3$	6.00×10^{3}	-5.40×10^{2}
2	$CH_2{=}CHCH_3 + O(^3P) \rightarrow CH_3CH_2CHO$	1.8×10^{3}	
3	$CH_2{=}CHCH_3 + O(^3P) \rightarrow CH_3\dot{O}_2 + CH_3C(O)\dot{O}_2$	1.8×10^{3}	
4	$CH_2{=}CHCH_3 + O(^3P) \rightarrow CH_3CH_2\dot{O}_2 + HO_2$	1.8×10^{3}	
5	$CH_2{=}CHCH_3 + O_3 \rightarrow CH_3CHO + CO$ $\rightarrow CH_3CHO + HO_2\cdot$	9.0×10^{-3} 1.5×10^{-2}	
6	$CH_2{=}CHCH_3 + O_3 \rightarrow CH_2O + CO$ $\rightarrow CH_2O + HO_2\cdot$	6.0×10^{-3} 1.5×10^{-2}	
7	$CH_2{=}CHCH_3 + NO_3 \rightarrow CH_3CH_2CHO + NO_2$	7.8	
8	$HOCH_2CH(\dot{O}_2)CH_3 + NO \rightarrow HOCH_2CH(\dot{O})CH_3 + NO_2$	1.0×10^{4}	
9	$CH_3CH_2\dot{O}_2 + NO \rightarrow CH_3CH_2\dot{O} + NO_2$	1.0×10^{4}	
10	$CH_3\dot{O}_2 + NO \rightarrow CH_3\dot{O} + NO_2$	1.0×10^{4}	
11	$CH_3C(O)\dot{O}_2 + NO \rightarrow CH_3\dot{O}_2 + NO_2 + CO_2$	5.4×10^{3}	
12	$CH_3CH_2C(O)\dot{O}_2 + NO \rightarrow CH_3CH_2\dot{O}_2 + NO_2 + CO_2$	5.4×10^{3}	
13	$CH_2(OH)\dot{O}_2 + NO \rightarrow CH_2(OH)\dot{O} + NO_2$	1.0×10^{4}	
14	$HOCH_2CH(\dot{O})CH_3 \xrightarrow{O_2} CH_3CHO + \dot{C}H_2OH$	$^{*}3.00 \times 10^{14}$	7.76×10^{3}
15	$HOCH_2CH(\dot{O})CH_3 + O_2 \rightarrow HOCH_2C(O)CH_3 + HO_2$	$^{*}6.7 \times 10^{4}$	
16	$CH_3CH_2\dot{O} + O_2 \rightarrow CH_3CHO + HO_2$	$^{*}2.0 \times 10^{3}$	
17	$CH_3\dot{O} + O_2 \rightarrow CH_2O + HO_2$	$^{*}2.0 \times 10^{3}$	
18	$\dot{C}H_2OH + O_2 \rightarrow CH_2(OH)\dot{O}_2$	$^{*}1.2 \times 10^{4}$	
19	$\dot{C}H_2OH + O_2 \rightarrow CH_2O + HO_2$	$^{*}1.2 \times 10^{3}$	
20	$CH_2(OH)\dot{O} + O_2 \rightarrow HC(O)OH + HO_2$	$^{*}1.4 \times 10^{3}$	
21	$CH_3CH_2CHO + h\nu \rightarrow CH_3CH_2\dot{O}_2 + CO_2 + HO_2$		
22	$CH_3CHO + h\nu \rightarrow CH_3\dot{O}_2 + CO_2 + HO_2$		
23	$CH_2O + h\nu \rightarrow CO + H_2$		
24	$CH_2O + h\nu \rightarrow CO + HO_2 + HO_2$		
25	$HOCH_2C(O)CH_3 + h\nu \rightarrow CH_3C(O)\dot{O}_2 + \dot{C}H_2OH$		
26	$CH_3CH_2CHO + OH \xrightarrow{O_2} CH_3CH_2C(O)\dot{O}_2 + H_2O$	2.0×10^{4}	
27	$CH_3CHO + OH \xrightarrow{O_2} CH_3C(O)\dot{O}_2 + H_2O$	2.0×10^{4}	
28	$CH_2O + OH \xrightarrow{O_2} HO_2 + CO$	2.0×10^{4}	
29	$HO_2 + NO_2 \rightarrow HO_2NO_2$	2.0×10^{3}	
30	$HO_2NO_2 \rightarrow HO_2 + NO_2$	$^{*}7.80 \times 10^{15}$	1.04×10^{4}
31	$CH_2(OH)\dot{O}_2 + NO_2 \rightarrow CH_2(OH)O_2NO_2$	7.8×10^{3}	
32	$CH_2(OH)O_2NO_2 \rightarrow CH_2(OH)\dot{O}_2 + NO_2$	$^{*}1.60 \times 10^{16}$	1.16×10^{4}
33	$CH_2(OH)CH(\dot{O}_2)CH_3 + NO_2 \rightarrow CH_2(OH)CH(O_2NO_2)CH_3$	7.8×10^{3}	
34	$CH_2(OH)CH(O_2NO_2)CH_3 \rightarrow CH_2(OH)CH(\dot{O}_2)CH_3 + NO_2$	$^{*}1.60 \times 10^{16}$	1.16×10^{4}
35	$CH_3C(O)O_2 + NO_2 \rightarrow CH_3C(\dot{O})O_2NO_2$	1.5×10^{3}	
36	$CH_3C(O)O_2NO_2 \rightarrow CH_3C(O)\dot{O}_2 + NO_2$	$^{*}1.02 \times 10^{16}$	1.35×10^{4}

continued....

Propene Mechanism (concluded)

37	$CH_3CH_2C(O)\dot{O}_2 + NO_2 \rightarrow$	$CH_3CH_2C(O)O_2NO_2$	1.5×10^3	
38	$CH_3CH_2C(O)O_2NO_2 \rightarrow$	$CH_3CH_2C(O)\dot{O}_2 + NO_2$	$^*1.02 \times 10^{16}$	1.35×10^{-4}
39	$CH_3\dot{O} + NO_2 \rightarrow$	CH_3ONO_2	2.0×10^4	
40	$CH_3\dot{O} + NO_2 \rightarrow$	$CH_2O + HNO_2$	2.2×10^3	
41	$CH_3CH_2\dot{O} + NO_2 \rightarrow$	$CH_3CH_2ONO_2$	2.0×10^4	
42	$CH_3CH_2\dot{O} + NO_2 \rightarrow$	$CH_3CHO + HNO_2$	2.2×10^3	
43	$CH_3(OH)CH(\dot{O})CH_3 + NO_2 \rightarrow$	$CH_3(OH)CH(ONO_2)CH_3$	2.0×10^4	
44	$CH_3(OH)CH(\dot{O})CH_3 + NO_2 \rightarrow$	$CH_3(OH)C(O)CH_3 + HNO_2$	2.2×10^3	
45	$CH_3\dot{O}_2 + NO_2 \rightarrow$	$CH_3O_2NO_2$	7.8×10^3	
46	$CH_3O_2NO_2 \rightarrow$	$CH_3\dot{O}_2 + NO_2$	$^*1.60 \times 10^{16}$	1.16×10^{-4}
47	$CH_3CH_2C(O)\dot{O}_2 + HO_2 \rightarrow$	$CH_3CH_2C(O)OOH$	4.0×10^3	
48	$CH_3C(O)\dot{O}_2 + HO_2 \rightarrow$	$CH_3C(O)OOH$	4.0×10^3	
49	$CH_2(OH)\dot{O}_2 + HO_2 \rightarrow$	$CH_2(OH)OOH$	4.0×10^3	
50	$CH_2(OH)CH_2CH_2\dot{O}_2 + HO_2 \rightarrow$	$CH_2(OH)CH_2CH_2OOH$	2.0×10^3	
51	$CH_3CH_2\dot{O}_2 + HO_2 \rightarrow$	CH_3CH_2OOH	2.0×10^3	
52	$CH_3C(O)\dot{O}_2 + CH_3C(O)\dot{O}_2 \rightarrow$	$CH_3\dot{O}_2 + CH_3\dot{O}_2 + 2CO_2$	2.4×10^3	
53	$CH_2(OH)CH_2CH_2\dot{O}_2 + CH_2(OH)CH_2CH_2\dot{O}_2 \rightarrow$	$CH_2(OH)CH_2CH_2\dot{O} + CH_2(OH)CH_2CH_2\dot{O} + O_2$	2.5×10^2	

[a] Units $ppm^{-1}\ min^{-1}$ except * min^{-1} .

TABLE 13 ETHENE MECHANISM

No.		A Factor[a]	Activation Energy K
1	$CH_2CH_2 + OH \xrightarrow{O_2} HOCH_2CH_2O_2$	3.26×10^3	-3.85×10^2
2	$CH_2CH_2 + O(^3P) \rightarrow CH_3CHO$	1.07×10^3	5.65×10^2
3	$CH_2CH_2 + O(^3P) \rightarrow CH_3O_2 + HO_2 + CO$	4.07×10^3	5.65×10^2
4	$CH_2CH_2 + NO_3 \rightarrow CH_3CHO + NO_3$	1.4	
5	$CH_2CH_2 + O_3 \rightarrow CH_2O + HO_2$ $\rightarrow CH_2O + CO$	2.66 1.06×10^1	2.56×10^3 2.56×10^3
6	$HOCH_2CH_2O_2 + NO \rightarrow HOCH_2CH_2O + NO_2$	1.0×10^4	
7	$CH_3O_2 + NO \rightarrow CH_3O + NO_2$	1.0×10^4	
8	$CH_3C(O)O_2 + NO \rightarrow CH_3O_2 + NO_2 + CO_2$	5.4×10^3	
9	$HOCH_2CH_2O + O_2 \rightarrow HOCH_2CHO + HO_2$	$^*1.0 \times 10^3$	
10	$CH_3O + O_2 \rightarrow CH_2O + HO_2$	$^*2.0 \times 10^3$	
11	$CH_2O + h\nu \xrightarrow{O_2} HO_2 + HO_2 + CO$		
12	$CH_2O + h\nu \rightarrow CO + H_2$		
13	$CH_3CHO + h\nu \xrightarrow{O_2} CH_3O_2 + CO + HO_2$		
14	$CH_2O + OH \xrightarrow{O_2} CO + HO_2 + H_2O$	2.0×10^4	
15	$CH_3CHO + OH \xrightarrow{O_2} CH_3C(O)O_2 + H_2O$	2.0×10^4	
16	$HOCH_2CHO + OH \xrightarrow{O_2} CH_2O + HO_2 + CO$	2.0×10^4	
17	$CH_3O_2 + HO_2 \rightarrow CH_3OOH + O_2$	2.0×10^3	
18	$HOCH_2CH_2O_2 + HO_2 \rightarrow HOCH_2CH_2OOH + O_2$	2.0×10^3	
19	$CH_3C(O)O_2 + HO_2 \rightarrow CH_3C(O)OOH + O_2$	4.0×10^3	
20	$CH_3C(O)O_2 + NO_2 \rightarrow CH_3C(O)O_2NO_2$	1.5×10^3	
21	$CH_3C(O)O_2NO_2 \rightarrow CH_3C(O)O_2 + NO_2$	$^*1.02 \times 10^{16}$	1.35×10^4
22	$HO_2 + NO_2 \rightarrow HO_2NO_2$	2.0×10^3	
23	$HO_2NO_2 \rightarrow HO_2 + NO_2$	$^*7.80 \times 10^{15}$	1.04×10^4
24	$CH_3O_2 + NO_2 \rightarrow CH_3O_2NO_2$	7.8×10^3	
25	$CH_3O_2NO_2 \rightarrow CH_3O_2 + NO_2$	$^*1.60 \times 10^{16}$	1.16×10^4
26	$HOCH_2CH_2O_2 + NO_2 \rightarrow HOCH_2CH_2O_2NO_2$	7.8×10^3	
27	$HOCH_2CH_2O_2NO_2 \rightarrow HOCH_2CH_2O_2 + NO_2$	$^*1.60 \times 10^{16}$	1.16×10^4
28	$CH_3C(O)O_2 + CH_3C(O)O_2 \rightarrow CH_3O_2 + CH_3O_2 + 2CO_2 + O_2$	2.4×10^3	
29	$CH_3O_2 + CH_3O_2 \rightarrow CH_3O + CH_3O + O_2$	2.0×10^2	
30	$HOCH_2CH_2O_2 + HOCH_2CH_2O_2 \rightarrow HOCH_2CH_2O + HOCH_2CH_2O + O_2$	2.0×10^2	
31	$HOCH_2CH_2O \xrightarrow{O_2} CH_2O + CH_2OH$	$^*1.0 \times 10^5$	
32	$CH_2OH + O_2 \rightarrow CH_2O + HO_2$	$^*1.2 \times 10^3$	

[a] Units ppm^{-1} min^{-1} except * min^{-1}.

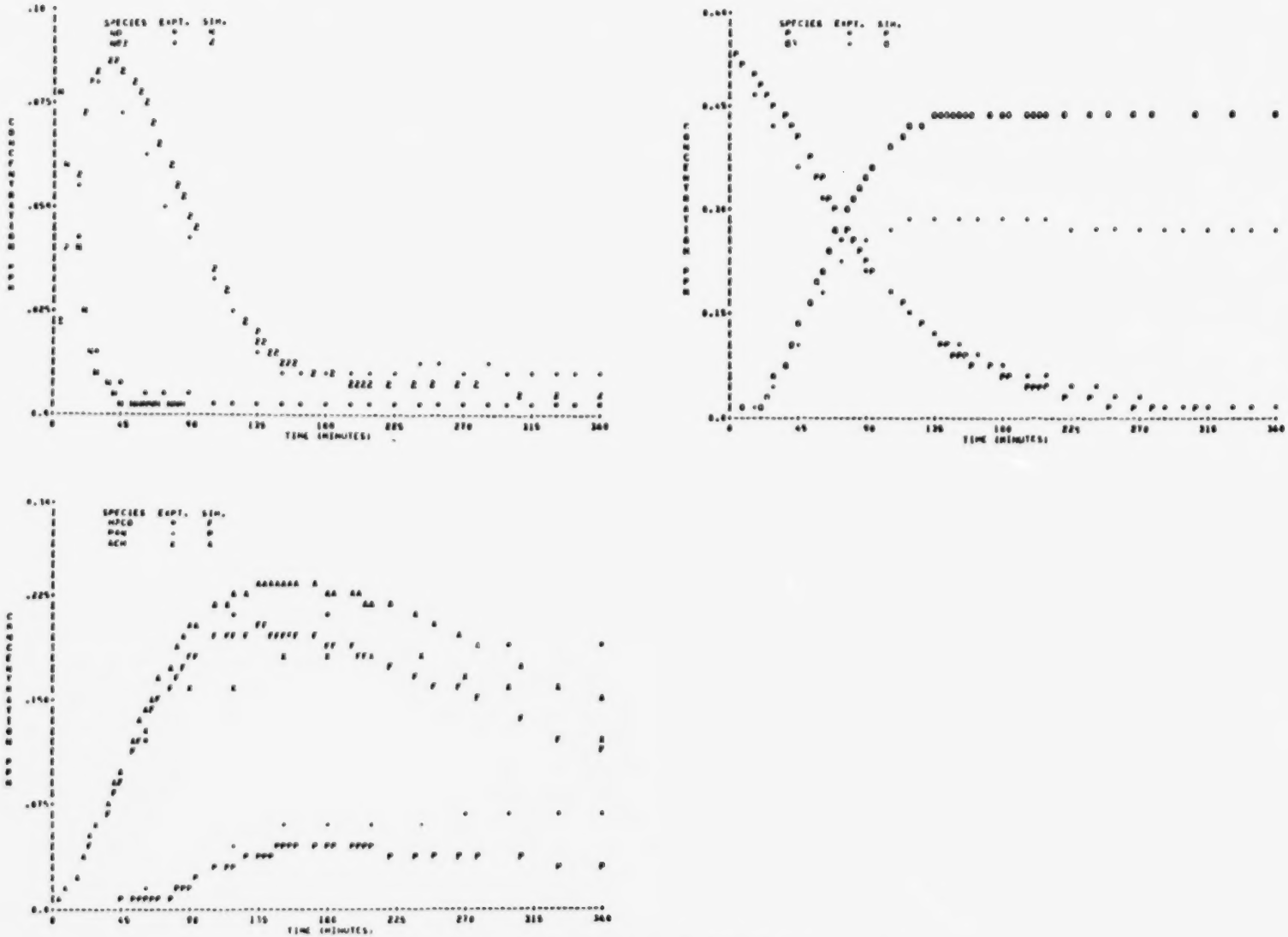

Figure 5. Simulation of SAPRC Propene Run.

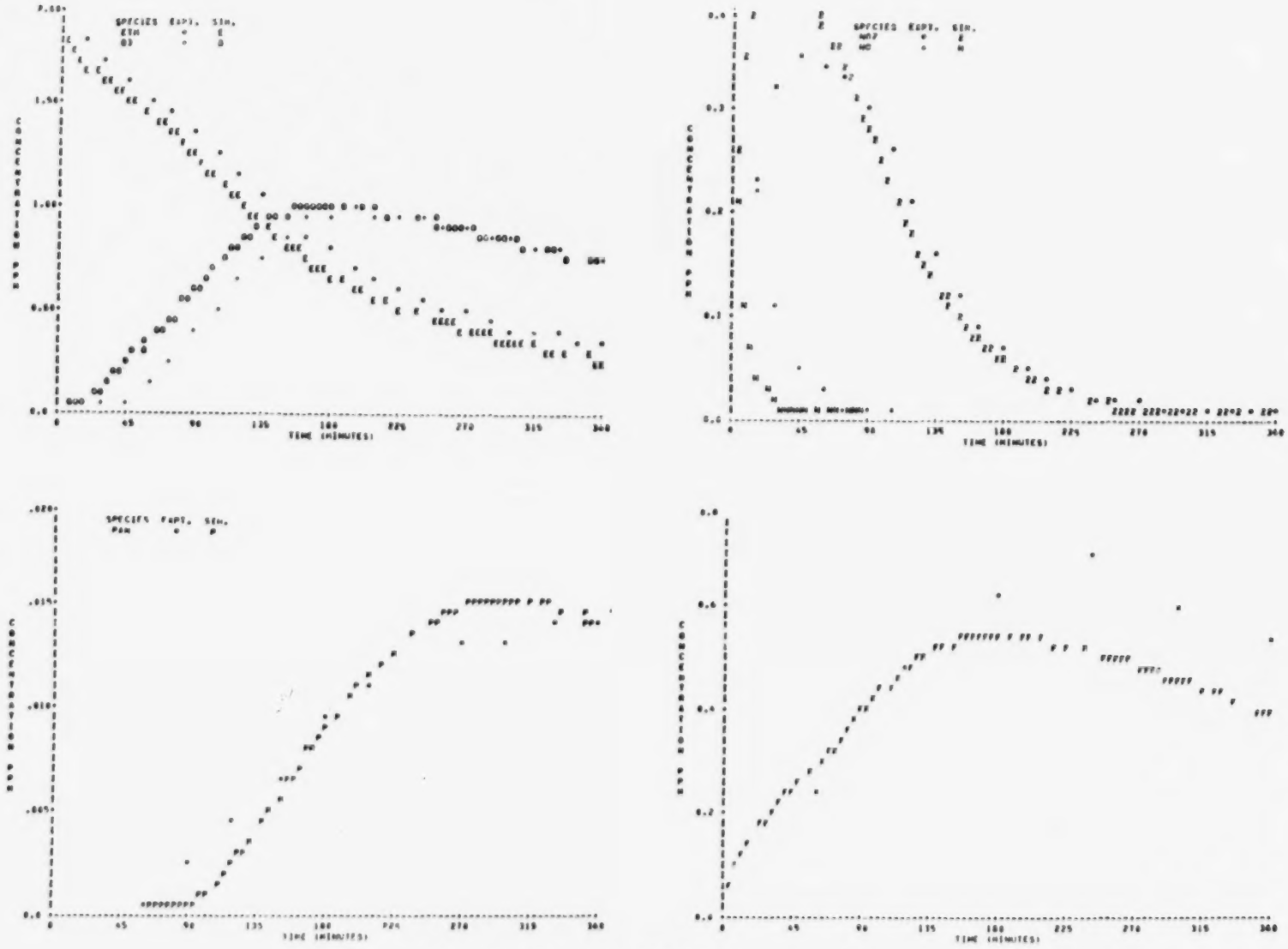

Figure 6. Simulation of SAPRC Ethene Run EC-156.

TABLE 14 SUMMARY OF INITIAL CONDITIONS FOR SMOG CHAMBER EXPERIMENTS FOR PROPENE[a]

No.	Propene	NO	NO_2	CH_2O	HONO	RH/NO_x	k_{NO_2}
256	0.11	0.520	0.044	0.042	0.000	0.19	0.30
257	0.112	0.530	0.032	0.371	0.000	0.86	0.30
276	0.54	0.410	0.106	0.016	0.000	1.06	0.35
277	0.56	0.098	0.010	0.005	0.000	5.22	0.35
278	1.02	0.366	0.128	0.017	0.000	2.04	0.35
279	1.14	0.730	0.244	0.017	0.000	1.17	0.35
314	1.08	0.684	0.246	0.000	0.000	1.16	0.55
315	0.97[c]	0.664	0.276	0.000	0.000	1.03	0.55
316	1.07[d]	0.735	0.246	0.000	0.000	1.09	0.55
317	0.49[e]	0.236	0.281	0.000	0.000	0.93	0.55
318	0.51[f]	0.172	0.331	0.000	0.000	1.02	0.55
319	0.50[g]	0.100	0.430	0.000	0.000	0.95	0.55
320	0.54	0.222	0.290	0.000	0.000	1.05	0.55
12.26.77R	0.99	0.28	0.12	0.000	0.020	2.48	- -
1.10.78R	1.08	0.32	0.14	0.000	0.020	2.35	- -
2.27.78R	1.32	0.37	0.12	0.000	0.005	2.69	- -
3.06.78R	1.26	0.39	0.12	0.000	0.000	2.47	- -
3.31.78R	1.27	0.39	0.091	0.000	0.004	3.09	- -
6.16.78B	0.67	0.42	0.21	0.000	0.001	1.06	- -
7.01.78B	0.51	0.61	0.32	0.000	0.015	0.55	- -
7.24.78R	0.99	0.78	0.18	0.000	0.020	1.03	- -
7.24.78B	0.49	0.80	0.17	0.000	0.020	0.51	- -
7.30.78B	0.42	0.40	0.084	0.000	0.010	0.88	- -
8.05.78R	0.28	0.21	0.052	0.000	0.030	1.07	- -
8.05.78B	0.51	0.43	0.145	0.000	0.030	0.89	- -
8.06.78R	0.56	0.43	0.121	0.000	0.030	1.02	- -
8.15.78R	0.48	0.43	0.109	0.000	0.030	0.89	- -
8.16.78R	0.52	0.62	0.070	0.000	0.020	0.75	- -
10.03.78B	0.45	0.35	0.14	0.000	0.010	0.92	- -
10.12.78B	0.44	0.36	0.12	0.000	0.010	0.92	- -

[a] Units in ppm.
[b] Units in min
[c] Temperature, 289.5 K.
[d] Temperature, 312.0 K.
[e] Initial PAN, 0.072 ppm.
[f] Initial PAN, 0.149 ppm.
[g] Initial PAN, 0.036 ppm.

TABLE 15 COMPARISON OF EXPERIMENTAL AND SIMULATION RESULTS FOR PROPENE CHAMBER EXPERIMENTS

No.	EXPERIMENTAL				SIMULATION			
	O_3-max		NO_2-max		O_3-max		NO_2-max	
	ppm	min	ppm	min	ppm	min	ppm	min
256	0.020	> 360	0.21	> 360	0.007	> 360	0.19	> 360
257	0.066	> 360	0.30	195	0.066	> 360	0.32	240
276	0.37	> 360	0.37	135	0.67	> 360	0.39	120
277	0.31	135	0.085	30	0.46	180	0.088	45
278	0.63	195	0.39	60	0.79	240	0.40	90
279	0.68	> 360	0.71	105	0.89	> 360	0.76	120
314	0.73	> 360	0.67	90	1.10	> 360	0.69	120
315	0.34	> 360	0.61	135	0.53	> 360	0.65	160
316	0.95	> 360	0.72	75	1.40	> 360	0.74	120
317	0.61	> 360	0.40	75	0.60	> 360	0.38	140
318	0.68	> 360	0.42	45	1.00	> 360	0.40	45
319	0.76	255	0.46	30	1.11	> 360	0.45	30
320	0.64	330	0.40	60	0.95	> 360	0.41	60
12.26.77R	0.38	700	0.31	525	0.23	720	0.27	480
1.10.78R	0.36	700	0.37	480	0.19	720	0.27	600
2.27.78R	0.59	570	0.38	540	0.88	720	0.33	480
3.06.78R	0.65	540	0.44	420	0.90	> 720	0.34	420
3.31.78R	0.82	480	0.42	370	1.17	> 720	0.36	420
6.16.78R	1.02	> 720	0.49	420	1.11	> 720	0.48	480
7.01.78B	0.56	820	0.68	470	0.77	> 840	0.70	480
7.24.78R	1.20	680	0.81	370	1.47	720	0.76	420
7.24.78B	0.29	> 720	0.66	540	0.60	> 720	0.73	520
7.30.78B	0.78	> 720	0.37	450	0.92	> 720	0.36	420
8.05.78R	0.62	720	0.25	300	0.61	720	0.23	360
8.05.78B	0.77	700	0.48	350	0.87	720	0.45	400
8.06.78R	0.50	> 600	0.51	280	0.63	> 720	0.46	400
8.15.78R	0.91	> 650	0.47	360	1.00	> 720	0.43	360
8.16.78R	0.73	> 720	0.53	450	0.87	> 720	0.53	420
10.03.78B	0.41	700	0.38	520	0.49	> 720	0.37	480
10.12.78B	0.46	> 720	0.37	510	0.39	> 720	0.35	540

TABLE 16 SUMMARY OF INITIAL CONDITIONS FOR SMOG CHAMBER EXPERIMENT FOR ETHENE

No.	Ethene	NO	NO_2	HONO	RH/NO_x	k_{NO_2}
142	0.95	0.32	0.16	0.050	1.98	0.33
143	2.03	0.39	0.11	0.050	4.06	0.33
156	1.99	0.38	0.12	0.050	3.98	0.33
285	1.95	0.79	0.22	0.000	1.93	0.39
286	3.76	0.71	0.24	0.000	3.96	0.39
287	4.00	0.40	0.12	0.000	7.69	0.39
6.16.78R	1.98	0.42	0.21	0.004	3.14	
8.21.78R	0.695	0.80	0.18	0.000	0.71	- -
9.19.78R	0.940	0.57	0.12	0.003	1.36	- -
10.17.78B	1.37	0.37	0.12	0.010	2.79	- -
10.18.78R	1.56	0.34	0.11	0.000	3.47	- -
11.19.78R	1.89	0.42	0.034	0.006	4.20	- -
11.20.78R	2.20	0.42	0.030	0.010	4.89	- -

Units in ppm.

TABLE 17 COMPARISON OF EXPERIMENTAL AND SIMULATION RESULTS FOR ETHENE CHAMBER EXPERIMENTS

No.	EXPERIMENTAL				SIMULATION			
	O_3-max		NO_2-max		O_3-max		NO_2-max	
	ppm	min	ppm	min	ppm	min	ppm	min
142	> 0.78	> 360	0.30	105	1.15	> 360	0.38	60
143	1.09	210	0.38	60	1.08	180	0.45	25
156	1.05	195	.36	45	1.08	180	0.44	25
285	> 0.84	> 360	0.71	160	> 1.00	> 360	0.71	190
286	1.08	180	0.76	70	1.50	200	0.75	100
287	0.96	135	0.45	45	1.30	140	.45	45
8.16.78R	1.10	480	0.48	320	2.04	660	0.52	420
8.21.78R	0.012	> 720	0.37	670	0.024	720	0.54	720
9.19.78R	1.03	700	0.51	430	0.61	720	0.47	600
10.17.78B	0.44	> 600	0.39	480	1.38	720	0.36	420
10.18.78R	0.71	690	0.31	500	1.14	720	0.35	540
11.19.78R	0.79	630	0.43	460	1.23	720	0.39	550
11.20.78R	0.75	630	0.42	480	1.32	720	0.41	480

large magnitude of the change for only a ten-degree change in temperature suggests a nonhomogeneous effect.

UNC DATA SET

UNC has reported data for propene and ethene. The results are also shown in Appendix B, typical runs are shown in Figures 7 and 8. Starting conditions are given in Table 14, and the O_3 and NO_2 maxima and times to maxima given in Table 15. The results are, in general, good; no systematic discrepancies between computed and experimental data are apparent except for the ozone. The computed ozone values average 18(± 35)% for the propene runs and 78(± 80)% for ethene. Note that the apparent discrepancy for NO_2 rate in some runs is due to the experimental measurement including PAN as NO_2. Substraction of the computed PAN concentration produces good agreement in all cases. A small initial amount of nitrous acid was assumed in the simulations to achieve the correct overall rate of reaction. The amounts are also given in Table 14.

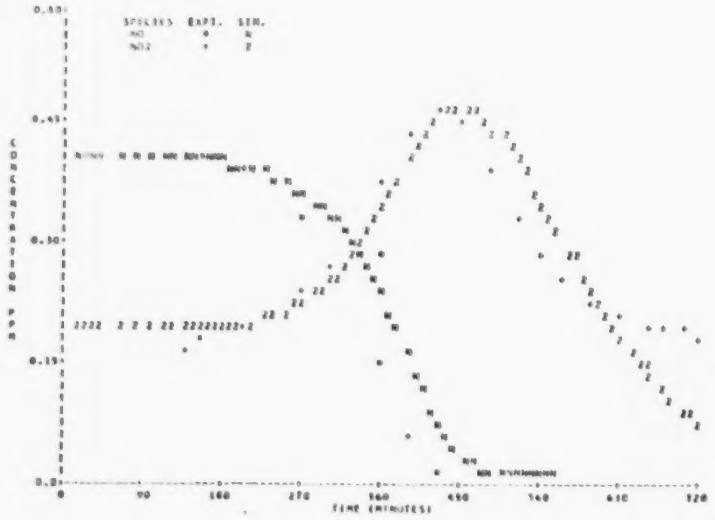

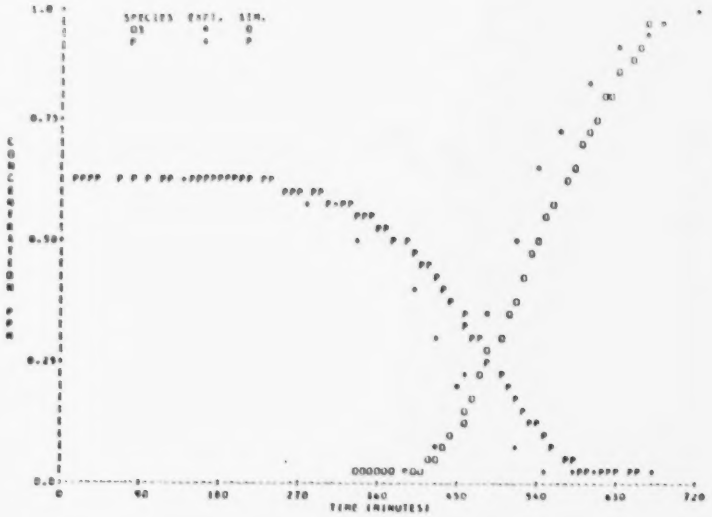

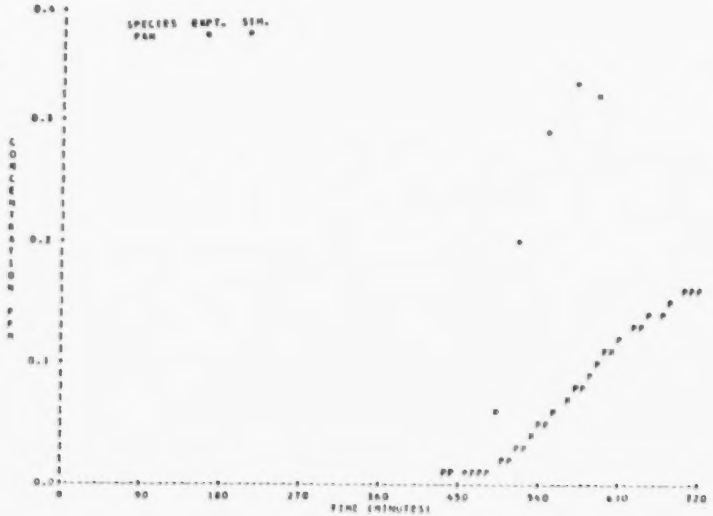

Figure 7. Simulation of UNC Propene Run 6.16.78 Blue.

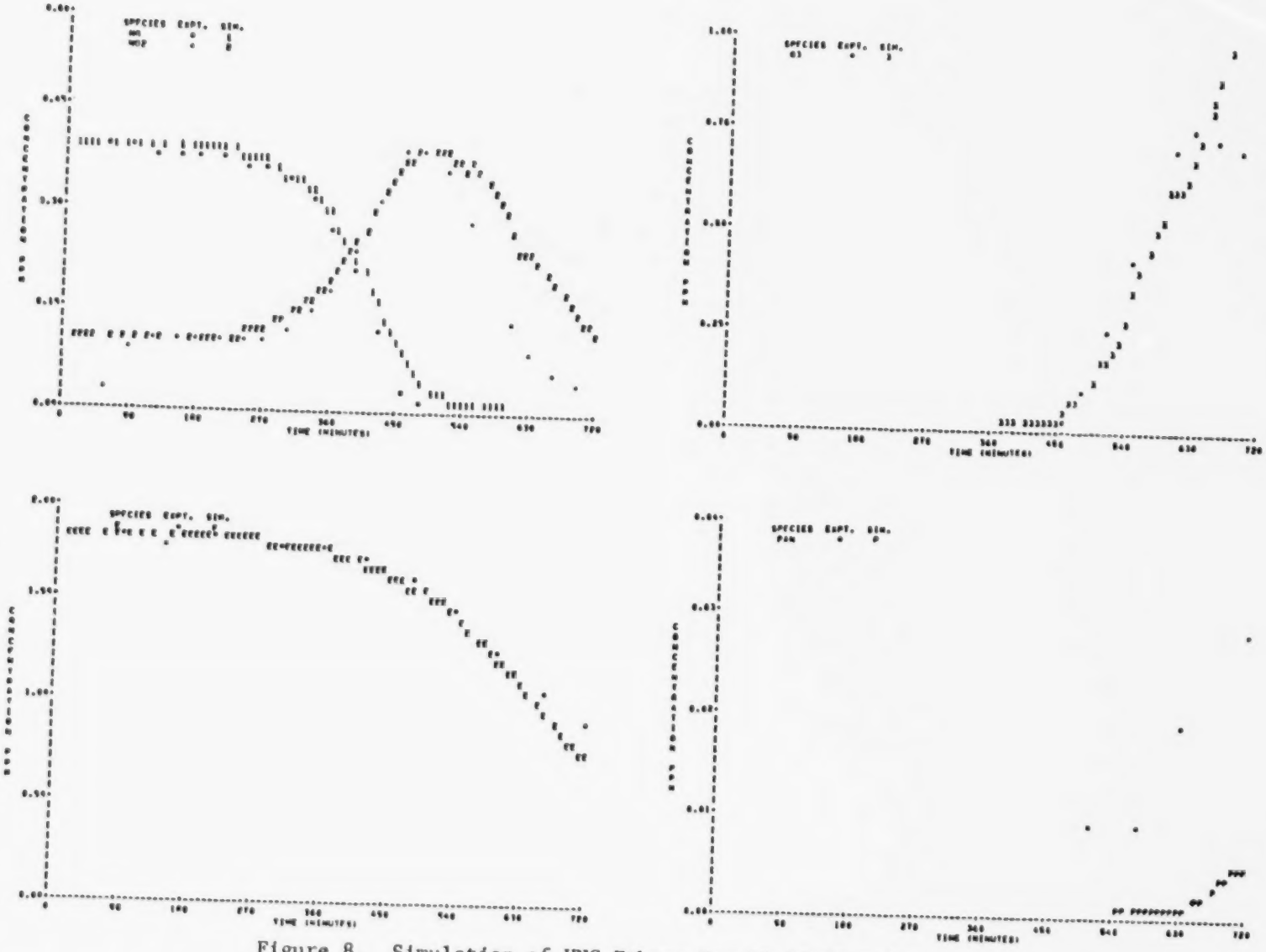

Figure 8. Simulation of UNC Ethene Run 11.19.78 Red.

SECTION 6

ALKANES

MECHANISM

Both SAPRC and UNC have reported data on butane-NO_x systems. The butane mechanism is given in Table 18. The major change from our previous report,[1] besides addition of the activation energy terms, is the reduction of reaction (16) in the table. This change improves the simulation of the butanone data as well as the agreement of the rate constant with values for similar reactions.

SAPRC DATA SET

The results for six SAPRC butane chamber runs are shown in Appendix C. Initial conditions are given in Table 19, and the NO_2 and O_3 maxima and the time to these maxima are given in Table 20. A typical result is shown in Figure 9. In all the simulations a standard heterogeneous radical input of 2×10^{-4} ppm min^{-1} of HO_2 radicals is assumed. In general there is good agreement between the computed and experimental results. In common with the propene set, there is a systematic tendency to overpredict ozone.

The results for the two nonstandard temperature runs (EC-308, 288.5 K; EC-309, 311.5 K) are similar to the results for the propene experiments. The increased reactivity at higher temperatures is adequately simulated, whereas the decrease in reactivity at low temperature is not, probably because of heterogeneous effects.

In summary these results are similar to the bulk of our previous work in the SAPRC butane-NO_x data set.

TABLE 18 n-BUTANE MECHANISM

No.		A Factor	Activation Energy
1	$CH_3CH_2CH_2CH_3 + OH \xrightarrow{O_2} CH_3CH_2CH_2CH_3\dot{O}_2 + H_2O$	8.87×10^3	8.20×10^2
2	$CH_3CH_2CH_2CH_3 + OH \xrightarrow{O_2} CH_3CH_2CH(\dot{O}_2)CH_3 + H_2O$	1.36×10^4	4.30×10^2
3	$CH_3CH_2CH_2CH_3 + O(^3P) \xrightarrow{O_2} CH_3CH_2CH_2CH_3\dot{O}_2 + OH$	6.4×10^1	
4	$CH_3CH_2CH_2CH_3\dot{O}_2 + NO \rightarrow CH_3CH_2CH_2CH_3\dot{O} + NO_2$	1.0×10^4	
5	$CH_3CH_2CH(\dot{O}_2)CH_3 + NO \rightarrow CH_3CH_2CH(\dot{O})CH_3 + NO_2$	1.0×10^4	
6	$CH_3CH_2CH_2C(O)\dot{O}_2 + NO \xrightarrow{O_2} CH_3CH_2\dot{O}_2 + NO_2 + CO_2$	5.4×10^3	
7	$CH_3CH_2C(O)\dot{O}_2 + NO \xrightarrow{O_2} CH_3CH_2\dot{O}_2 + NO_2 + CO_2$	5.4×10^3	
8	$CH_3C(O)\dot{O}_2 + NO \xrightarrow{O_2} CH_3\dot{O}_2 + NO_2 + CO_2$	5.4×10^3	
9	$CH_3CH_2(\dot{O}_2)C(O)CH_3 + NO \xrightarrow{O_2} NO_2 + HO_2 + CH_3C(O)C(O)CH_3$	5.4×10^3	
10	$HOCH_2CH_2CH_2CH_2\dot{O}_2 + NO \rightarrow HOCH_2CH_2CH_2CH_2\dot{O} + NO_2$	1.0×10^4	
11	$CH_3CH_2CH_2\dot{O}_2 + NO \rightarrow CH_3CH_2CH_2\dot{O} + NO_2$	1.0×10^4	
12	$CH_3CH_2\dot{O}_2 + NO \rightarrow CH_3CH_2\dot{O} + NO_2$	1.0×10^4	
13	$CH_3\dot{O}_2 + NO \rightarrow CH_3\dot{O} + NO$	1.0×10^4	
14	$CH_3CH_2CH(\dot{O})CH_3 \xrightarrow{O_2} CH_3CH_2\dot{O}_2 + CH_3CHO$	* 1.05×10^{14}	7.35×10^3
15	$CH_3CH_2CH_2CH_2\dot{O} \xrightarrow{O_2} CH_3(\dot{O}_2)CH_2CH_2CH_2OH$	* 1.51×10^{13}	3.87×10^3
16	$CH_3CH_2CH(\dot{O})CH_3 + O_2 \rightarrow CH_3CH_2CH(O)CH_3 + HO_2$	* 5.15×10^9	1.76×10^3
17	$CH_3CH_2CH_2CH_2\dot{O} + O_2 \rightarrow CH_3CH_2CH_2CHO + HO_2$	* 1.02×10^8	2.01×10^3
18	$CH_3CH_2CH_2\dot{O} + O_2 \rightarrow CH_3CH_2CHO + HO_2$	* 1.02×10^8	2.01×10^3
19	$CH_3CH_2\dot{O} + O_2 \rightarrow CH_3CHO + HO_2$	* 1.02×10^8	2.01×10^3
20	$CH_3\dot{O} + O_2 \rightarrow CH_2O + HO_2$	* 1.63×10^8	2.01×10^3
21	$CH_2O + h\nu \xrightarrow{2O_2} HO_2 + HO_2 + CO$		
22	$CH_2O + h\nu \rightarrow H_2 + CO$		
23	$CH_3CHO + h\nu \xrightarrow{2O_2} CH_3\dot{O}_2 + HO_2 + CO$		
24	$CH_3CH_2CHO + h\nu \xrightarrow{2O_2} CH_3CH_2\dot{O}_2 + HO_2 + CO$		
25	$CH_3CH_2CH_2CHO + h\nu \xrightarrow{2O_2} CH_3CH_2CH_2\dot{O}_2 + HO_2 + CO$		
26	$CH_3CH_2CH_2CHO + h\nu \rightarrow CH_3CHO + C_2H_4$		
27	$CH_3CH_2C(O)CH_3 + h\nu \xrightarrow{2O_2} CH_3C(O)\dot{O}_2 + CH_3CH_2\dot{O}_2$		
28	$CH_2O + OH \xrightarrow{O_2} CO + HO_2 + H_2O$	2.0×10^4	
29	$CH_3CHO + OH \xrightarrow{O_2} CH_3C(O)\dot{O}_2 + H_2O$	2.0×10^4	
30	$CH_3CH_2CHO + OH \xrightarrow{O_2} CH_3CH_2C(O)\dot{O}_2 + H_2O$	2.0×10^4	
31	$CH_3CH_2CH_2CHO + OH \xrightarrow{O_2} CH_3CH_2CH_2C(O)\dot{O}_2 + H_2O$	2.0×10^4	
32	$CH_3CH_2C(O)CH_3 + OH \xrightarrow{O_2} CH_3CH(\dot{O}_2)C(O)CH_3 + H_2O$	5.2×10^3	
33	$CH_3CH_2CH_2C(O)\dot{O}_2 + HO_2 \rightarrow CH_3CH_2CH_2C(O)OOH + O_2$	4.0×10^3	
34	$CH_3CH_2C(O)\dot{O}_2 + HO_2 \rightarrow CH_3CH_2C(O)OOH + O_2$	4.0×10^3	
35	$CH_3C(O)\dot{O}_2 + HO_2 \rightarrow CH_3C(O)OOH + O_2$	4.0×10^3	
36	$HOCH_2CH_2CH_2CH_2\dot{O}_2 + HO_2 \rightarrow HOCH_2CH_2CH_2CH_2OOH + O_2$	2.0×10^3	

Table 18. n-Butane Mechanism (continued)

37	$CH_3CH(\dot{O}_2)C(O)CH_3 + HO_2$	$\rightarrow CH_3CH(OOH)C(O)CH_3 + O_2$	2.0×10^{3}	
38	$CH_3CH_2CH(\dot{O}_2)CH_3 + HO_2$	$\rightarrow CH_3CH_2CH(CH_3)OOH + O_2$	2.0×10^{3}	
39	$CH_3CH_2CH_2CH_2\dot{O}_2 + HO_2$	$\rightarrow CH_3CH_2CH_2CH_2OOH + O_2$	2.0×10^{3}	
40	$CH_3CH_2CH_2\dot{O}_2 + HO_2$	$\rightarrow CH_3CH_2CH_2OOH + O_2$	2.0×10^{3}	
41	$CH_3CH_2\dot{O}_2 + HO_2$	$\rightarrow CH_3CH_2OOH + O_2$	2.0×10^{3}	
42	$CH_3\dot{O}_2 + HO_2$	$\rightarrow CH_3OOH + O_2$	2.0×10^{3}	
43	$CH_3CH_2CH_2C(O)\dot{O}_2 + NO_2$	$\rightarrow CH_3CH_2CH_2C(O)O_2NO_2$	1.5×10^{3}	
44	$CH_3CH_2C(O)\dot{O}_2 + NO_2$	$\rightarrow CH_3CH_2C(O)O_2NO_2$	1.5×10^{3}	
45	$CH_3C(O)\dot{O}_2 + NO_2$	$\rightarrow CH_3C(O)O_2NO_2$	1.5×10^{3}	
46	$CH_3CH_2CH_2C(O)O_2NO_2$	$\rightarrow CH_3CH_2CH_2C(O)\dot{O}_2 + NO_2$	$^{*}1.02 \times 10^{16}$	1.35×10^{-4}
47	$CH_3CH_2C(O)O_2NO_2$	$\rightarrow CH_3CH_2C(O)\dot{O}_2 + NO_2$	$^{*}1.02 \times 10^{16}$	1.35×10^{-4}
48	$CH_3C(O)O_2NO_2$	$\rightarrow CH_3C(O)\dot{O}_2 + NO_2$	$^{*}1.02 \times 10^{16}$	1.35×10^{-4}
49	$CH_3\dot{O} + NO_2$	$\rightarrow CH_3ONO_2$	1.5×10^{4}	
50	$CH_3\dot{O} + NO_2$	$\rightarrow CH_2O + HNO_2$	4.4×10^{3}	
51	$CH_3CH_2\dot{O} + NO_2$	$\rightarrow CH_3CH_2ONO_2$	1.5×10^{4}	
52	$CH_3CH_2\dot{O} + NO_2$	$\rightarrow CH_3CHO + HNO_2$	2.9×10^{3}	
53	$CH_3CH_2CH_2\dot{O} + NO_2$	$\rightarrow CH_3CH_2CH_2ONO_2$	1.5×10^{4}	
54	$CH_3CH_2CH_2\dot{O} + NO_2$	$\rightarrow CH_3CH_2CHO + HNO_2$	2.9×10^{3}	
55	$CH_3CH_2CH_2CH_2\dot{O} + NO_2$	$\rightarrow CH_3CH_2CH_2CH_2ONO_2$	1.5×10^{4}	
56	$CH_3CH_2CH_2CH_2\dot{O} + NO_2$	$\rightarrow CH_3CH_2CH_2CHO + HNO_2$	1.5×10^{3}	
57	$CH_3CH_2CH(\dot{O})CH_3 + NO_2$	$\rightarrow CH_3CH_2CH(ONO_2)CH_3$	1.5×10^{4}	
58	$CH_3CH_2CH(\dot{O})CH_3 + NO_2$	$\rightarrow CH_3CH_2C(O)CH_3 + HNO_2$	1.5×10^{4}	
59	$HO_2 + NO_2$	$\rightarrow HO_2NO_2$	2.0×10^{3}	
60	HO_2NO_2	$\rightarrow HO_2 + NO_2$	$^{*}7.80 \times 10^{15}$	1.04×10^{-4}
61	$CH_3\dot{O}_2 + NO_2$	$\rightarrow CH_3O_2NO_2$	7.8×10^{3}	
62	$CH_3O_2NO_2$	$\rightarrow CH_3\dot{O}_2 + NO_2$	$^{*}1.60 \times 10^{16}$	1.16×10^{-4}
63	$CH_3CH_2\dot{O}_2 + NO_2$	$\rightarrow CH_3CH_2O_2NO_2$	7.8×10^{3}	
64	$CH_3CH_2O_2NO_2$	$\rightarrow CH_3CH_2\dot{O}_2 + NO_2$	$^{*}1.60 \times 10^{16}$	1.16×10^{-4}
65	$CH_3CH_2CH_2\dot{O}_2 + NO_2$	$\rightarrow CH_3CH_2CH_2O_2NO_2$	7.8×10^{3}	
66	$CH_3CH_2CH_2O_2NO_2$	$\rightarrow CH_3CH_2CH_2\dot{O}_2 + NO_2$	$^{*}1.60 \times 10^{16}$	1.16×10^{-4}
67	$CH_3CH_2CH_2CH_2\dot{O}_2 + NO_2$	$\rightarrow CH_3CH_2CH_2CH_2O_2NO_2$	7.8×10^{3}	
68	$CH_3CH_2CH_2CH_2O_2NO_2$	$\rightarrow CH_3CH_2CH_2CH_2\dot{O}_2 + NO_2$	$^{*}1.60 \times 10^{16}$	1.16×10^{-4}
69	$CH_3CH_2CH(O_2)CH_3 + NO_2$	$\rightarrow CH_3CH_2CH(O_2NO_2)CH_3$	7.8×10^{3}	
70	$CH_3CH_2CH(O_2NO_2)CH_3$	$\rightarrow CH_3CH_2CH(\dot{O}_2)CH_3 + NO_2$	$^{*}1.6 \times 10^{16}$	1.16×10^{-4}
71	$CH_3CH_2CH(\dot{O}_2)CH_3 + CH_3CH_2CH(\dot{O}_2)CH_3$	$\rightarrow CH_3CH_2CH(\dot{O})CH_3 + CH_3CH_2CH(\dot{O})CH_3 + O_2$	2.0×10^{3}	
72	$CH_3CH_2CH_2CH_2\dot{O}_2 + CH_3CH_2CH_2CH_2\dot{O}_2$	$\rightarrow CH_3CH_2CH_2CH_2O + CH_3CH_2CH_2CH_2O + O_2$	2.0×10^{2}	

continued . . .

Table 18. n-Butane Mechanism (concluded)

73	$CH_3CH_2CH_2\dot{O}_2 + CH_3CH_2CH_2\dot{O}_2 \rightarrow CH_3CH_2CH_2\dot{O} + CH_3CH_2CH_2\dot{O} + O_2$		2.0×10^2	
74	$CH_3CH_2\dot{O}_2 + CH_3CH_2\dot{O}_2 \rightarrow CH_3CH_2\dot{O} + CH_3CH_2\dot{O} + O_2$		2.0×10^2	
75	$CH_3\dot{O}_2 + CH_3O_2 \rightarrow CH_3\dot{O} + CH_3\dot{O} + O_2$		2.0×10^2	
76	$CH_3C(O)\dot{O}_2 + CH_3C(O)\dot{O}_2 \rightarrow CH_3\dot{O}_2 + CH_3\dot{O}_2 + 2CO_2 + O_2$		2.4×10^3	
77	$CH_2(\dot{O})CH_2CH_2CH_2OH \xrightarrow{O_2} CH_2(OH)CH_2CH_2CH(OH)\dot{O}_2$		$^*9.51 \times 10^{12}$	3.27×10^3
78	$CH_2(OH)CH_2CH_2CH(OH)\dot{O}_2 + NO \rightarrow CH_2(OH)CH_2CH_2CH(OH)\dot{O} + NO_2$		1.0×10^4	
79	$CH_2(OH)CH_2CH_2CH(OH)\dot{O}_2 + HO_2 \rightarrow$ stable product		4.0×10^3	
80	$CH_2(OH)CH_2CH_2CH(OH)\dot{O} \xrightarrow{O_2} CH(OH)(\dot{O}_2)CH_2CH_2CH(OH)_2$		$^*9.51 \times 10^{12}$	3.27×10^3
81	$CH(OH)(\dot{O}_2)CH_2CH_2CH_2(OH)_2 + NO \rightarrow CH(OH)(\dot{O})CH_2CH_2CH(OH)_2$		1.0×10^4	
82	$CH(OH)(\dot{O}_2)CH_2CH_2CH_2(OH)_2 + HO_2 \rightarrow$ stable product		4.0×10^3	
83	$CH(OH)(\dot{O})CH_2CH_2CH(OH)_2 \xrightarrow{O_2} CH(OH)_2CH_2CH_2C(OH)_2\dot{O}_2$		$^*4.76 \times 10^{12}$	2.31×10^3
84	$CH(OH)_2CH_2CH_2C(OH)_2\dot{O}_2 + NO \rightarrow CH(OH)_2CH_2CH_2C(OH)\dot{O}$		1.0×10^4	
85	$CH(OH)_2CH_2CH_2C(OH)_2\dot{O}_2 + HO_2 \rightarrow$ stable product		4.0×10^3	
86	$CH(OH)_2CH_2CH_2C(OH)_2\dot{O} \xrightarrow{O_2} C(OH)_2(\dot{O}_2)CH_2CH_2C(OH)_2$		$^*4.76 \times 10^{12}$	6.44×10^3
87	$C(OH)_2(\dot{O}_2)CH_2CH_2C(OH)_2 + NO \rightarrow C(OH)_2(\dot{O})CH_2CH_2C(OH)_2$		1.0×10^4	
88	$C(OH)_2(\dot{O}_2)CH_2CH_2C(OH)_2 + HO_2 \rightarrow$ stable products		4.0×10^3	

[a] Units $ppm^{-1}\ min^{-1}$, except * units min^{-1}.

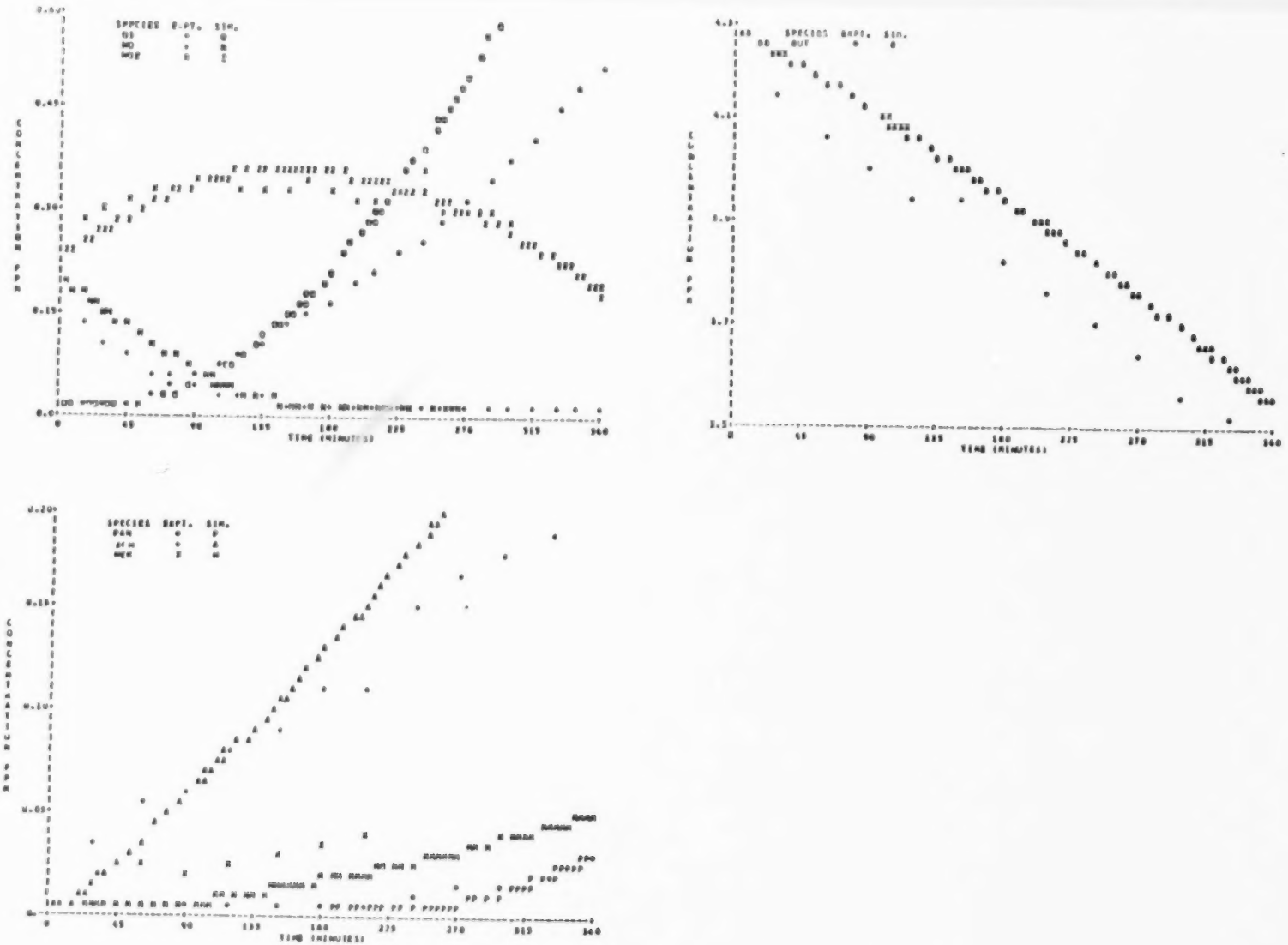

Figure 9. Simulation of SAPRC n-Butane Run EC-309.

TABLE 19 SUMMARY OF INITIAL CONDITIONS OF MISCELLANEOUS SMOG CHAMBER EXPERIMENTS[a]

No.	Subst.	NO	NO_2	HONO	RH/NO_x	k_{NO_2}[b]
	n-Butane					
304	4.28	0.349	0.117	0.000	9.18	9.43
305	4.30	0.078	0.020	0.000	43.9	0.43
306	6.44	0.147	0.040	0.000	34.4	0.43
307[c]	6.44	0.083	0.019	0.000	63.1	0.43
308[d]	4.05	0.305	0.178	0.000	8.39	0.43
309	4.31	0.203	0.272	0.000	9.07	0.43
7.21.78R	1.83	0.189	0.054	0.020	7.53	- -
7.22.78R	2.09	0.432	0.116	0.020	3.81	- -
2.27.78R	3.37	0.189	0.077	0.020	12.7	- -
	CH_2O					
250	0.33	0.011	0.012	0.000	14.3	0.30
251	0.19	0.080	0.033	0.000	1.71	0.30
252	0.36	0.392	0.103	0.000	0.73	0.30
255	0.33	0.006	0.010	0.000	20.63	0.30
9.14.77R	1.05	0.293	0.104	0.000	2.64	- -
9.15.78B	2.00	0.211	0.057	0.000	7.46	- -
9.21.78B	1.97	0.190	0.067	0.000	7.67	- -
	A_cH					
253	0.546	0.011	0.009	0.000	27.3	0.30
254	0.472	0.085	0.027	0.000	4.32	0.30
12.28.77B	1.91	0.29	0.117	0.000	4.69	- -
8.08.78R	0.46	0.42	0.095	0.000	0.89	- -

[a] Units in ppm.
[b] Units in min^{-1}.
[c] Temperature, 288.5 K.
[d] Temperature, 311.5 K.

TABLE 20 COMPARISON OF EXPERIMENTAL AND SIMULATION RESULTS FOR MISCELLANEOUS CHAMBER EXPERIMENTS

No.	EXPERIMENTAL				SIMULATION			
	O_3-max		NO_2-max		O_3-max		NO_2-max	
	ppm	min	ppm	min	ppm	min	ppm	min
304	0.36	> 435	0.32	180	0.98	> 435	0.35	170
305	0.40	> 360	0.077	90	0.76	> 360	0.075	80
306	0.54	> 405	0.15	100	0.99	> 400	0.15	90
307	0.42	> 390	0.078	60	0.84	> 390	0.08	60
308	0.04	> 360	0.28	345	0.35	> 360	0.35	220
309	0.56	360	0.36	90	0.91	> 360	0.35	160
7.21.78R	0.72	> 720	0.22	400	0.84	> 720	0.20	180
7.22.78R	0.13	> 720	0.43	660	0.19	> 720	0.42	660
2.27.78R	0.72	680	0.27	300	0.62	> 720	0.22	600
250	0.21	360	0.22	330	0.21	230	0.012	0
251	0.25	315	0.08	30	0.063	360	0.07	60
252	0.02	> 360	0.20	180	0.013	> 360	0.20	170
255	0.15	315	- -	- -	0.18	240	0.01	0
9.14.77R	0.62	> 720	0.28	300	0.52	720	0.30	360
9.15.78B	0.55	630	0.22	300	0.93	650	0.21	300
9.21.78B	0.74	630	0.25	300	1.25	660	0.22	300
253	0.125	> 360	- -	- -	0.14	> 360	0.013	90
254	0.20	> 360	0.06	90	0.16	> 360	0.082	180
12.26.77B	0.039	700	0.33	660	0.60	720	0.28	360
8.08.78R	0.51	770	0.42	470	0.75	780	0.34	480

UNC DATA SET

The results for the selected UNC butane runs are shown in Appendix C. Initial conditions are given in Table 19 and results summarized in Table 20. A typical result is shown in Figure 10. The results are generally in good agreement. A small variable amount of initial nitrous acid was used to increase the overall reaction rate of the simulations to match the experimental data. The amounts used are listed in Table 19.

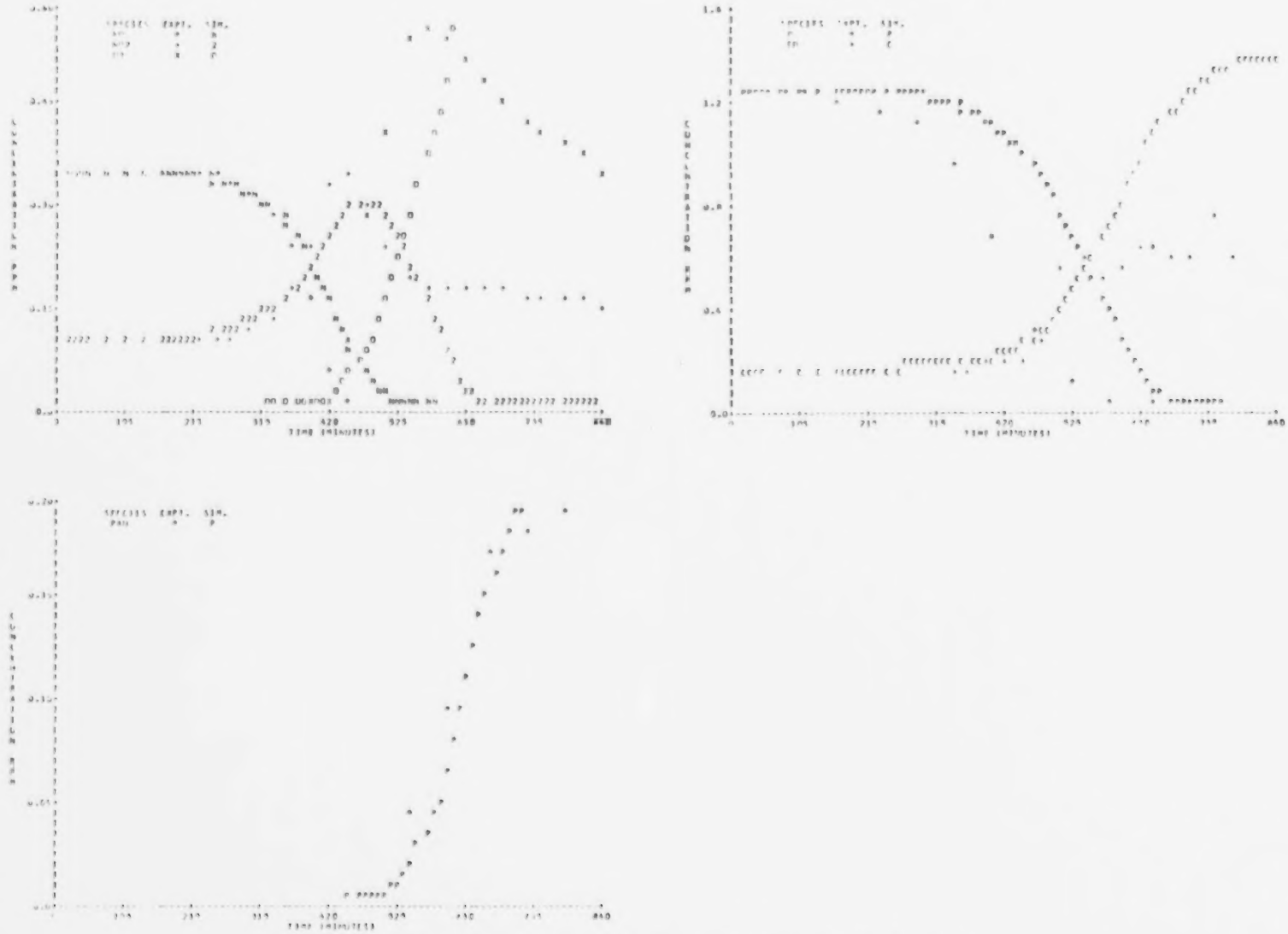

Figure 10. Simulation of UNC n-Butane Run 7.27.78 Red.

SECTION 7

ALDEHYDES

MECHANISM

Both SAPRC and UNC have reported experiments for acetaldehyde and formaldehyde chamber experiments. The aldehyde mechanisms are subsets of the alkane and alkene mechanism, but are given explicitly in Table 21 for convenience.

SAPRC DATA SET

The six SAPRC aldehyde runs have been modeled and are shown in Appendix C. Initial conditions are in Table 19 and the results are summarized in Table 20. Typical results for acetaldehyde and formaldehyde are shown in Figures 11 and 12. Aldehydes present a difficult analytical problem and there is considerable scatter in their concentration measurements. However, in general the results are in good agreement.

UNC DATA SET

The UNC aldehyde chamber runs are given in Appendix C. Initial conditions are in Table 19 and results are summarized in Table 20. A typical result for acetaldehyde is shown in Figure 13, and for formaldehyde in Figure 14. As in the SAPRC data set there is considerable scatter in the hydrocarbon measurement, but in general the results are in agreement.

TABLE 21 ALDEHYDE MECHANISM

No.		A-Factor[a]	Activation Energy
1	$CH_3CHO + h\nu \xrightarrow{O_2} CH_3O_2 + CO + HO_2$		
2	$CH_2O + h\nu \rightarrow CO + HO_2 + HO_2$		
3	$CH_2O + h\nu \rightarrow CO$		
4	$CH_3CHO + OH \xrightarrow{O_2} CH_3C(O)\dot{O}_2 + H_2O$	2.0×10^7	
5	$CH_2O + OH \rightarrow HO_2 + CO + H_2O$	2.0×10^4	
6	$CH_3C(O)\dot{O}_2 + NO \rightarrow CH_3\dot{O}_2 + NO_2 + CO_2$	5.4×10^4	
7	$CH_3C(O)\dot{O}_2 + NO_2 \rightarrow CH_3C(O)O_2NO_2$	1.5×10^4	
8	$CH_3C(O)O_2NO_2 \rightarrow CH_3C(O)\dot{O}_2 + NO_2$	1.02×10^{16}	1.35×10^4
9	$CH_3\dot{O}_2 + NO_2 \rightarrow CH_3O_2NO_2$	7.8×10^3	
10	$CH_3O_2NO_2 \rightarrow CH_3\dot{O}_2 + NO_2$	$^*1.6 \times 10^{16}$	1.1×10^4
11	$CH_3\dot{O}_2 + NO \rightarrow CH_3\dot{O} + NO_2$	1.0×10^4	
12	$CH_3\dot{O} + O_2 \rightarrow CH_2O + HO_2$	$^*2.0 \times 10^9$	
13	$CH_3\dot{O} + NO_2 \rightarrow CH_3ONO_2$	2.0×10^4	
14	$CH_3\dot{O} + NO_2 \rightarrow CH_2O + HNO_2$	2.2×10^3	
15	$CH_3C(O)\dot{O}_2 + CH_3C(O)\dot{O}_2 \rightarrow CH_3\dot{O}_2 + CH_3\dot{O}_2 + 2CO_2$	2.4×10^3	
16	$CH_3C(O)\dot{O}_2 + HO_2 \rightarrow CH_3C(O)OOH$	4.0×10^3	
17	$CH_3\dot{O} + HO_2 \rightarrow CH_3OOH$	2.0×10^3	

[a] Units in $ppm^{-1}\ min^{-1}$, except * min^{-1}.

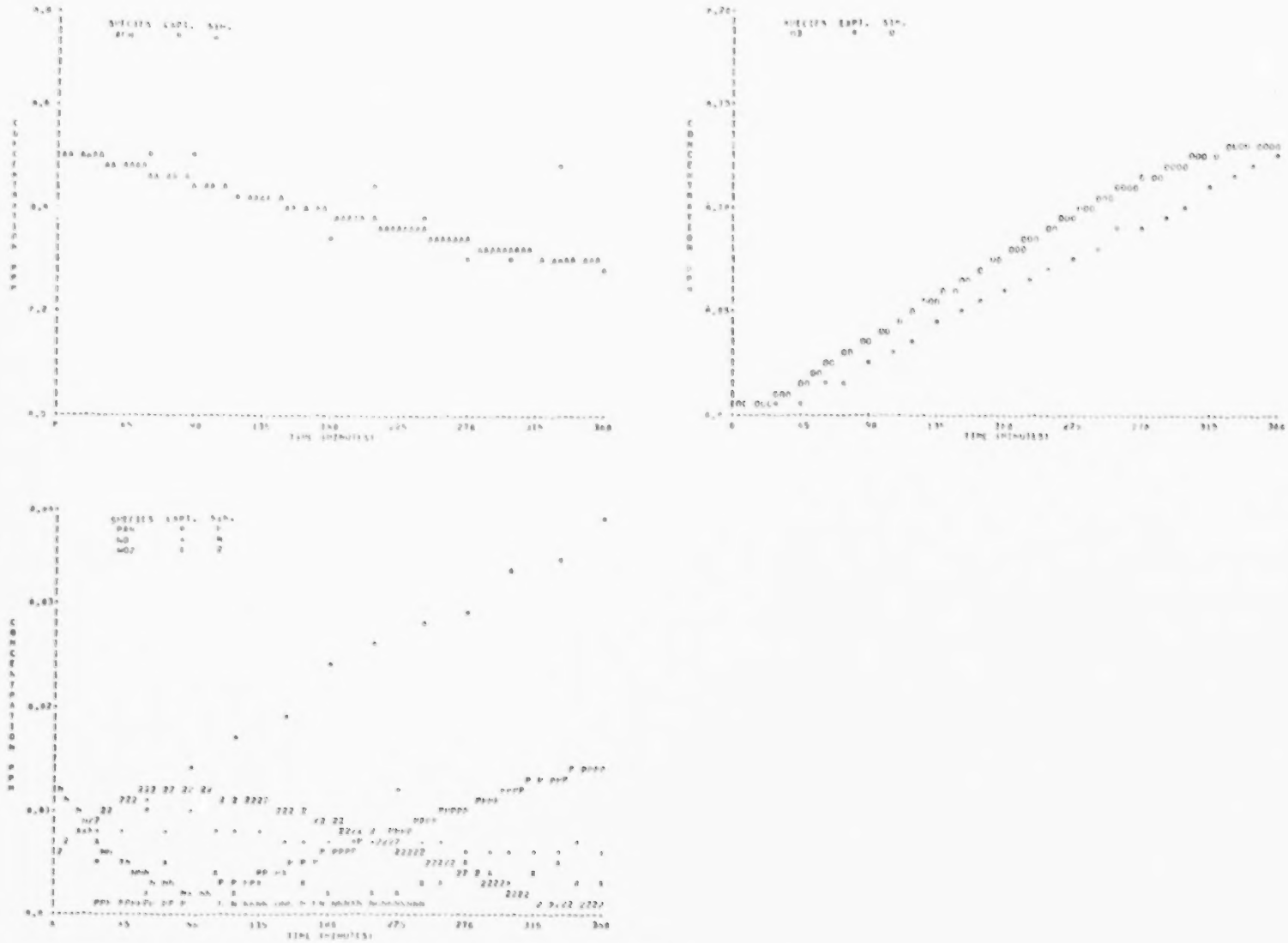

Figure 11. Simulation of SAPRC Acetaldehyde Run EC-253.

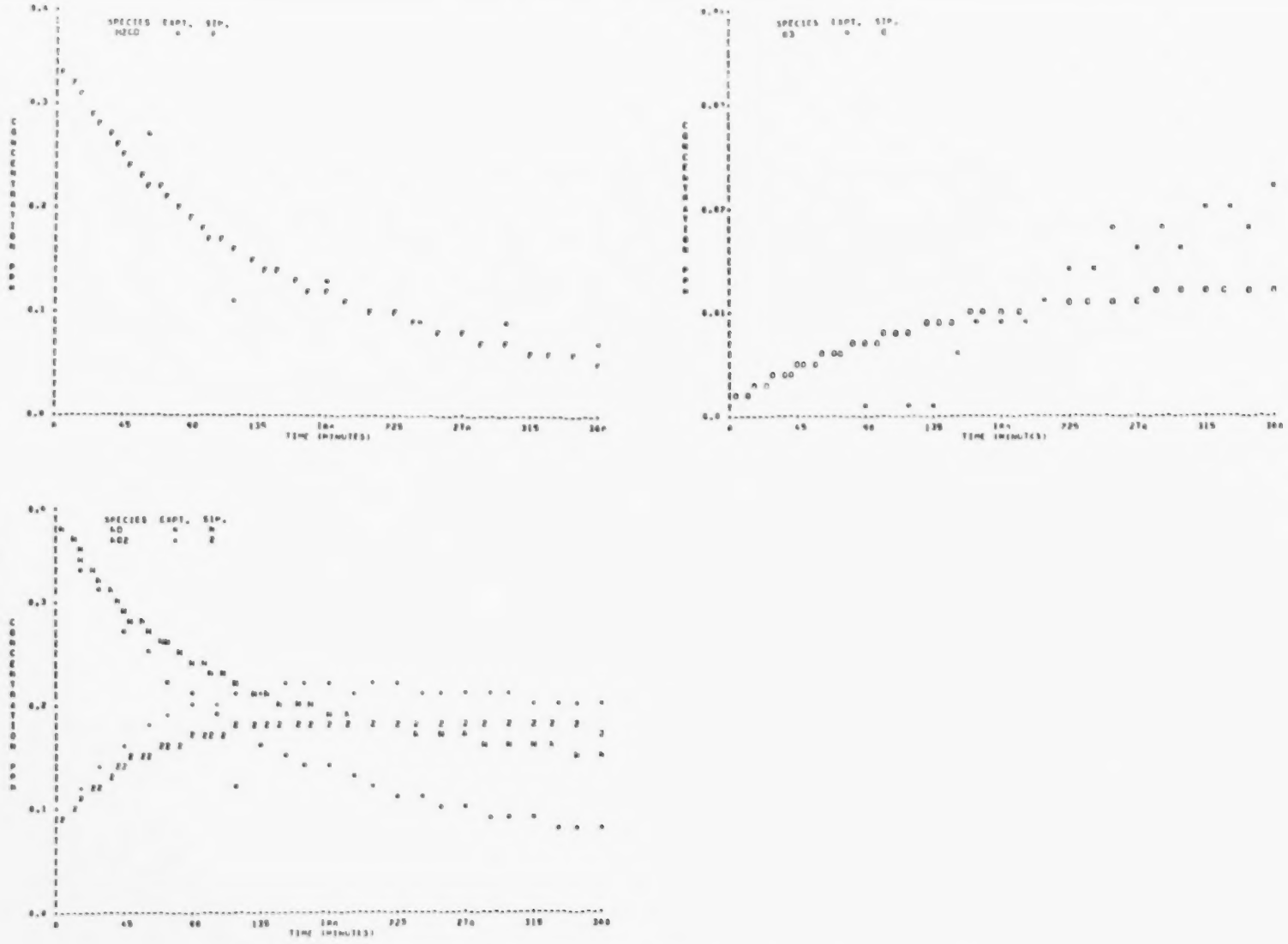

Figure 12. Simulation of SAPRC Formaldehyde Run EC-252.

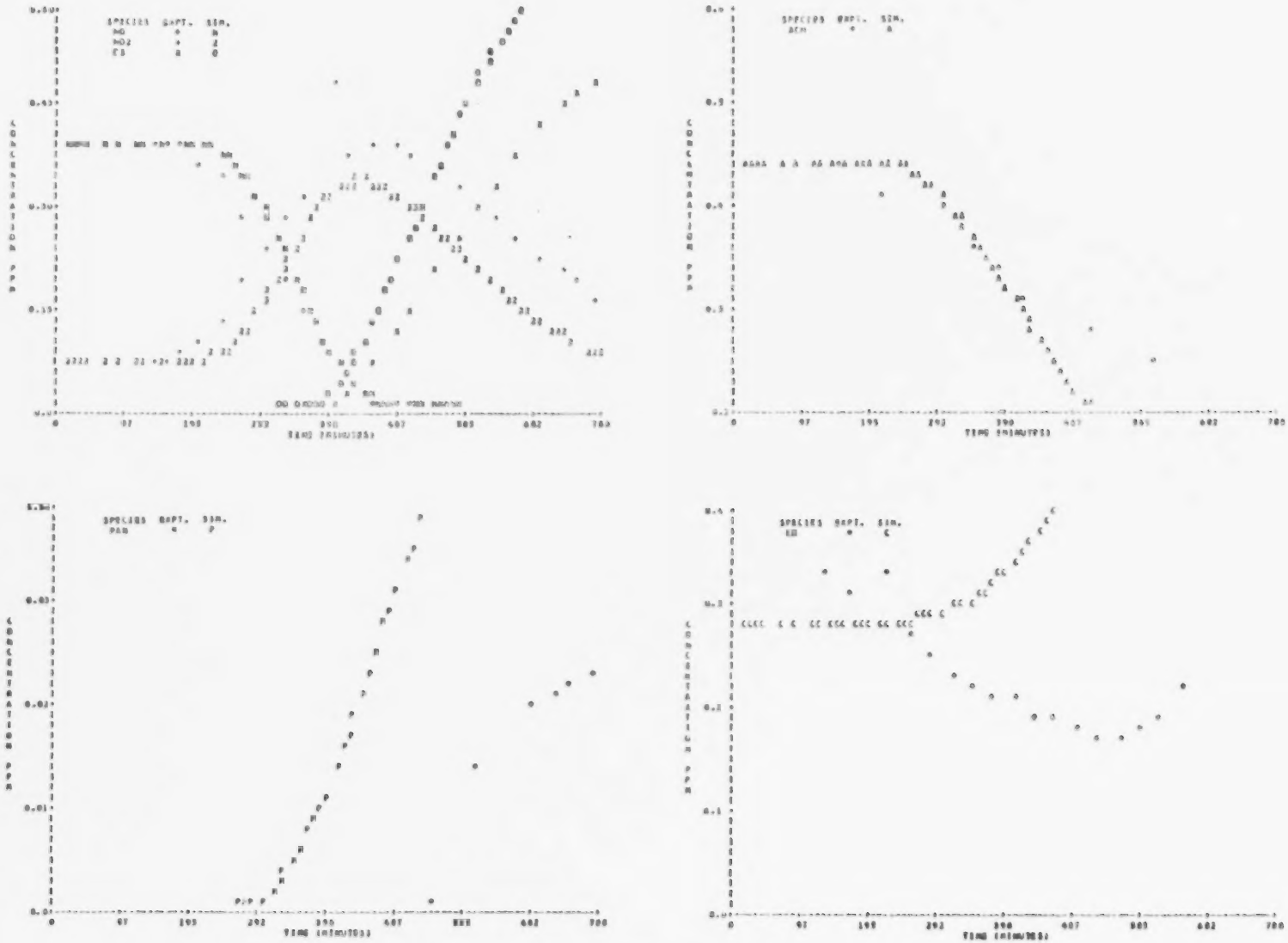

Figure 13. Simulation of UNC Acetaldehyde Run 8.08.78 Red.

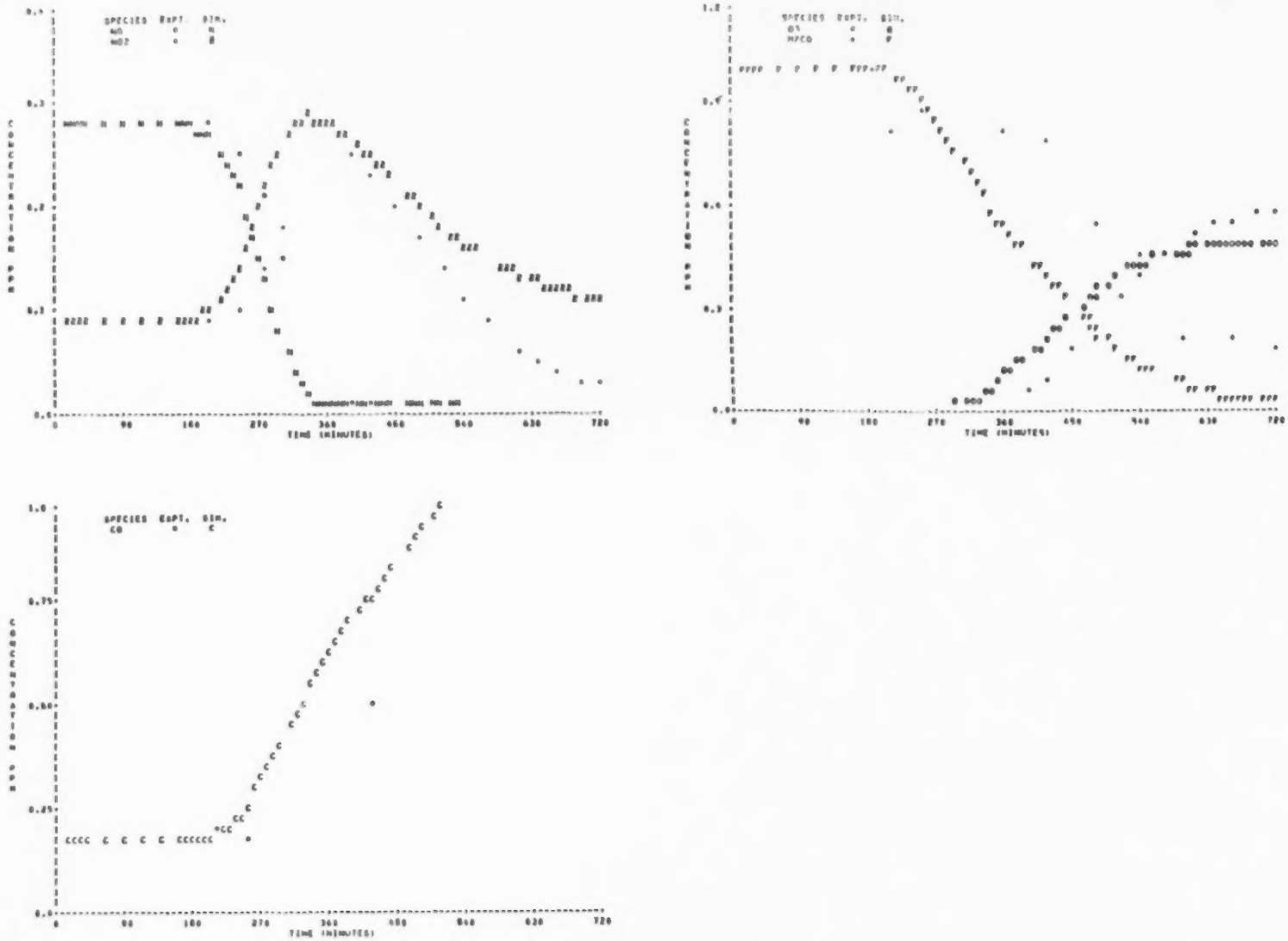

Figure 14. Simulation of UNC Formaldehyde Run 9.14.77 Red.

REFERENCES

1. D. G. Hendry, A. C. Baldwin, J. R. Barker, and D. M. Golden, "Computer Modeling of Simulated Photochemical Smog," EPA Report 600/3-78-059, June 1978.

2. J. N. Pitts, Jr., et al., "Mechanisms of Photochemical Reactions in Urban Air," EPA Report 600/3-77-0146, February 1977, and subsequent quarterly reports.

3. H. E. Jeffries, D. L. Fox, and R. M. Kamen, "Outdoor Smog Chamber Studies: Effect of Hydrocarbon Reduction on Nitrogen Dioxide," EPA Report 650/3-75-011, June 1975 and subsequent quarterly reports.

4. K. L. Demerjian, J. A. Kerr, and J. G. Calvert, Adv. Environ. Sci., 4, 1 (1974).

5. H. Niki, E. E. Daby, and W. Weinstock, Adv. Chem. Series, 113, 16 (1972).

6. T. A. Hecht, J. H. Seinfeld, and M. C. Dodge, Environ. Sci. Technol., 8, 327 (1974).

7. G. Z. Whitten et al., "Modeling of Simulated Photochemical Smog with Kinetics Mechanisms," EPA Report 600/3-79-001, January 1979.

8. W.P.L. Carter, A. C. Lloyd, J. L. Srung, and J. N. Pitts, Jr., Int. J. Chem. Kinetics, 11, 45 (1979).

9. K. R. Darnall, R. Atkinson, and J. N. Pitts, Jr., J. Phys. Chem., 83, 1943 (1979).

10. D. G. Hendry, R. A. Kenley, J. E. Davenport, and B. Y. Lan, "Reactions of Oxy Radicals in the Atmosphere," EPA Report 600/3-79-020, March 1979.

11. D. G. Hendry and R. A. Kenley, "Abstracts of Papers," Part II, 178th American Chemical Society National Meeting, PHYS-251, September 1979.

12. J. T. Herron and R. E. Huie, J. Amer. Chem. Soc., 99, 5430 (1977).

13. K. L. Schere and K. L. Demerjian, "Calculation of Selected Photolytic Rate Constants over a Diurnal Range," EPA Report 600/4-77-015, 1977.

14. G. Z. Whitten and J. P. Meyer, "CHEMK: A Computer Modeling Scheme for Chemical Kinetics," Systems Applications, Incorporated, San Rafael, California, 1975.

15. A. C. Hindmarsh, "GEAR: Ordinary Differential Equation Systems Solver," Lawrence Livermore Laboratory Report UCID 3001, Rev. 2, 1972.

16. C. W. Gear, Comm. Amer. Comp. Mach., 14, 1976 (1971).

17. J. G. Calvert, Environ. Sci. Tech., 10, 256 (1976).

18. W. A. Lonneman, S. L. Kopcynski, P. E. Danley, and F. D. Sutterfield, Environ. Sci. Tech., 8, 229 (1974).

19. W. A. Lonneman, R. L. Seila, and J. J. Bufalini, Environ. Sci. Tech., 12, 459 (1978).

20. D. D. Davis, W. Bollinger, and S. Fischer, J. Phys. Chem., 79, 293 (1975).

21. D. D. Davis, "Investigation of Important Hydroxyl Radical Reactions in the Perturbed Troposphere," EPA Report 600/3-77-11, October 1977.

22. R. A. Perry, R. Atkinson, and J. N. Pitts, Jr., J. Phys. Chem., 81, 296 (1977).

23. D. A. Hansen, R. Atkinson, and J. N. Pitts, Jr., J. Phys. Chem., 79, 1763 (1975).

24. R. Atkinson and J. N. Pitts, Jr., J. Phys. Chem., 79, 295 (1975).

25. D. G. Hendry, T. Mill, L. Piszkiewicz, J. A. Howard, and H. K. Eigenmann, J. Phys. Chem. Ref. Data, 3, 937 (1974).

26. T. W. Nakagawa, L. J. Andrews, and R. M. Keefer, J. Amer. Chem. Soc., 82, 269 (1960).

27. S. M. Japar and H. Niki, J. Phys. Chem., 79, 1629 (1975).

28. G. J. Doyle, A. C. Lloyd, K. R. Darnall, A. M. Winer, and J. N. Pitts, Jr., Environ. Sci. Tech., 9, 237 (1975).

29. R. J. O'Brien, P. J. Green, and R. M. Doty, "Chemical Kinetic Data Needs for Modeling the Lower Troposphere," NBS Special Pub. 557, August 1979, p. 93.

30. J. M. Heuss and W. A. Glasson, Environ. Sci. Tech., 2, 1109 (1968).

31. S. L. Kopczynski, R. L. Kuntz, J. J. Bufalini, Environ. Sci. Tech., 9, 648 (1975).

32. M. Hoshino, H. Akimoto, and M. Okuda, Bull. Chem. Soc. Japan, 51, 718 (1978).

33. H. Akimoto, M. Hoshino, G. Inone, M. Okuda, Bull. Chem. Soc. Japan, 51, 2496 (1978).

34. K. Nojima, K. Fukaga, S. Fukui, and S. Kanno, Chemosphere, 3, 247 (1974).

35. R. A. Kenley, J. E. Davenport, and D. G. Hendry, J. Phys. Chem., 82, 1095 (1978).

36. J. R. Barker, S. W. Benson, and D. M. Golden, Int. J. Chem. Kinetics, 9, 31 (1977).

37. D. G. Hendry and R. A. Kenley, "Atmospheric Chemistry of Peroxynitrates in Nitrogenous Air Pollutants, D. Grosjean, Ed., Ann Arbor Science, 1979, p. 137.

38. S. W. Benson, The Foundation of Chemical Kinetics, McGraw-Hill Book Company, Inc., New York, 1960, p. 33.

39. R. Atkinson, K. R. Darnall, and J. N. Pitts, Jr., J. Phys. Chem., 82, 2759 (1978).

40. H. Niki, P..O. Maker, C. M. Savage, and C. P. Breitenbach, J. Phys. Chem., 82, 132 (1978).

41. R. Atkinson and J. N. Pitts, Jr., J. Phys. Chem., 79, 541 (1975).

42. J. A. Howard, Adv. Free Radical Chemistry, 4, 49 (1972).

43. D. G. Hendry, "Chemical Kinetic Data Needs for Modeling the Lower Troposphere," NBS Special Publication 557, August 1979, p. 85.

44. D. G. Hendry, "Atmospheric Reaction Products of Organic Compounds," EPA Report 560/12-79-001, June 1979.

45. C. S. Parmenter, J. Chem. Phys., 41, 658 (1964).

46. H. Niki, P. D. Maker, C. M. Savage, and L. P. Breitenbach, "FTIR Studies of Gaseous and Particulate Nitrogenous Compounds," in Nitrogenous Air Pollutants, Ed., D. Grosjean, Ann Arbor Science, Ann Arbor, Michigan, 1979, p. 1.

47. D. G. Hendry, unpublished data.

48. R. A. Perry, R. Atkinson, and J. N. Pitts, Jr., J. Phys. Chem., 81, 1607 (1977).

49. M. C. Dodge and R. R. Arnts, Int. J. Chem. Kinetics, 11, 399 (1978).

50. D. G. Hendry and R. A. Kenley, J. Amer. Chem. Soc., 99, 3198 (1977).

51. A. C. Baldwin and D. M. Golden, J. Phys. Chem., 82, 644 (1978).

52. A. C. Baldwin, J. R. Barker, D. M. Golden, and D. G. Hendry, J. Phys. Chem., 81, 2483 (1977).

53. R. F. Hampson and D. Garvin, "Reaction Rate and Photochemical Data for Atmospheric Chemistry - 1977," NBS Special Publication 513, 1977.

Appendix A

SIMULATION OF AROMATIC HYDROCARBON CHAMBER RUNS

TABLE A-1. PHOTOLYSIS RATE CONSTANTS FOR TOLUENE AND m-XYLENE CHAMBER RUNS (in min^{-1})

EC No.	NO_2	HNO_2	H_2O_2	$O_3(^1D)$	$O_3(^3P)$	H_2CO(rad)	H_2CO(molec)
77-86	0.16	4.5×10^{-2}	3.3×10^{-4}	6.0×10^{-4}	6.6×10^{-4}	5.6×10^{-4}	8.0×10^{-4}
266-272	0.35	0.11	7.7×10^{-4}	1.2×10^{-3}	1.7×10^{-3}	1.2×10^{-3}	2.2×10^{-3}
273	0.37	0.12	8.2×10^{-4}	1.3×10^{-3}	1.8×10^{-3}	1.3×10^{-3}	2.4×10^{-3}
327-340	0.40	0.12	7.8×10^{-4}	7.9×10^{-4}	1.6×10^{-3}	7.8×10^{-4}	2.5×10^{-3}
343-346	0.38	0.11	7.6×10^{-4}	1.0×10^{-3}	1.6×10^{-3}	8.2×10^{-4}	2.4×10^{-3}

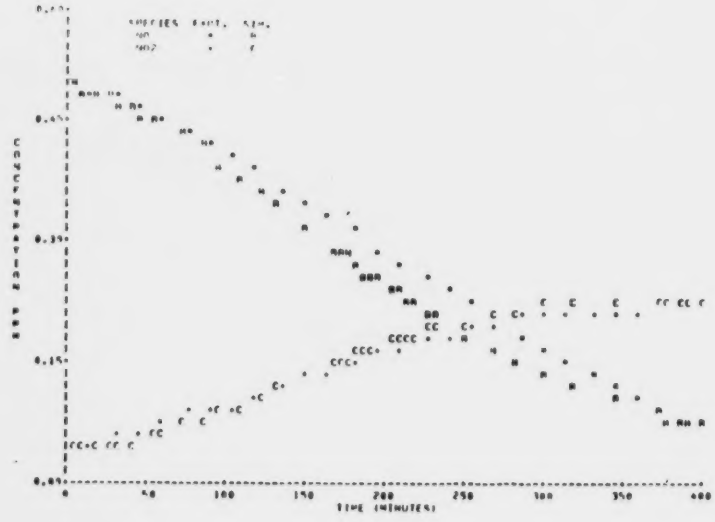

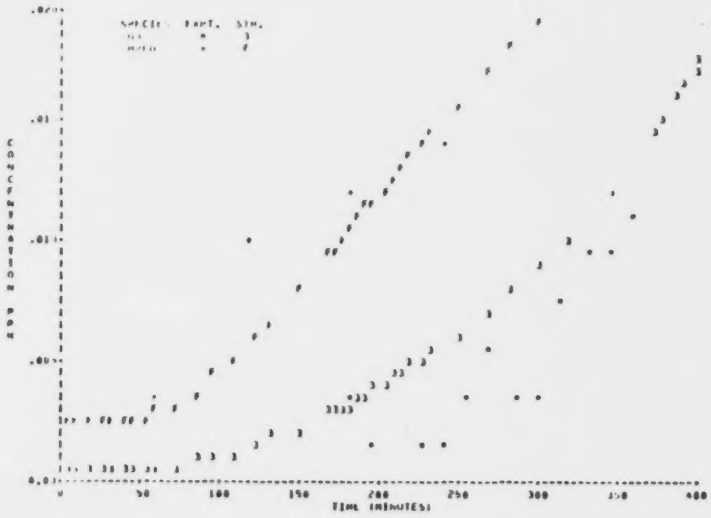

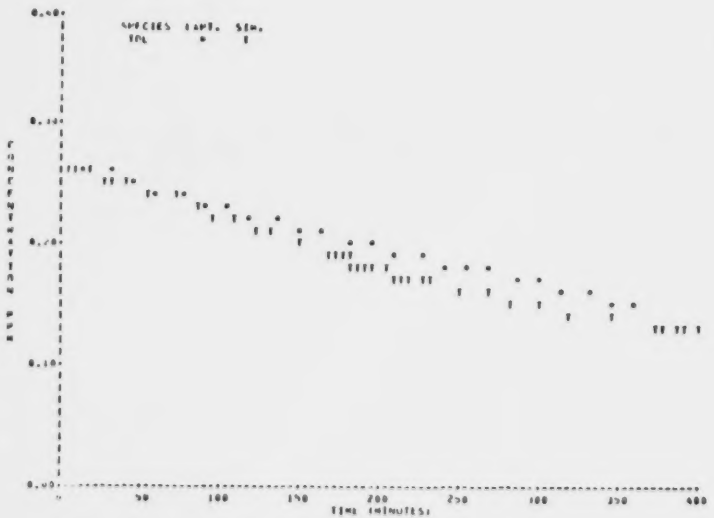

FIGURE A-1 SAPRC EC-77

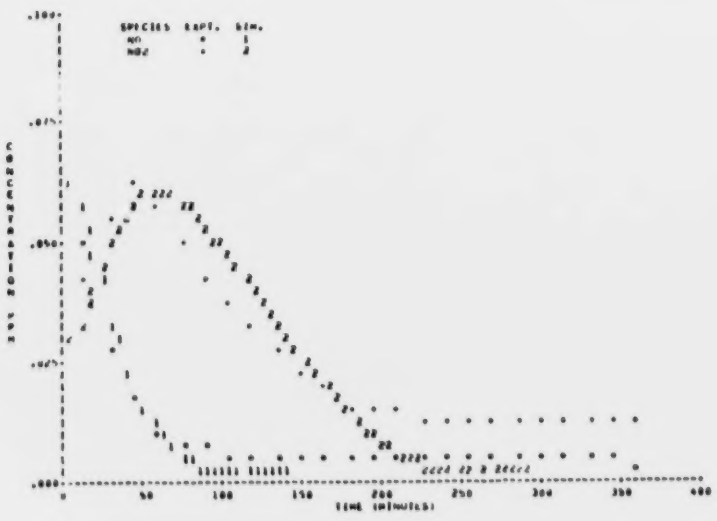

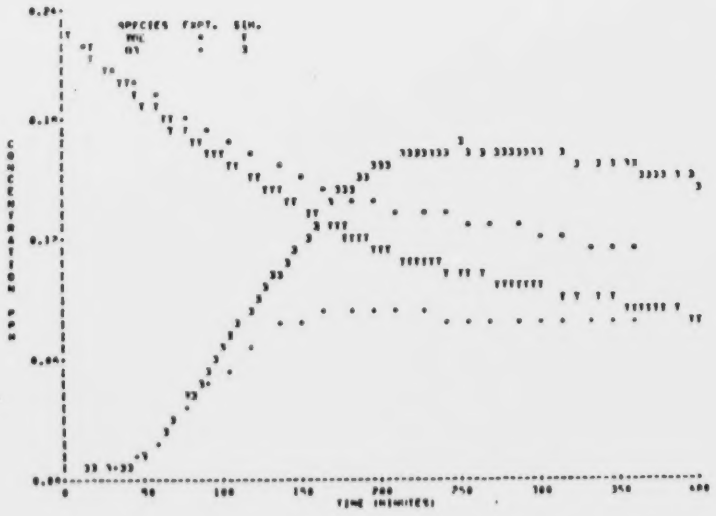

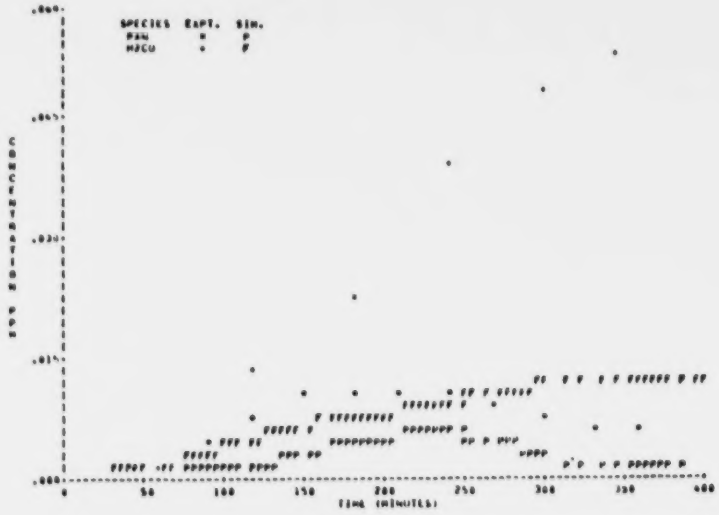

FIGURE A-2 SAPRC EC-78

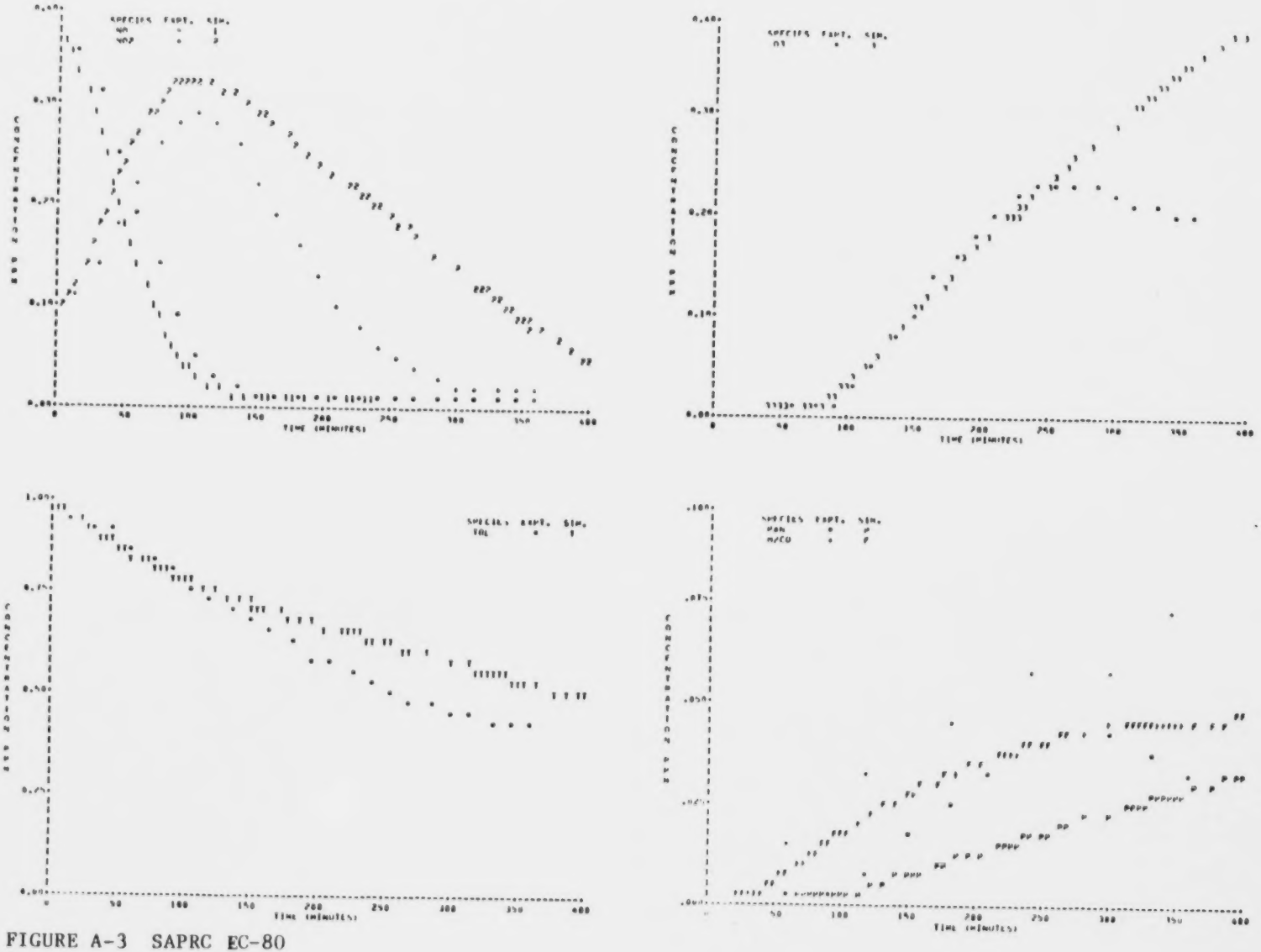

FIGURE A-3 SAPRC EC-80

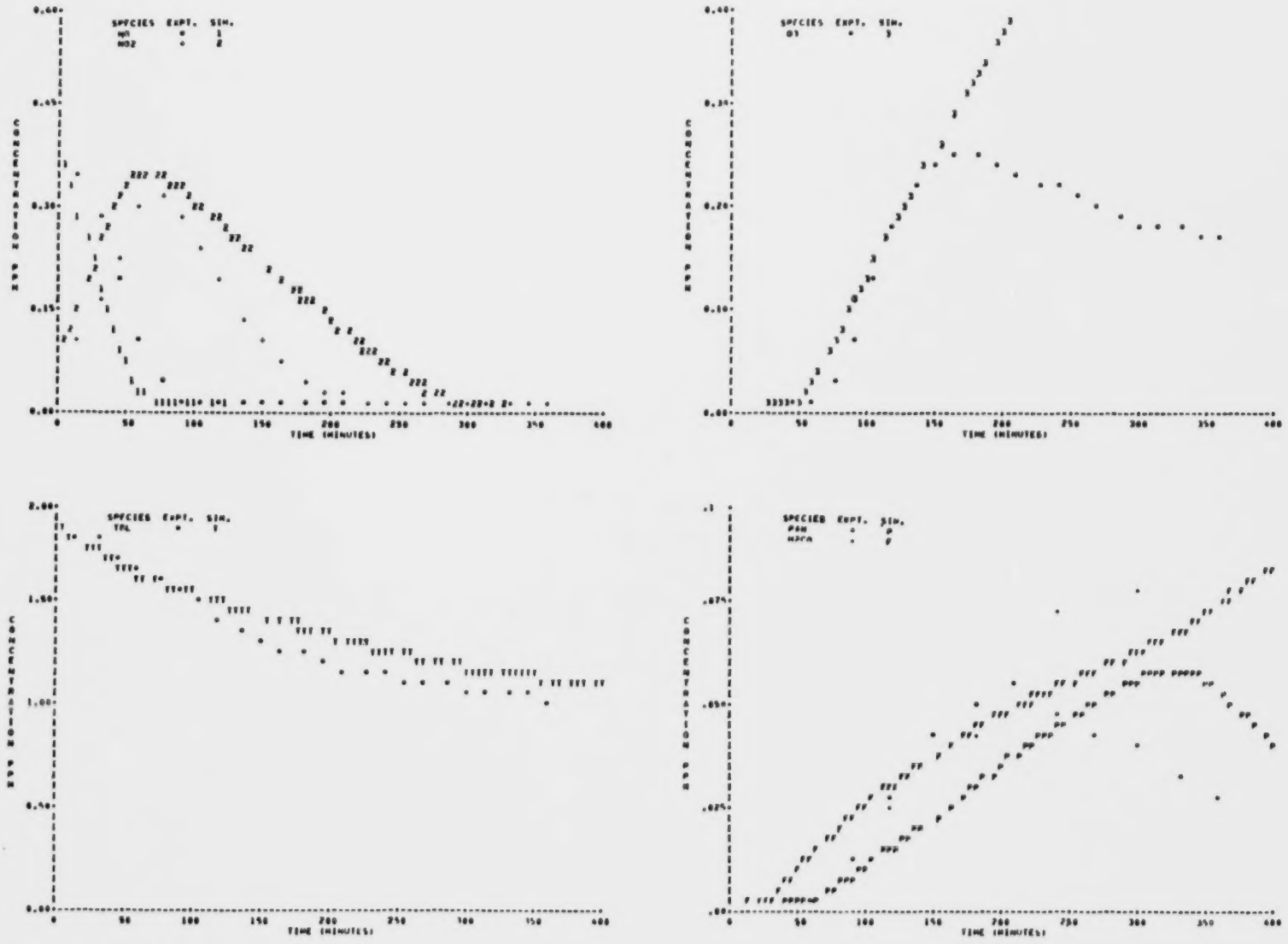

FIGURE A-4 SAPRC EC-81

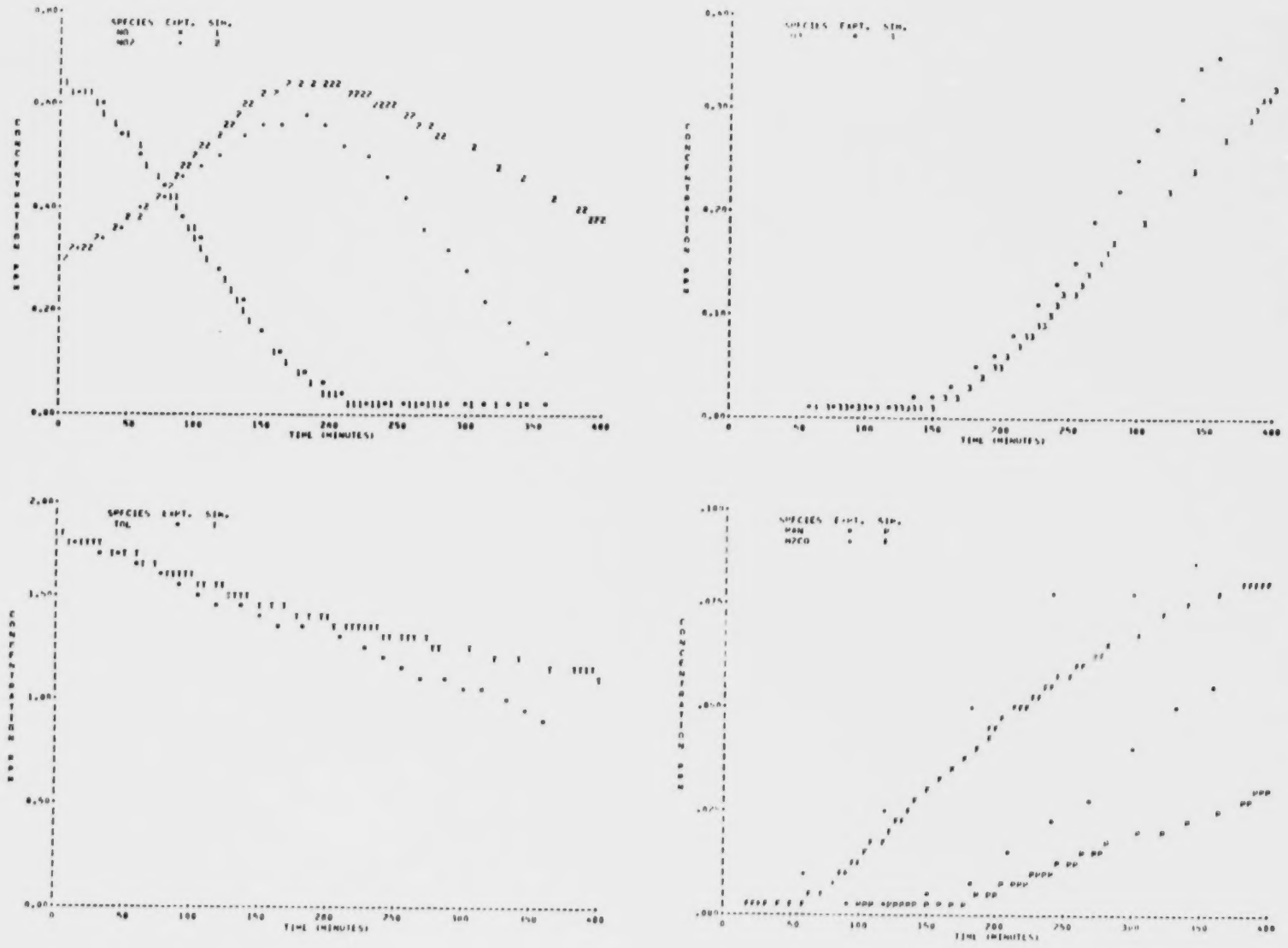

FIGURE A-5 SAPRC EC-82

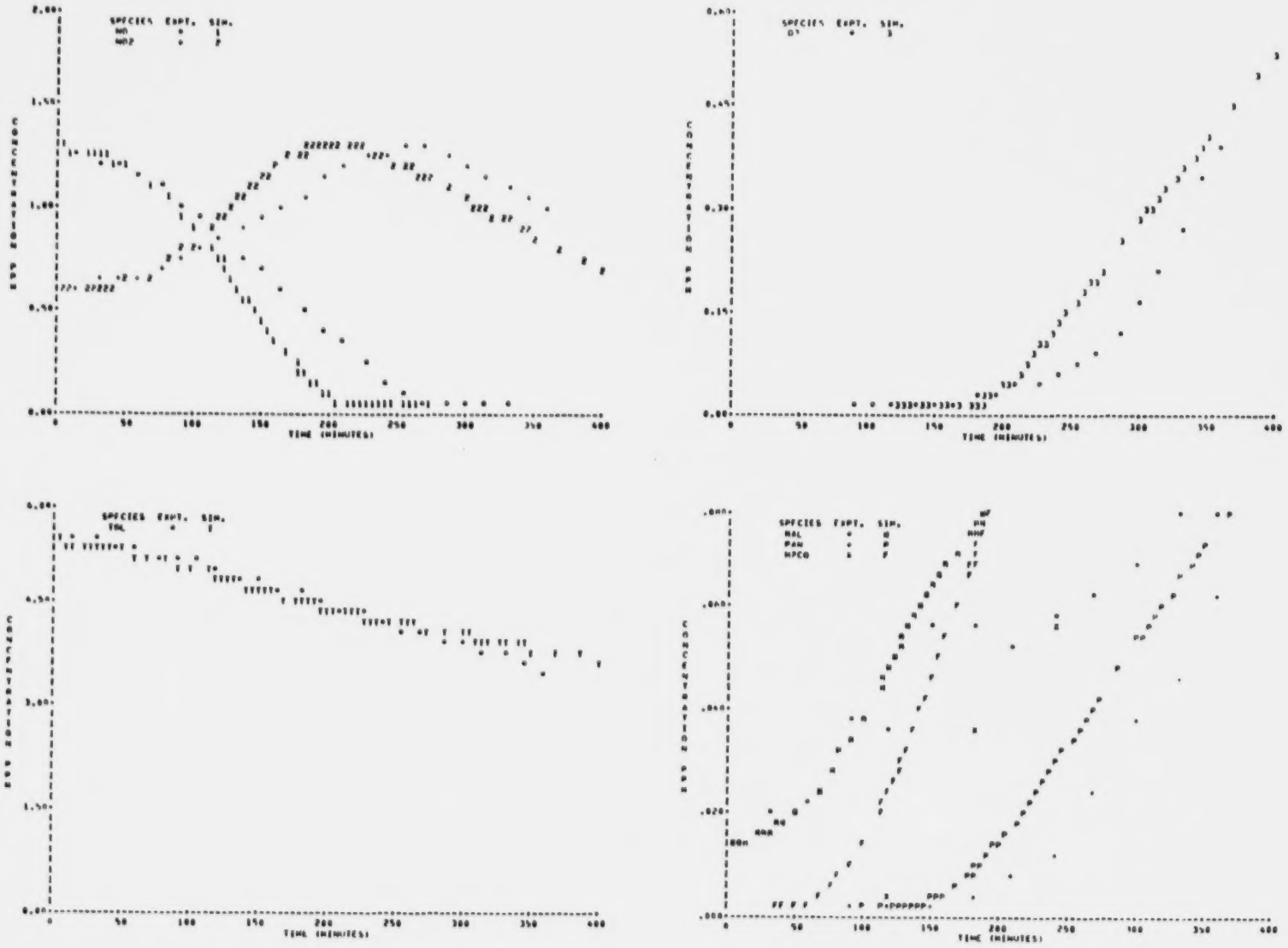

FIGURE A-6 SAPRC EC-83

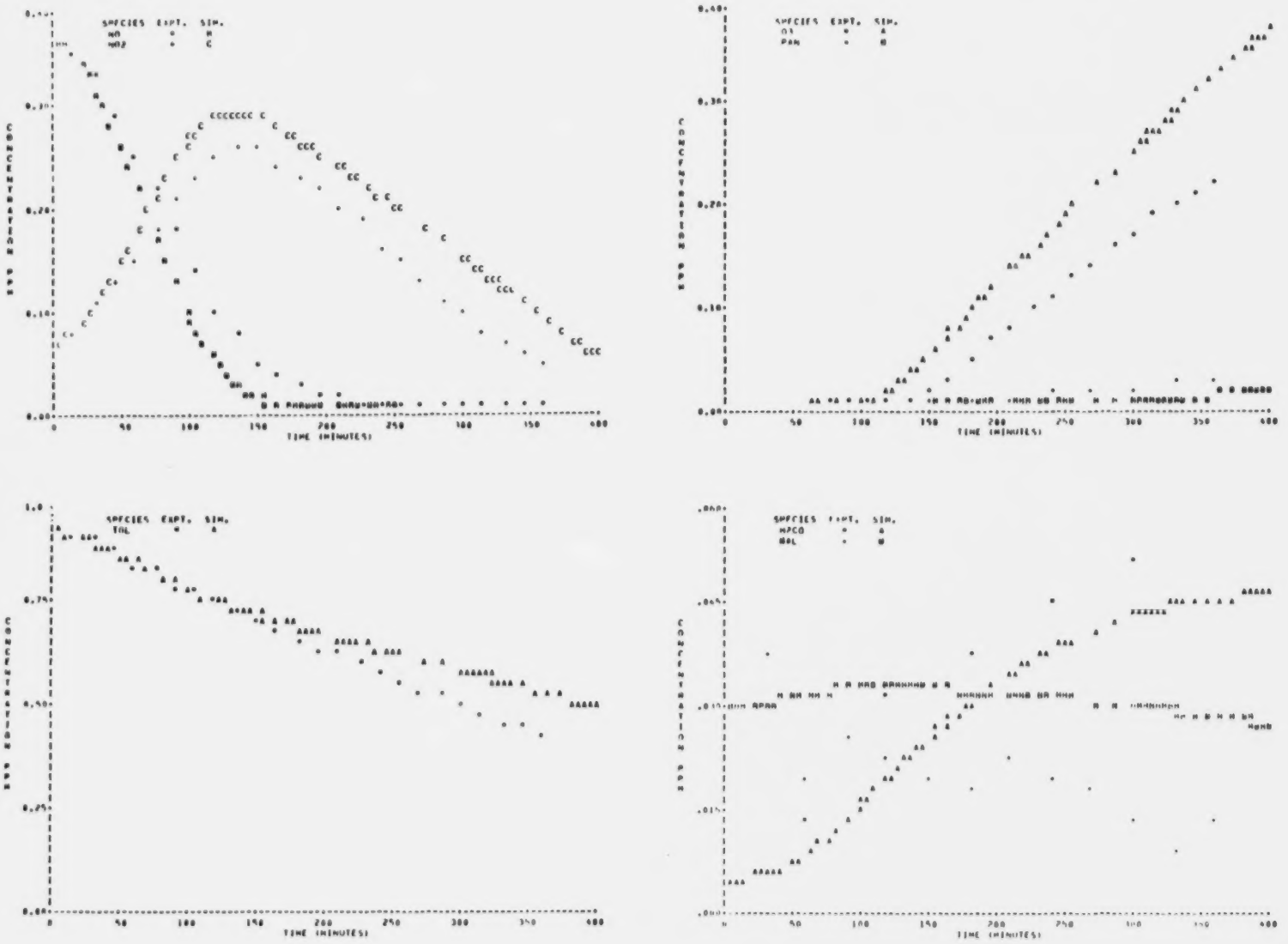

FIGURE A-7 SAPRC EC-84

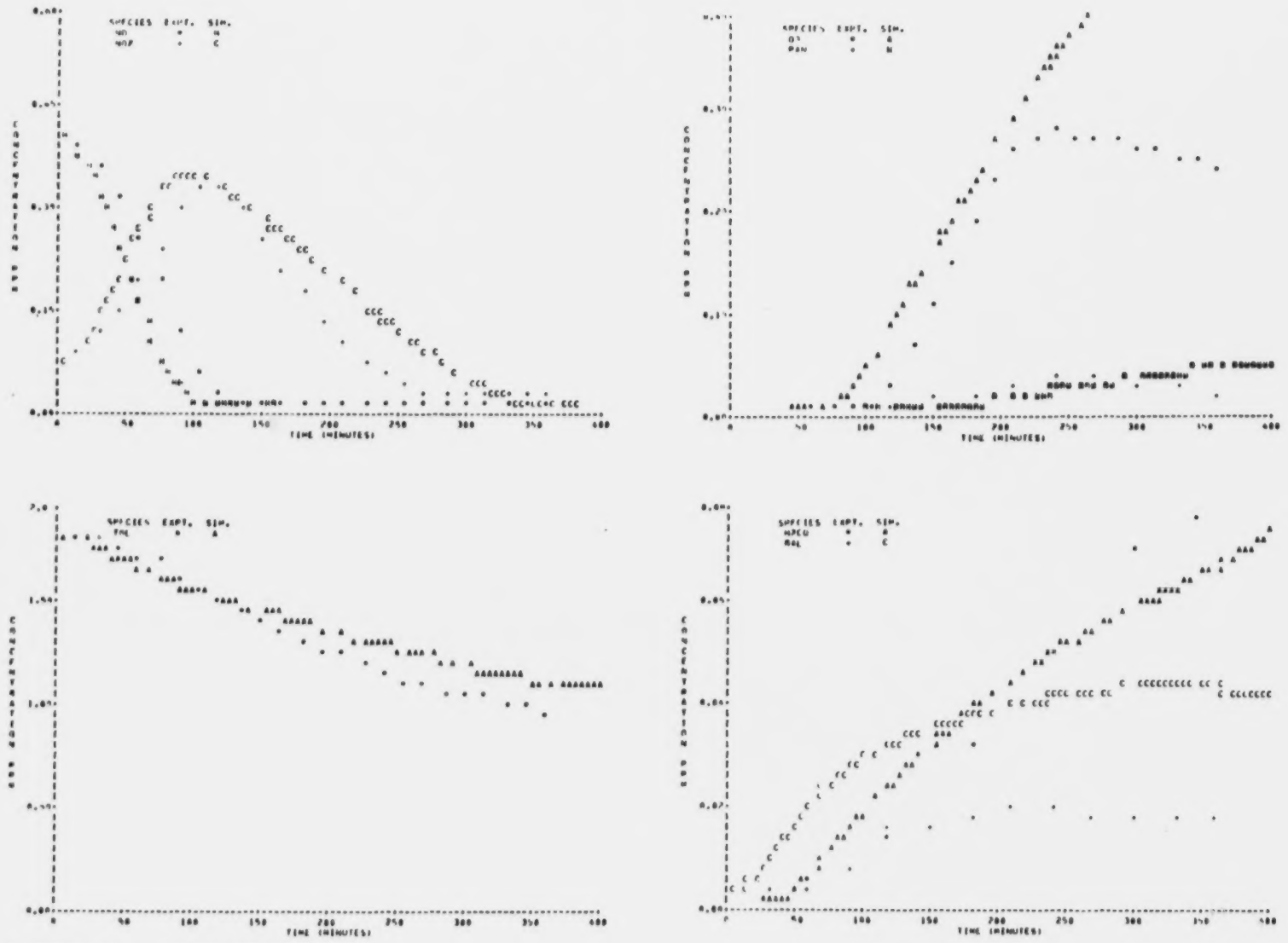

FIGURE A-8 SAPRC EC-85

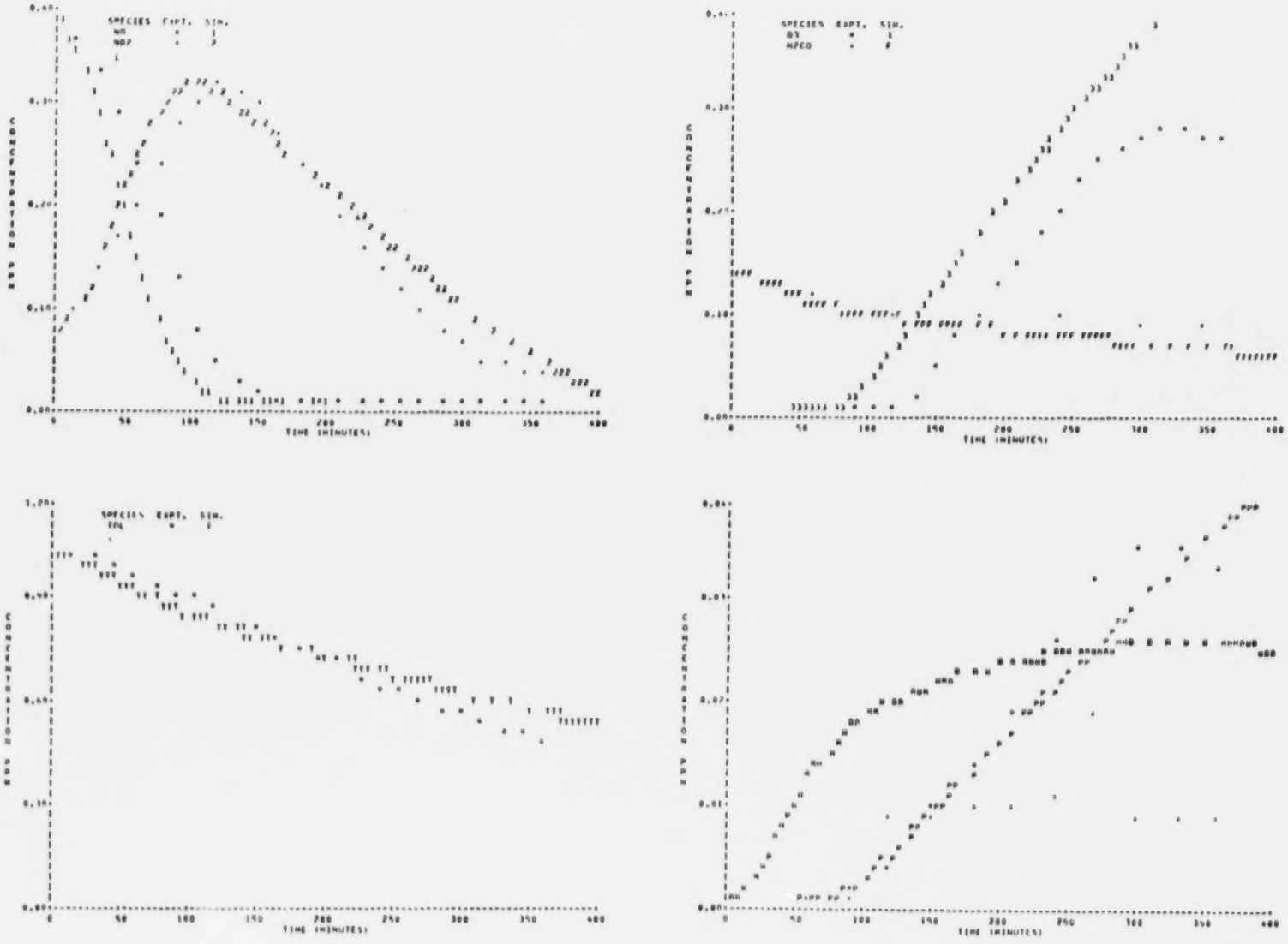

FIGURE A-9 SAPRC EC-86

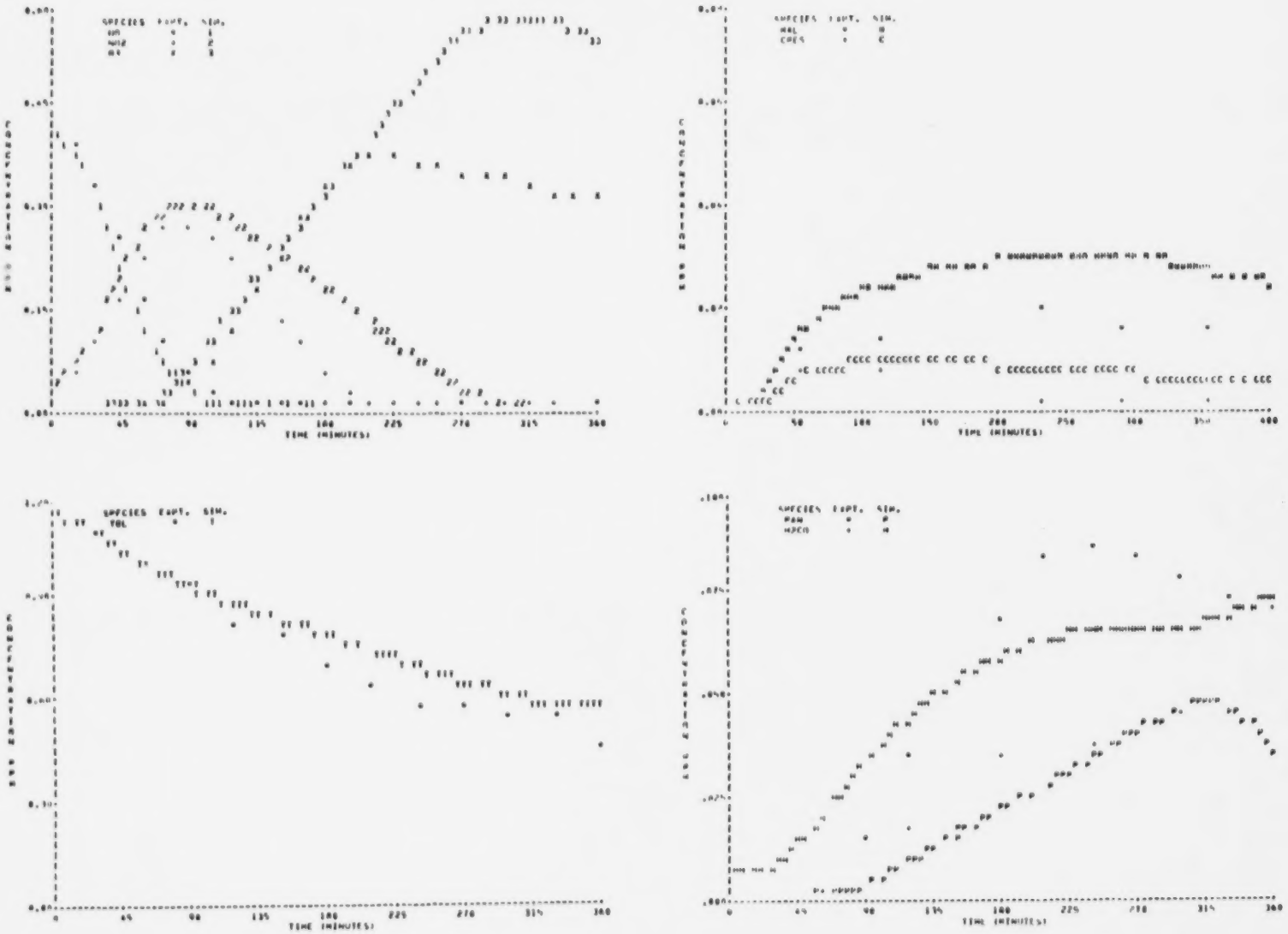

FIGURE A-10 SAPRC EC-266

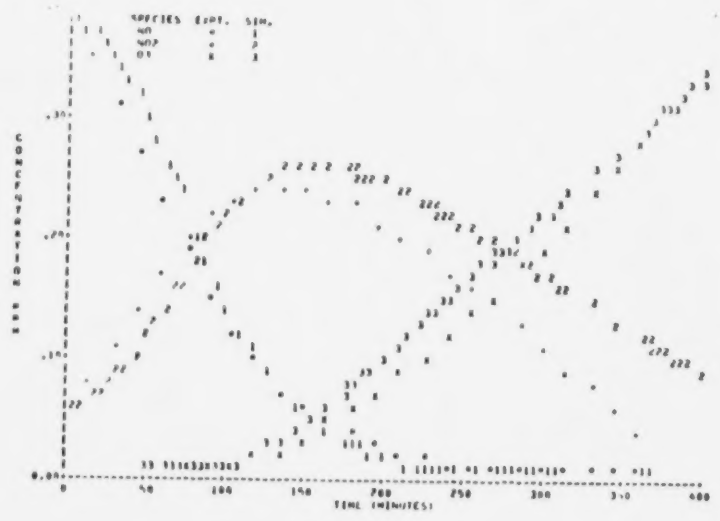

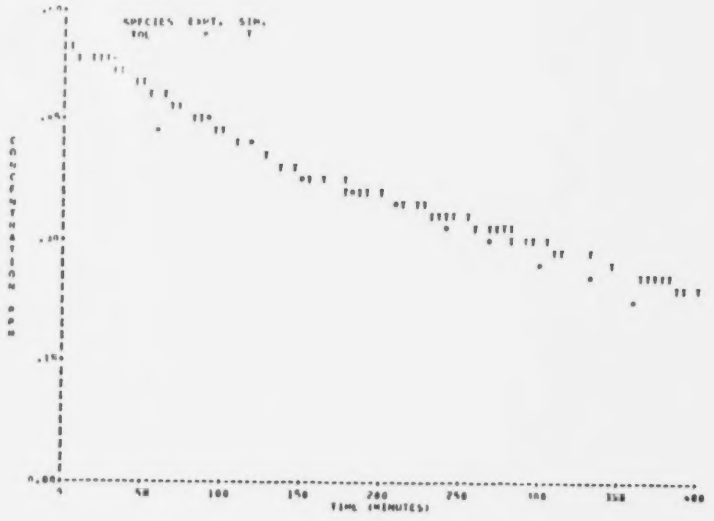

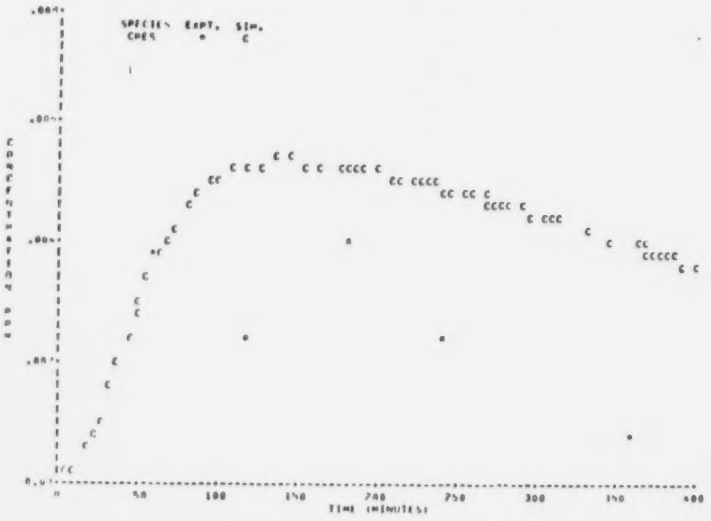

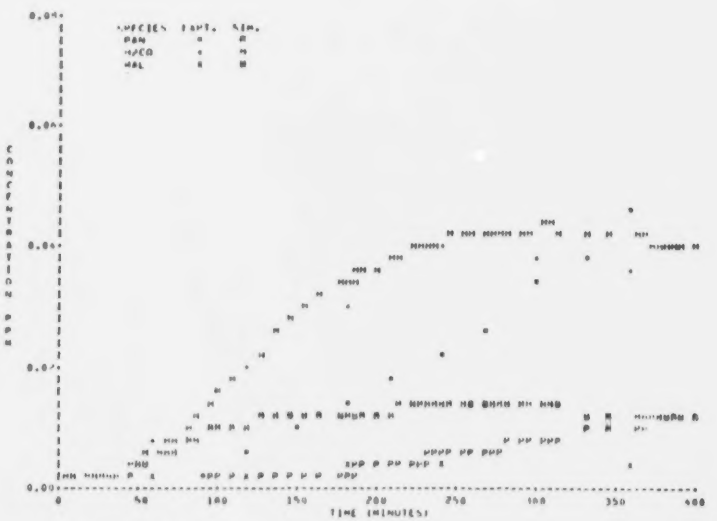

FIGURE A-11 SAPRC EC-269

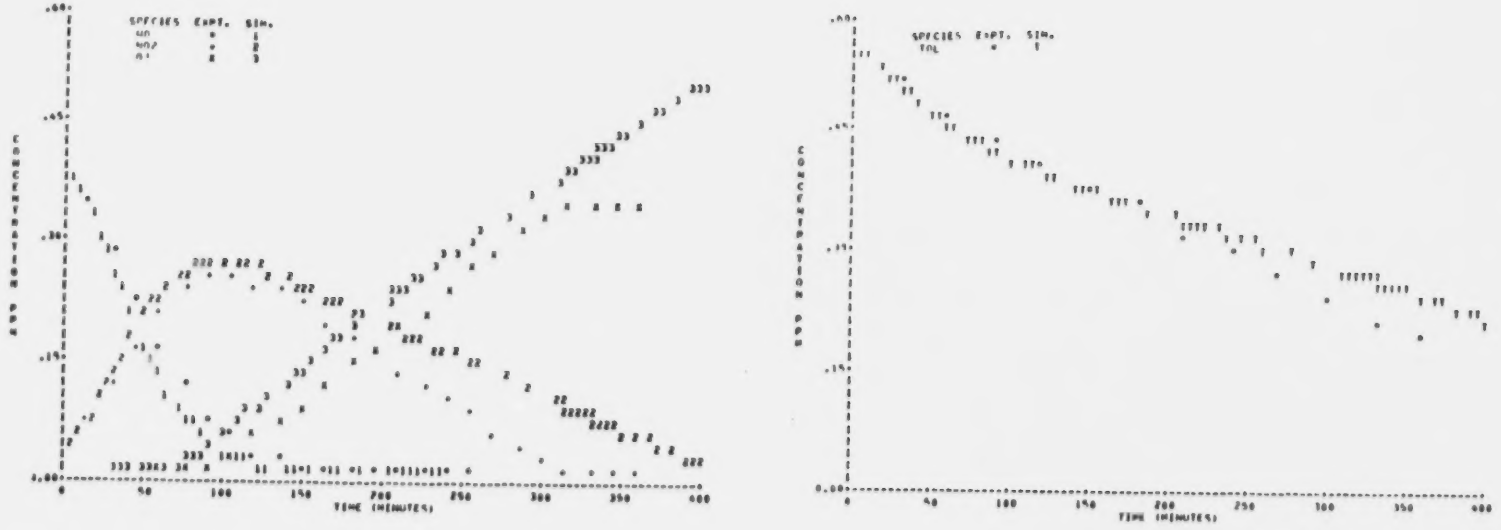

FIGURE A-12 SAPRC EC-270

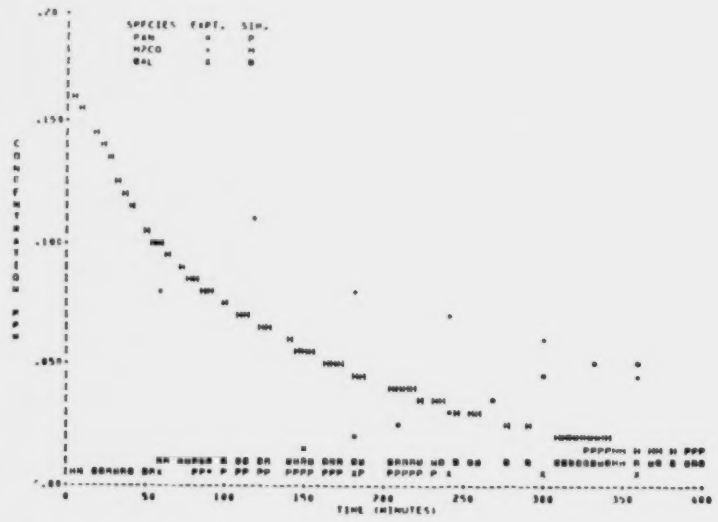

FIGURE A-12 SAPRC EC-270

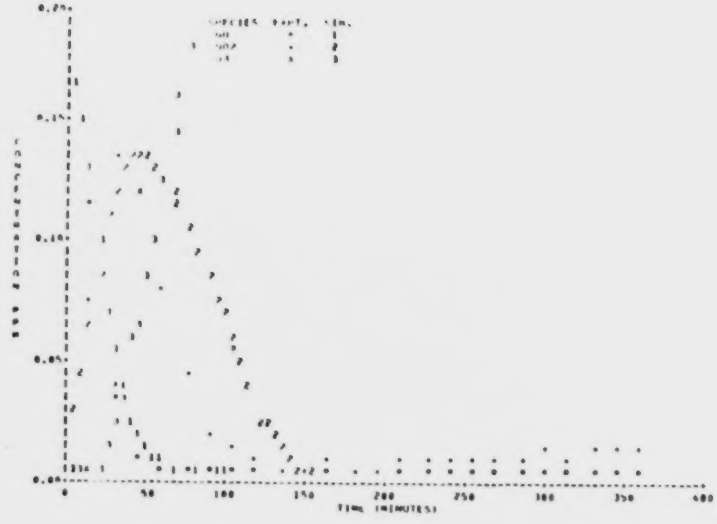

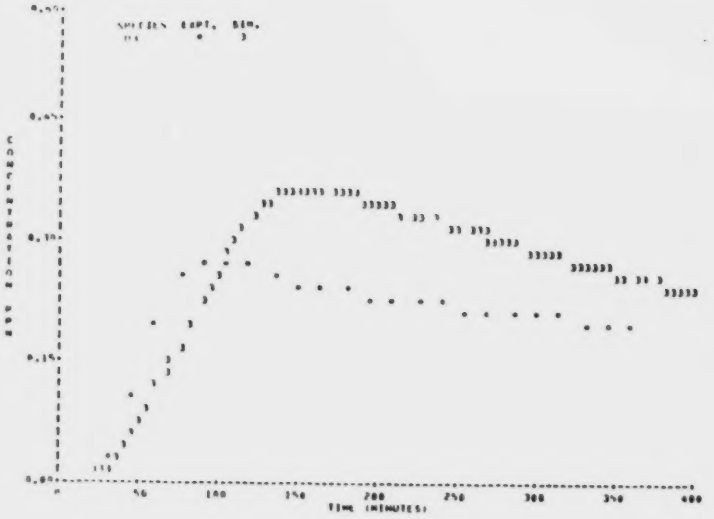

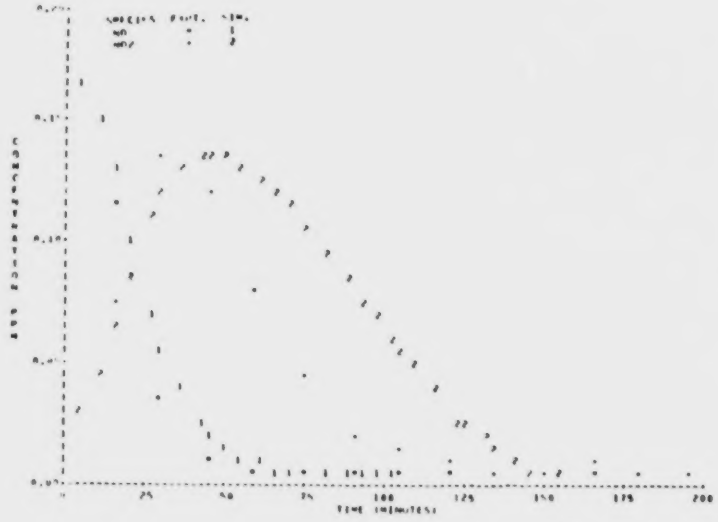

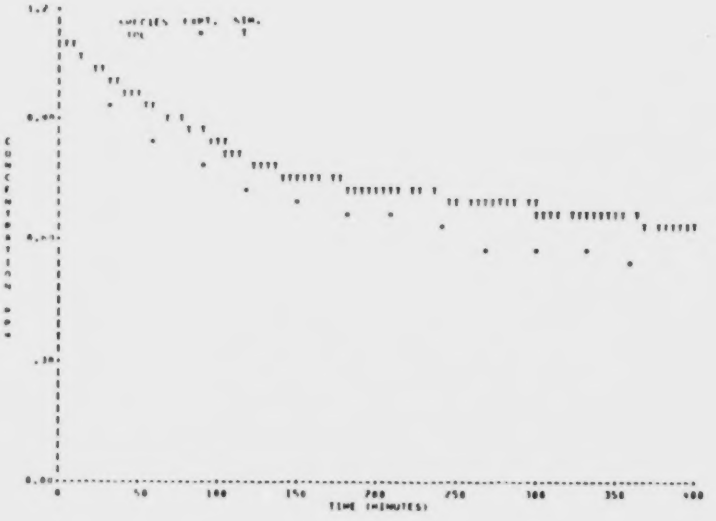

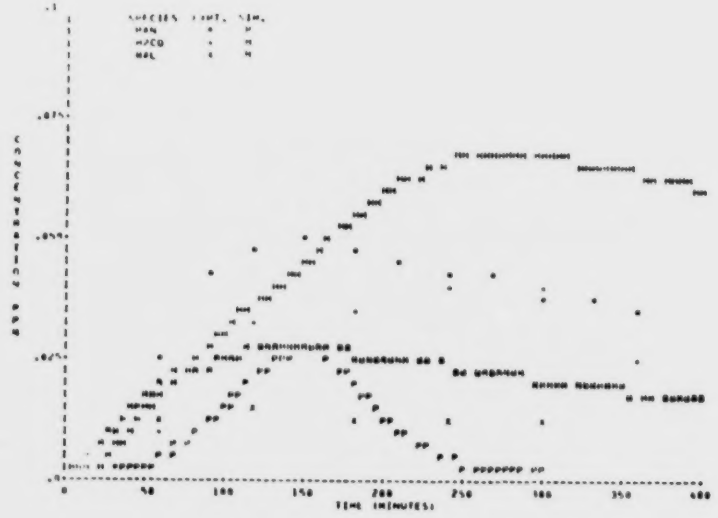

FIGURE A-13 SAPRC EC-271

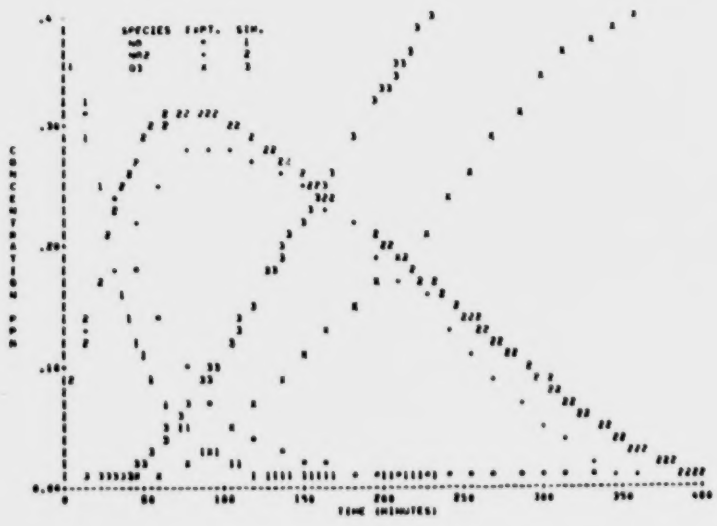
SPECIES EXPT. SIM.
CONCENTRATION PPM
TIME (MINUTES)

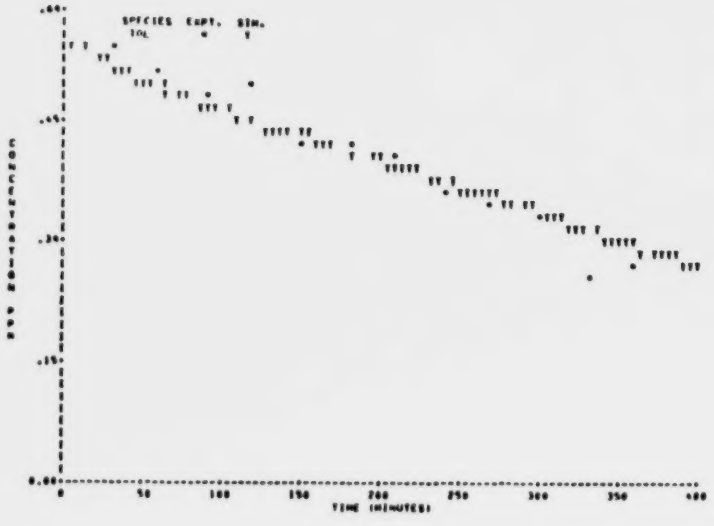
SPECIES EXPT. SIM.
CONCENTRATION PPM
TIME (MINUTES)

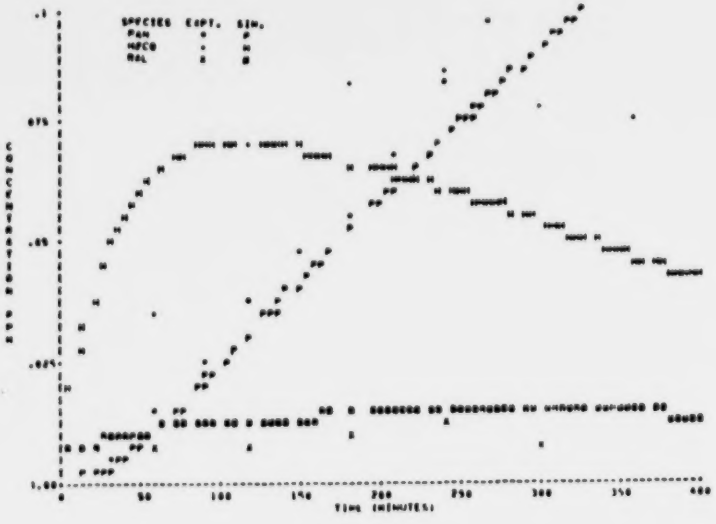
SPECIES EXPT. SIM.
CONCENTRATION PPM
TIME (MINUTES)

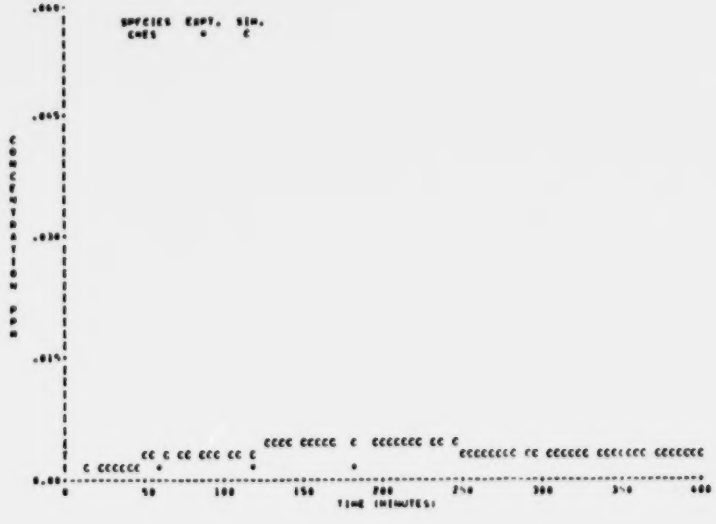
SPECIES EXPT. SIM.
CONCENTRATION PPM
TIME (MINUTES)

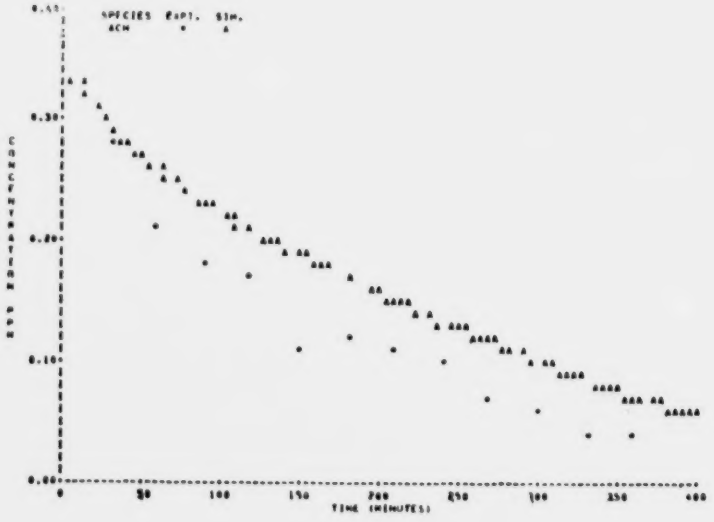

FIGURE A-14 SAPRC EC-272

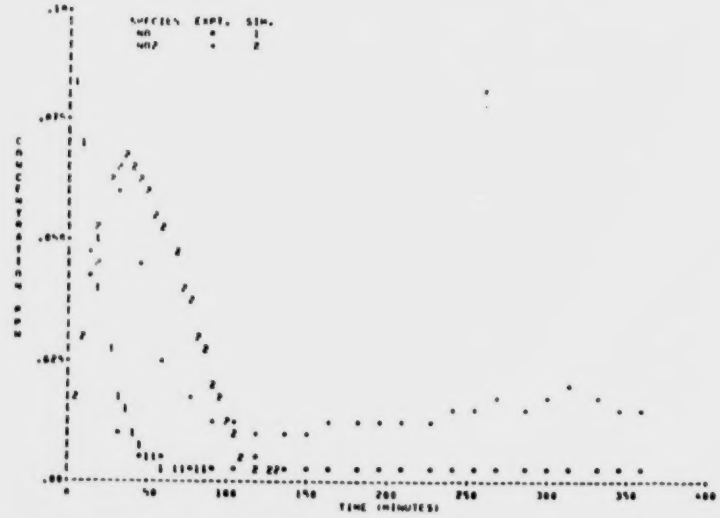
SPECIES EXPT. SIM.
NO
NO2
CONCENTRATION PPM
TIME (MINUTES)

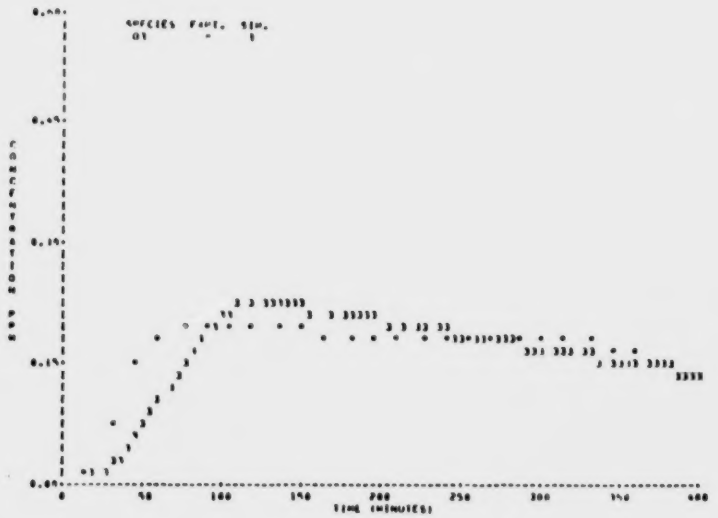
SPECIES EXPT. SIM.
O3
CONCENTRATION PPM
TIME (MINUTES)

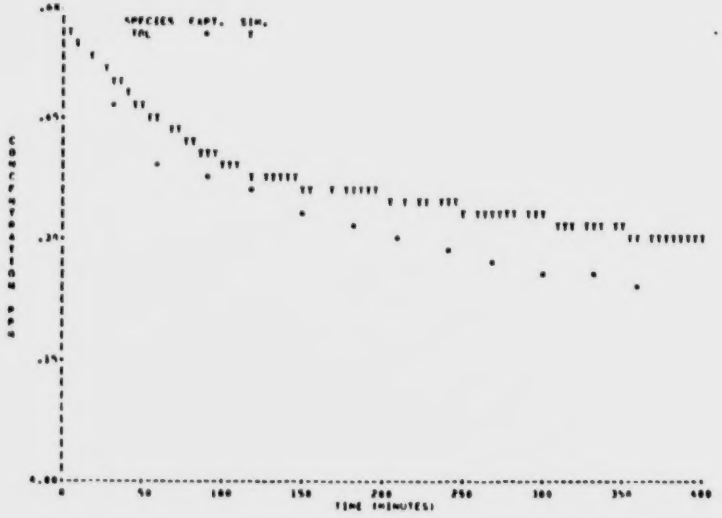
SPECIES EXPT. SIM.
TOL
CONCENTRATION PPM
TIME (MINUTES)

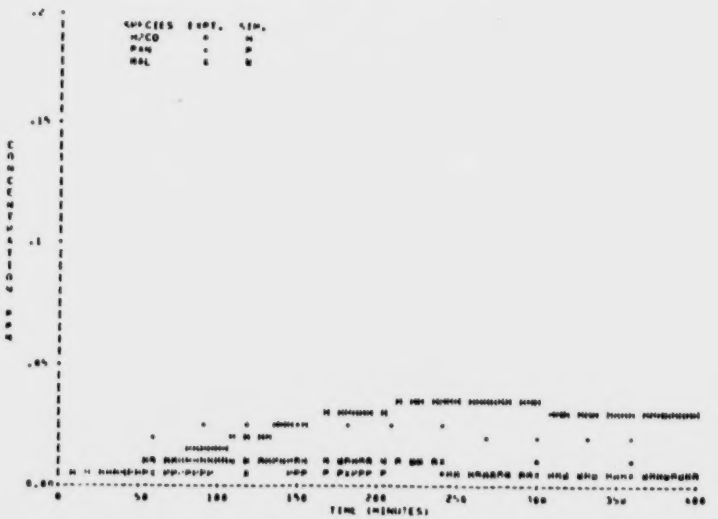
SPECIES EXPT. SIM.
H2CO
PAN
RAL
CONCENTRATION PPM
TIME (MINUTES)

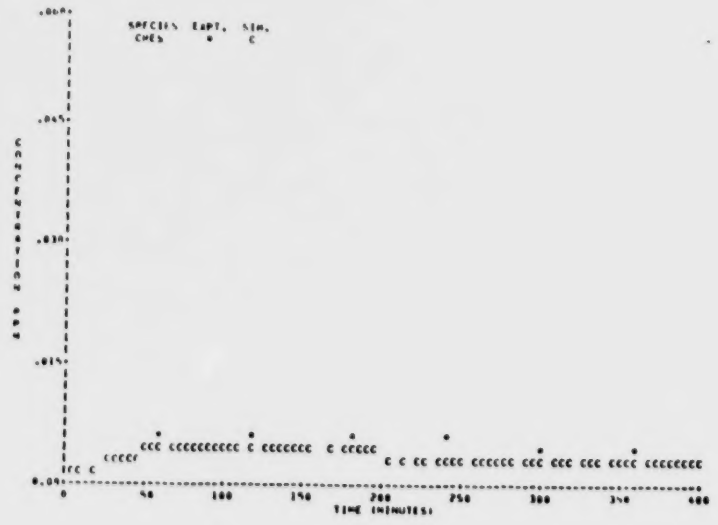

Figure A-15 SAPRC EC-273

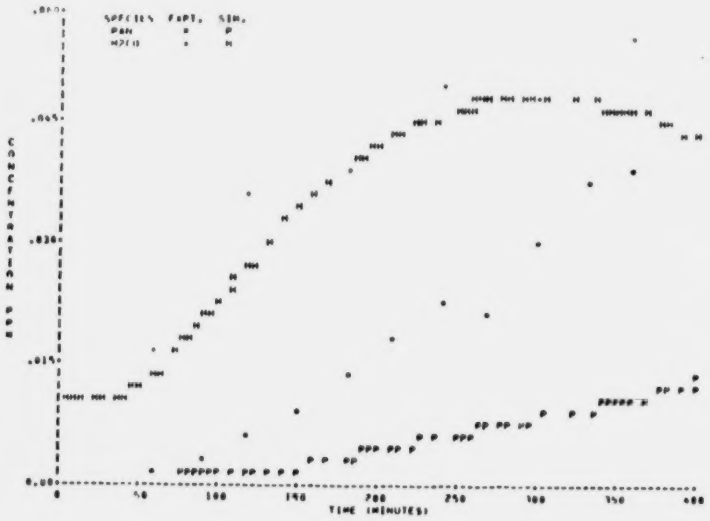

FIGURE A-16 SAPRC EC-327

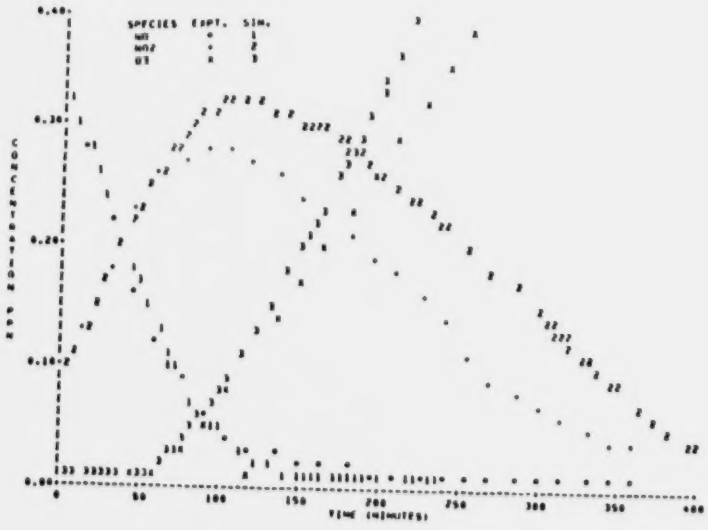
SPECIES EXPT. SIM.
NO
NO2
O3
CONCENTRATION PPM
TIME (MINUTES)

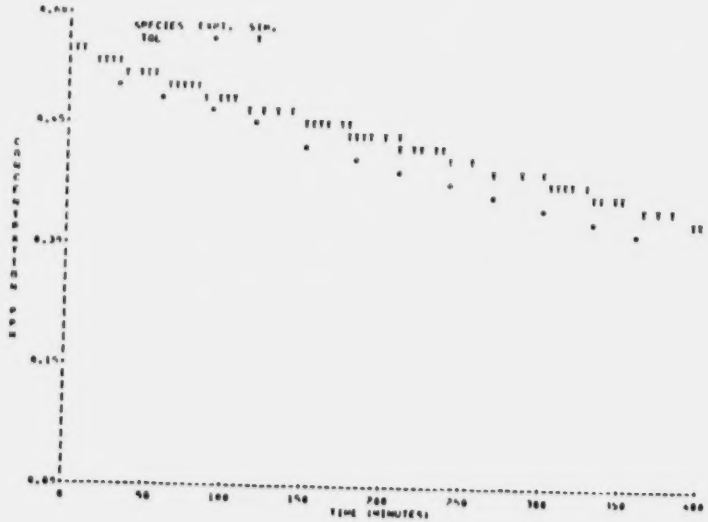
SPECIES EXPT. SIM.
TOL
CONCENTRATION PPM
TIME (MINUTES)

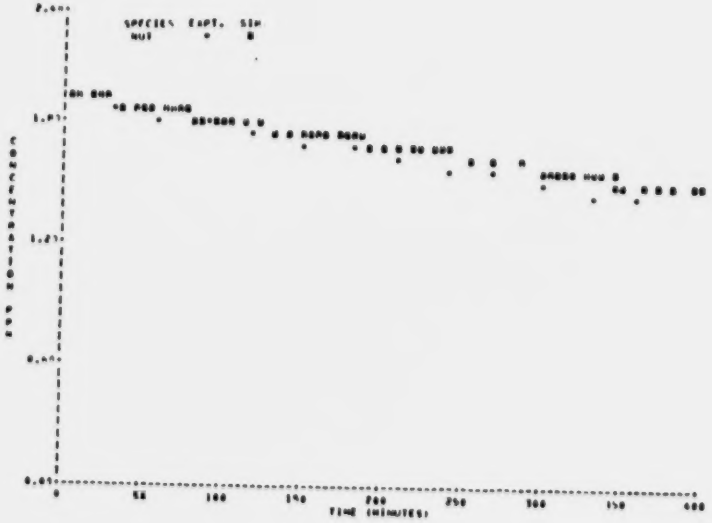
SPECIES EXPT. SIM
NO2
CONCENTRATION PPM
TIME (MINUTES)

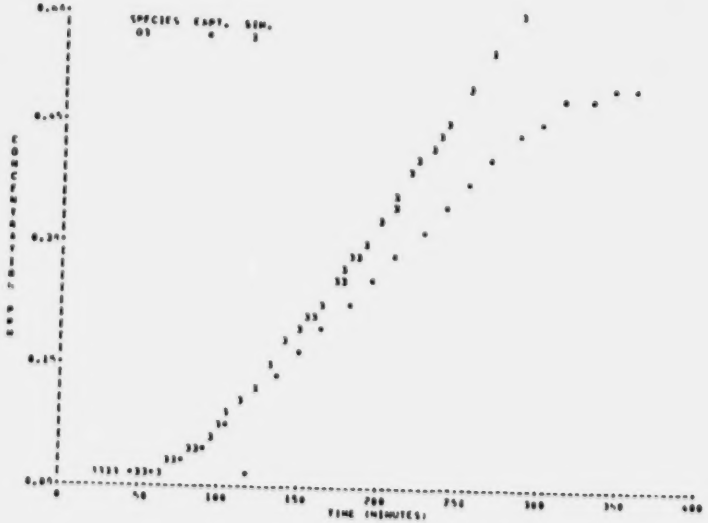
SPECIES EXPT. SIM.
O3
CONCENTRATION PPM
TIME (MINUTES)

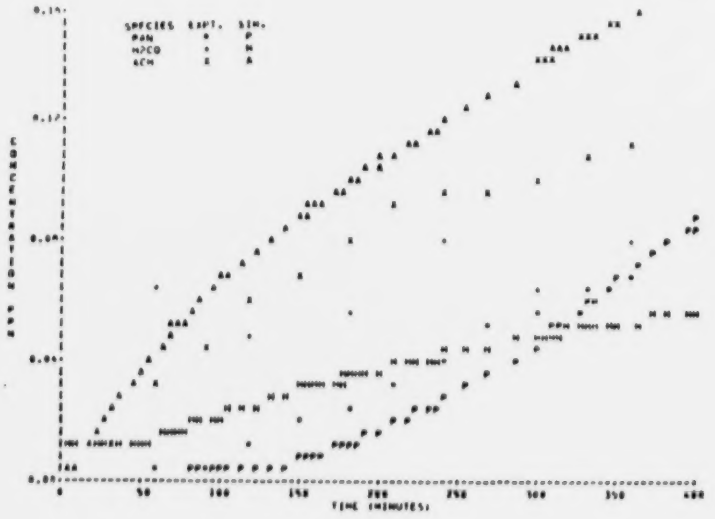

FIGURE A-17 SAPRC EC-328

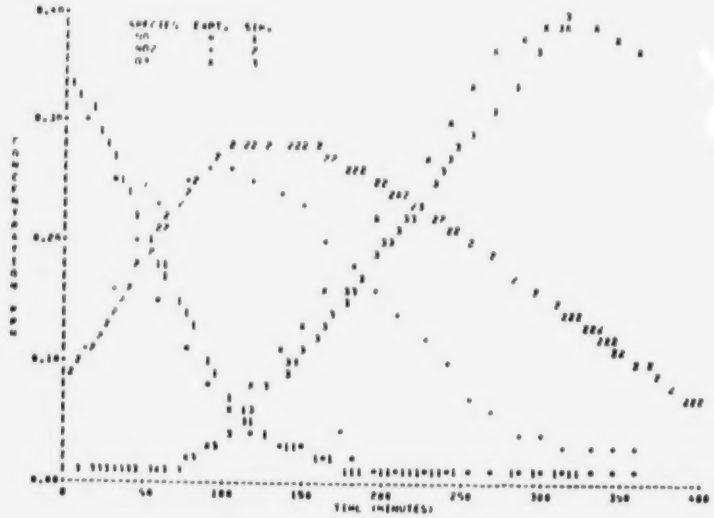
SPECIES EXPT. SIM.
TIME (MINUTES)

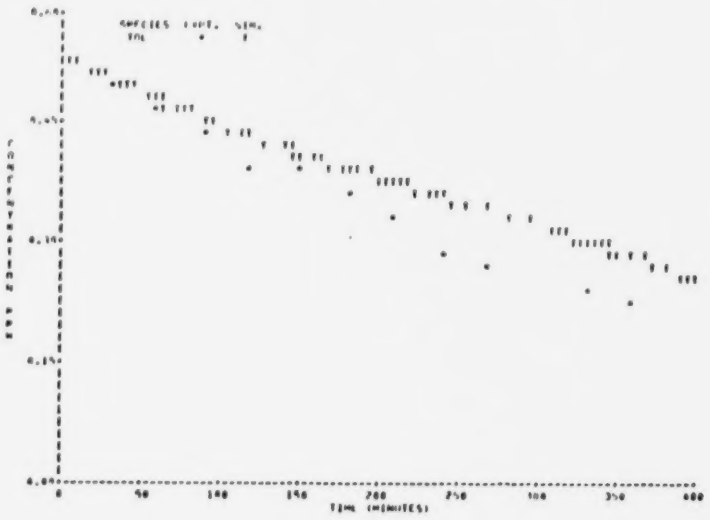
SPECIES EXPT. SIM.
TIME (MINUTES)

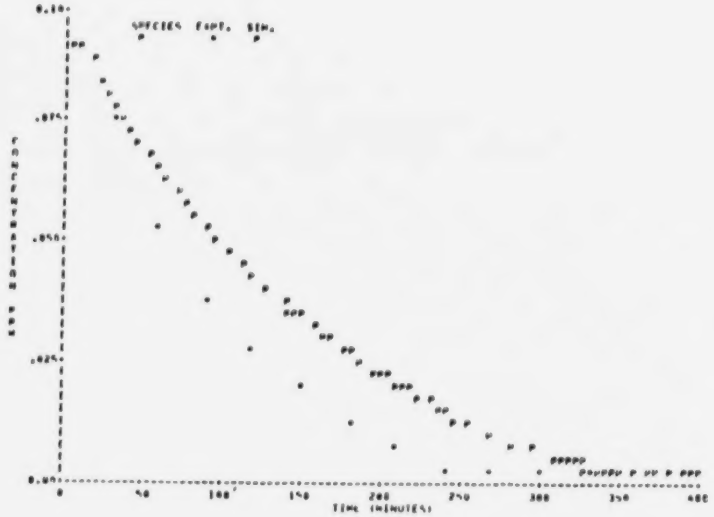
SPECIES EXPT. SIM.
TIME (MINUTES)

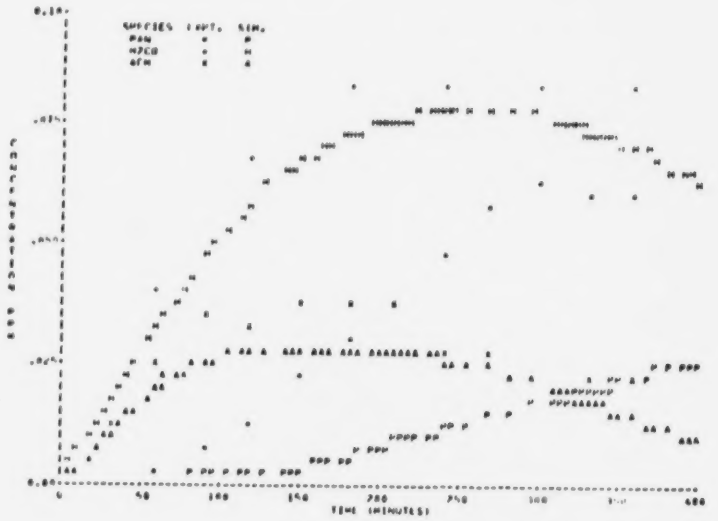
SPECIES EXPT. SIM.
TIME (MINUTES)

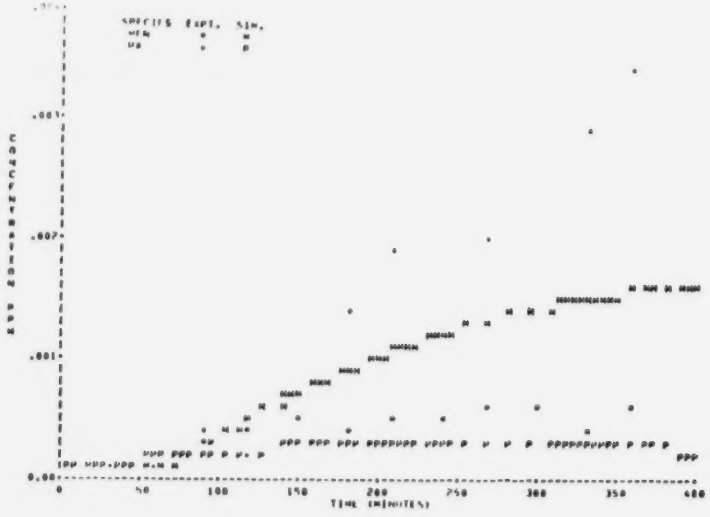

FIGURE A-18 SAPRC EC-329

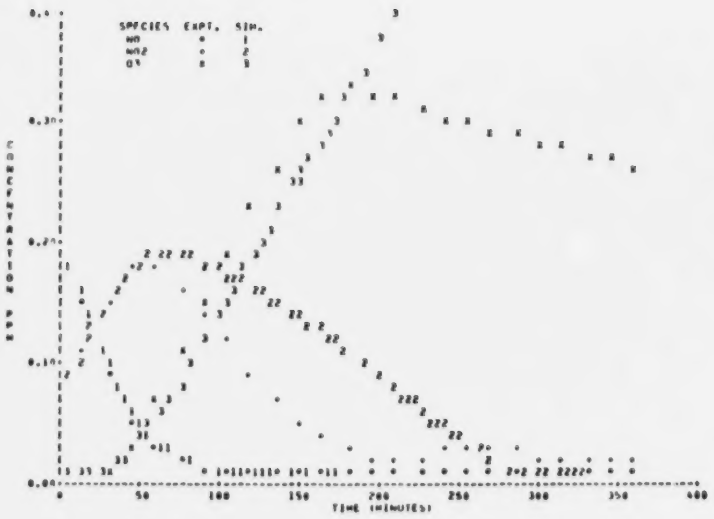

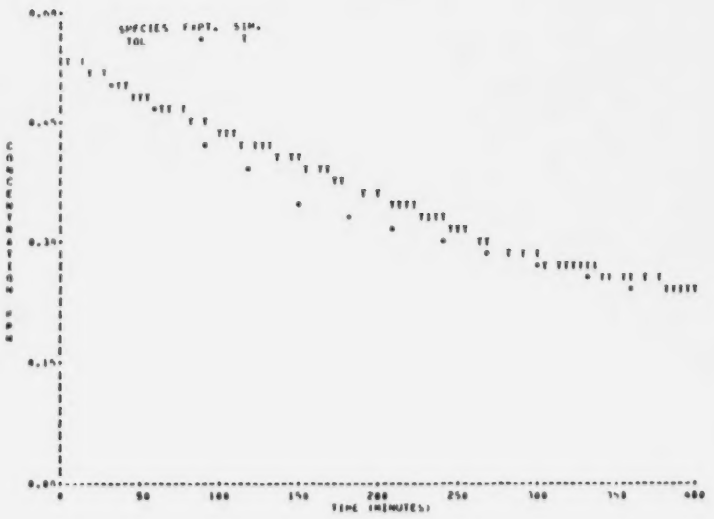

FIGURE A-19 SAPRC EC-330

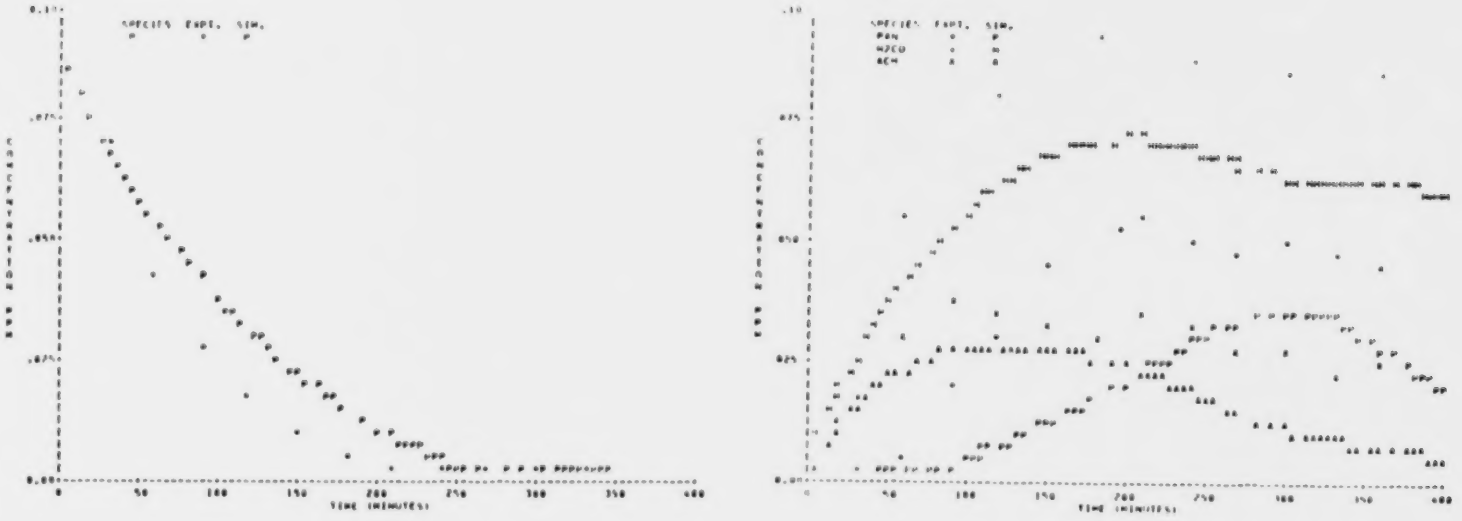

FIGURE A-19 SAPRC EC-330

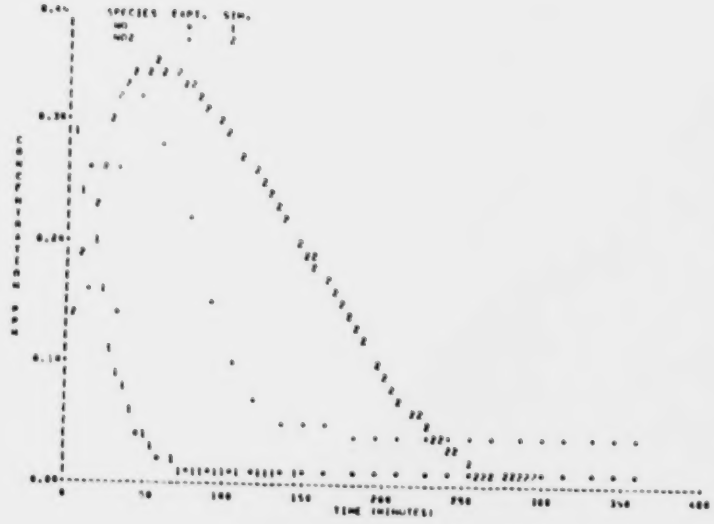
SPECIES EXPT. SIM.
NO
NO2
PPM CONCENTRATION
TIME (MINUTES)

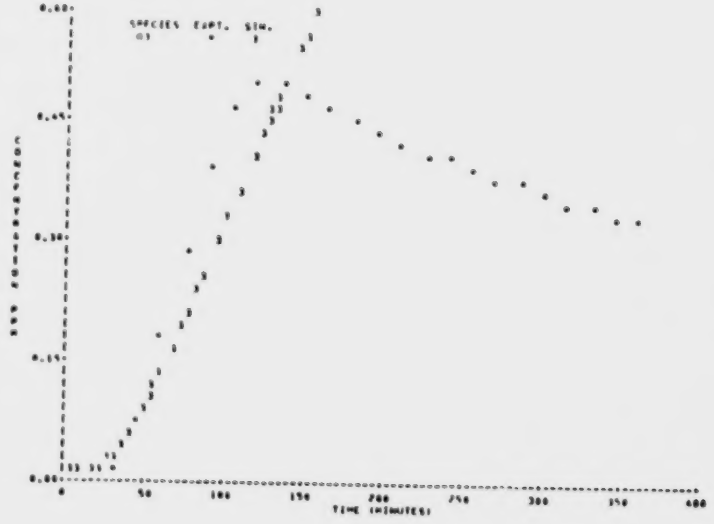
SPECIES EXPT. SIM.
O3
PPM CONCENTRATION
TIME (MINUTES)

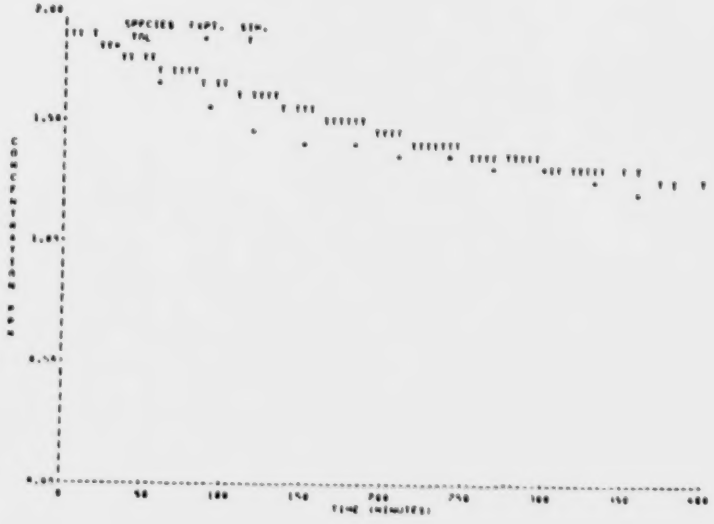
SPECIES EXPT. SIM.
PPM CONCENTRATION
TIME (MINUTES)

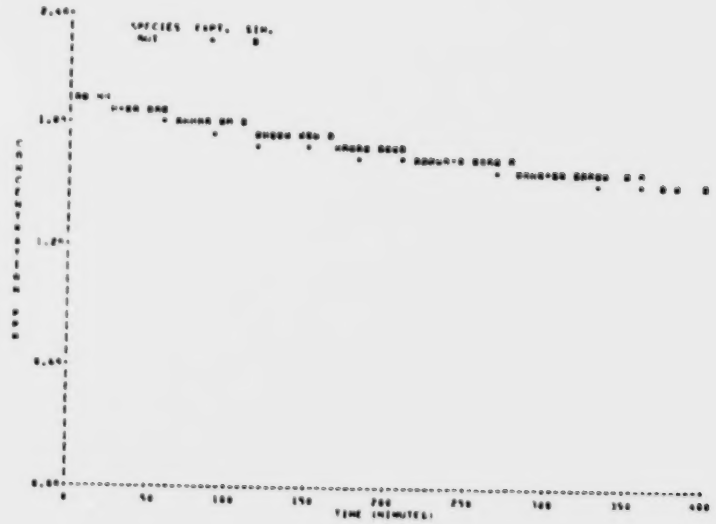
SPECIES EXPT. SIM.
PPM CONCENTRATION
TIME (MINUTES)

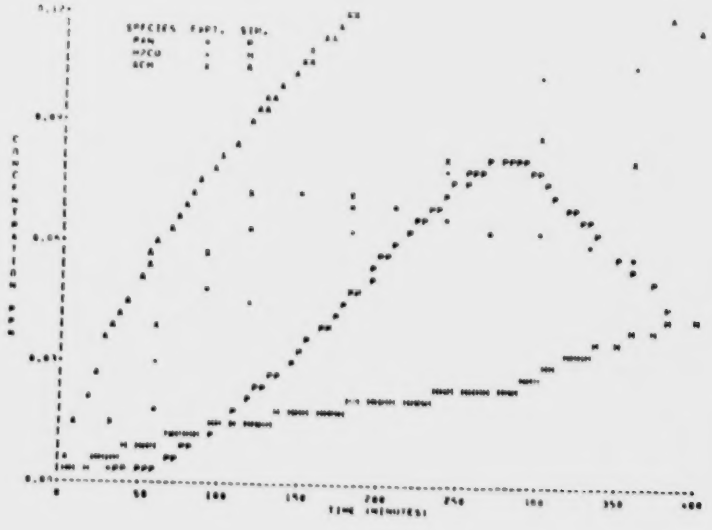

FIGURE A-20 SAPRC EC-331

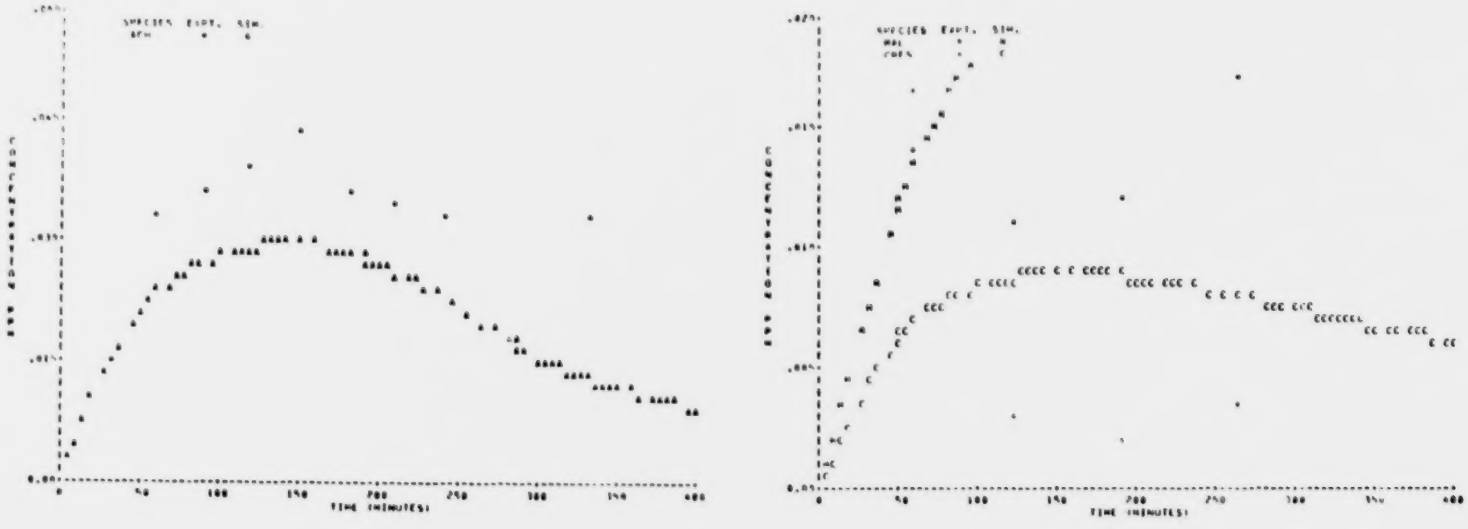

FIGURE A-21 SAPRC EC-334

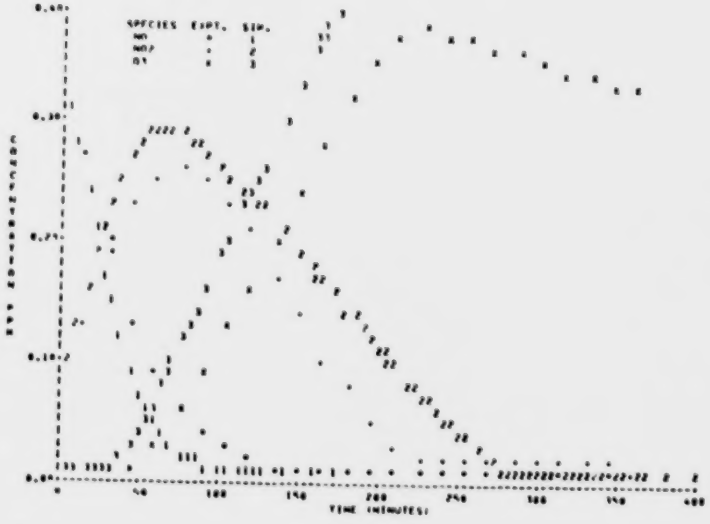
SPECIES EXPT. SIM.
NO
NO2
O3
TIME (MINUTES)

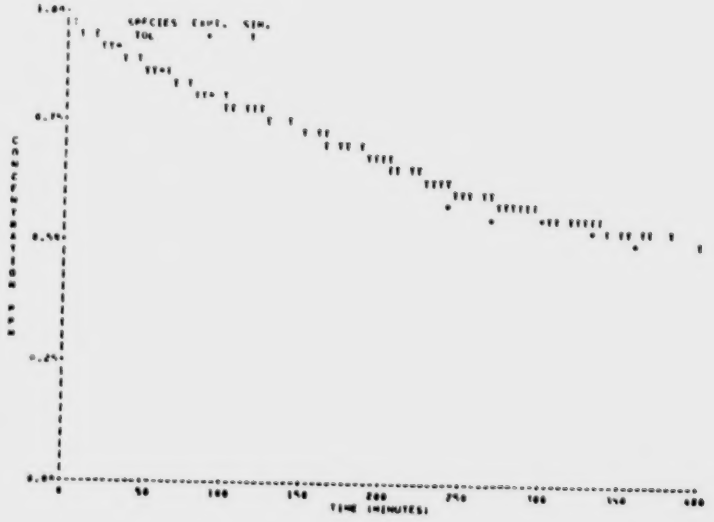
SPECIES EXPT. SIM.
TOL
TIME (MINUTES)

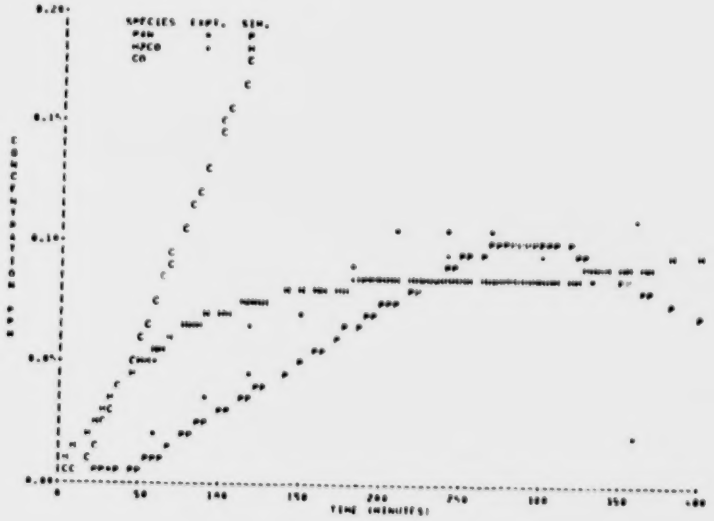
SPECIES EXPT. SIM.
PAN
HPCO
CO
TIME (MINUTES)

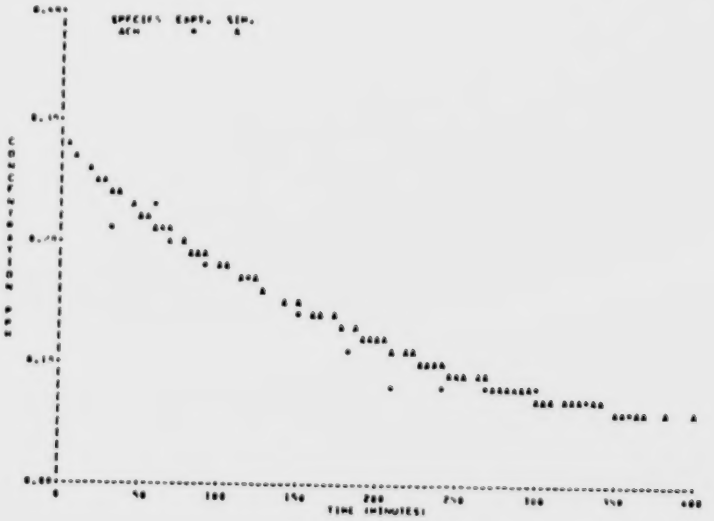
SPECIES EXPT. SIM.
ACH
TIME (MINUTES)

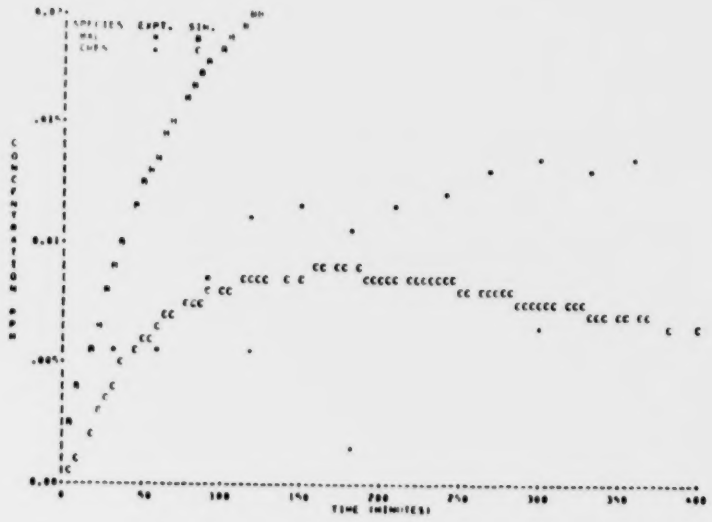

FIGURE A-22 SAPRC EC-335

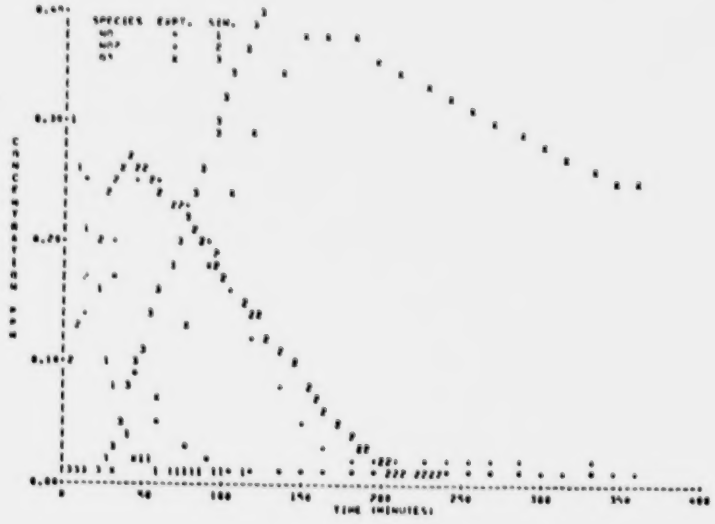
SPECIES EXPT. SIM.
TIME (MINUTES)

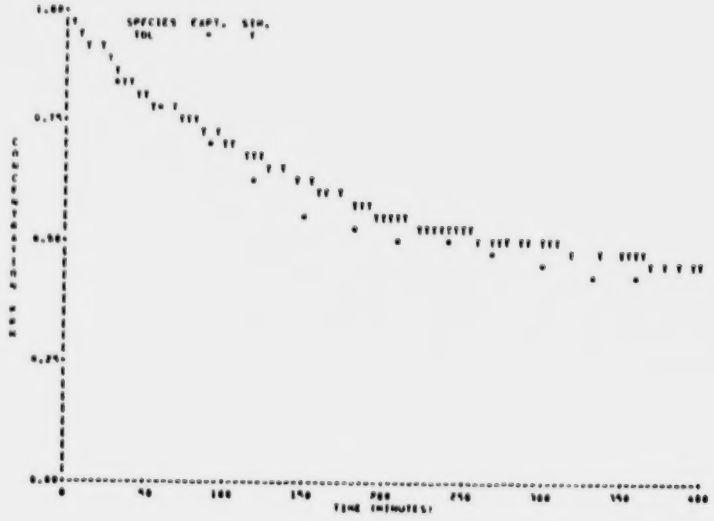
SPECIES EXPT. SIM.
TOL
TIME (MINUTES)

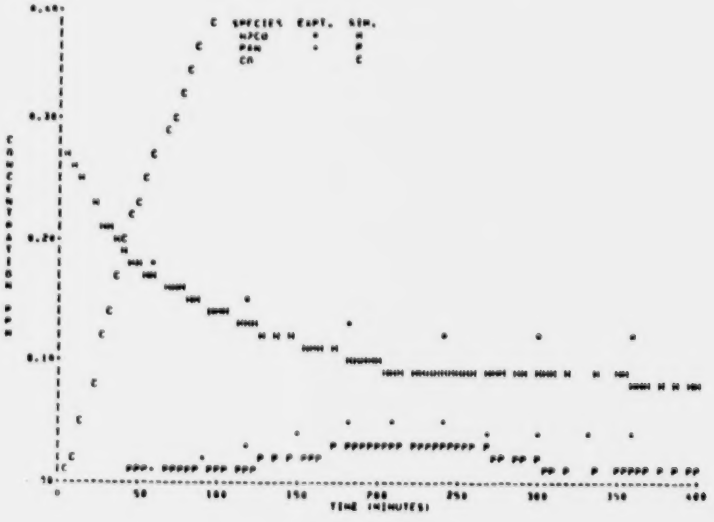
SPECIES EXPT. SIM.
HCHO
PAN
CO
TIME (MINUTES)

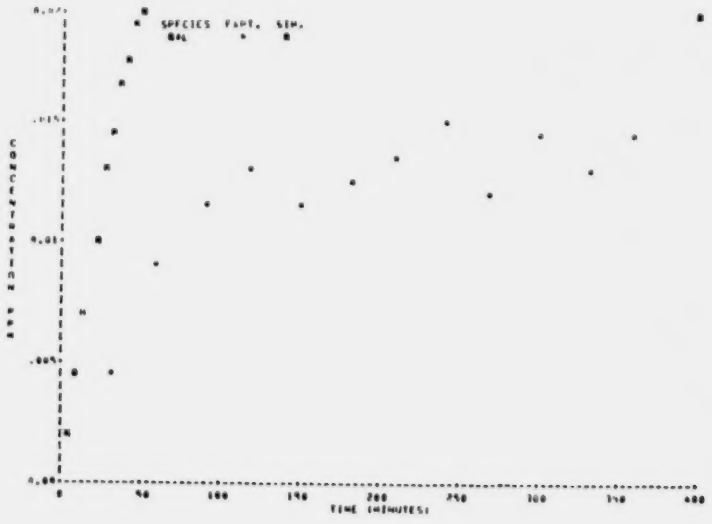

FIGURE A-23 SAPRC EC-336

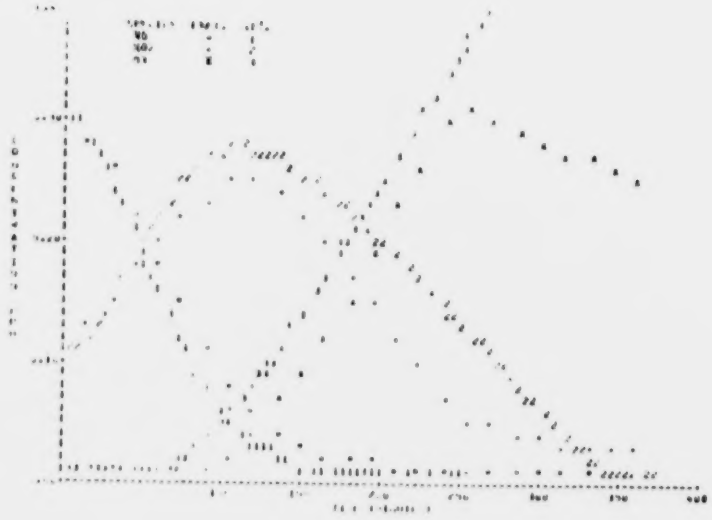

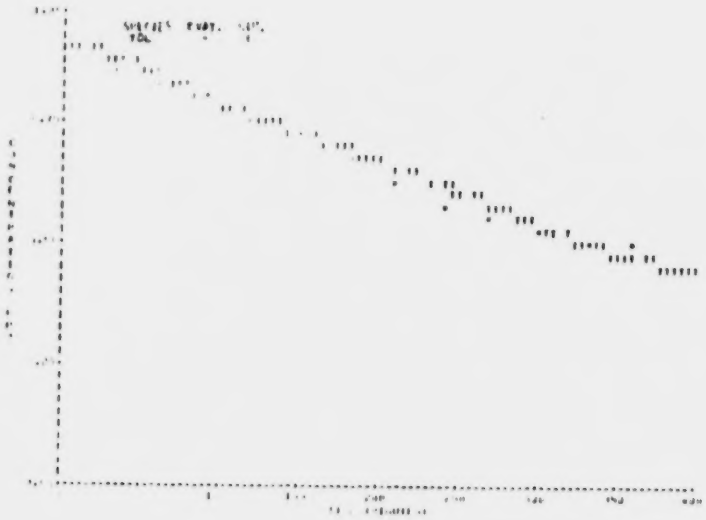

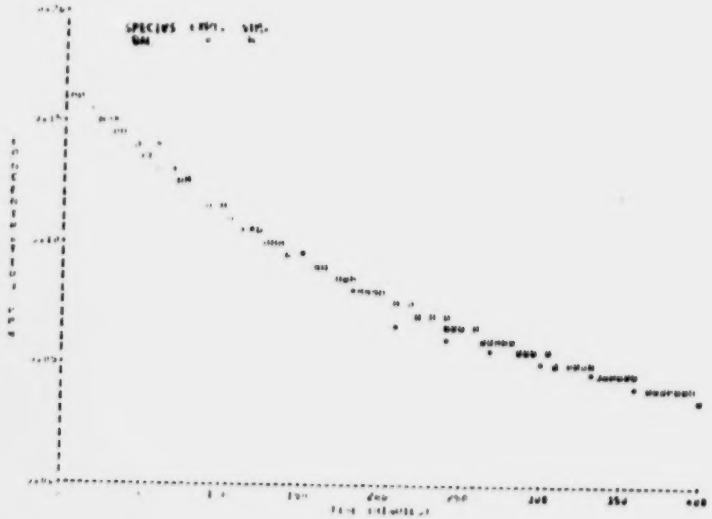

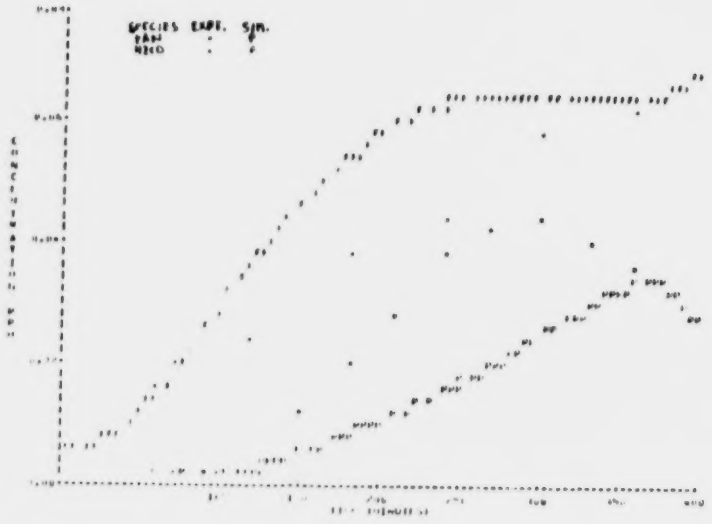

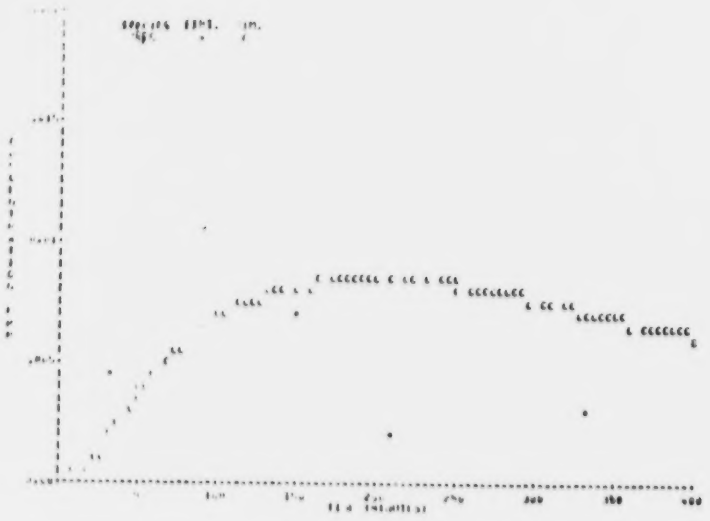

FIGURE A-24 SAPRC EC-337

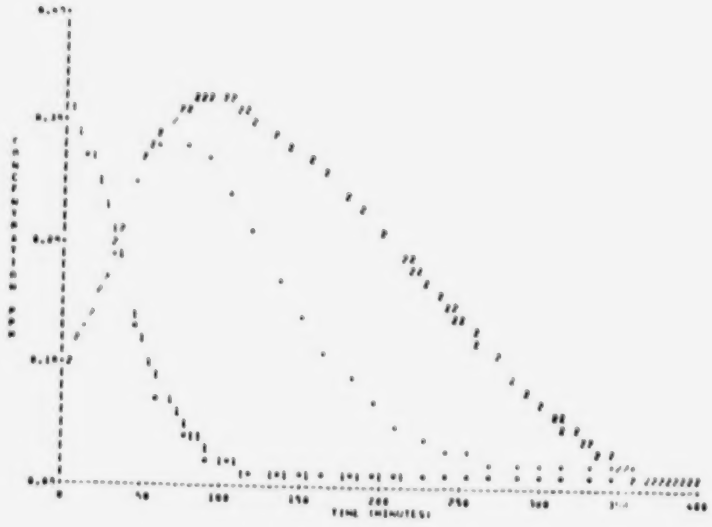

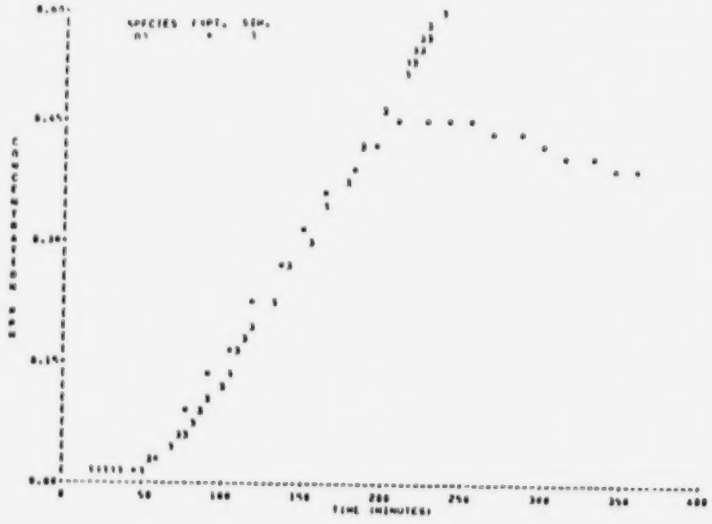
SPECIES EXPT. SIM.
OUT

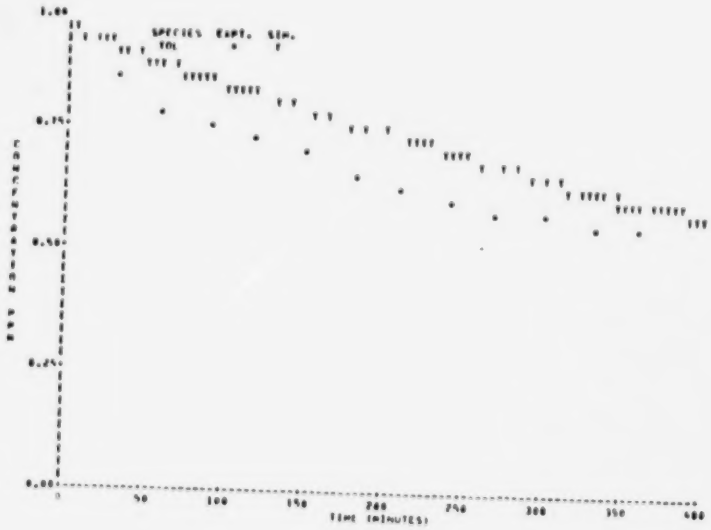
SPECIES EXPT. SIM.
TOL

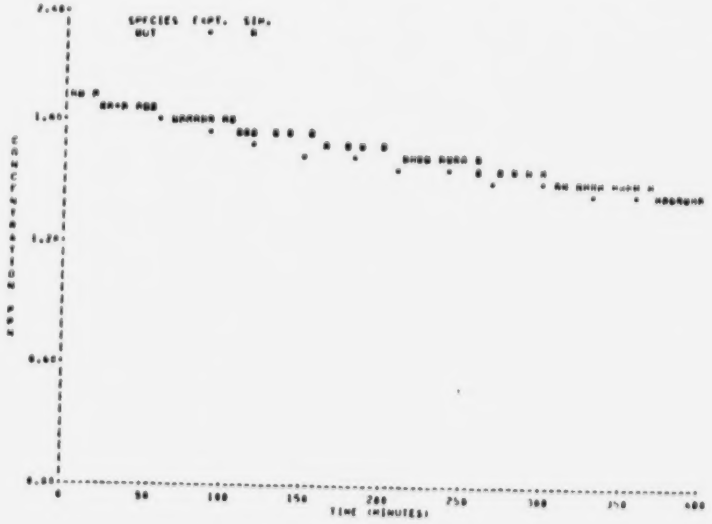
SPECIES EXPT. SIM.
OUT

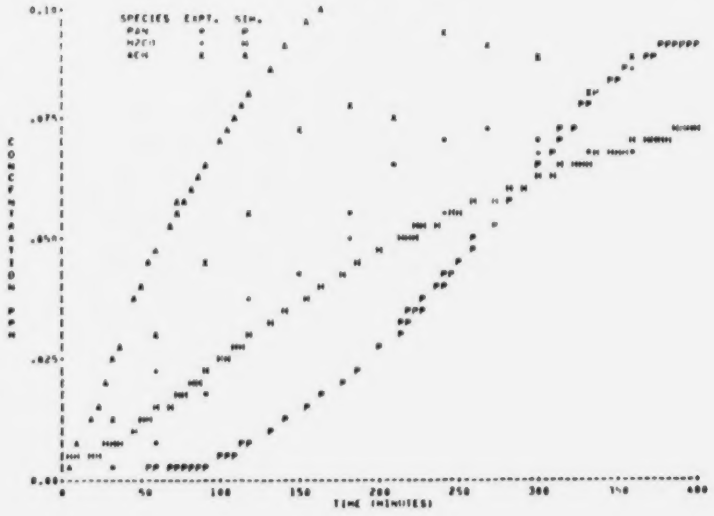

FIGURE A-25 SAPRC EC-338

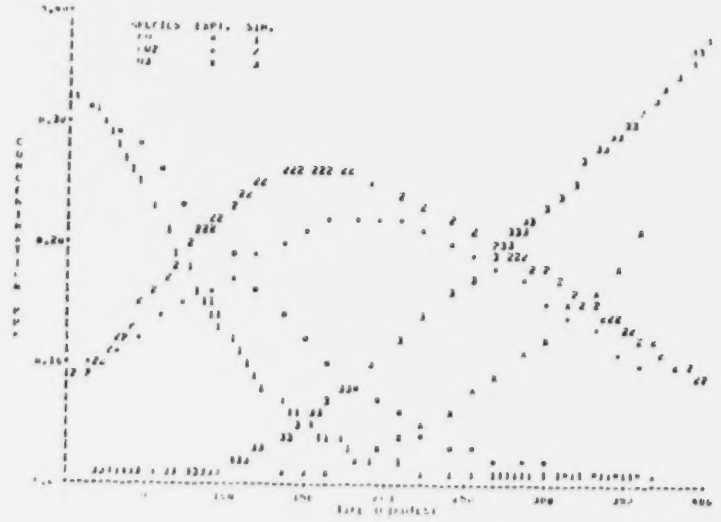

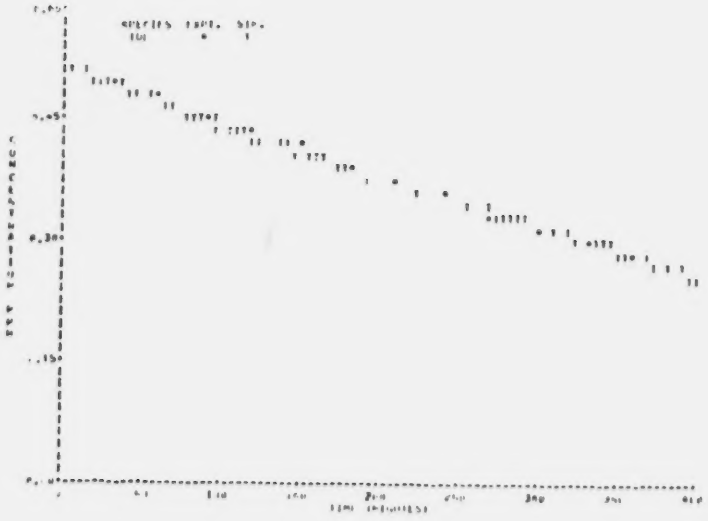

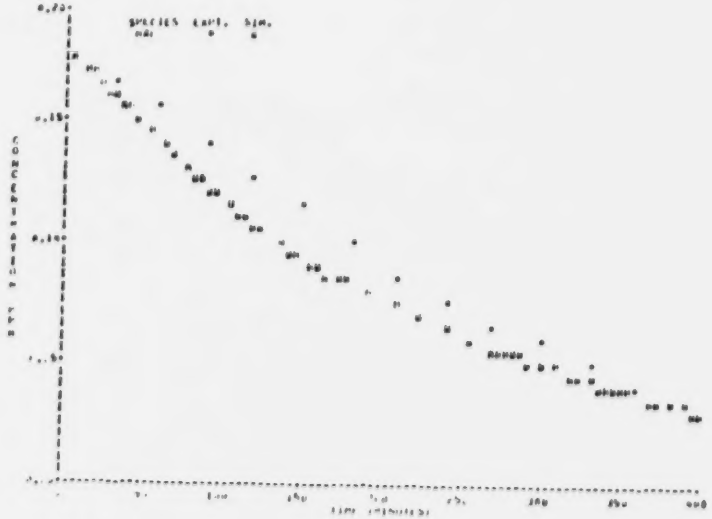

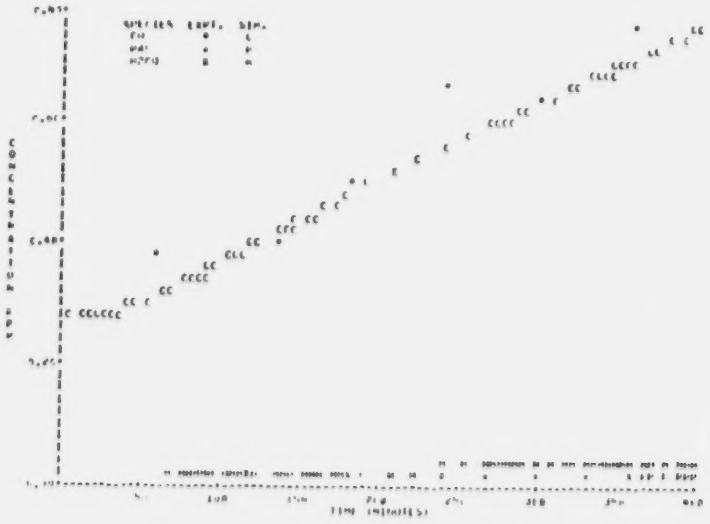

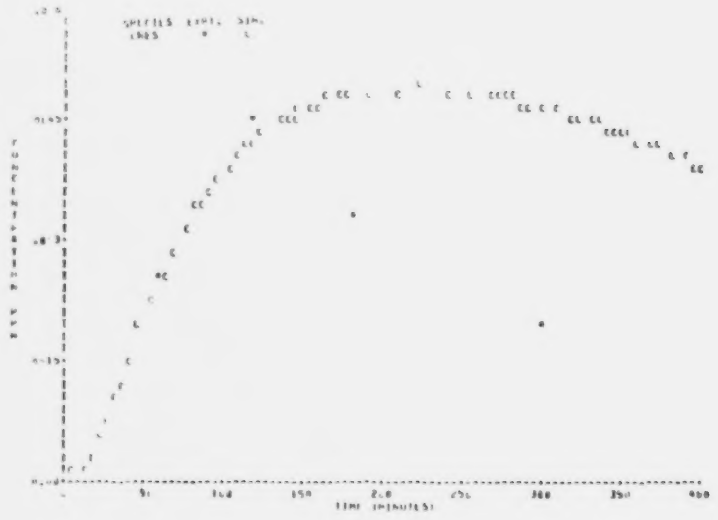

FIGURE A-26 SAPRC EC-339

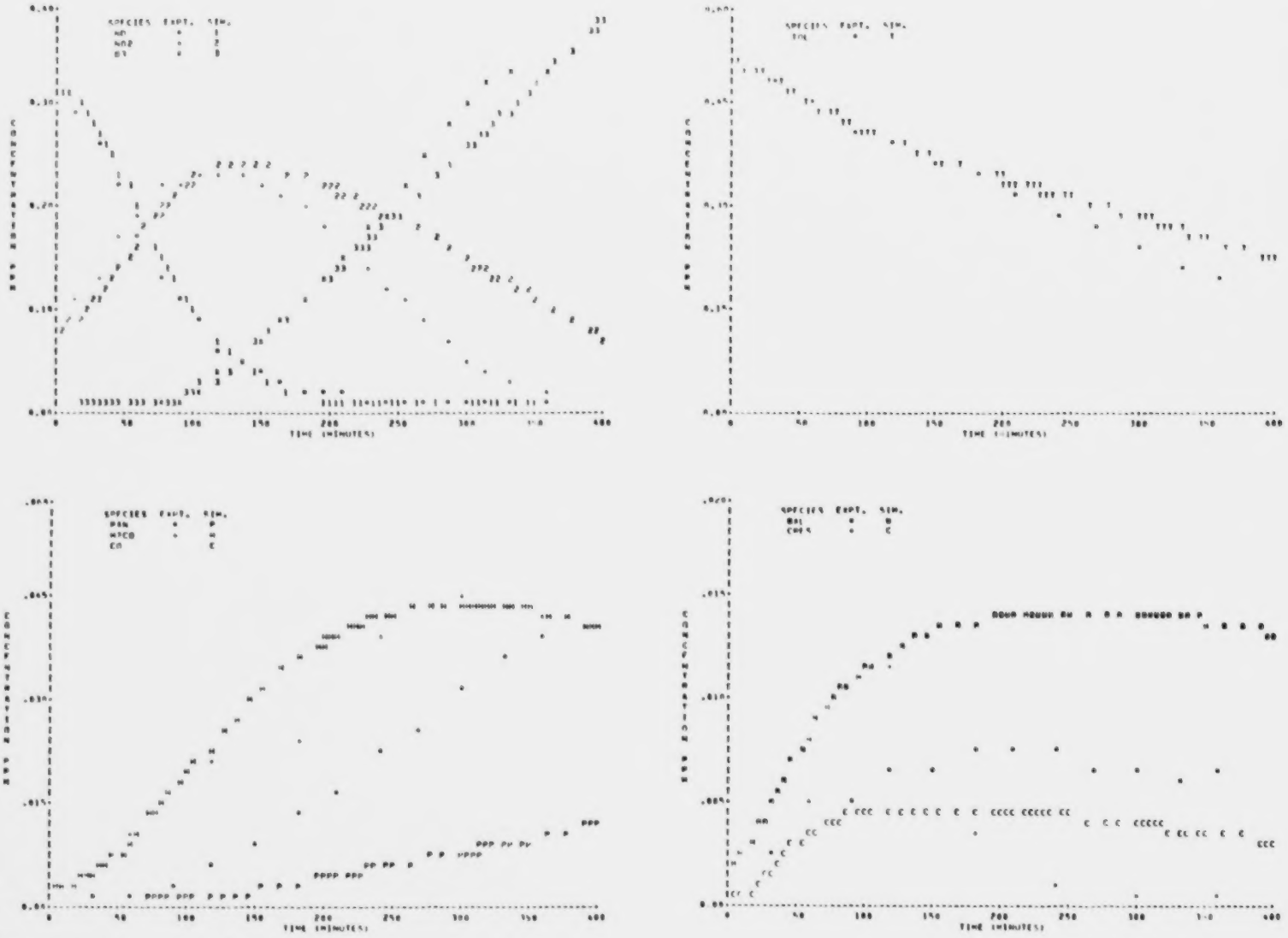

FIGURE A-27 SAPRC EC-340

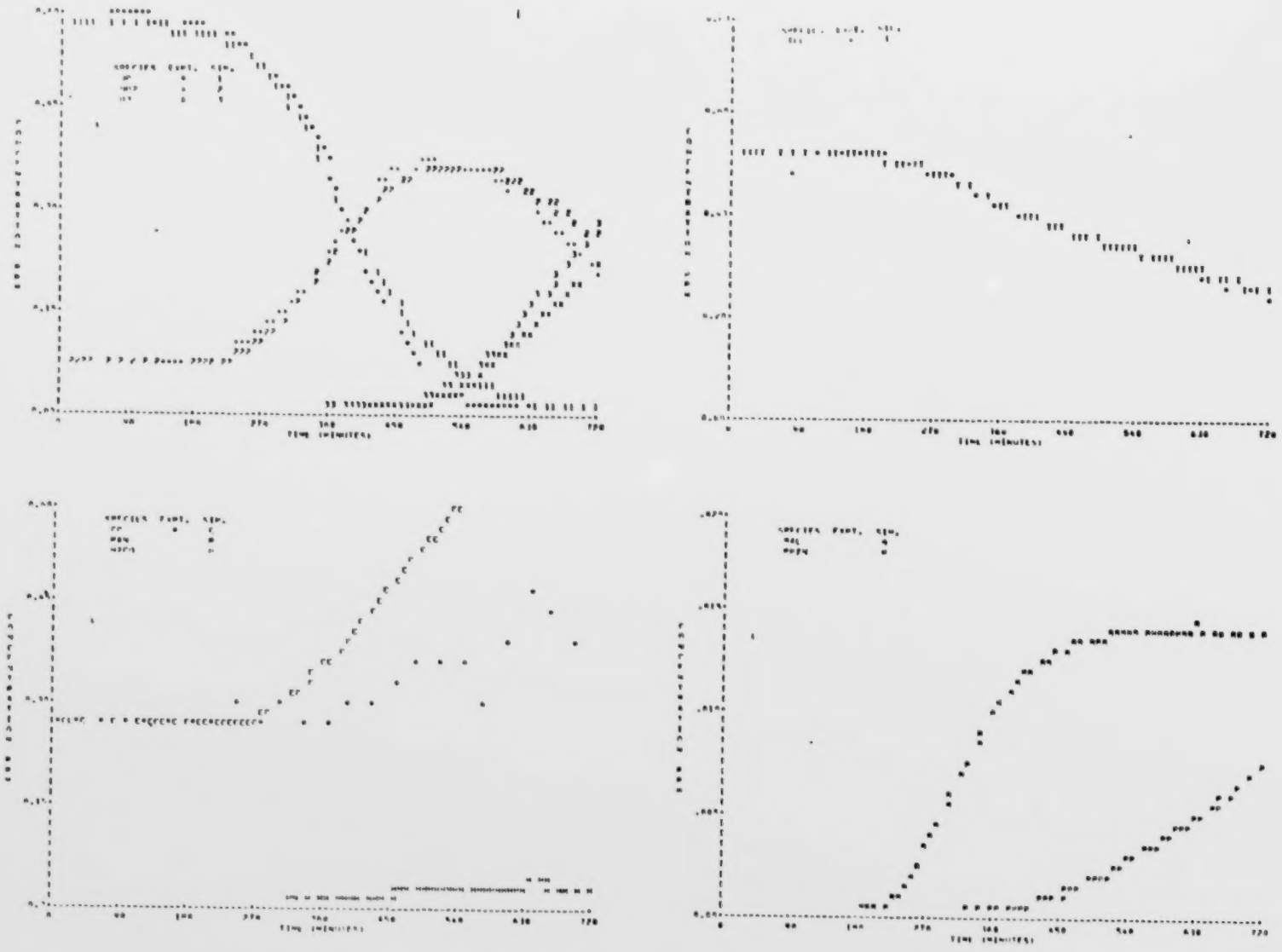

FIGURE A-28 UNC 8.16.78 RED

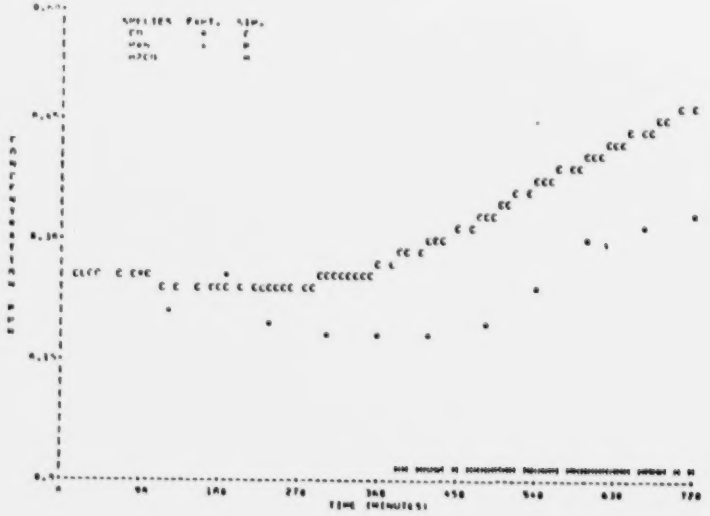

FIGURE A-29 UNC 9.14.78 RED

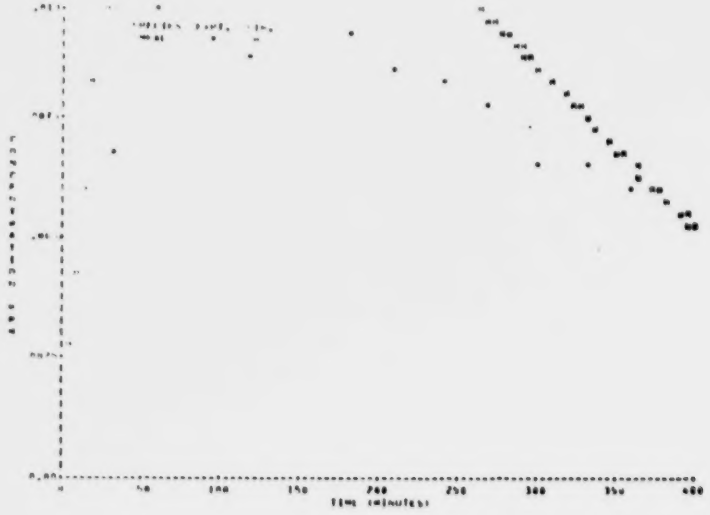

FIGURE A-30 SAPRC EC-343

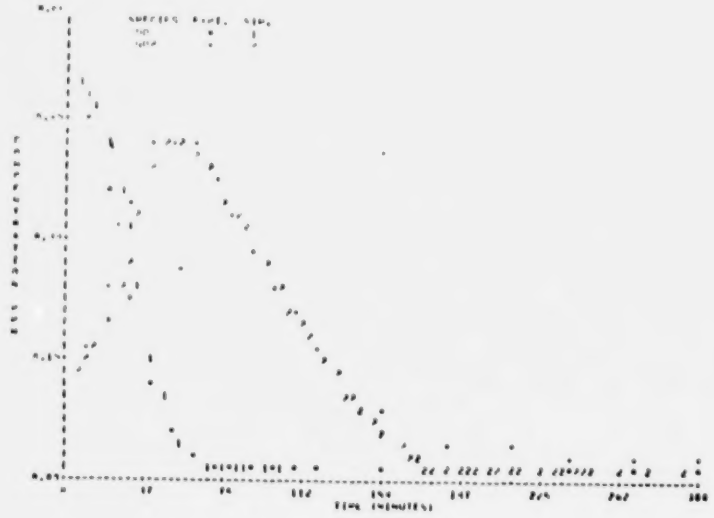

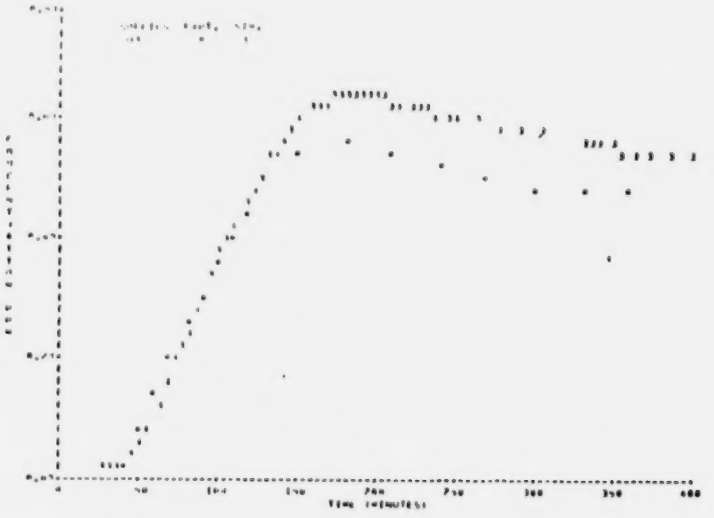

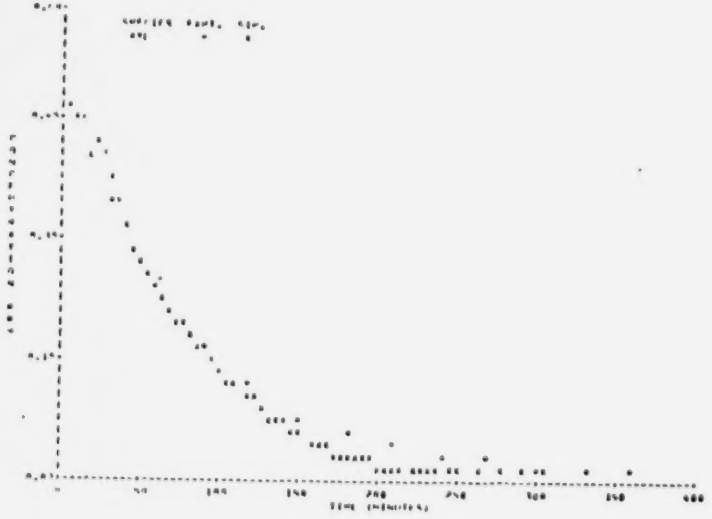

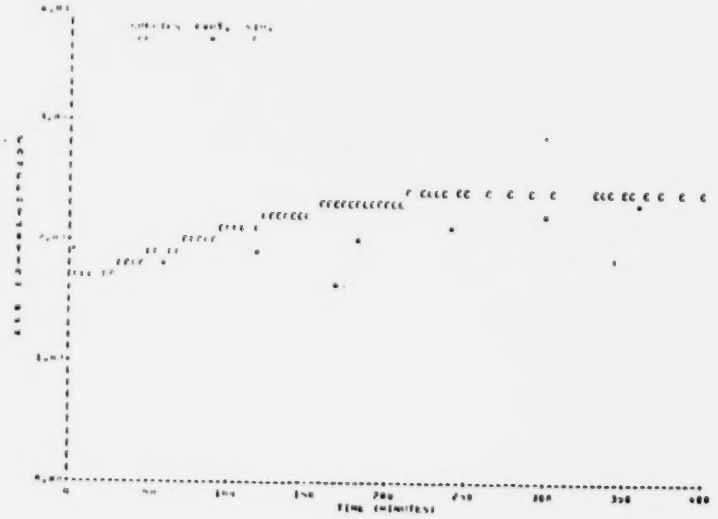

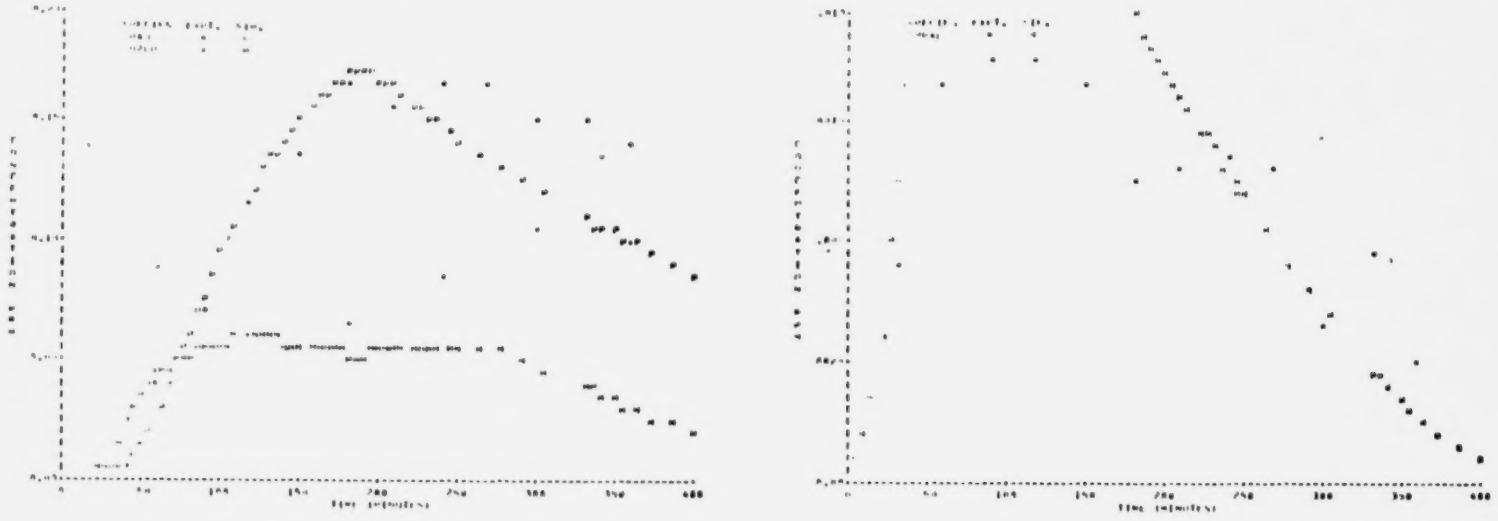

FIGURE A-31 SAPRC EC-344

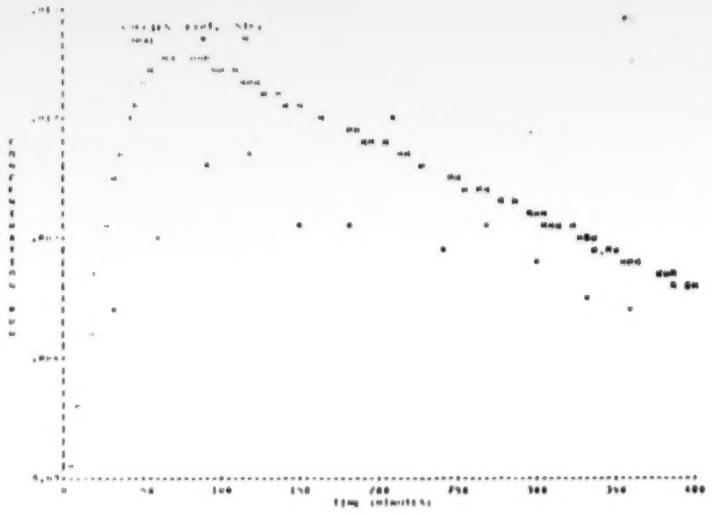

FIGURE A-32 SAPRCE EC-345

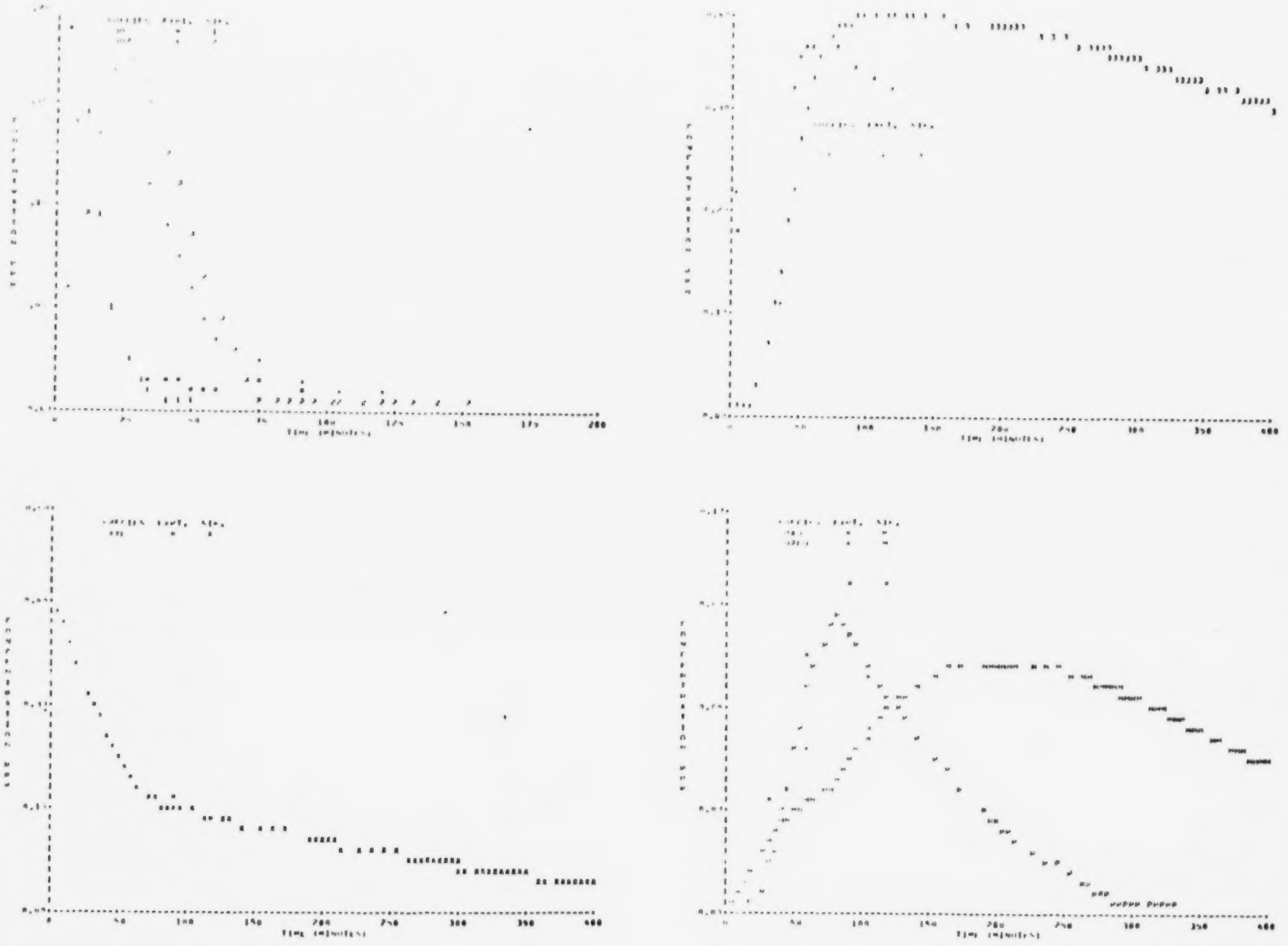

FIGURE A-33 SAPRC EC-346

Appendix B

SIMULATION OF ALKENE CHAMBER RUNS

TABLE B-1. PHOTOLYSIS RATE CONSTANTS FOR PROPENE AND ALKENE CHAMBER RUNS (in min^{-1})

EC-No.	NO_2	HNO_2	H_2O_2	$O_3(^1D)$	$O_3(^3P)$	H_2CO(rad)	H_2CO(molec)	CH_3CHO
142-143	0.33	9.5×10^{-2}	6.5×10^{-4}	1.1×10^{-3}	1.2×10^{-3}	9.0×10^{-4}	2.4×10^{-3}	4.4×10^{-4}
156	0.33	9.5×10^{-2}	6.5×10^{-4}	1.1×10^{-3}	1.2×10^{-3}	9.0×10^{-4}	2.4×10^{-3}	4.4×10^{-4}
256-257	0.30	8.0×10^{-2}	5.7×10^{-4}	8.4×10^{-4}	1.2×10^{-3}	8.4×10^{-4}	1.6×10^{-3}	4.0×10^{-4}
276-279	0.35	0.11	7.6×10^{-4}	1.2×10^{-3}	1.7×10^{-3}	1.2×10^{-3}	2.1×10^{-3}	6.0×10^{-4}
285-287	0.39	0.12	6.5×10^{-4}	1.3×10^{-3}	1.8×10^{-3}	1.3×10^{-3}	2.4×10^{-3}	6.5×10^{-4}
314	0.48	0.14	1.0×10^{-3}	1.5×10^{-3}	2.2×10^{-3}	1.1×10^{-3}	3.4×10^{-3}	8.0×10^{-4}
315	0.49	0.15	1.1×10^{-3}	1.7×10^{-3}	2.3×10^{-3}	1.2×10^{-3}	3.4×10^{-3}	8.0×10^{-4}
316	0.51	0.15	1.1×10^{-3}	1.7×10^{-3}	2.3×10^{-3}	1.2×10^{-3}	3.4×10^{-3}	8.0×10^{-4}
317-318	0.53	0.16	1.1×10^{-3}	1.3×10^{-3}	2.3×10^{-3}	1.2×10^{-3}	3.5×10^{-3}	8.0×10^{-4}
319-320	0.55	0.16	1.1×10^{-3}	1.2×10^{-3}	2.3×10^{-3}	1.2×10^{-3}	3.7×10^{-3}	8.0×10^{-4}

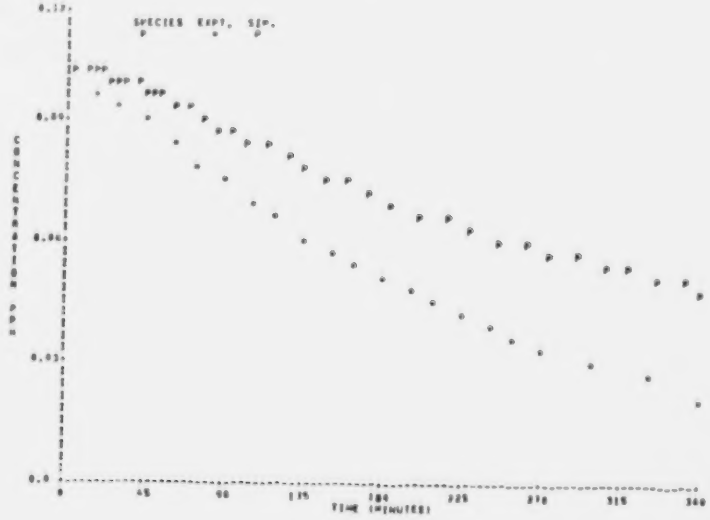

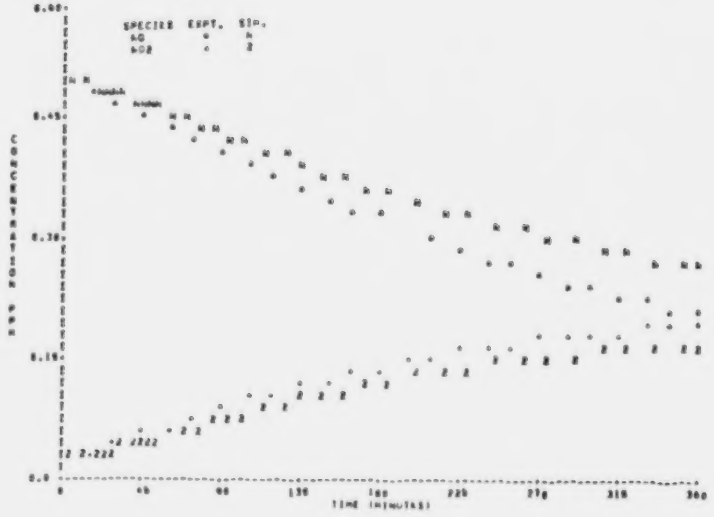

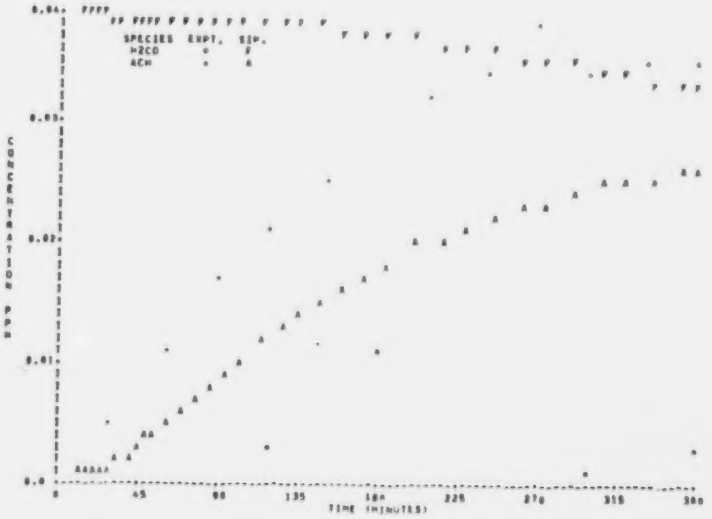

FIGURE B-1 SAPRC EC-256

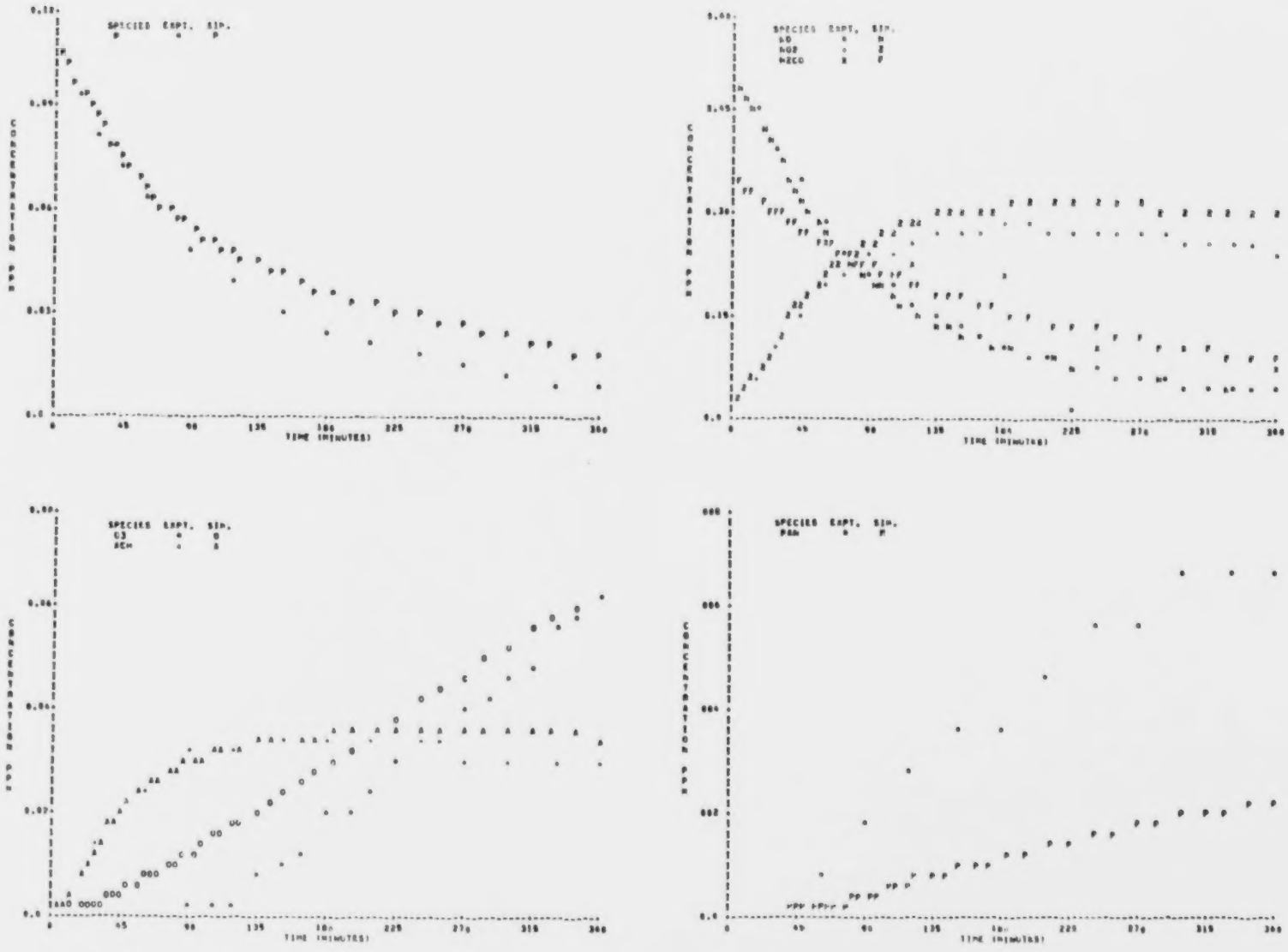

FIGURE B-2 SAPRC EC-257

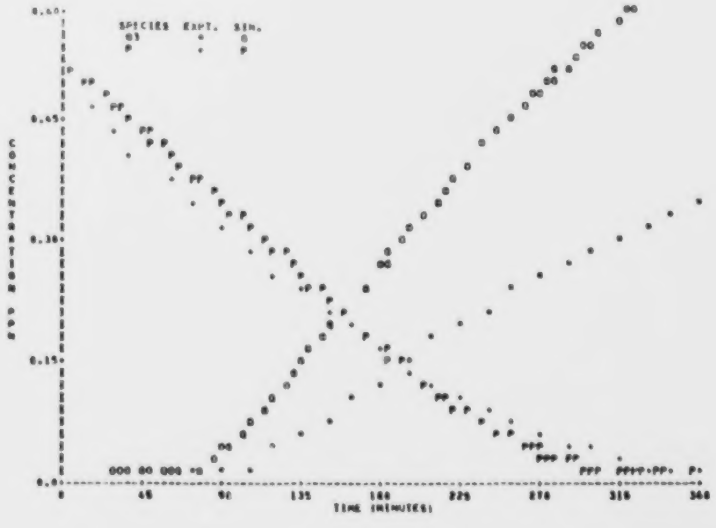

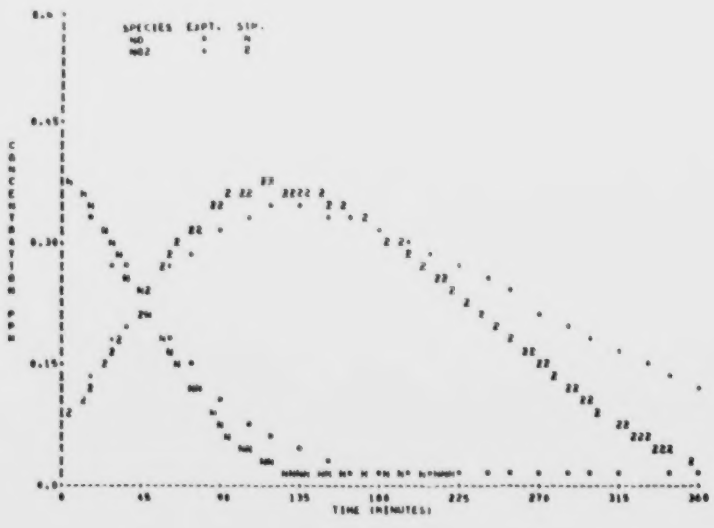

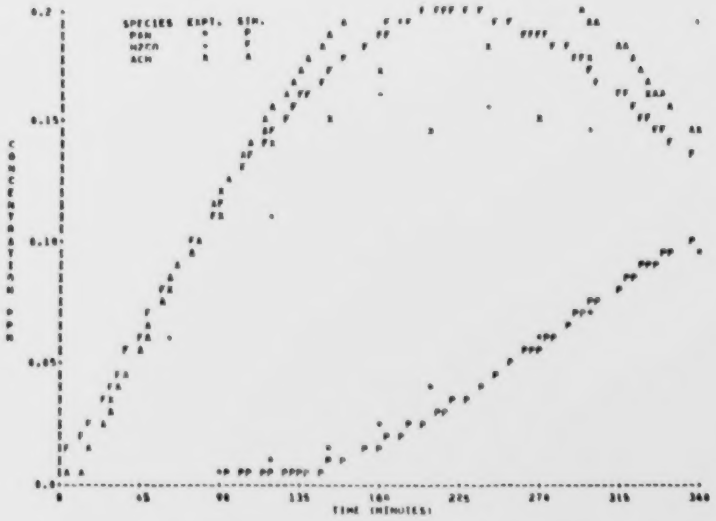

FIGURE B-3 SAPRC EC-276

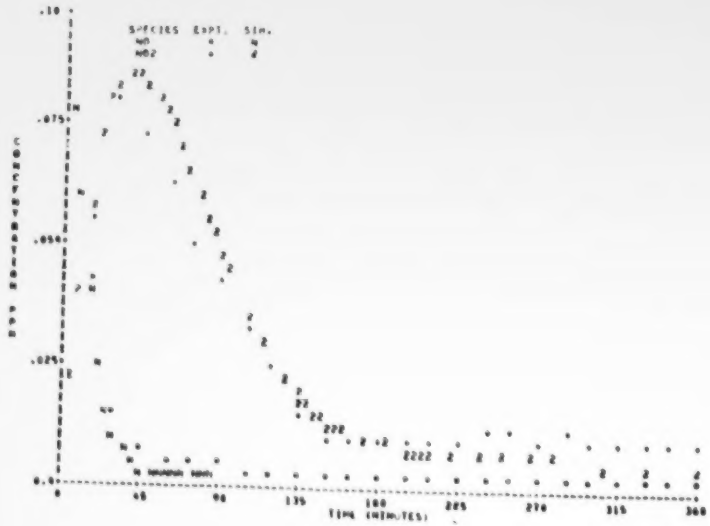

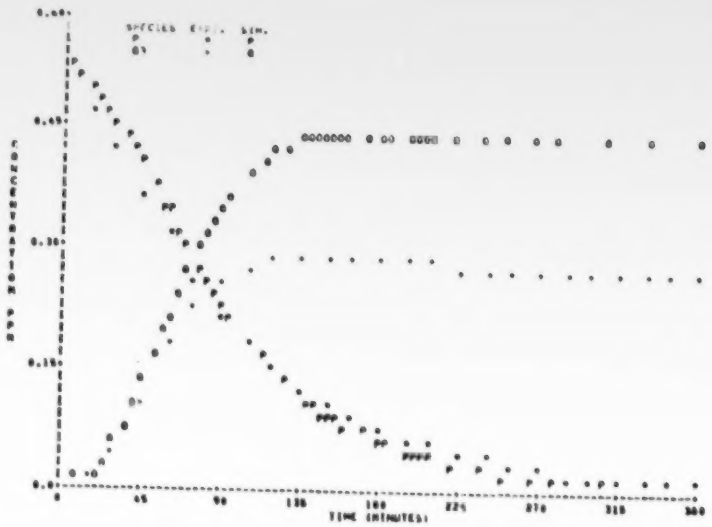

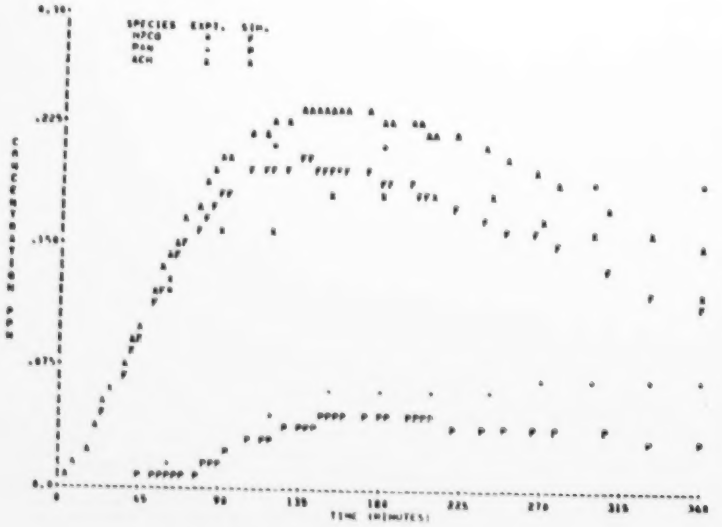

FIGURE B-4 SAPRC EC-277

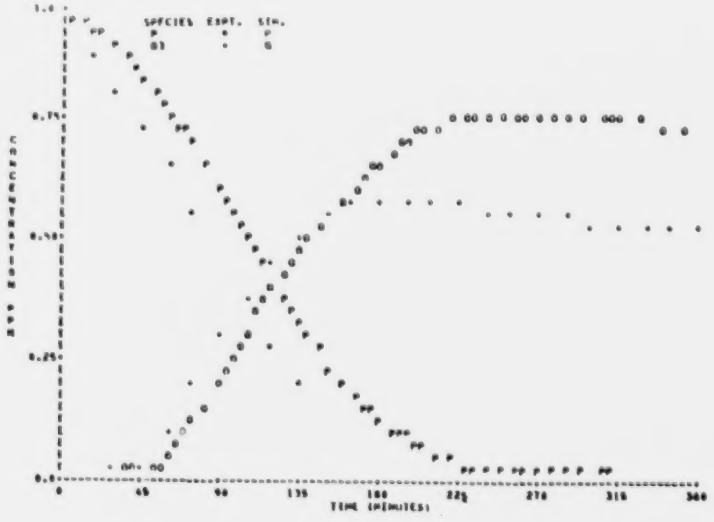

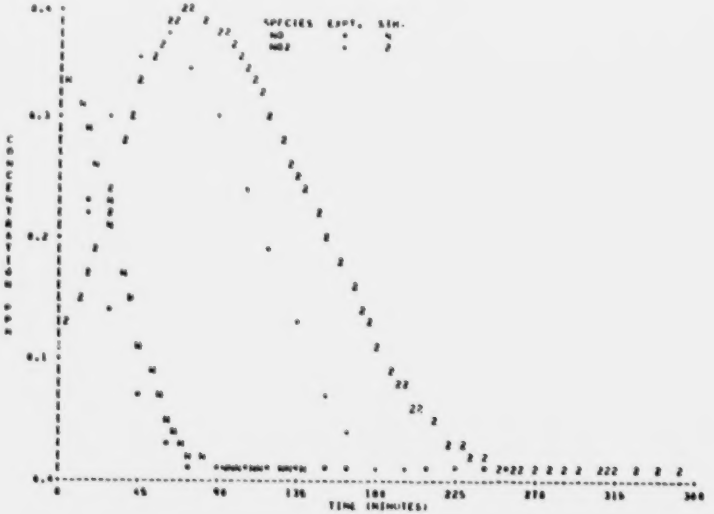

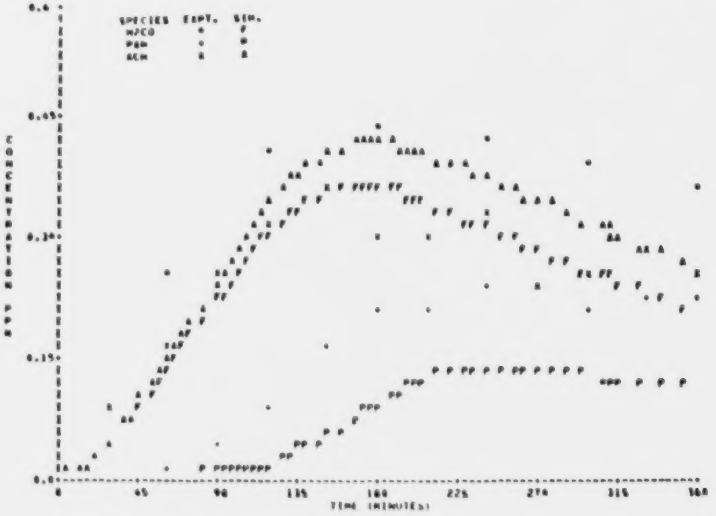

FIGURE B-5 SAPRC EC-278

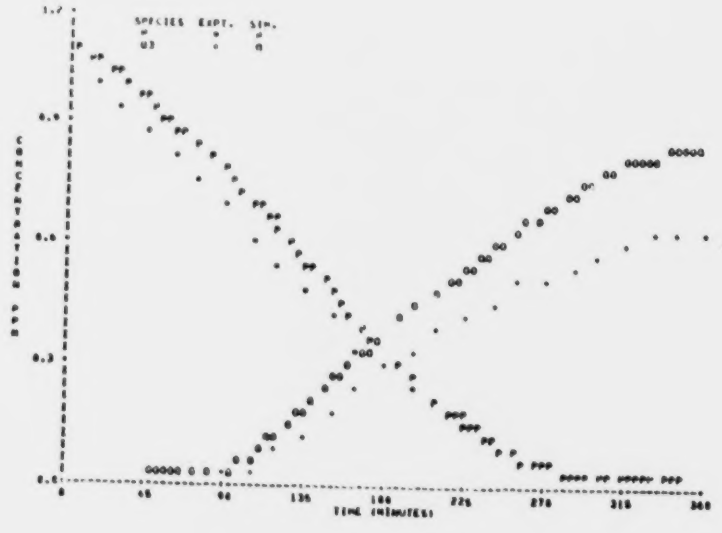

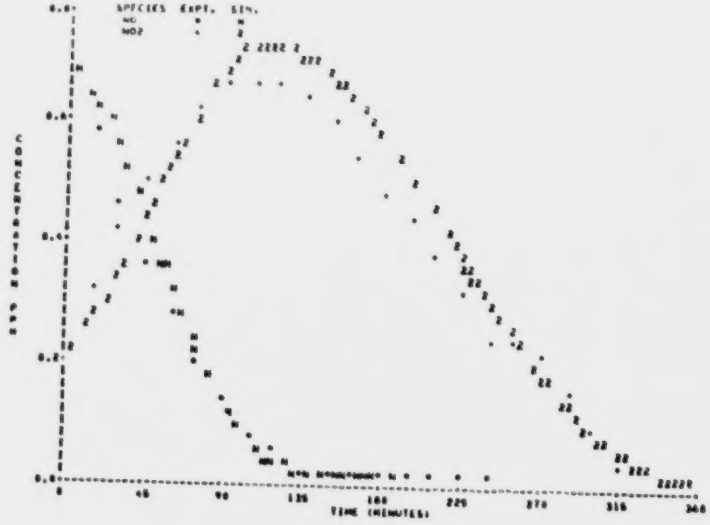

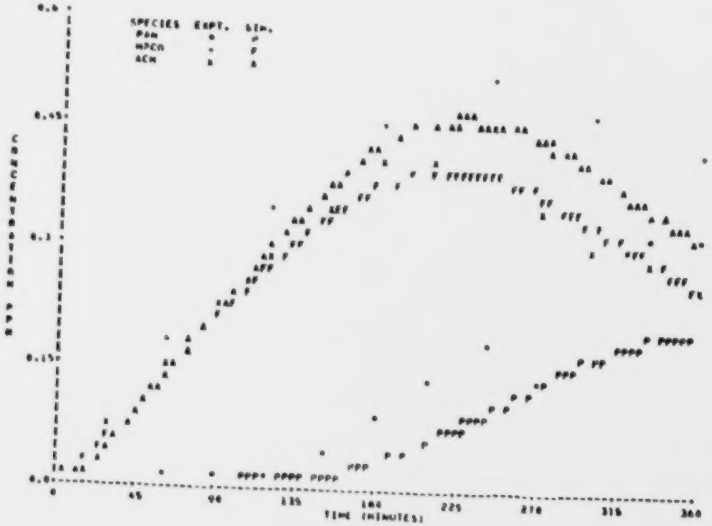

FIGURE B-6 SAPRC EC-279

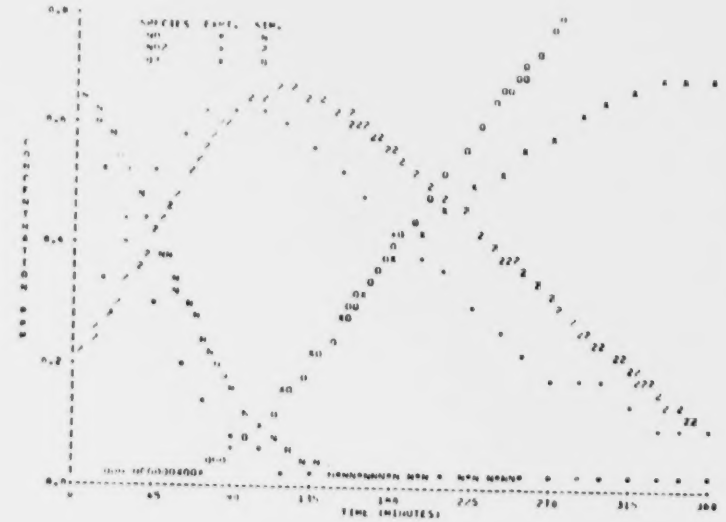

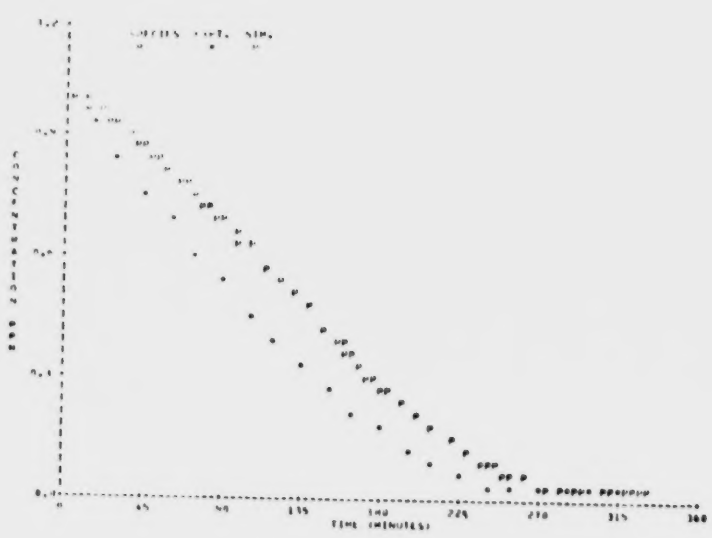

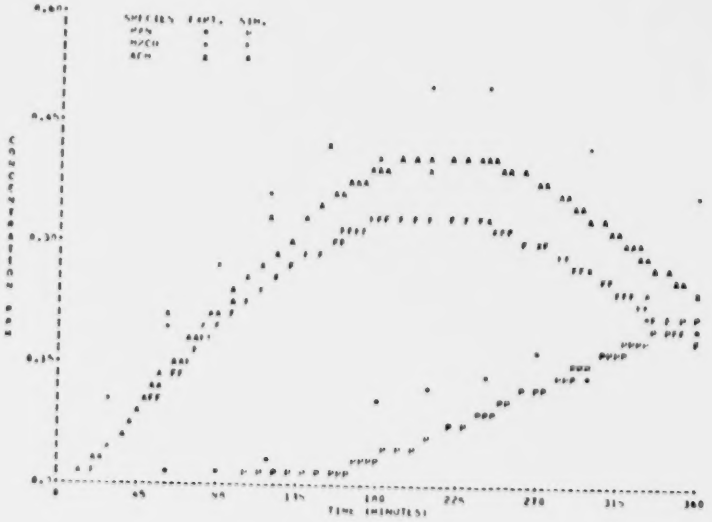

FIGURE B-7 SAPRC EC-314

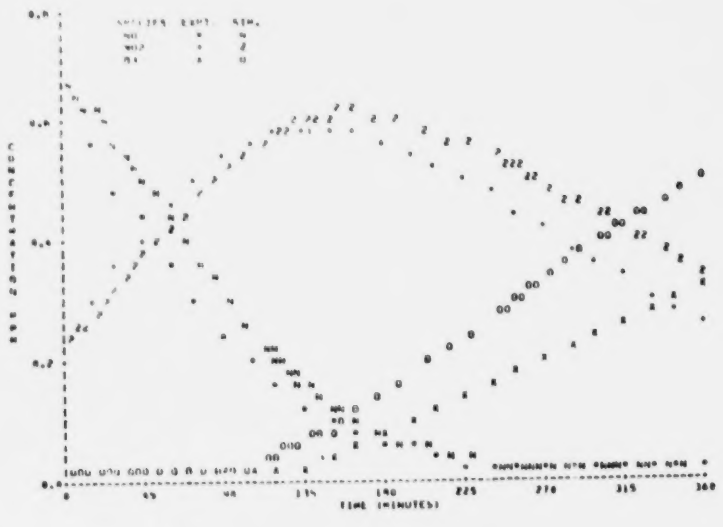

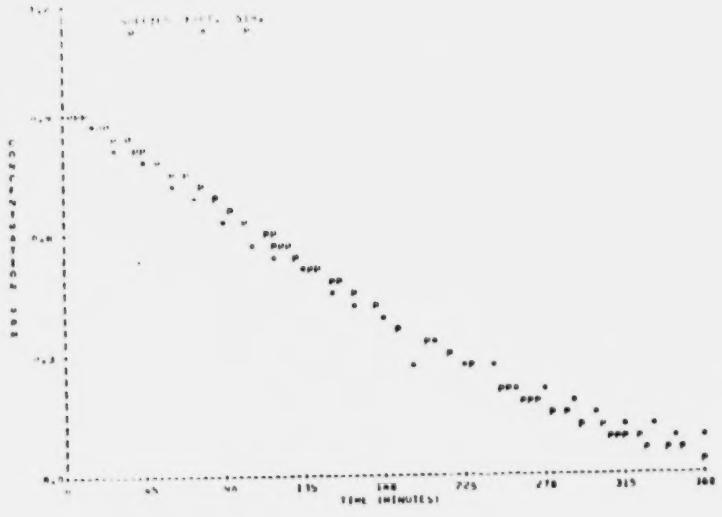

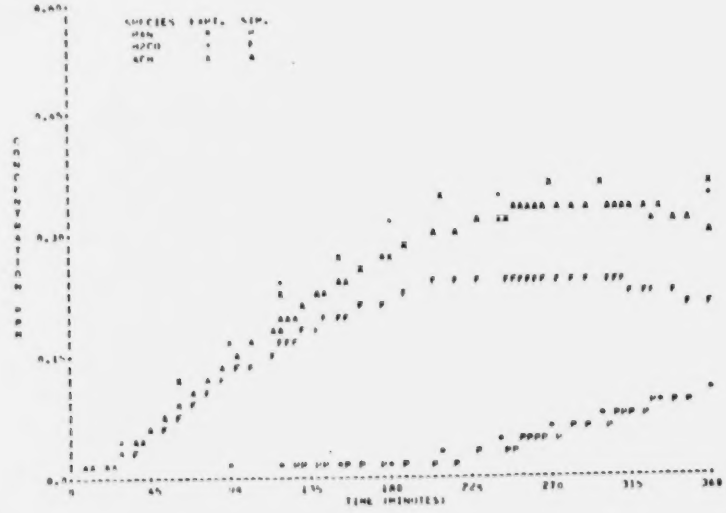

FIGURE B-8 SAPRC EC-315

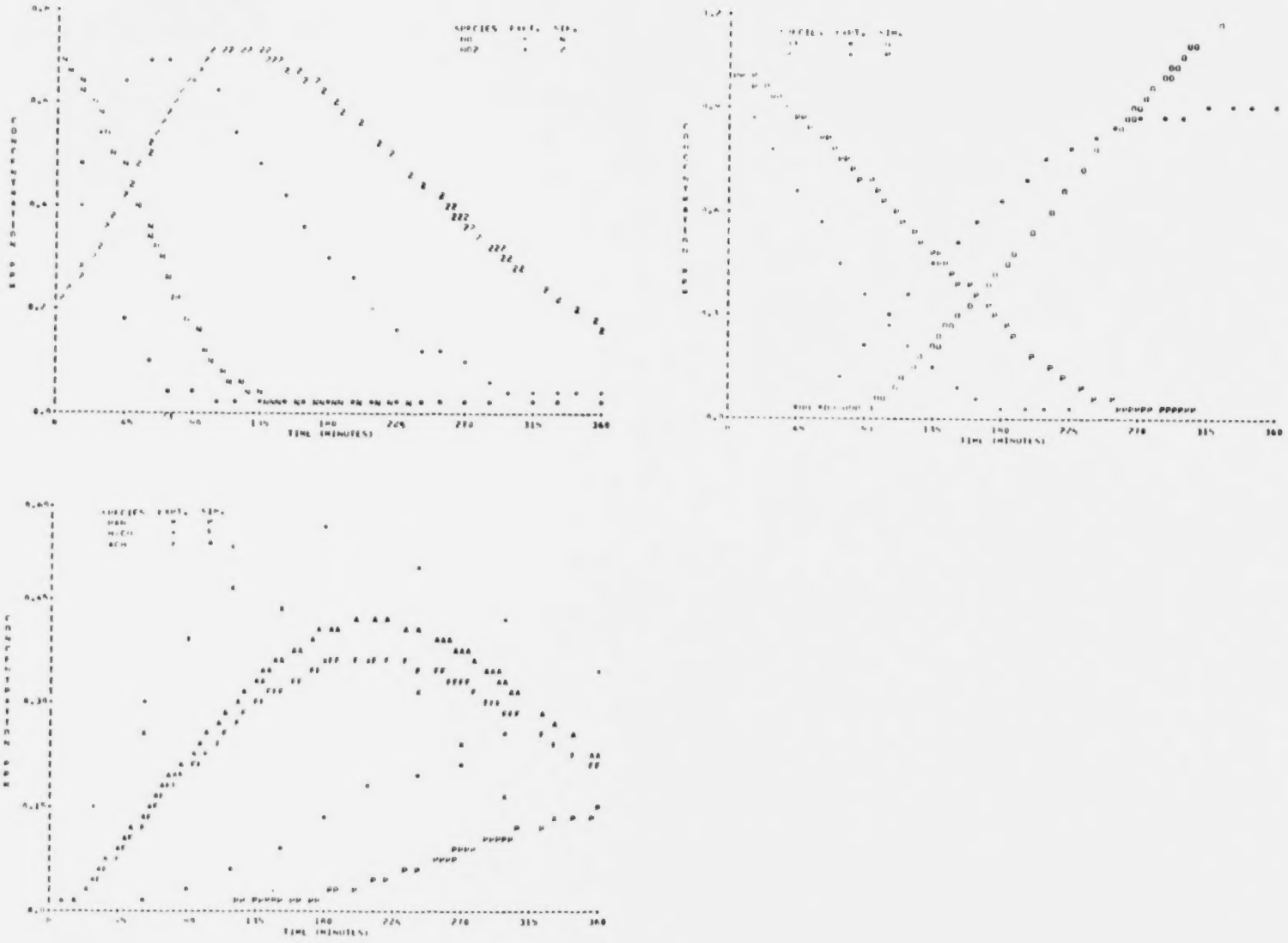

FIGURE B-9 SAPRC EC-316

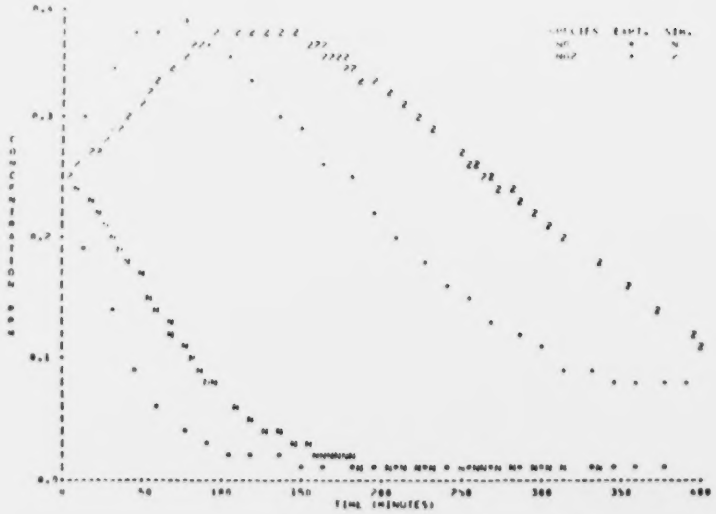

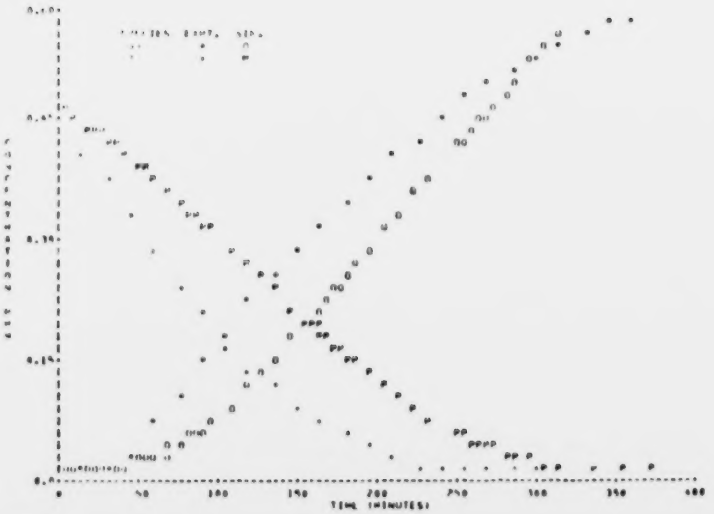

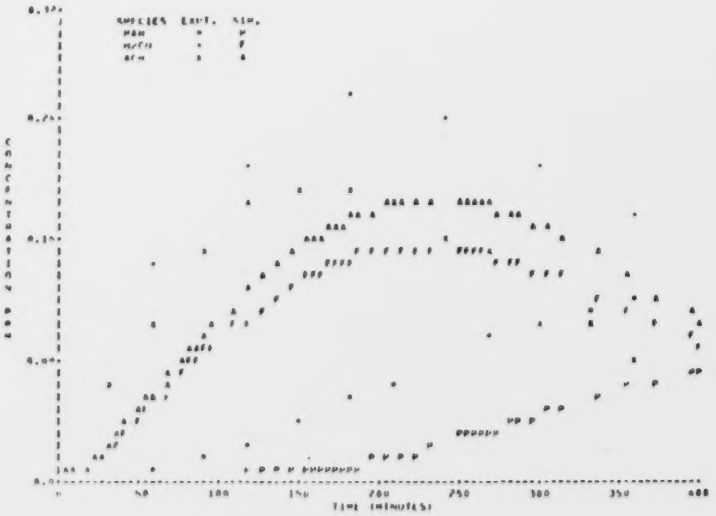

FIGURE B-10 SAPRC EC-317

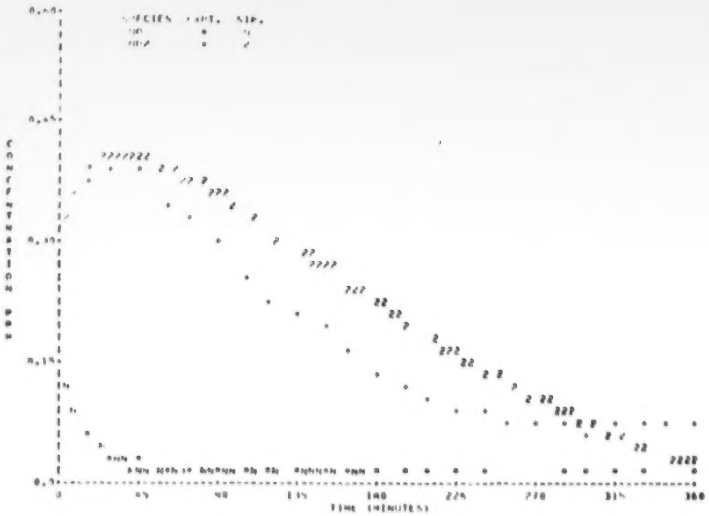

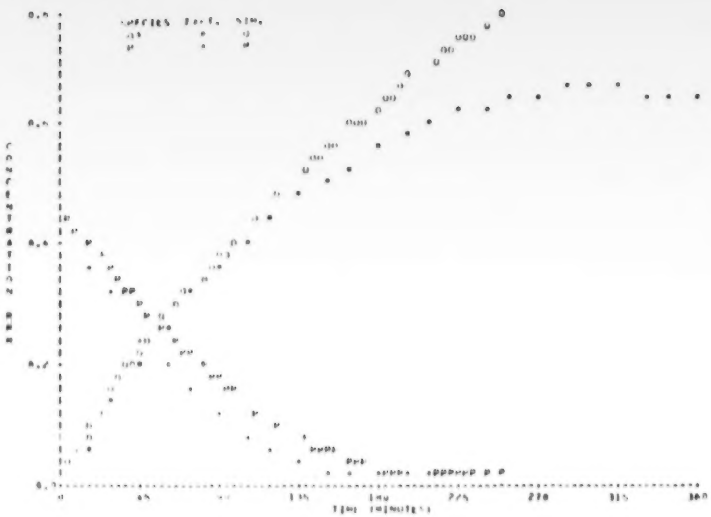

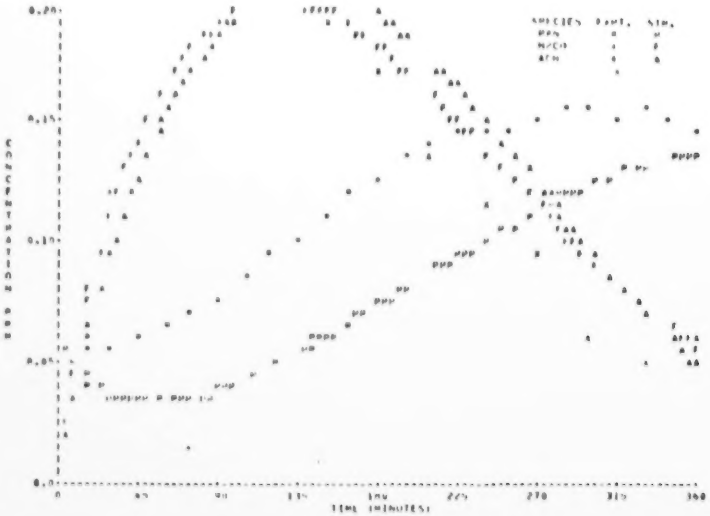

FIGURE B-11 SAPRC EC-318

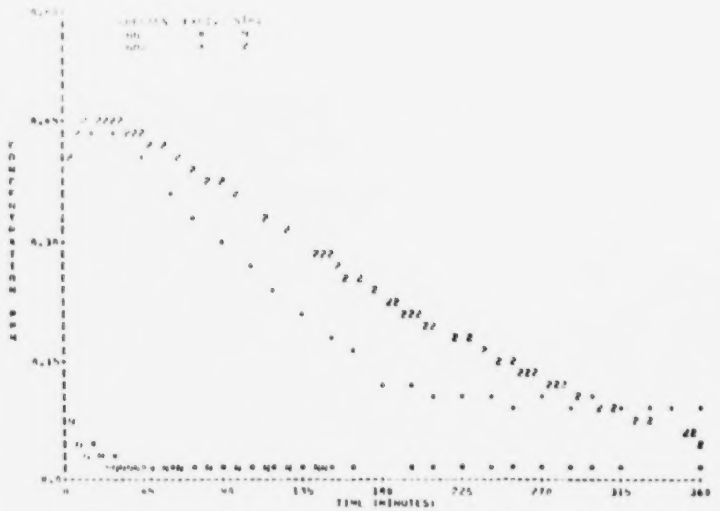

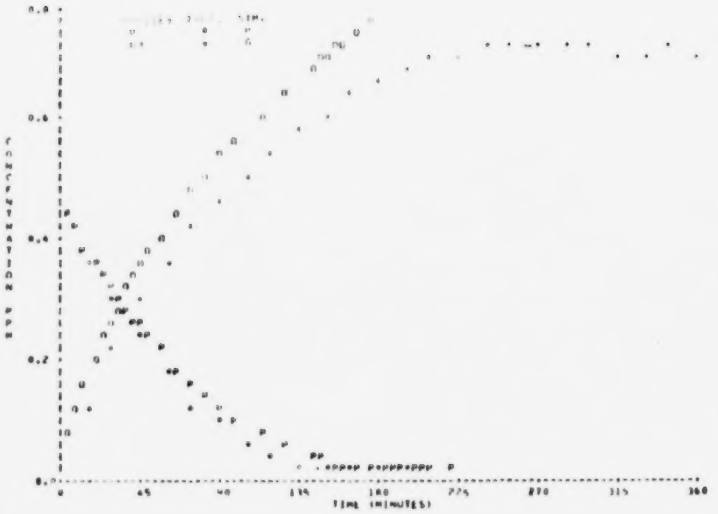

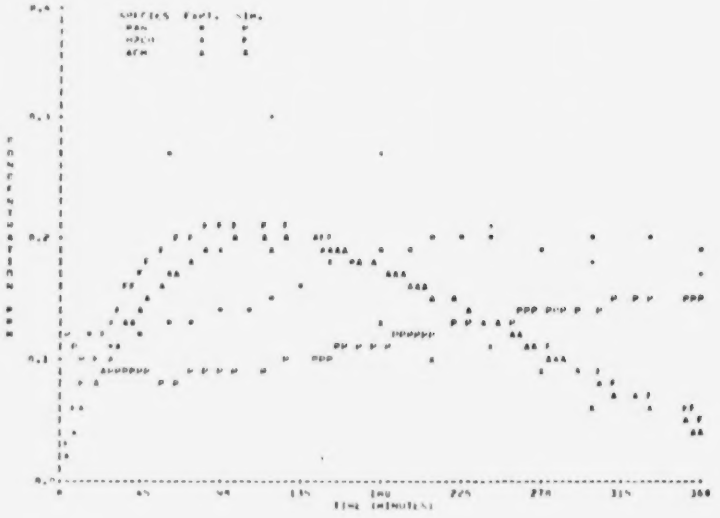

FIGURE B-12 SAPRC EC-319

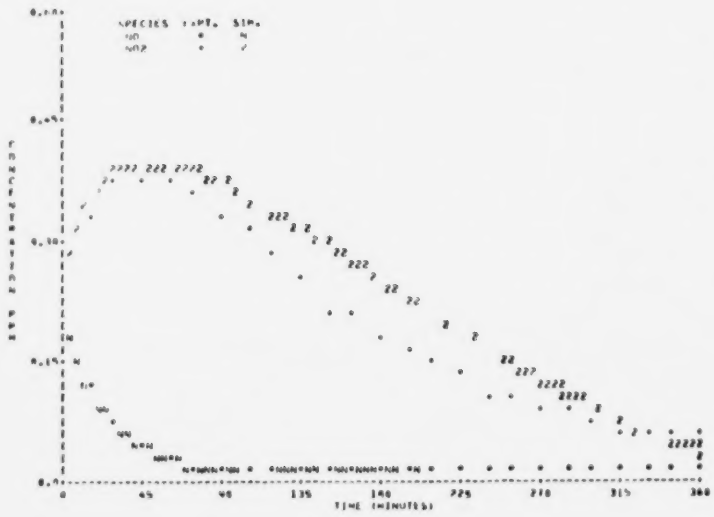

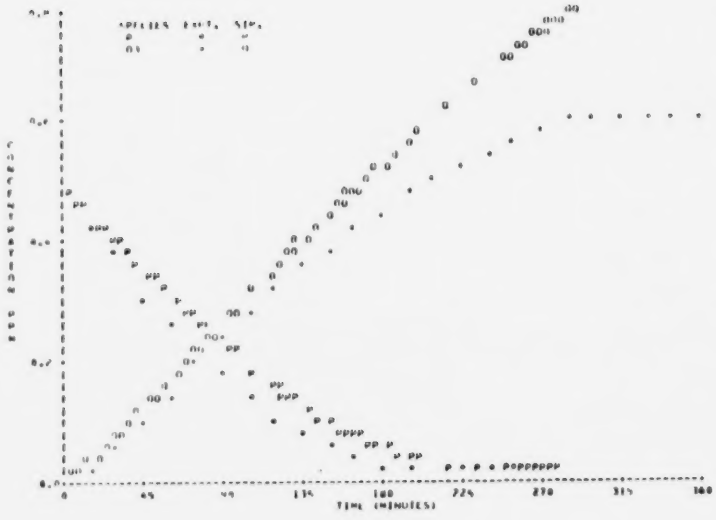

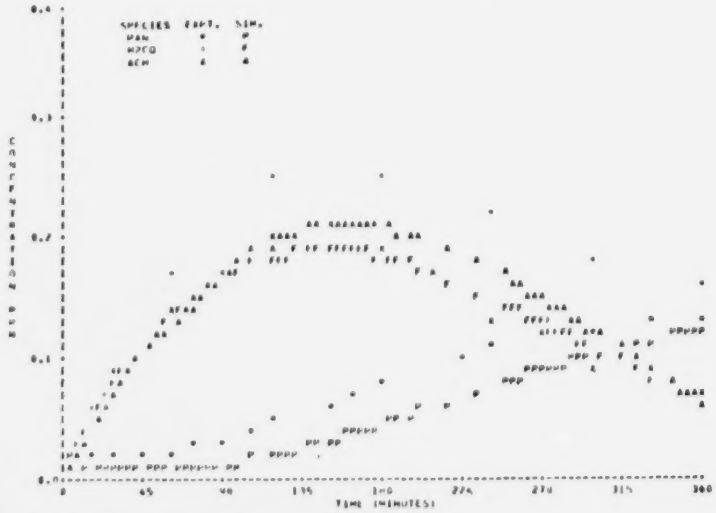

FIGURE B-13 SAPRC EC-320

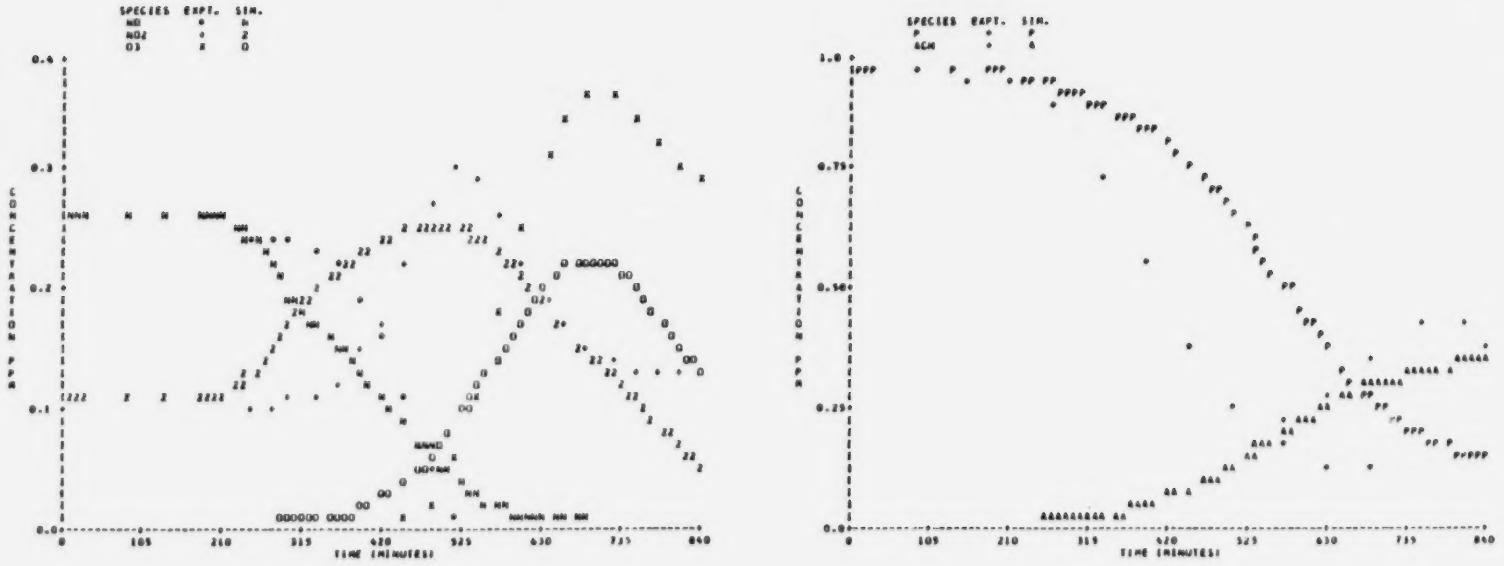

FIGURE B-14 UNC 12.26.77 Red

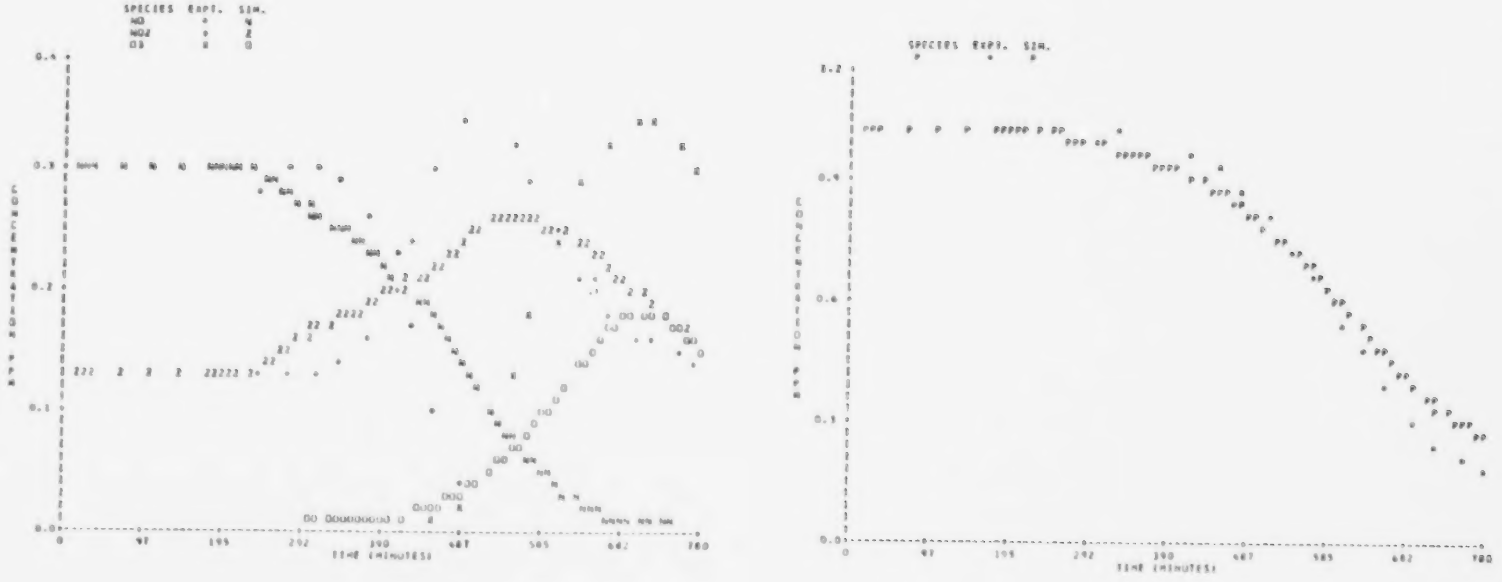

FIGURE B-15 UNC 1.10.78 Red

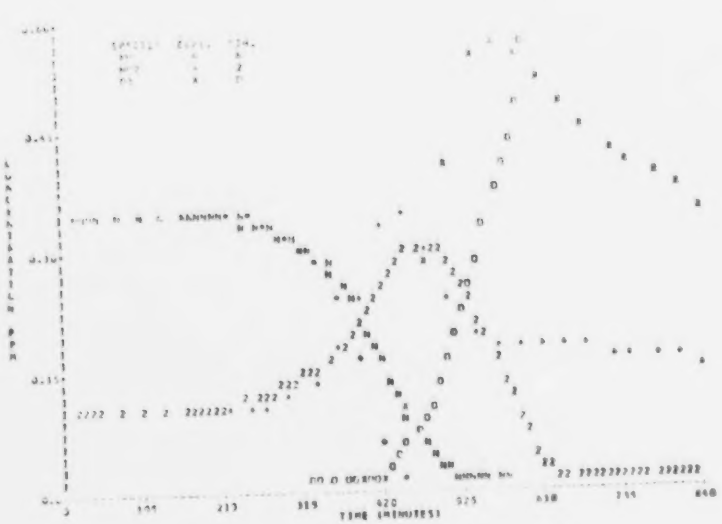

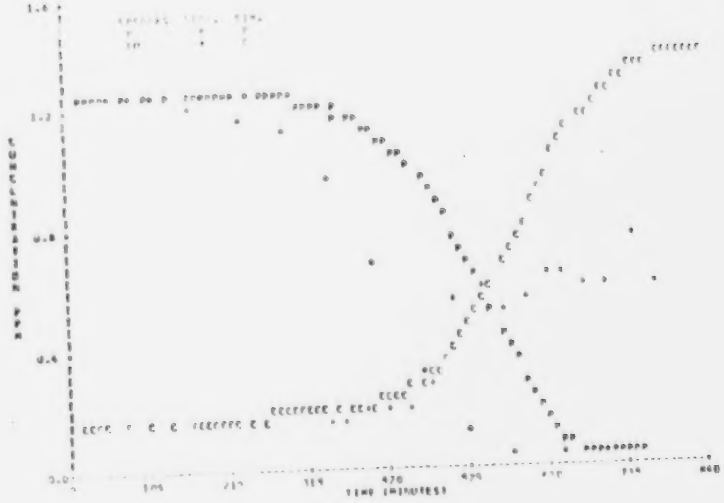

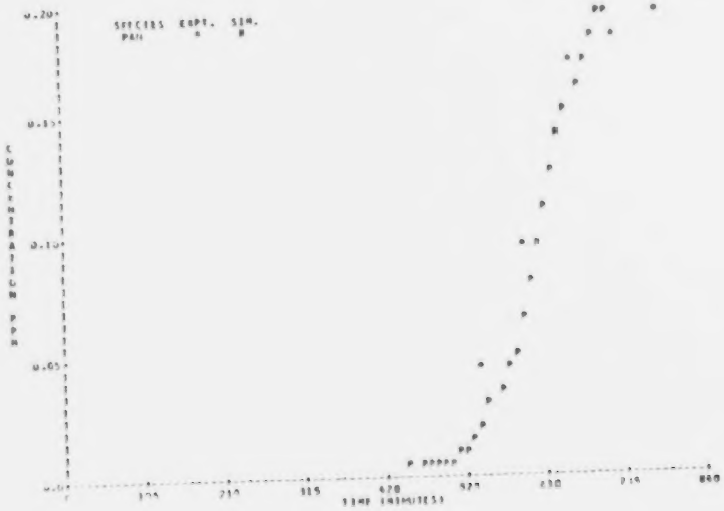

FIGURE B-16 UNC 2.27.78 Red

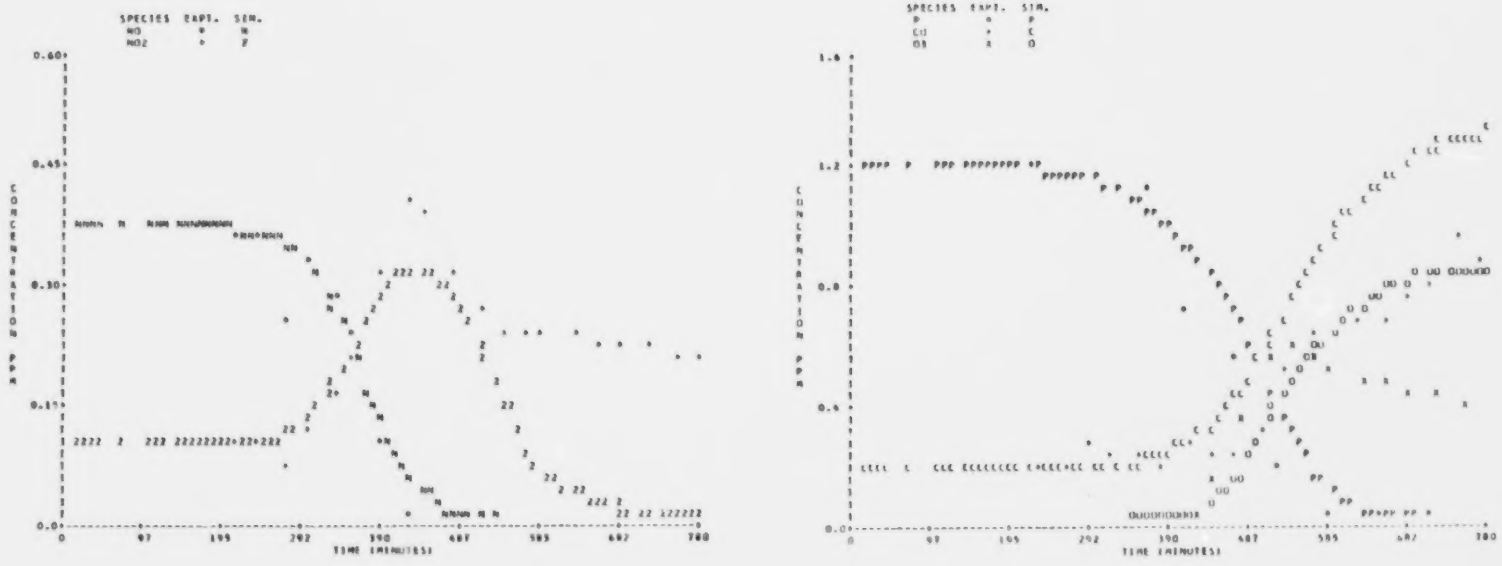

FIGURE B-17 UNC 3.06.78 Red

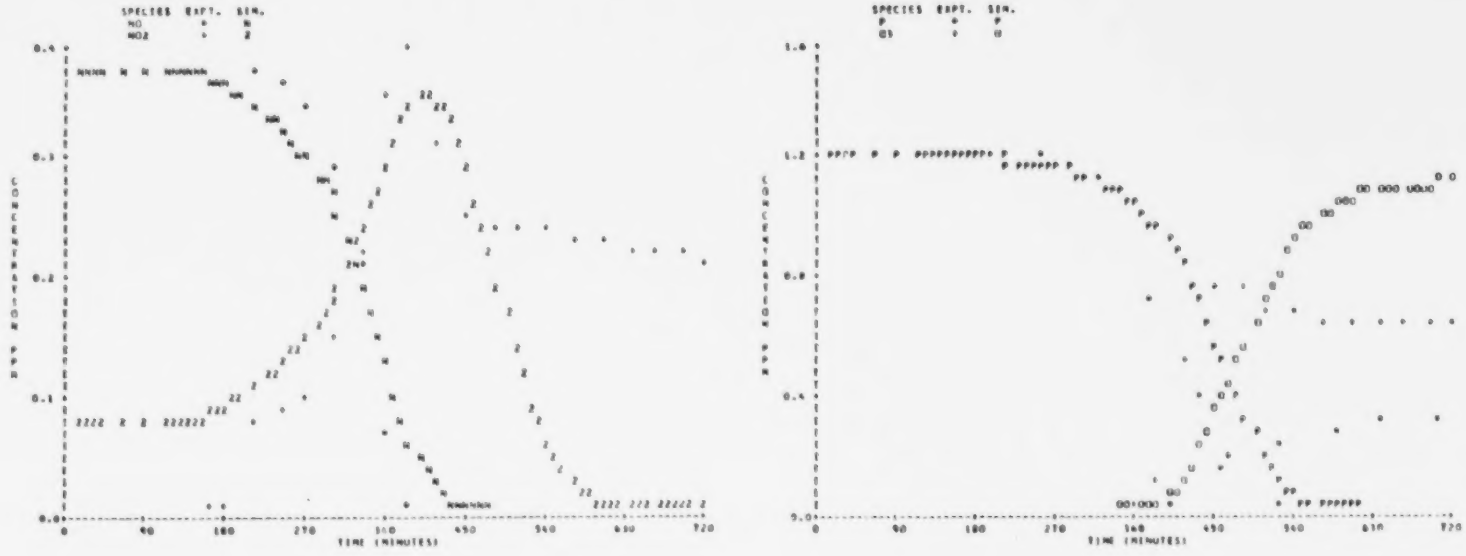

FIGURE B-18 UNC 3.31.78 Red

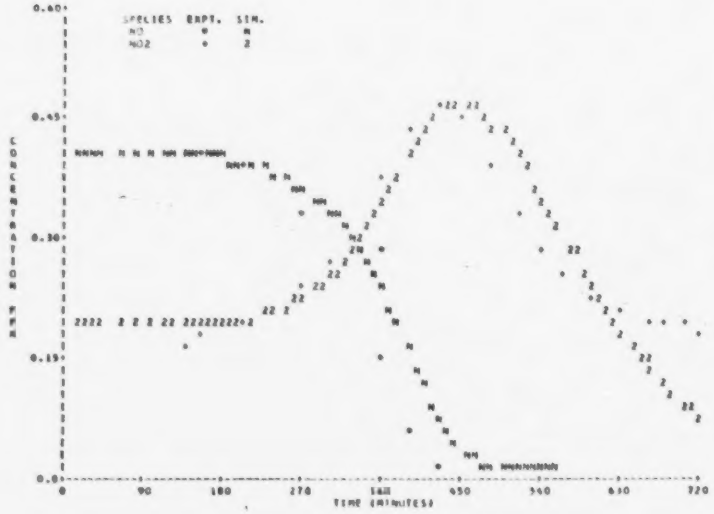

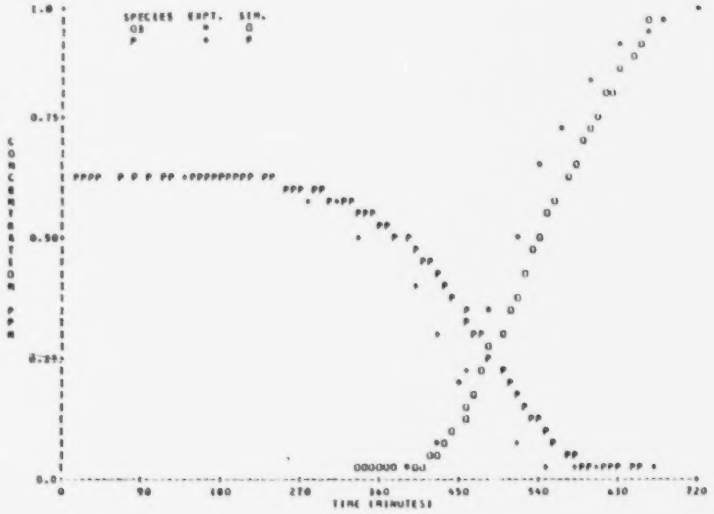

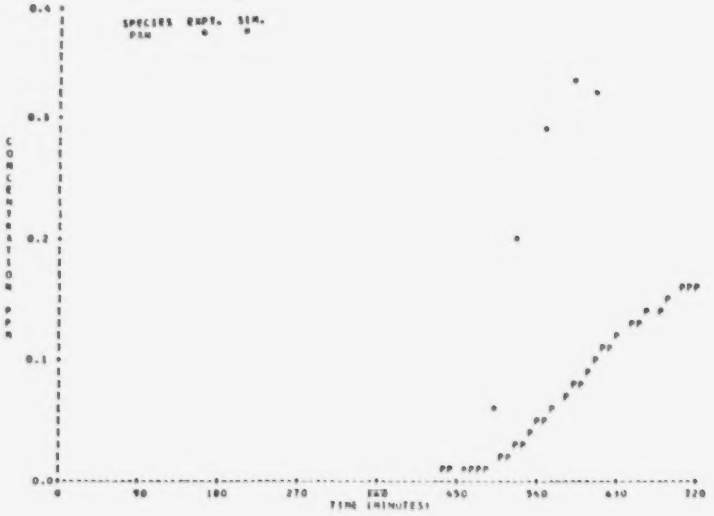

FIGURE B-19 UNC 6.16.78 Blue

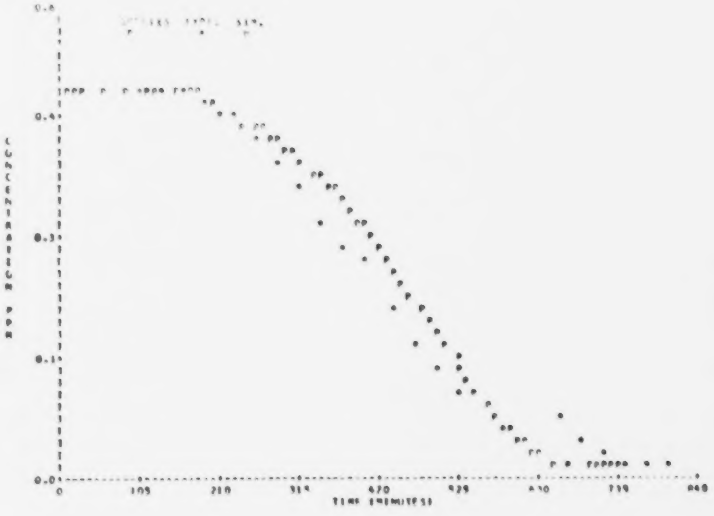

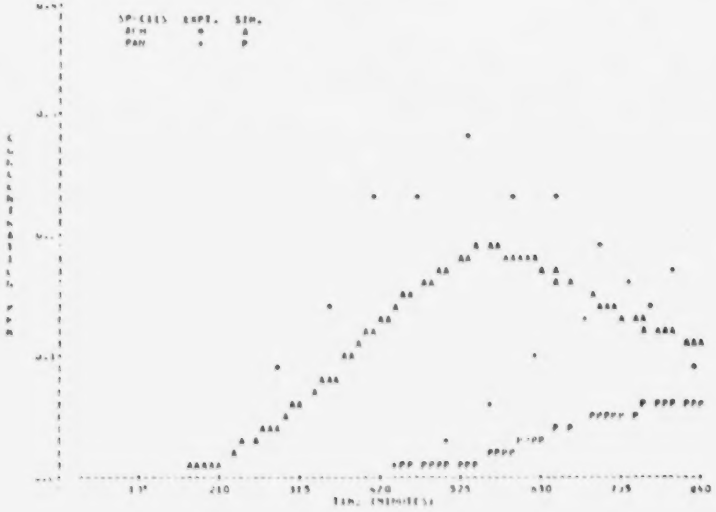

FIGURE B-20 UNC 7.01.78 Blue

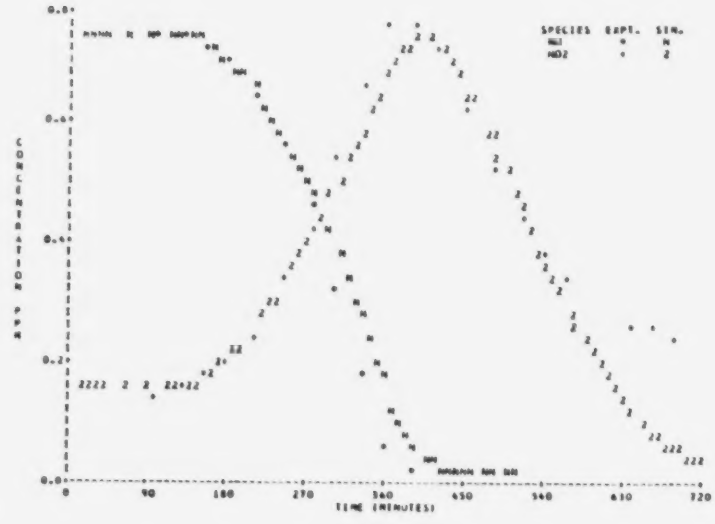

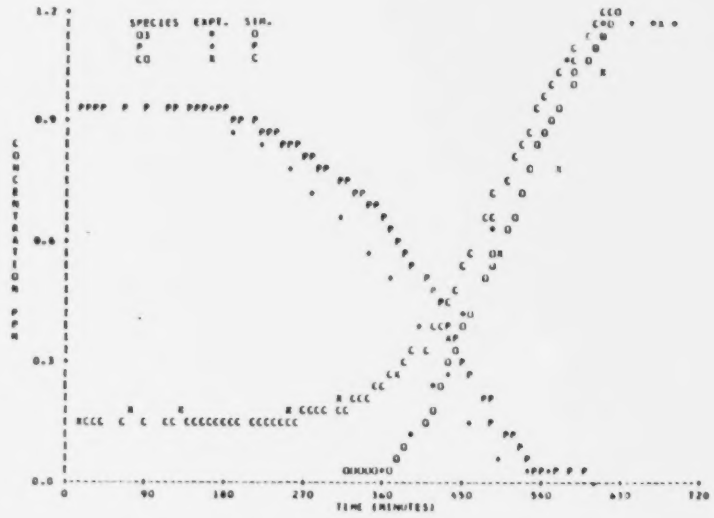

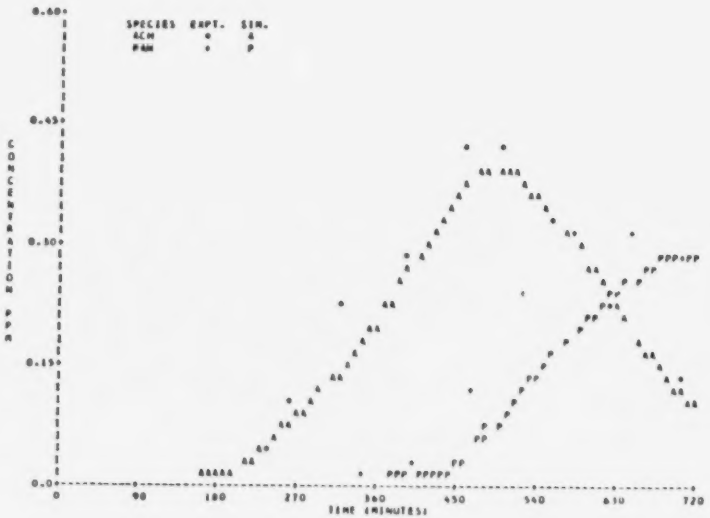

FIGURE B-21 UNC 7.24.78 Red

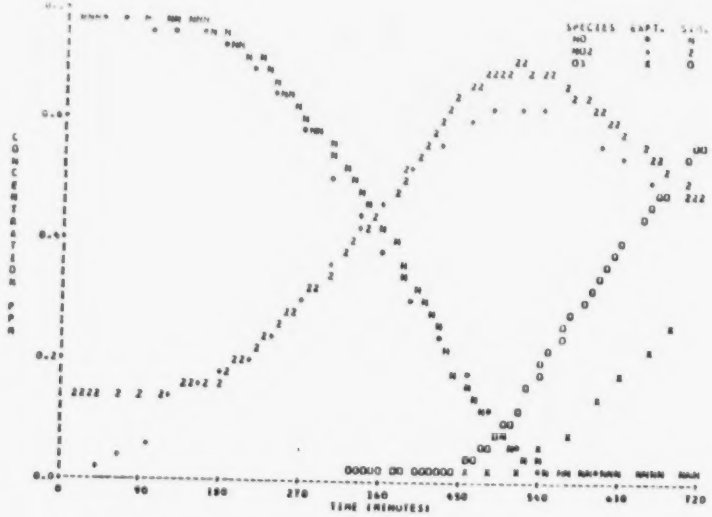

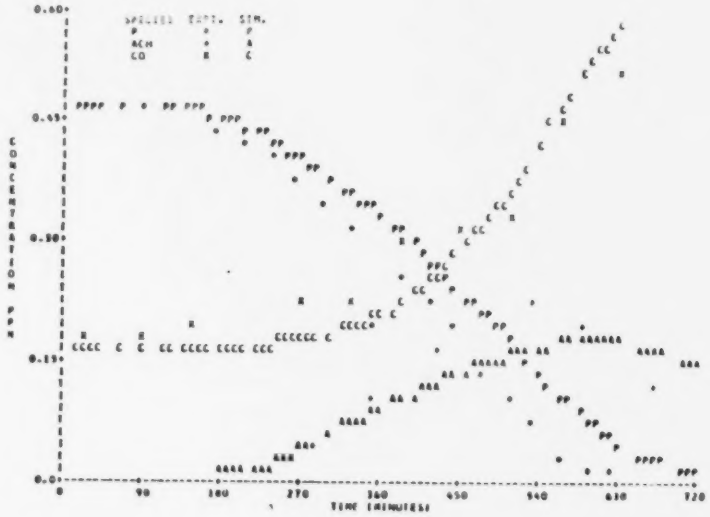

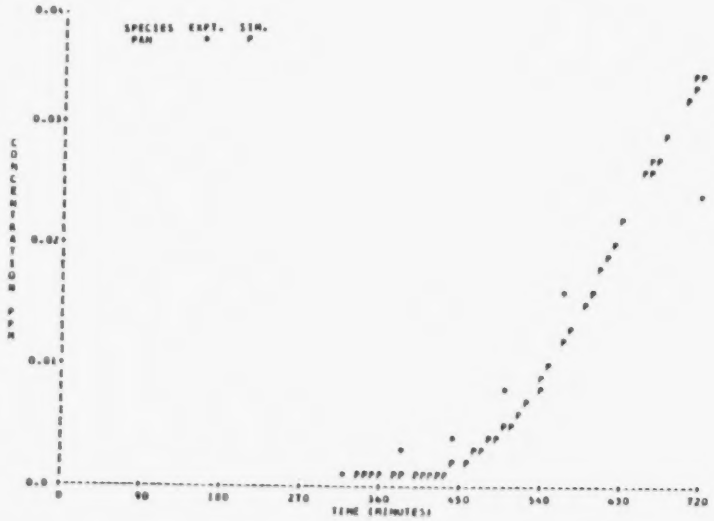

FIGURE B-22 UNC 7.24.78 Blue

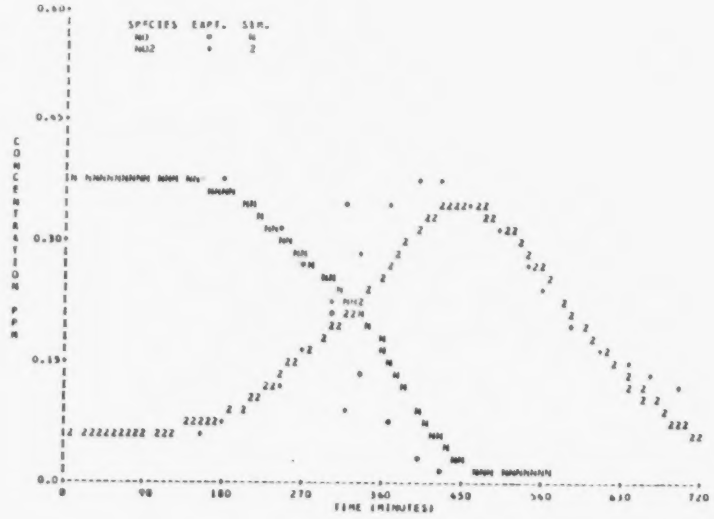

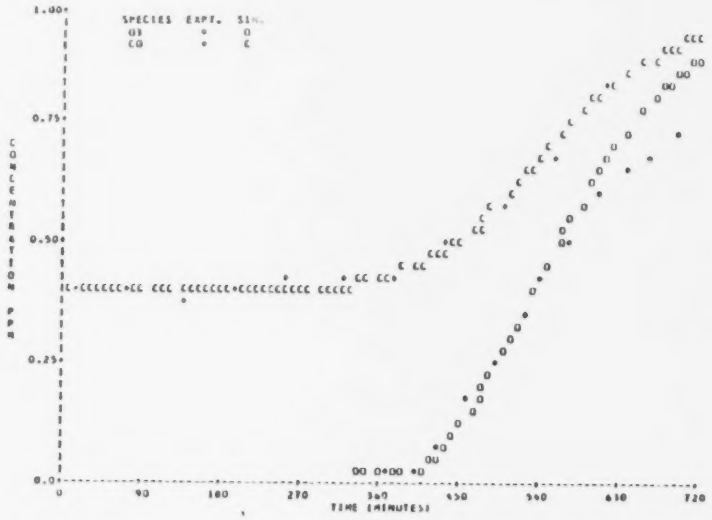

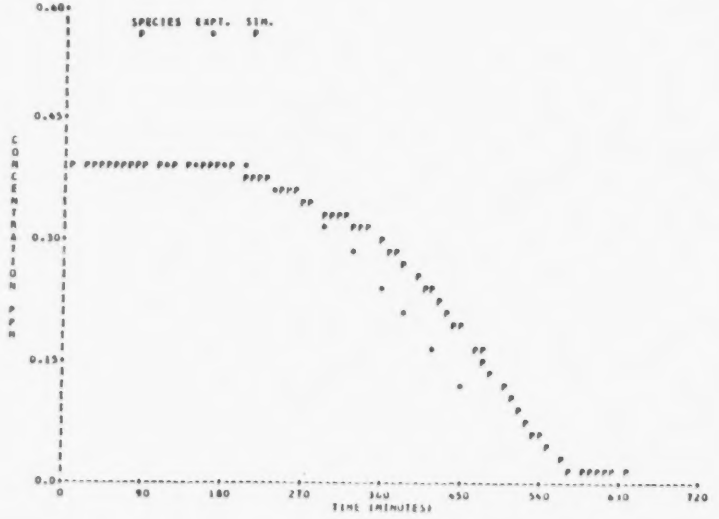

FIGURE B-23 UNC 7.30.78 Blue

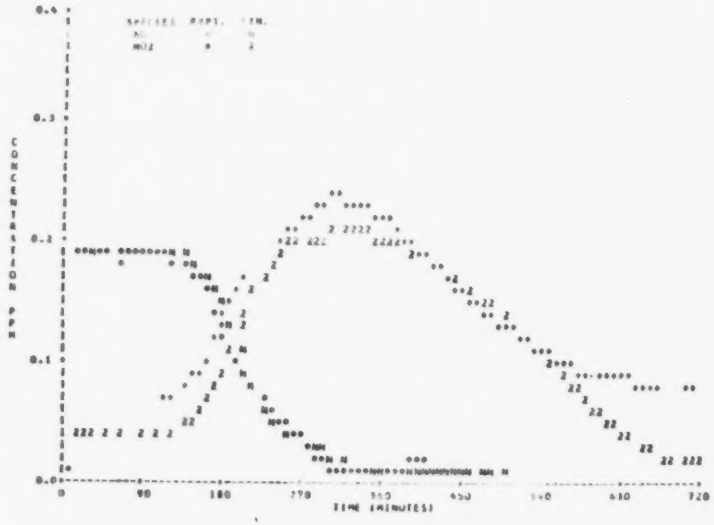

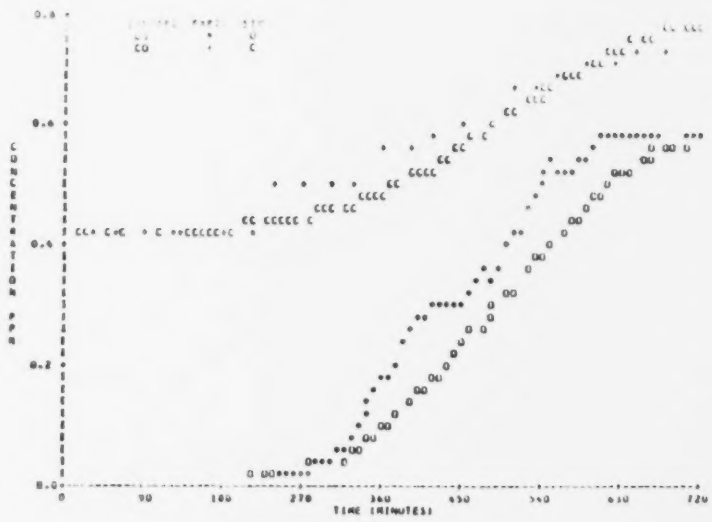

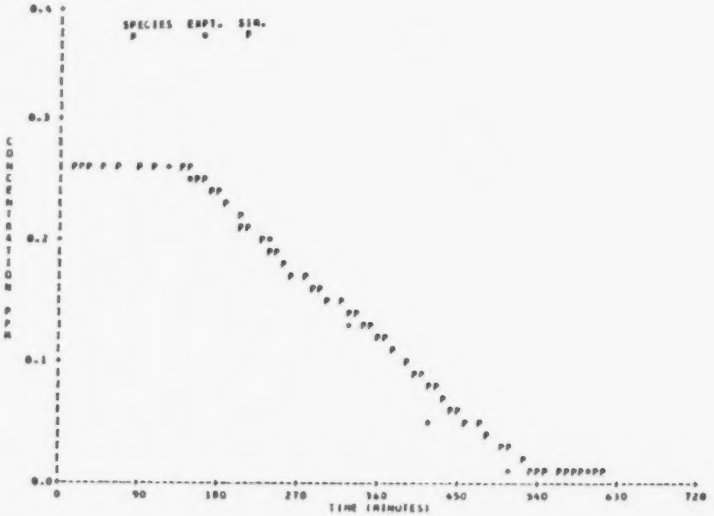

FIGURE B-24 UNC 8.05.78 Red

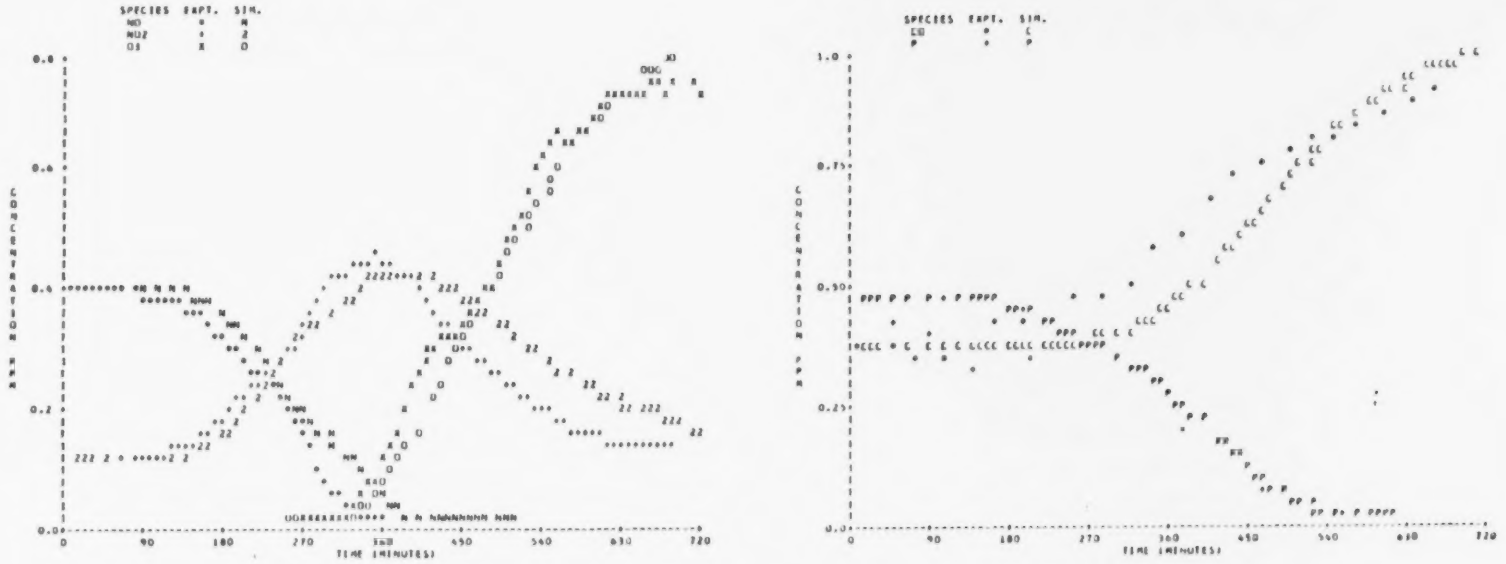

FIGURE B-25 UNC 8.05.78 Blue

Reproduced from
best available copy.

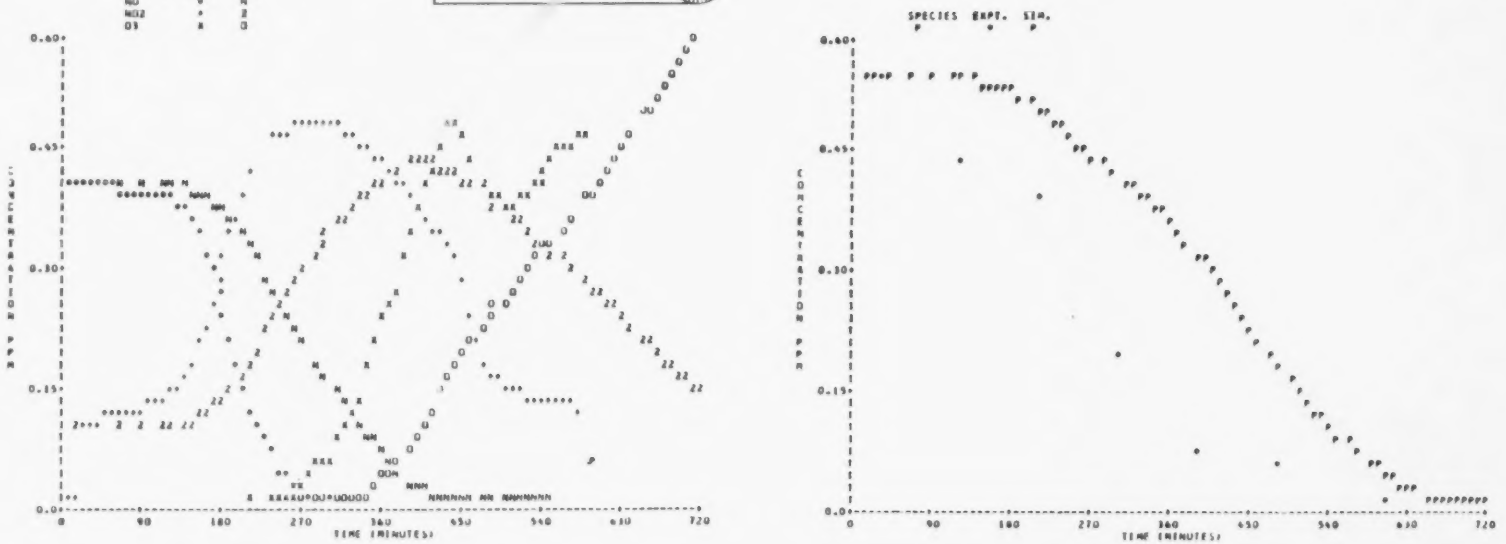

FIGURE B-26 UNC 8.06.78 Red

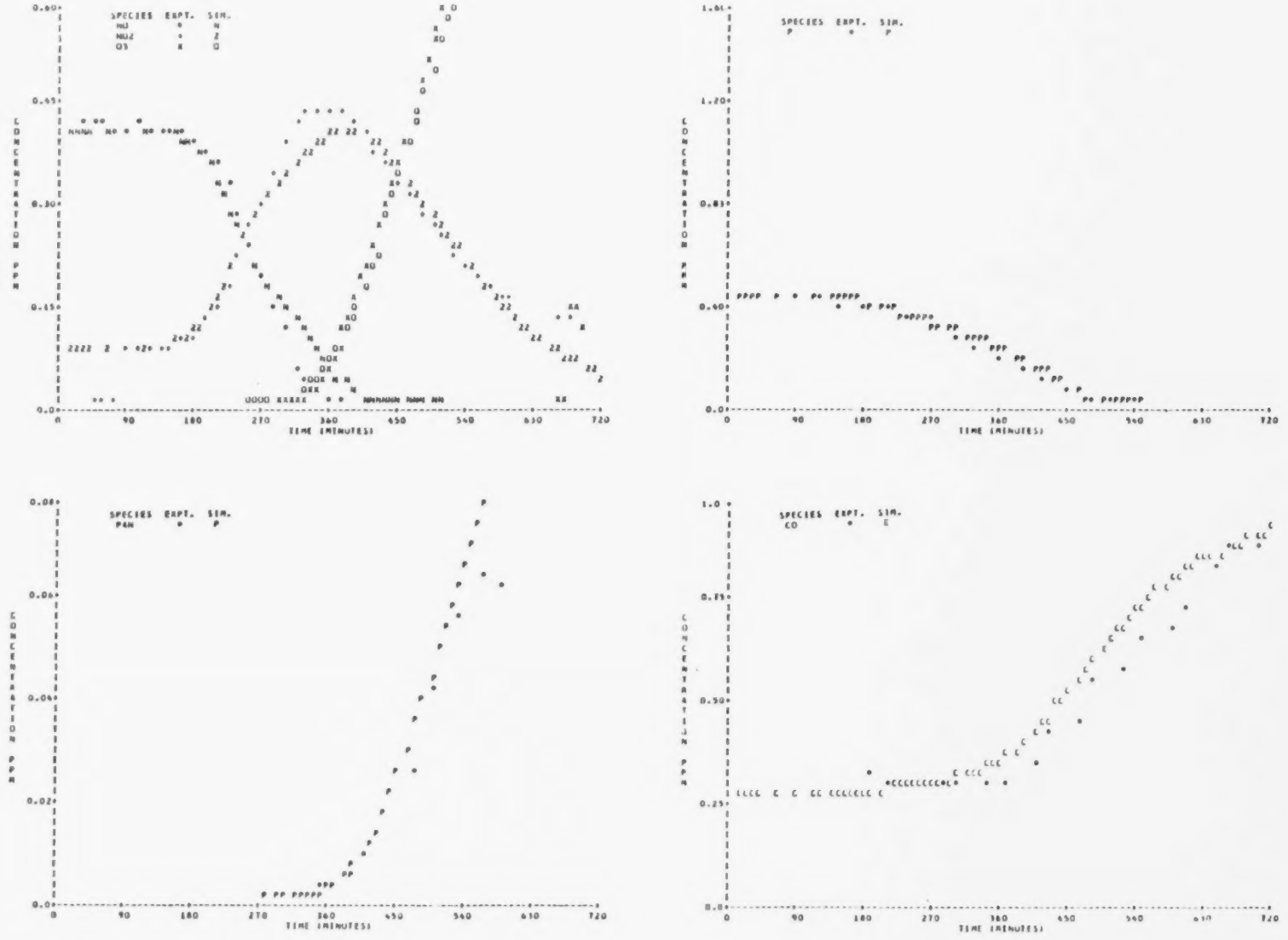

FIGURE B-27 UNC 8.15.78 Red

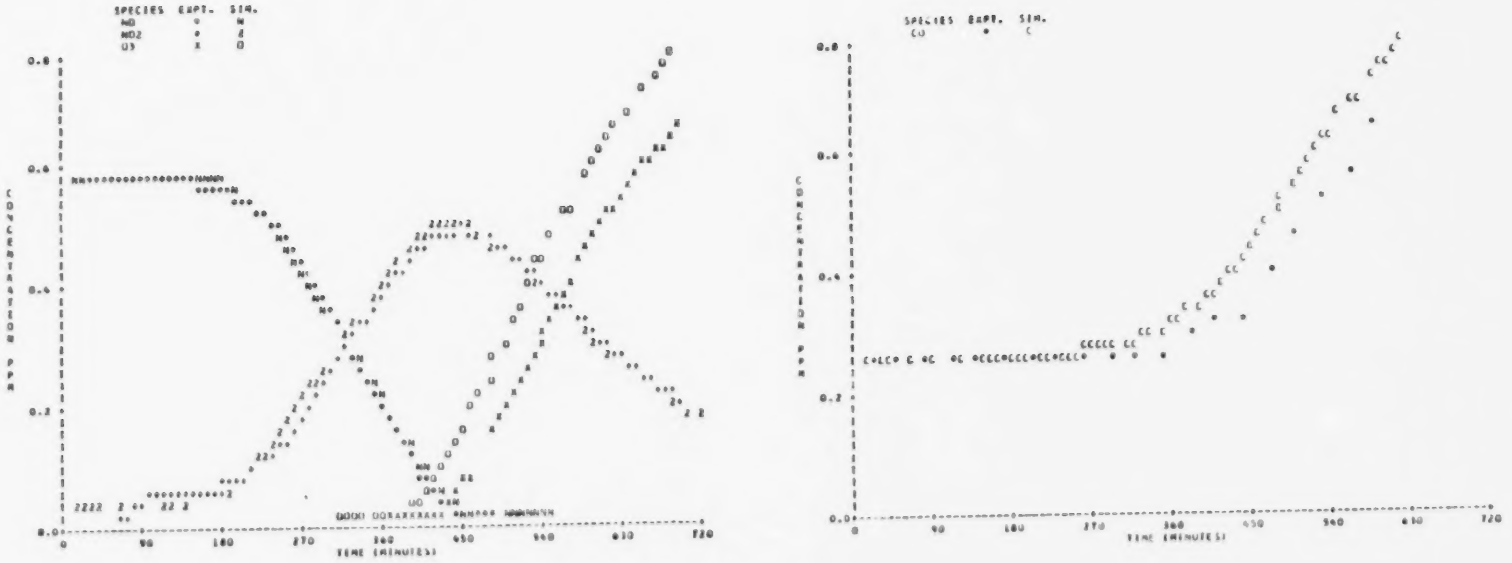

FIGURE B-28 UNC 8.16.78 Red

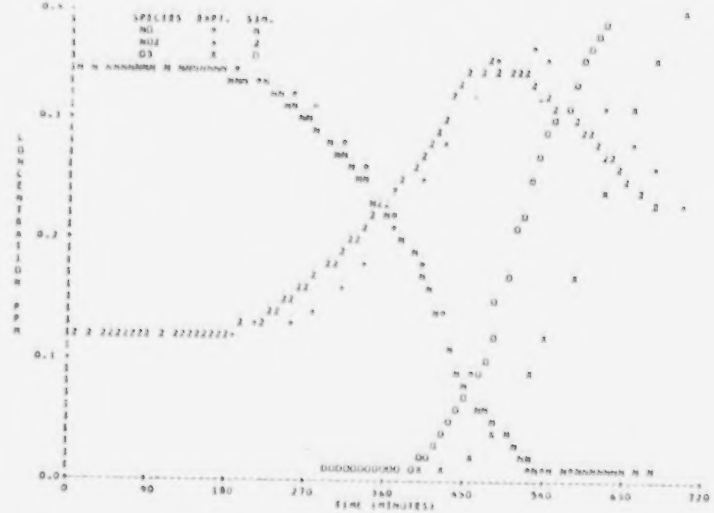

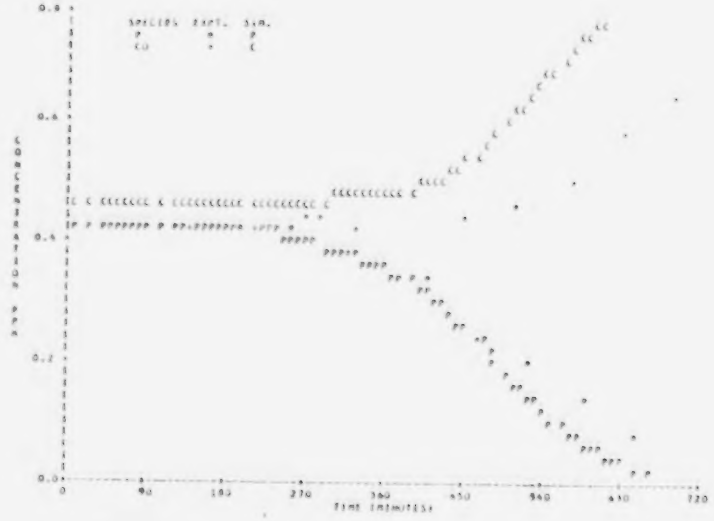

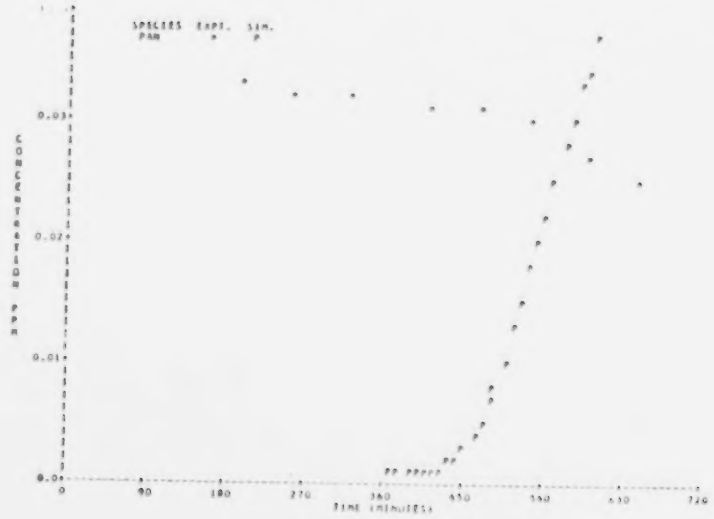

FIGURE B-29 UNC 10.03.78 Blue

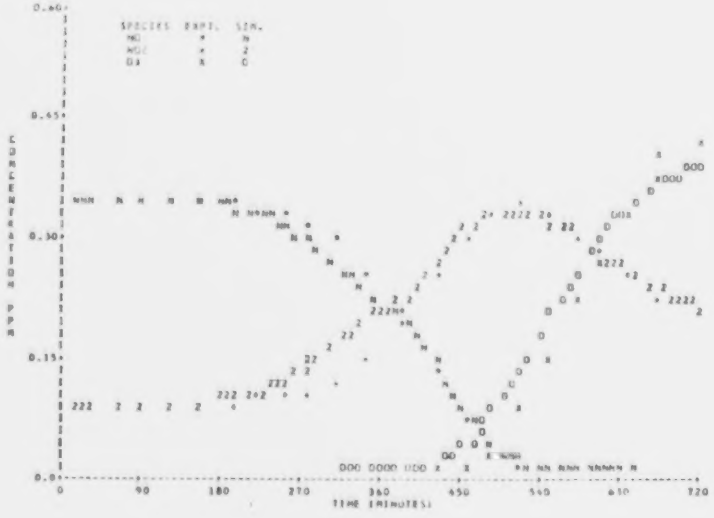

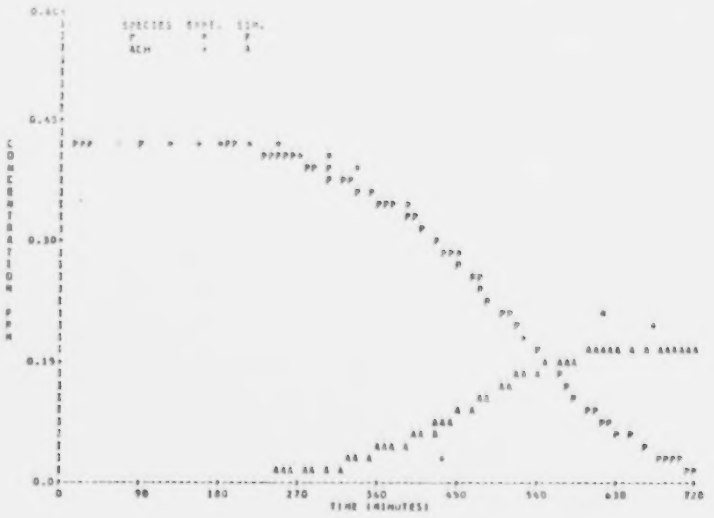

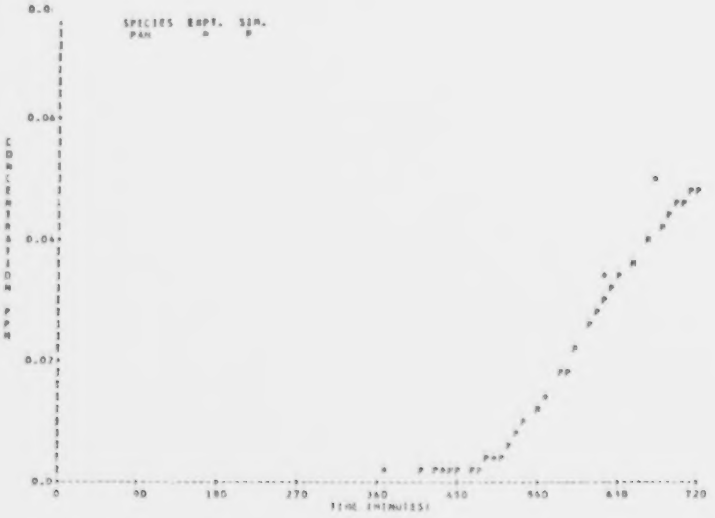

FIGURE B-30 UNC 10.12.78 Blue

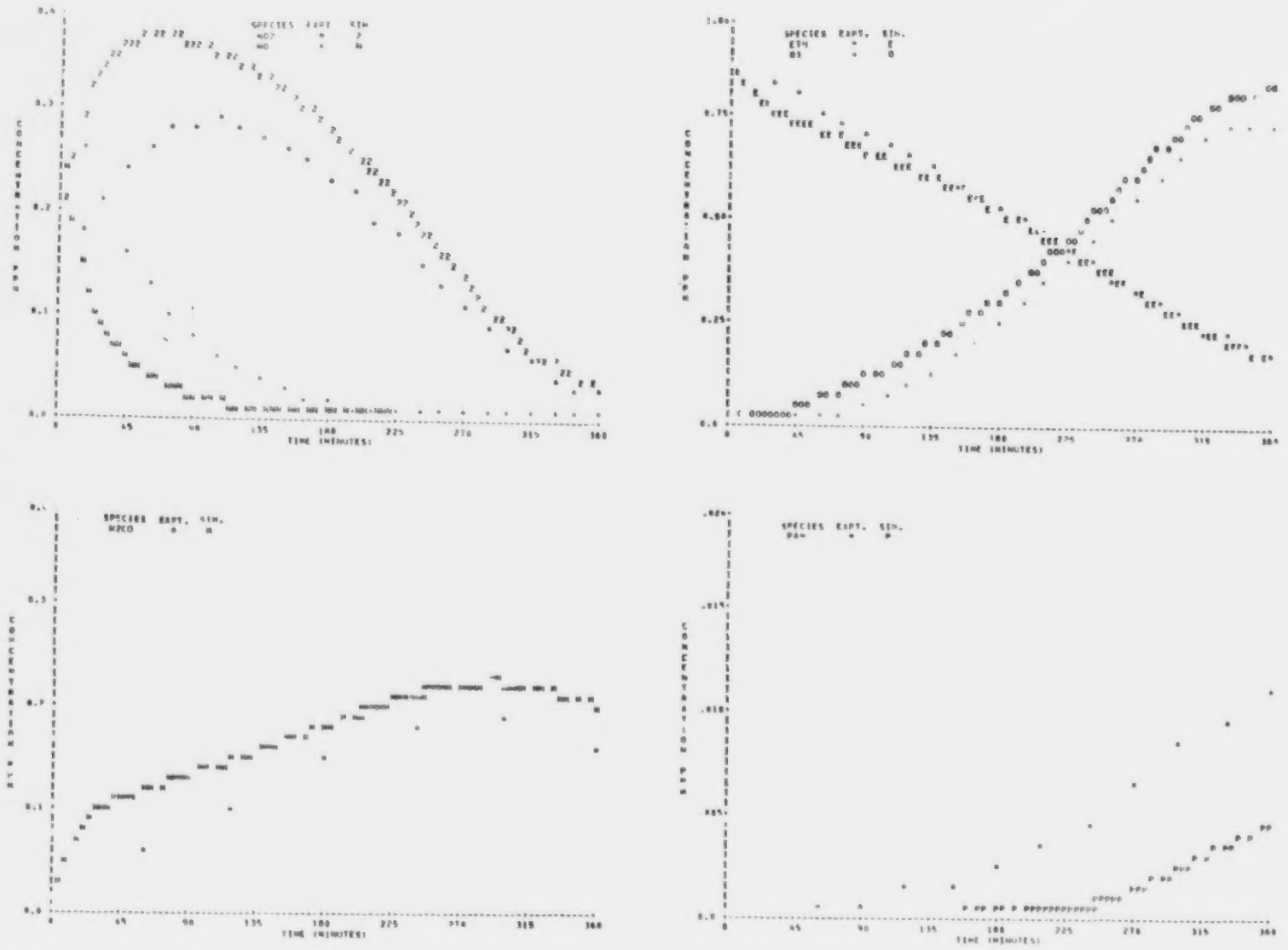

FIGURE B-31 SAPRC EC-142

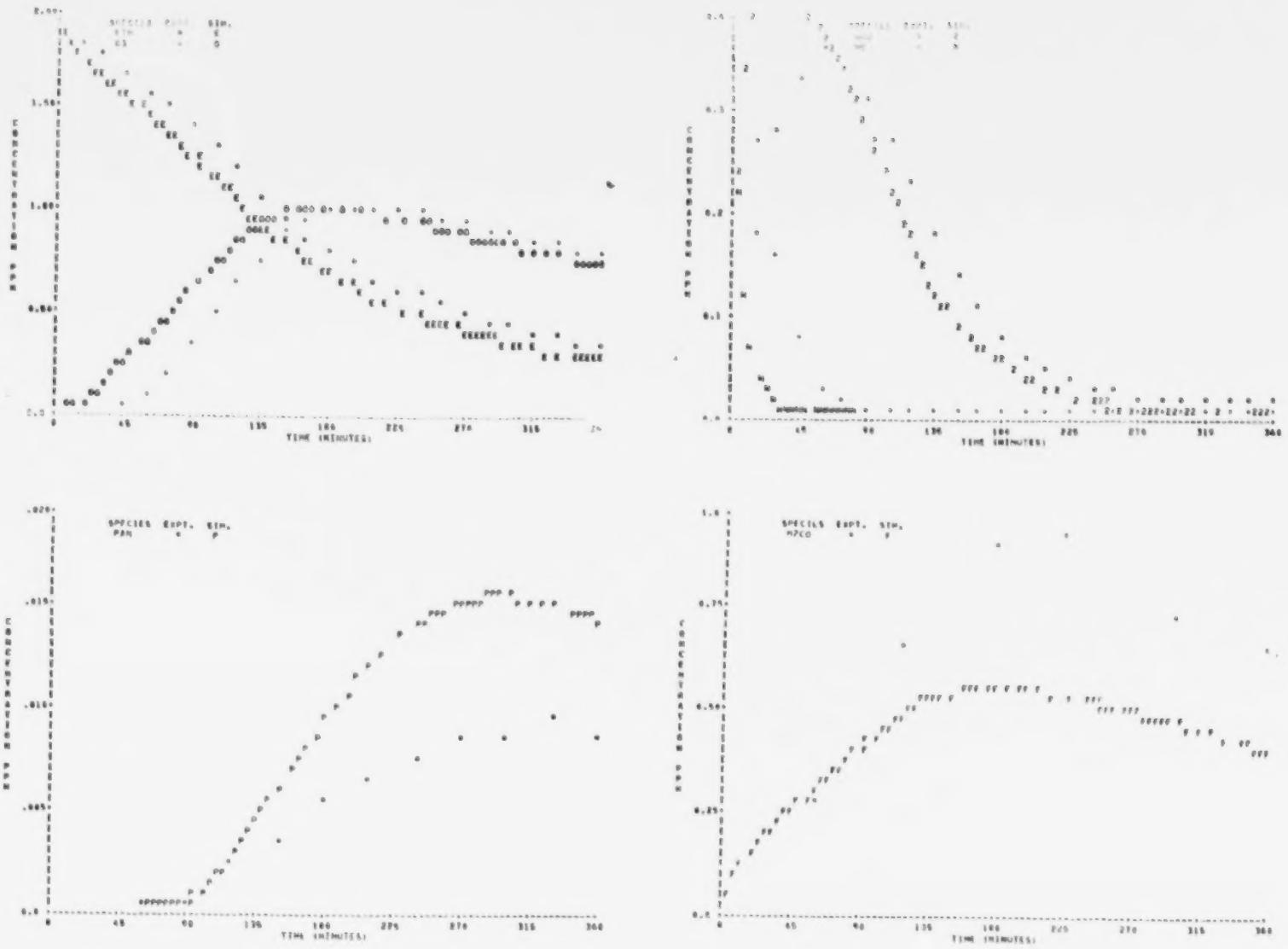

FIGURE B-32 SAPRC EC-143

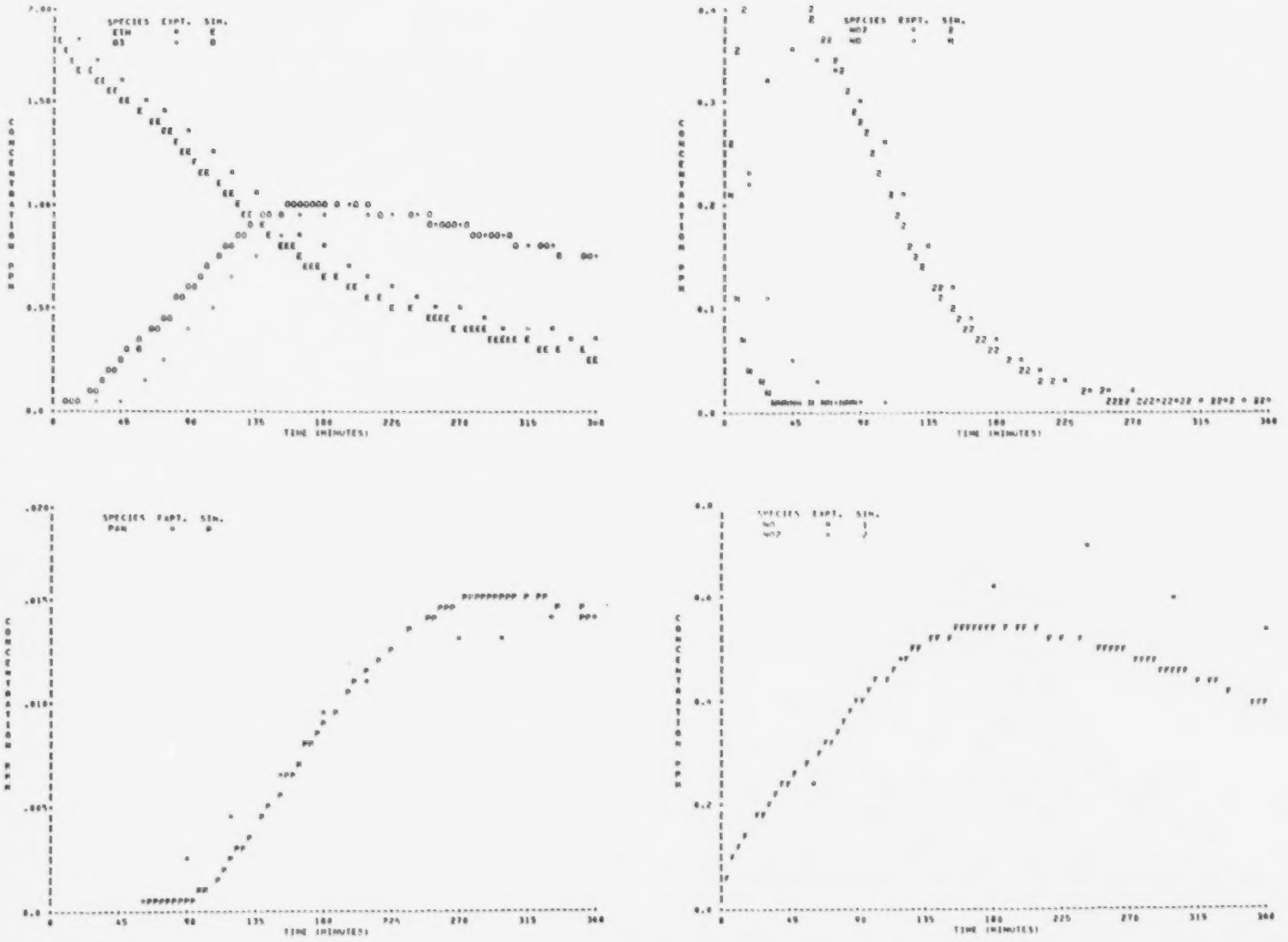

FIGURE B-33 SAPRC EC-156

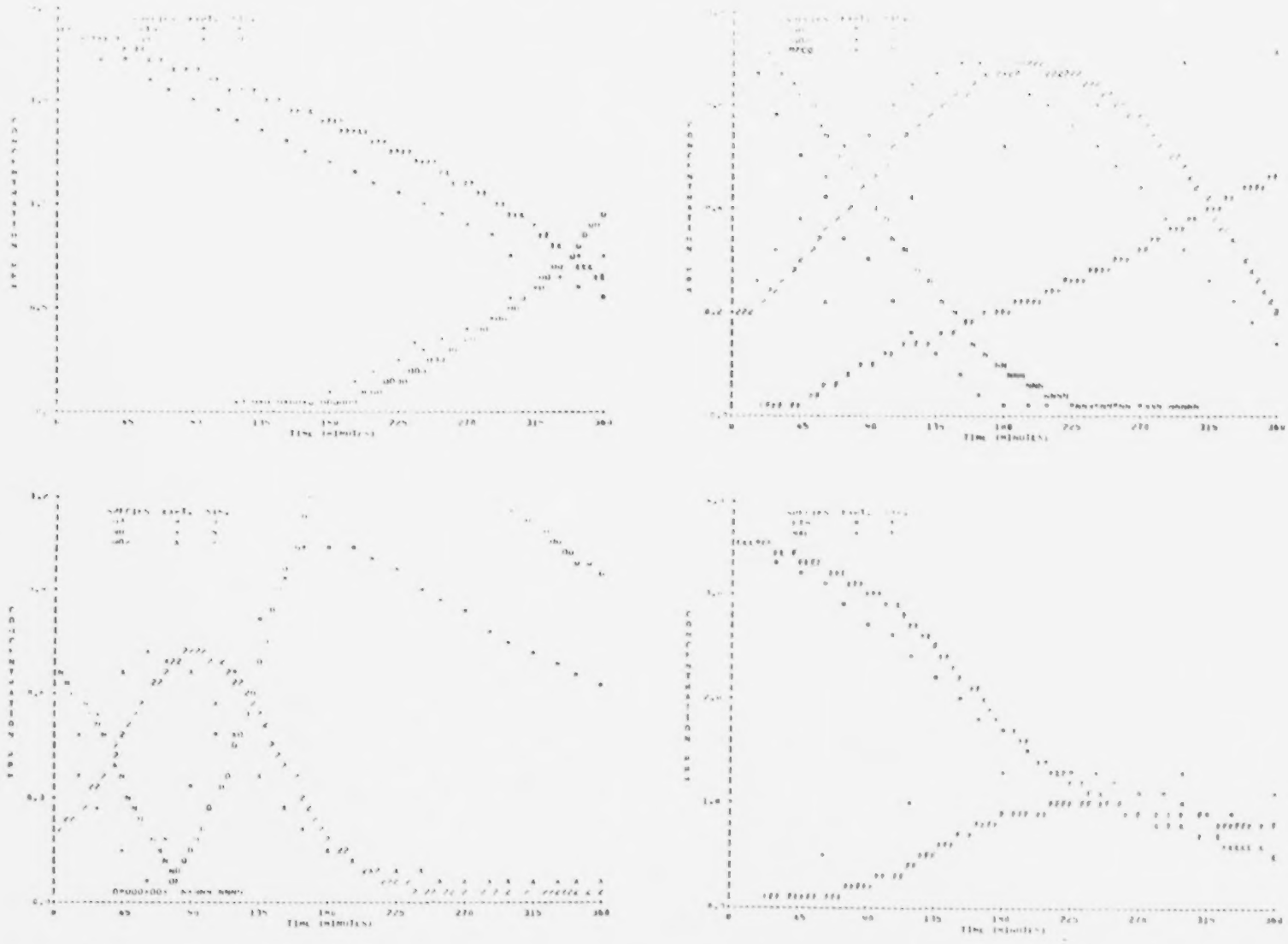

FIGURE B-34 SAPRC EC-285

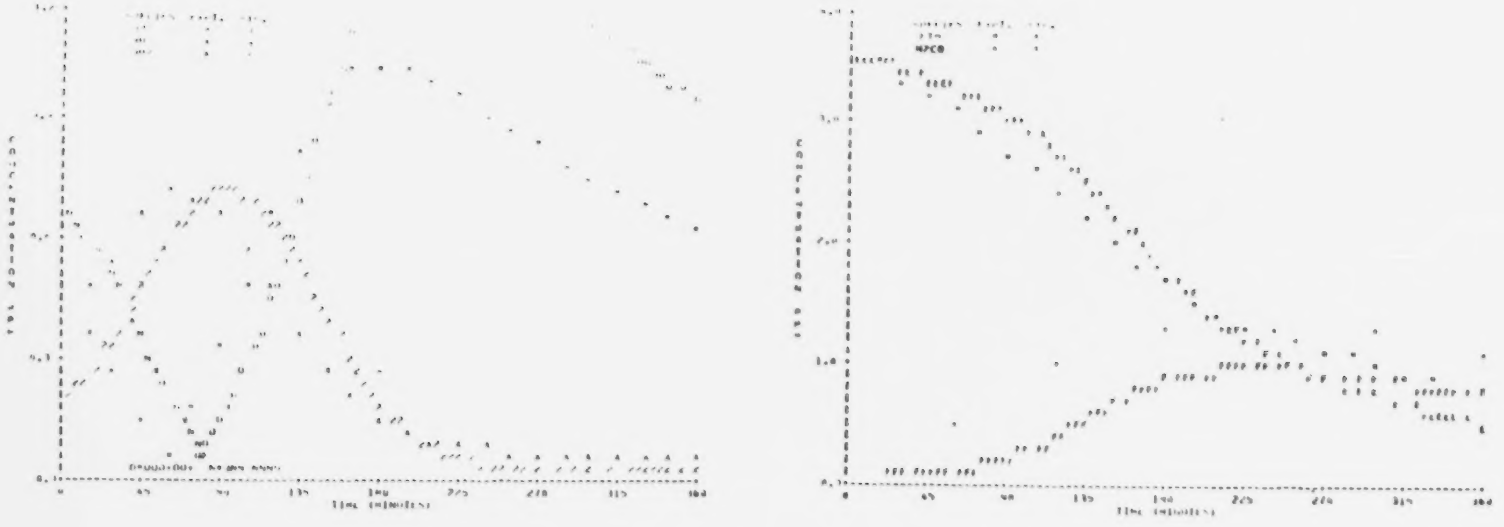

FIGURE B-35 SAPRC EC-286

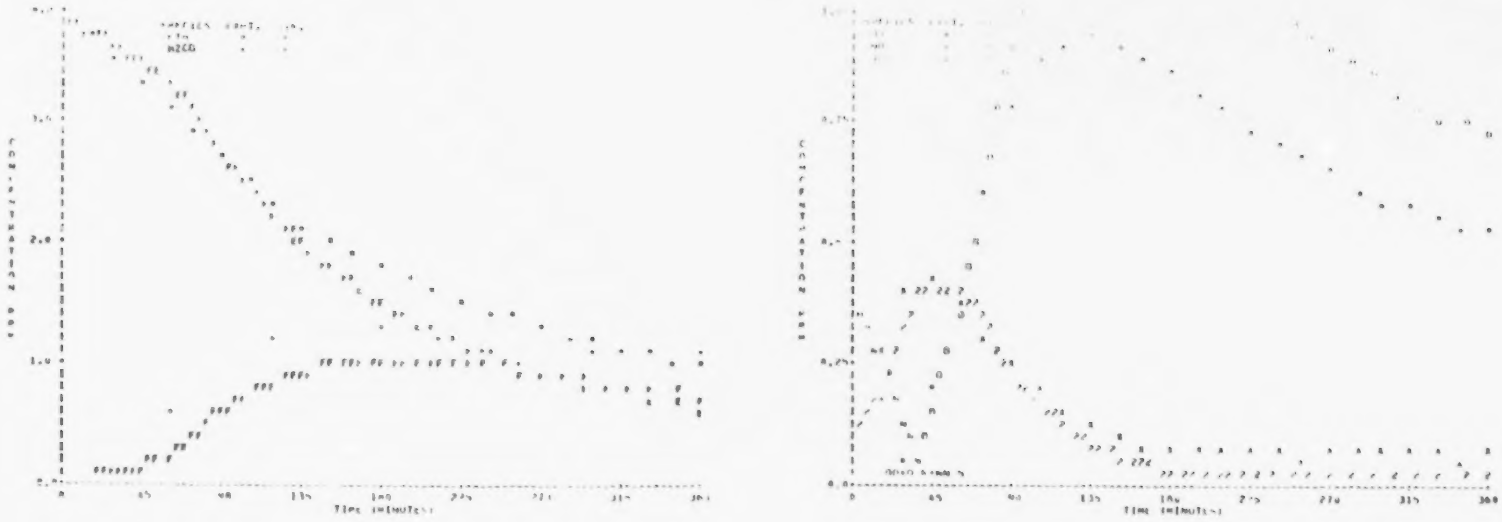

FIGURE B-36 SAPRC EC-287

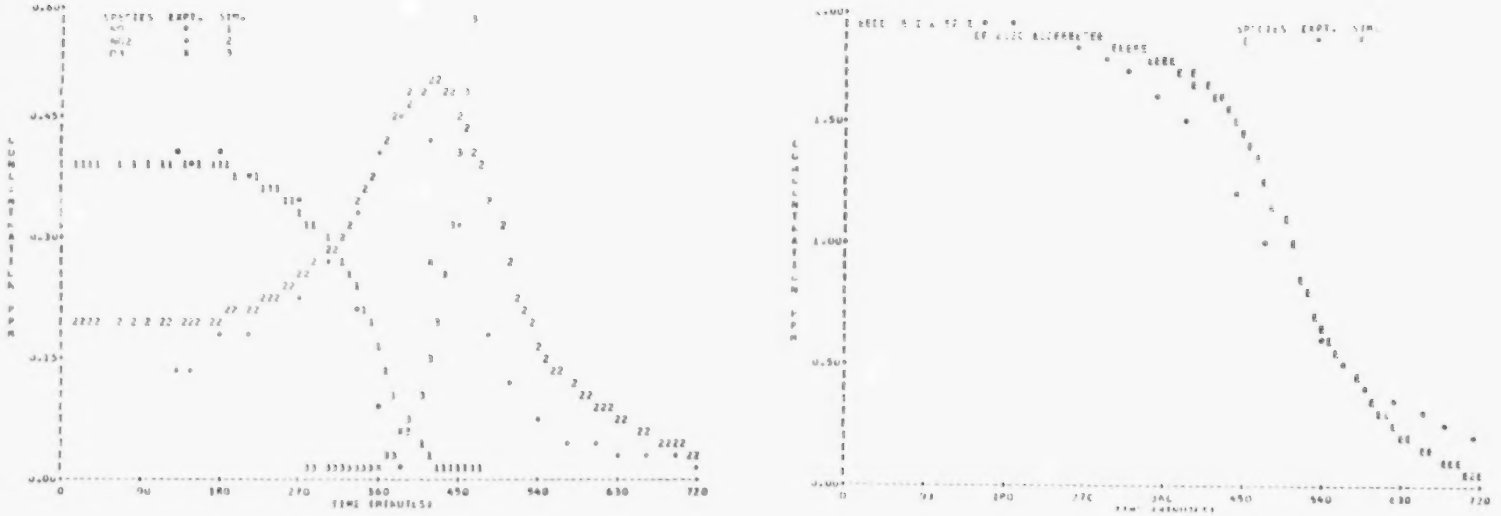

FIGURE B-37 UNC 6.16.78 Red

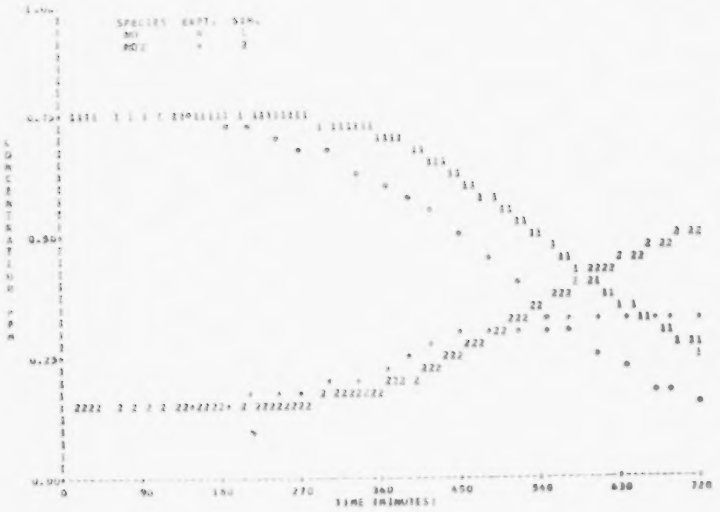

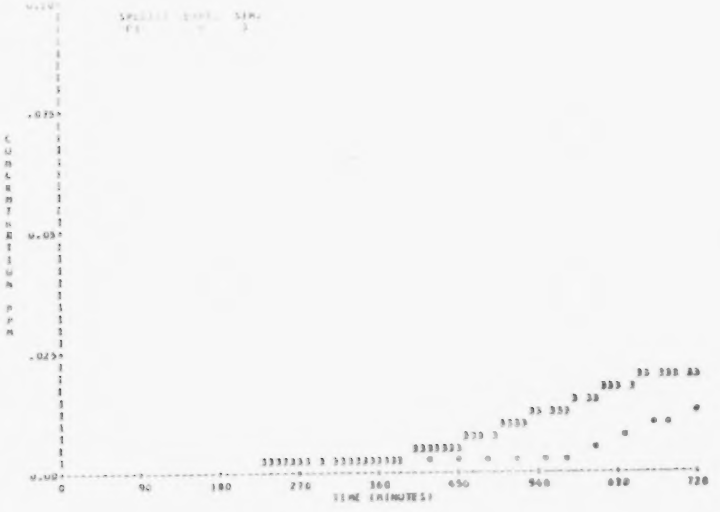

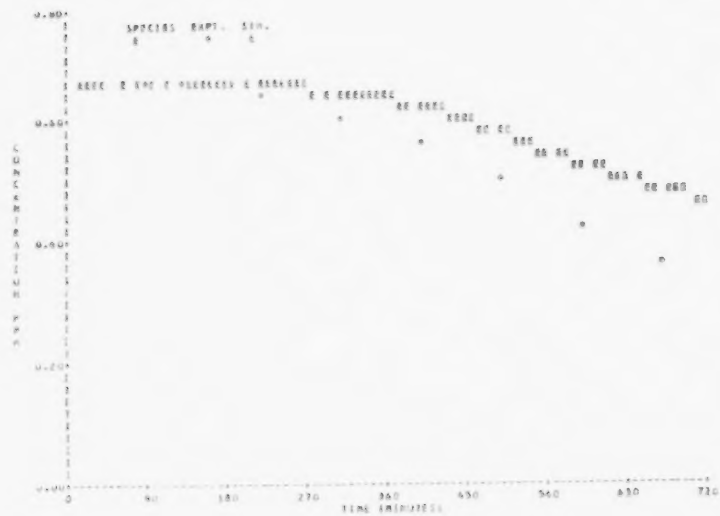

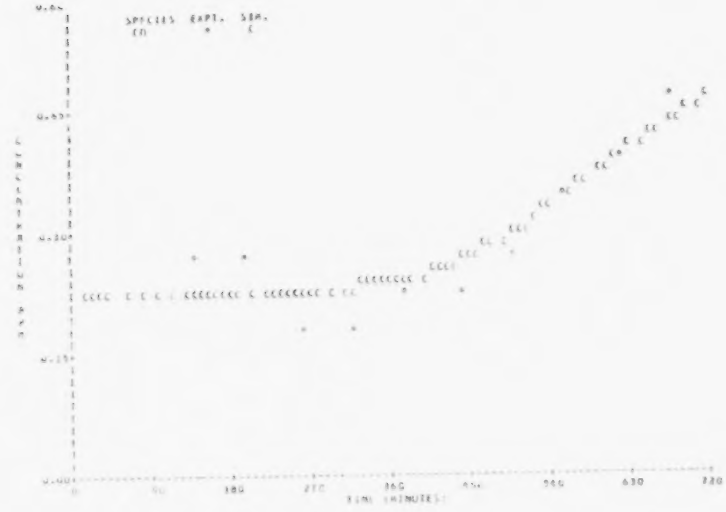

FIGURE B-38 UNC 8.21.78 Rec

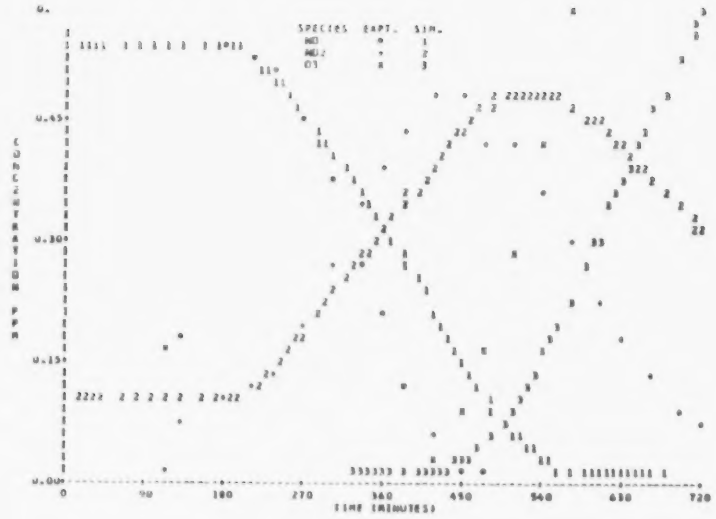

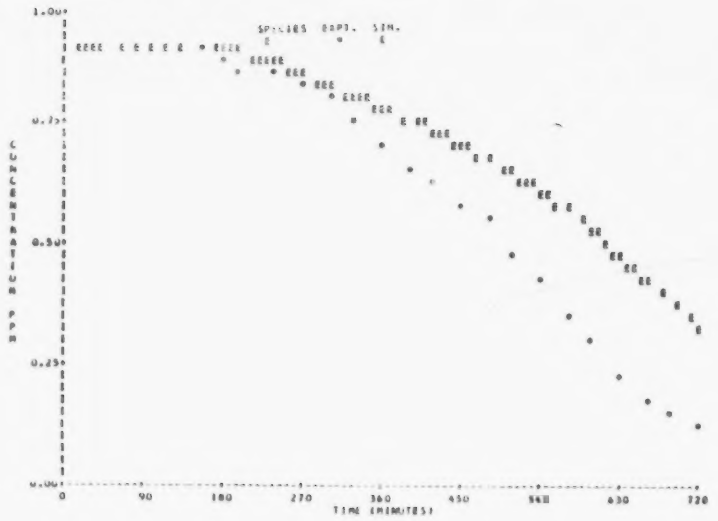

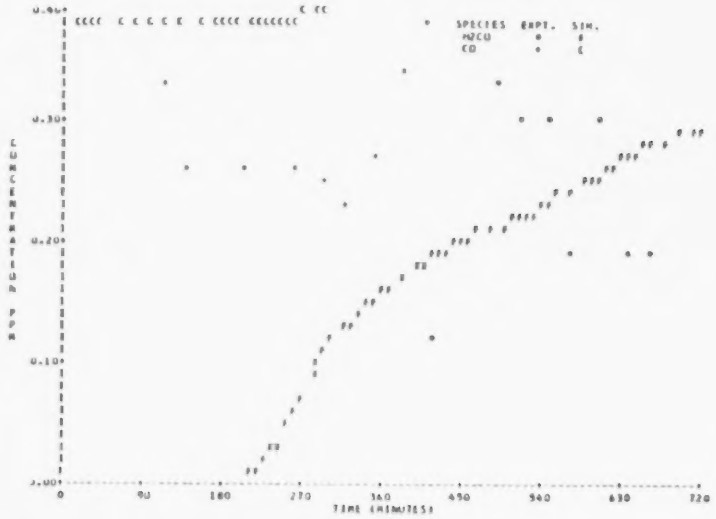

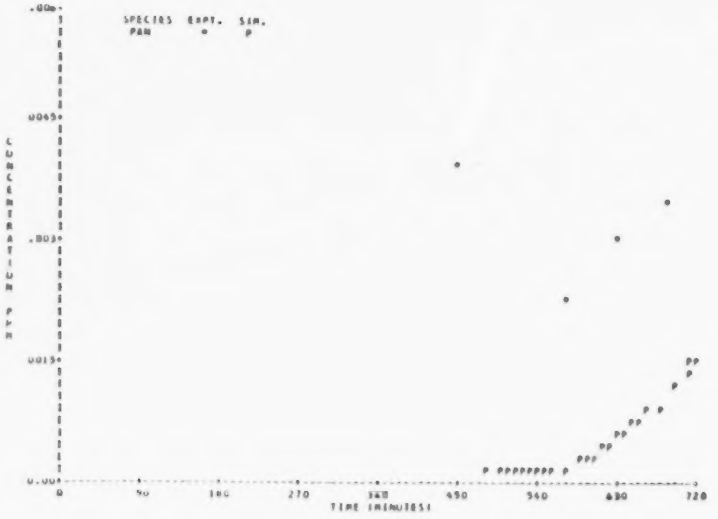

FIGURE B-39 UNC 9.19.78 Red

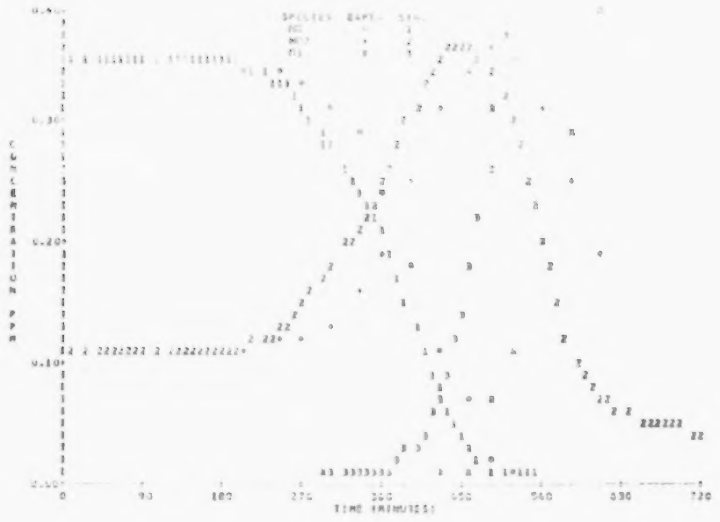

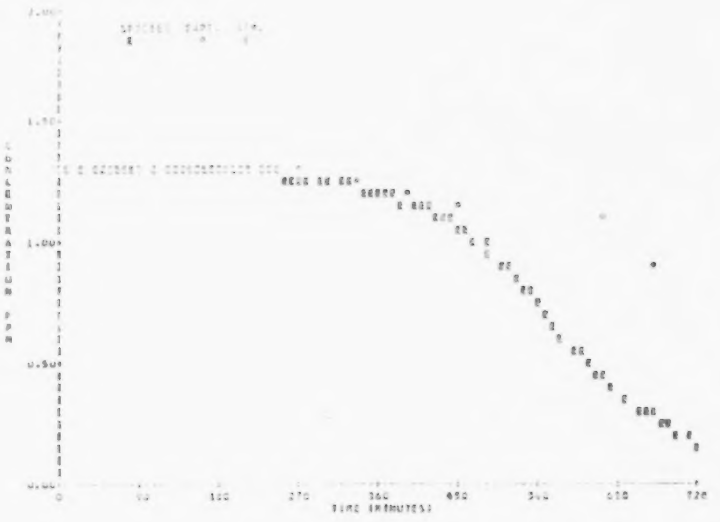

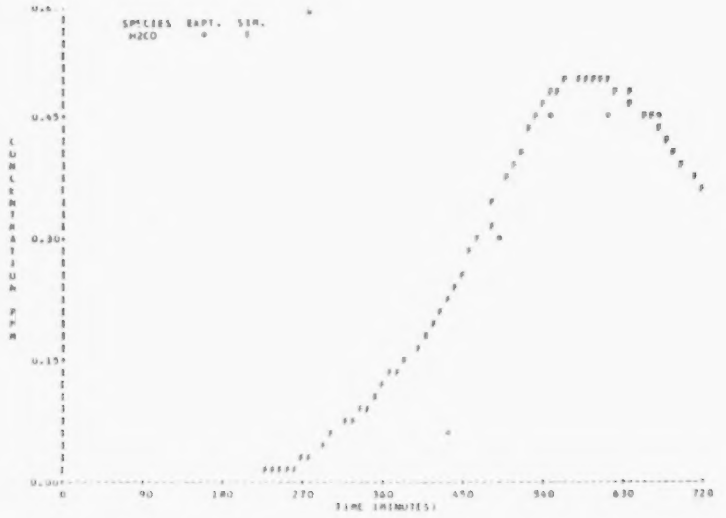

FIGURE B-40 UNC 10.17.78 Red

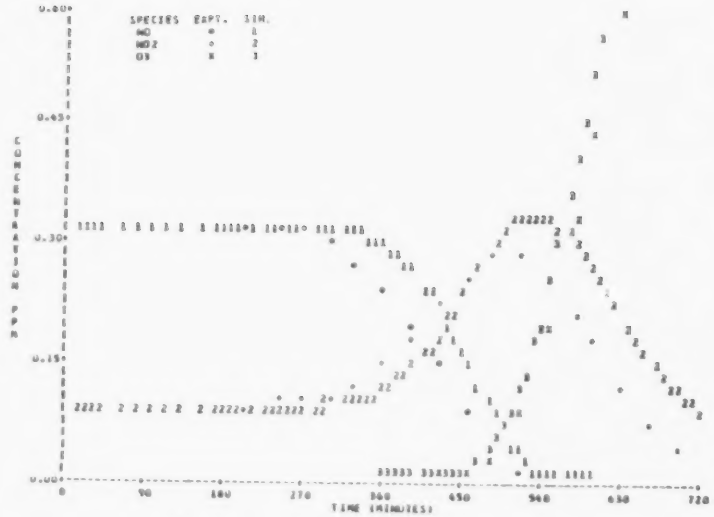

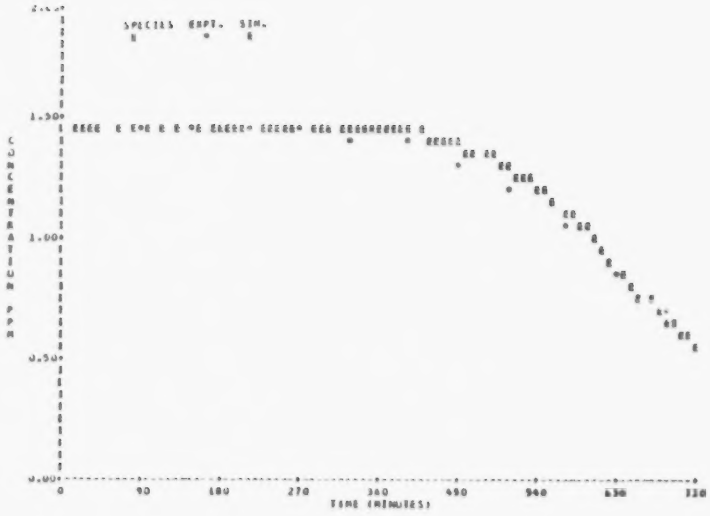

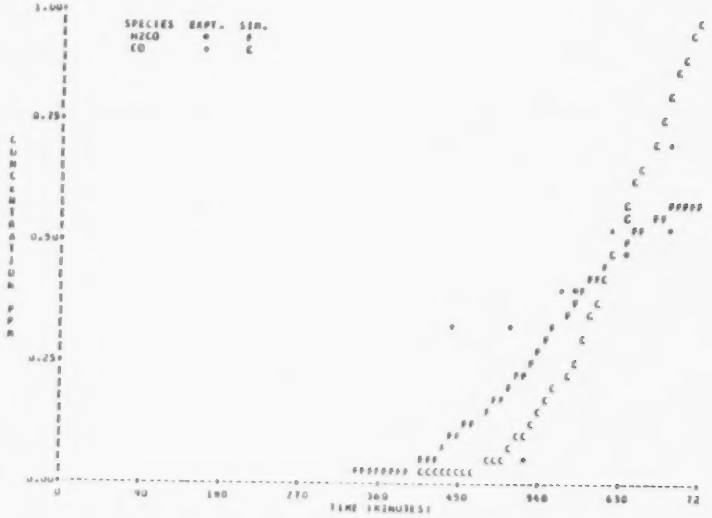

FIGURE B-41 UNC 10.18.78 Red

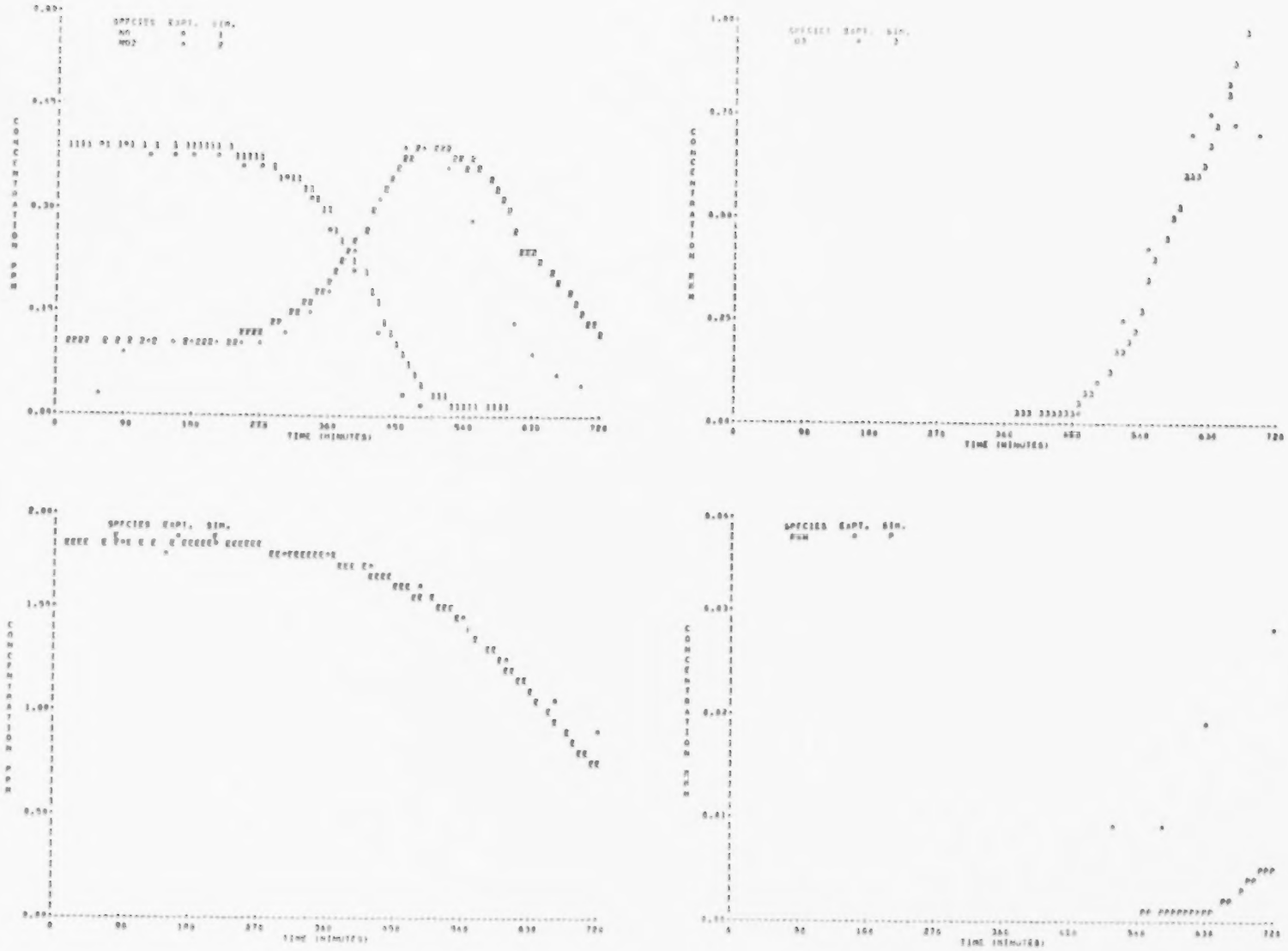

FIGURE B-42 UNC 11.19.78 Red

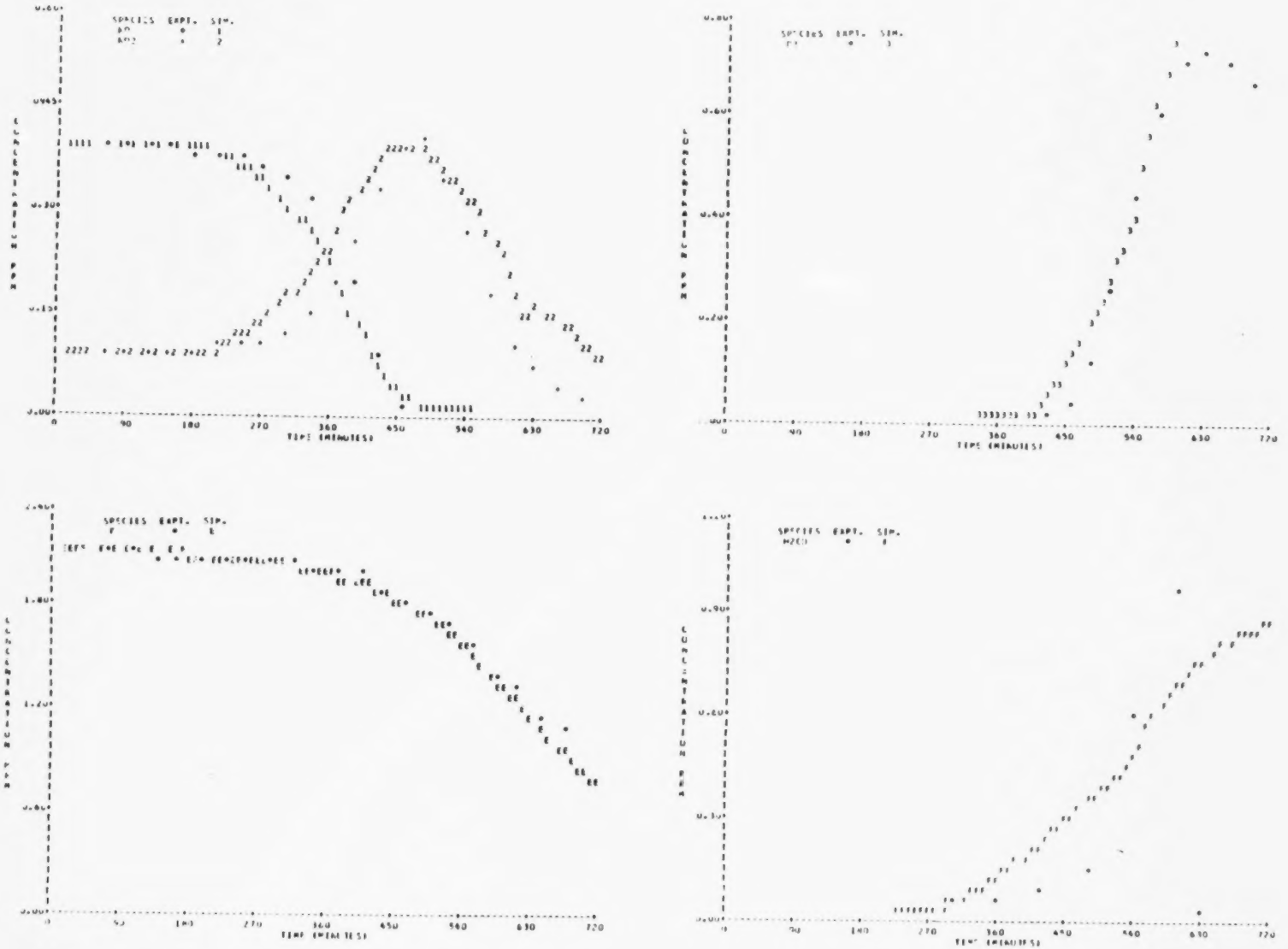

FIGURE B-43 UNC 11.20.78 Red

Appendix C

SIMULATION OF n-BUTANE AND ALDEHYDE CHAMBER RUNS

TABLE C-1. PHOTOLYSIS RATE CONSTANTS FOR n-BUTANE, FORMALDEHYDE, AND ACETALDEHYDE CHAMBER RUNS (in min^{-1})

EC-No.	NO_2	HNO_2	H_2O_2	$O_3(^1D)$	$O_3(^3P)$	H_2CO(rad)	H_2CO(molec)	CH_3CHO	C_2H_5CHO	C_3H_7CHO rad	C_3H_7CHO molec	$C_2H_5C(O)CH_3$
250-255	0.30	8.0×10^{-2}	5.7×10^{-4}	8.4×10^{-6}	1.2×10^{-3}	8.4×10^{-4}	1.6×10^{-3}	4.0×10^{-4}	--	--	--	--
304-307	0.43	0.13	9.1×10^{-4}	1.6×10^{-5}	2.0×10^{-3}	1.0×10^{-3}	2.9×10^{-3}	7.0×10^{-4}	1.4×10^{-3}	1.0×10^{-3}	6.0×10^{-4}	4.6×10^{-4}
308	0.44	0.13	9.3×10^{-4}	1.6×10^{-5}	2.1×10^{-3}	1.0×10^{-3}	3.0×10^{-3}	7.2×10^{-4}	1.4×10^{-3}	1.0×10^{-3}	6.1×10^{-4}	4.7×10^{-4}
309	0.45	0.13	9.5×10^{-4}	1.7×10^{-5}	2.1×10^{-3}	1.0×10^{-3}	3.1×10^{-3}	7.4×10^{-4}	1.5×10^{-3}	1.0×10^{-3}	6.3×10^{-4}	4.8×10^{-4}

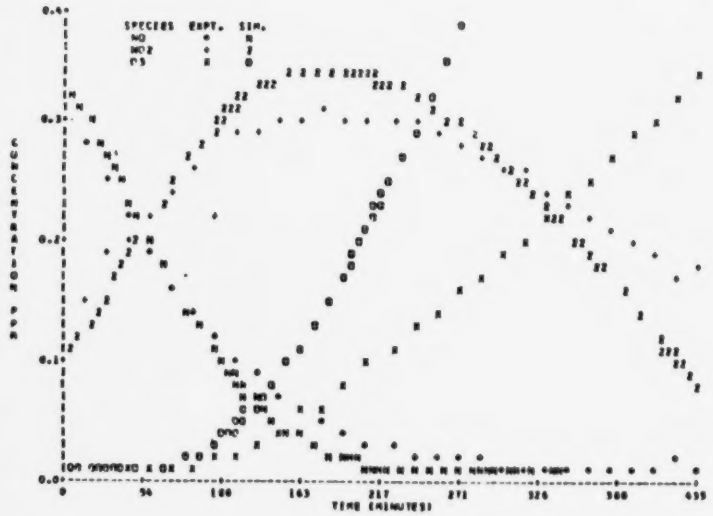

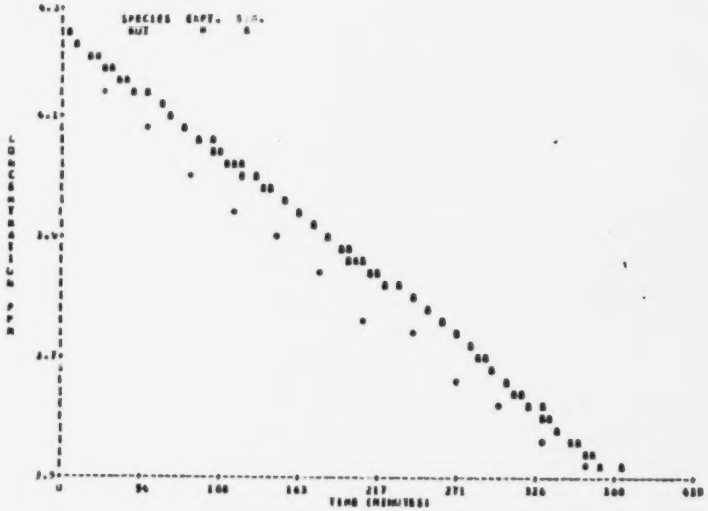

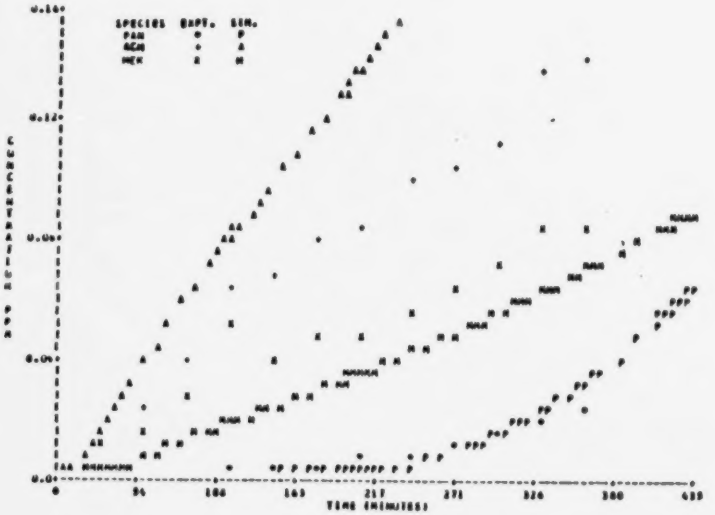

FIGURE C-1 SAPRC EC-304

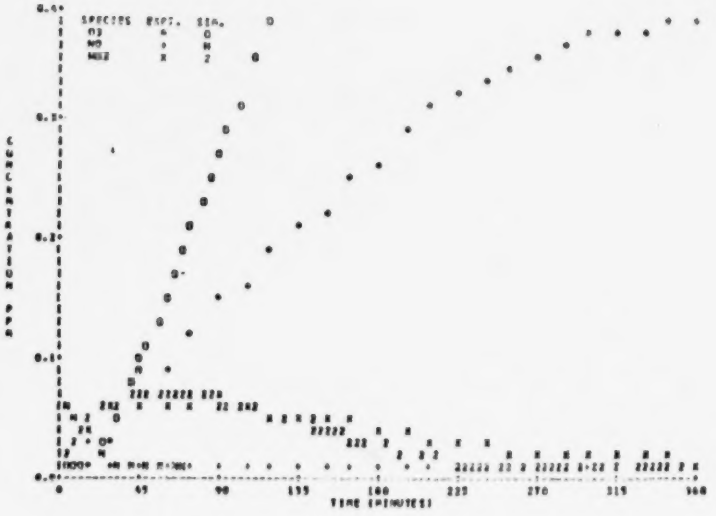

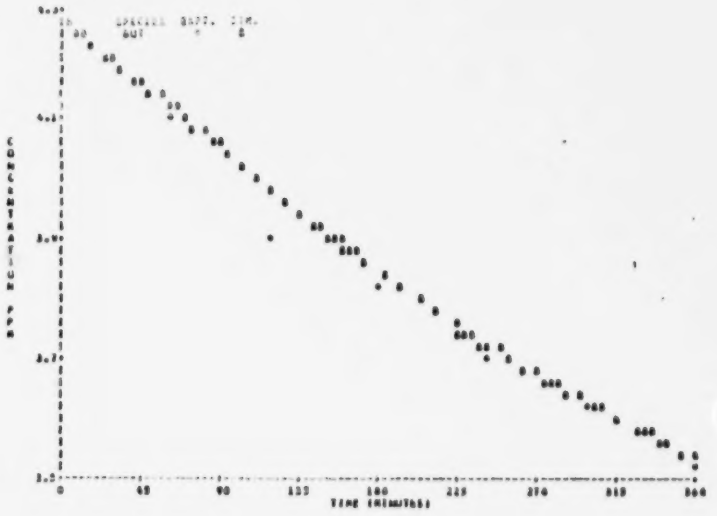

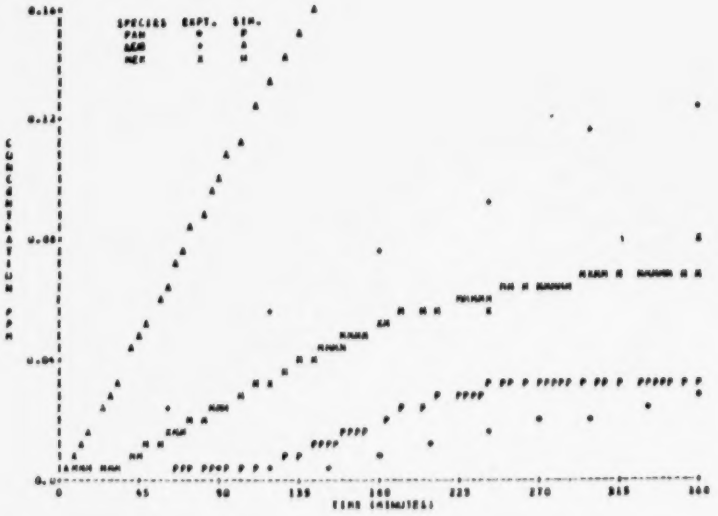

FIGURE C-2 SAPRC EC-305

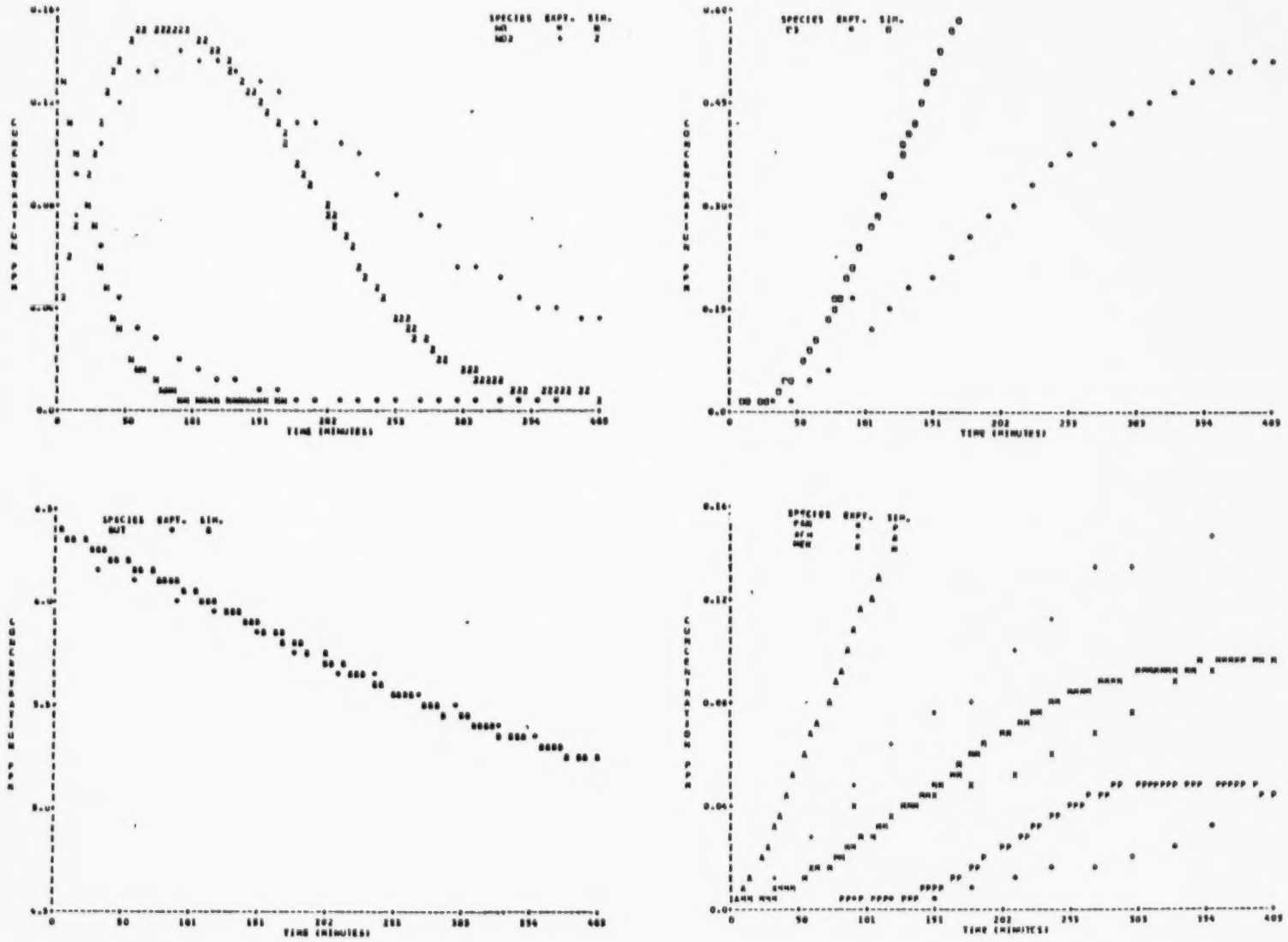

FIGURE C-3 SAPRC EC-306

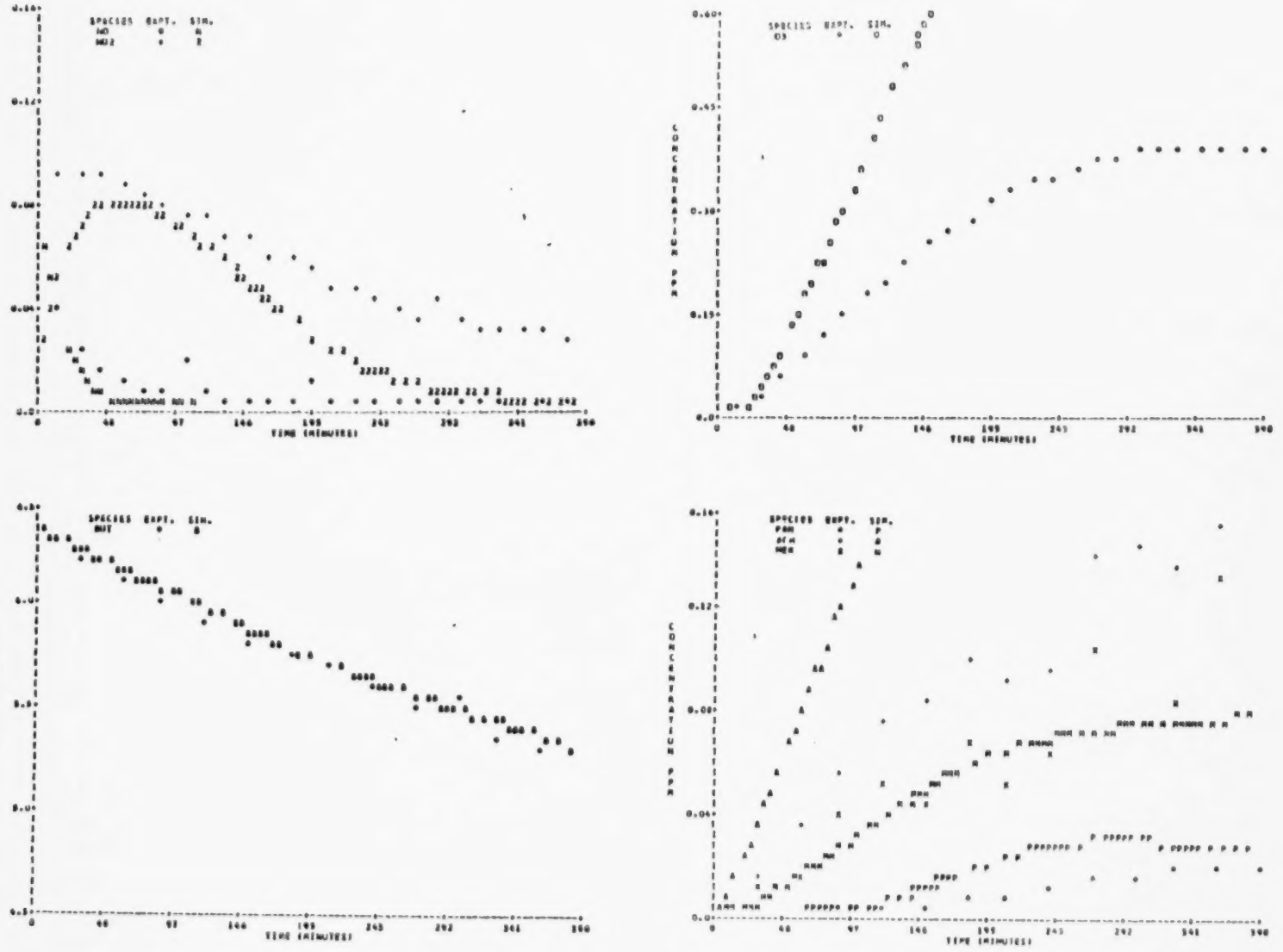

FIGURE C-4 SAPRC EC-307

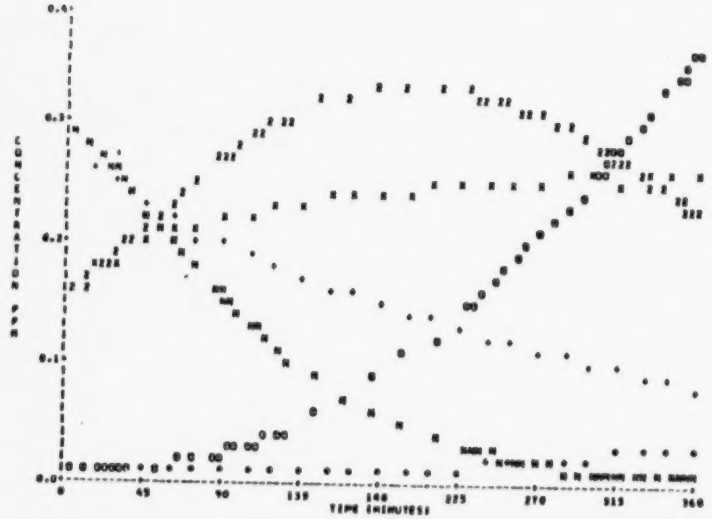

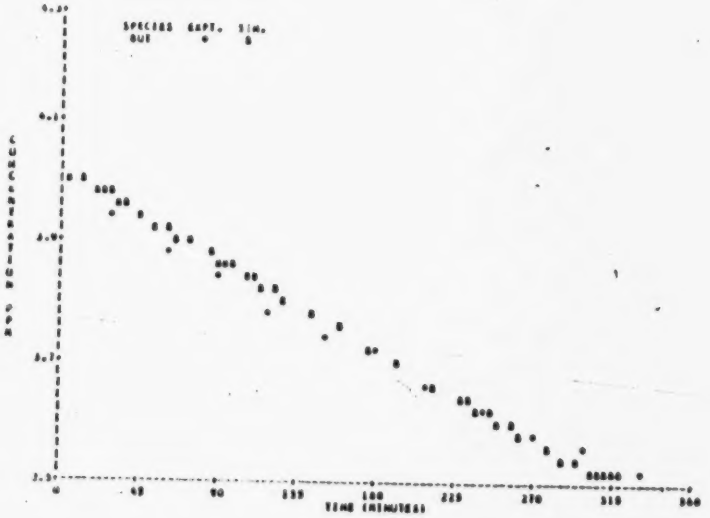

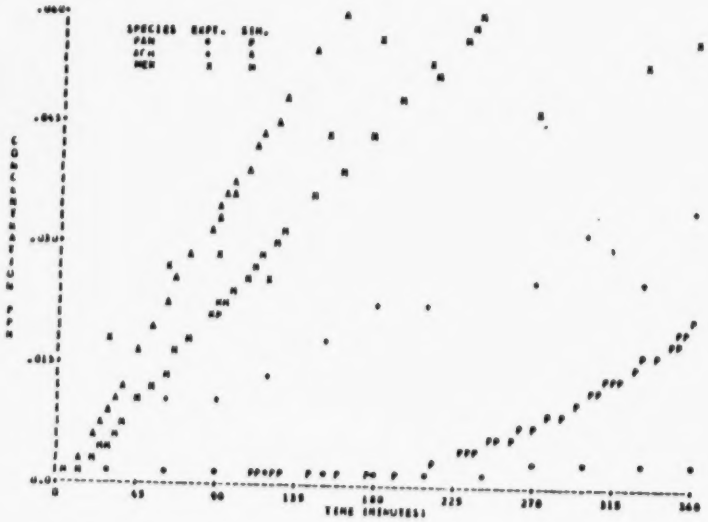

FIGURE C-5 SAPRC EC-308

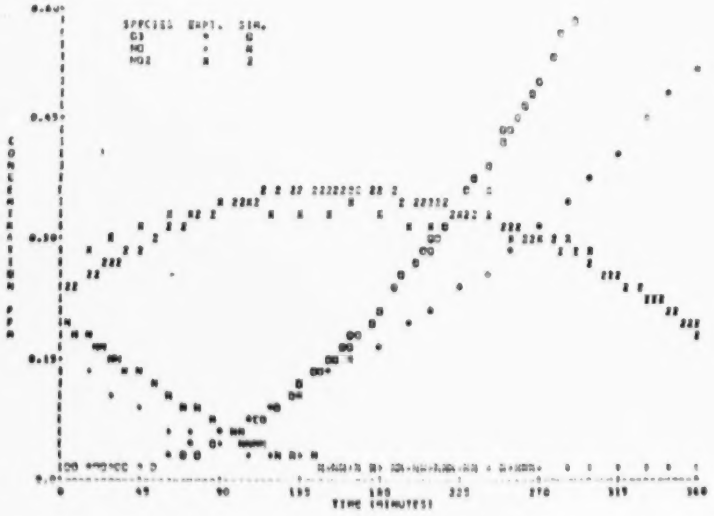

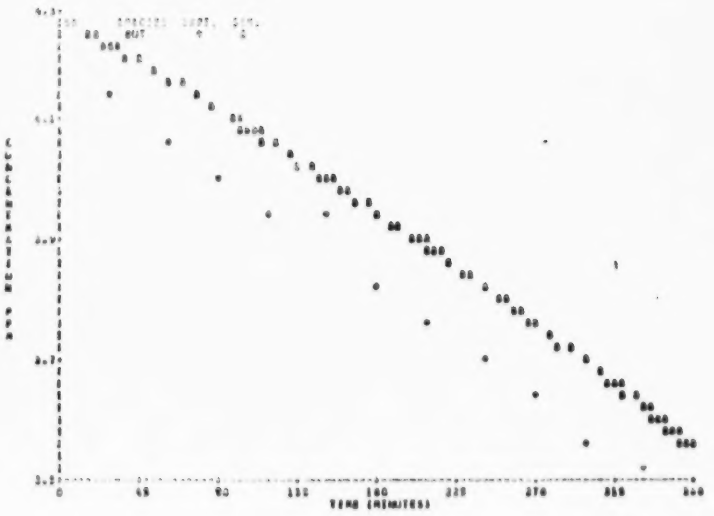

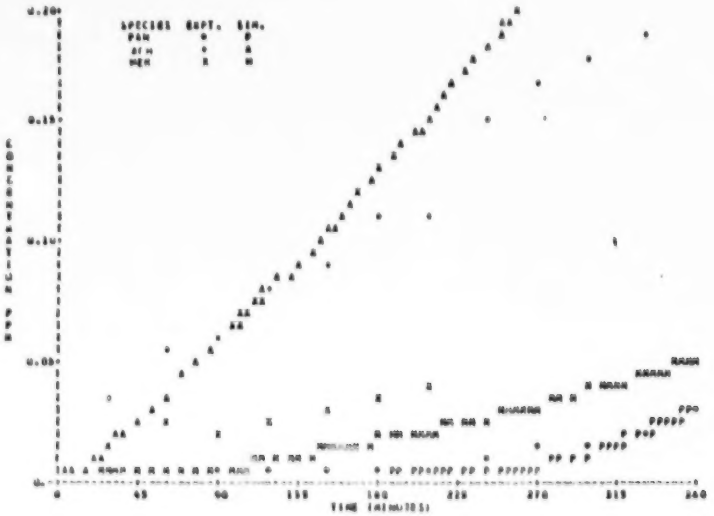

FIGURE C-6 SAPRC EC-309

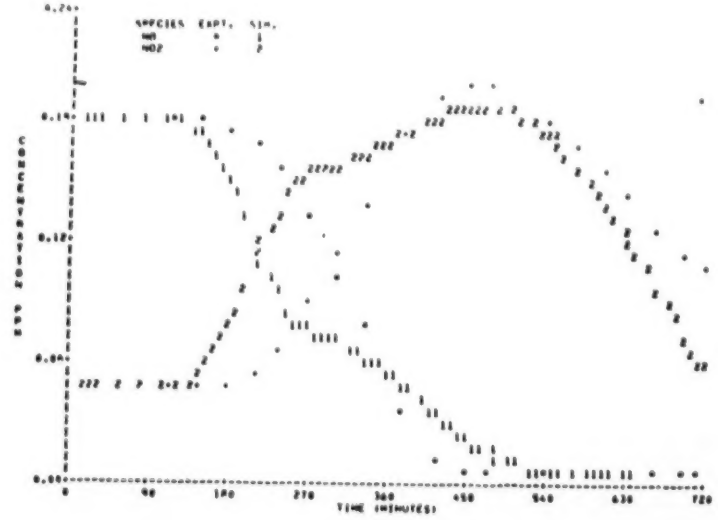

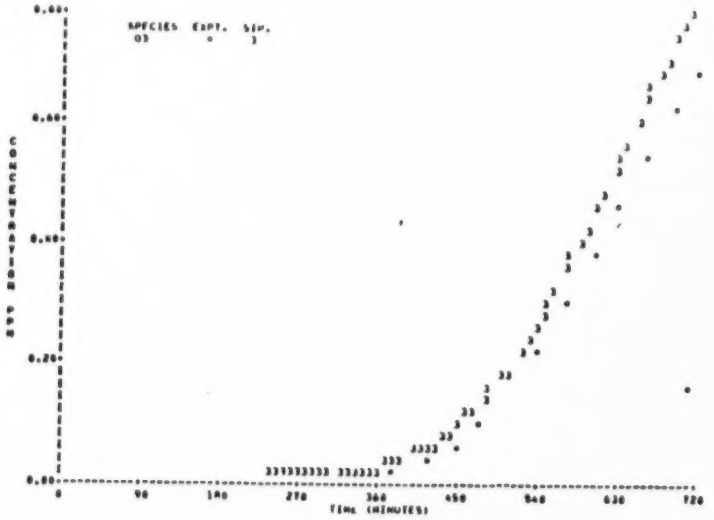

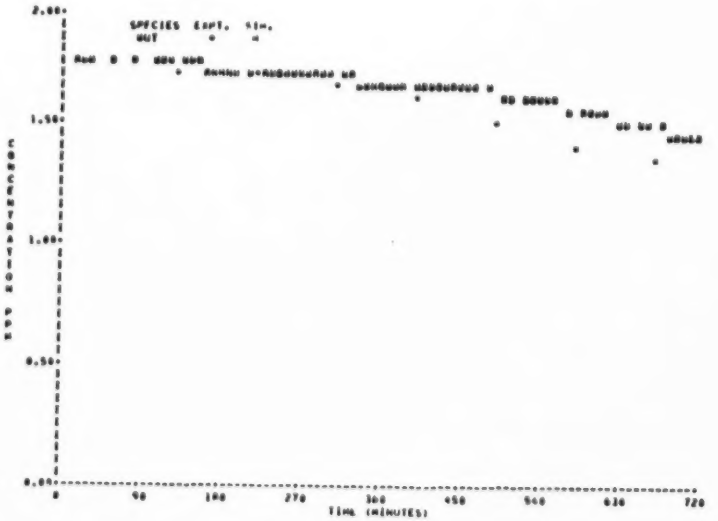

FIGURE C-7 UNC 7.21.78 Red

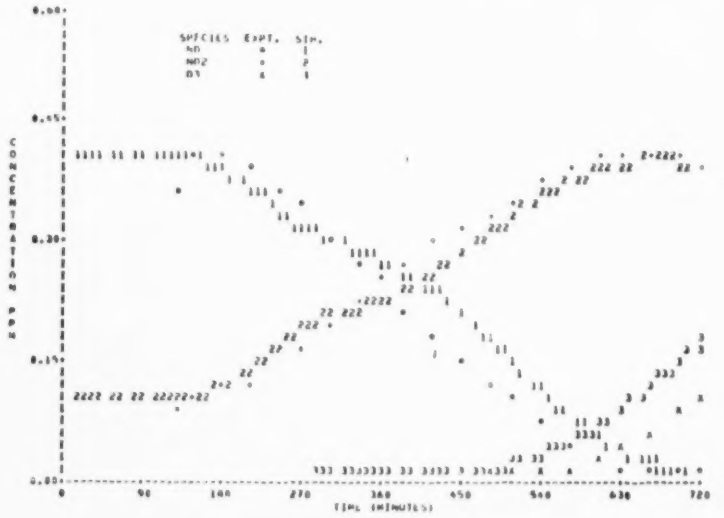

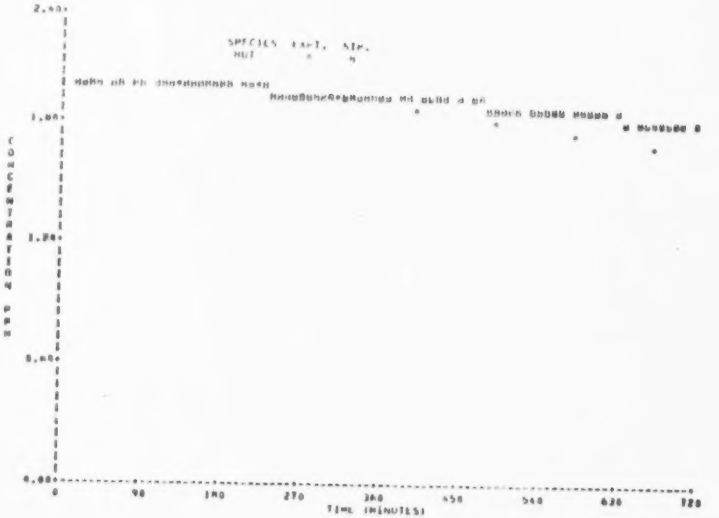

FIGURE C-8 UNC 7.22.78 Red

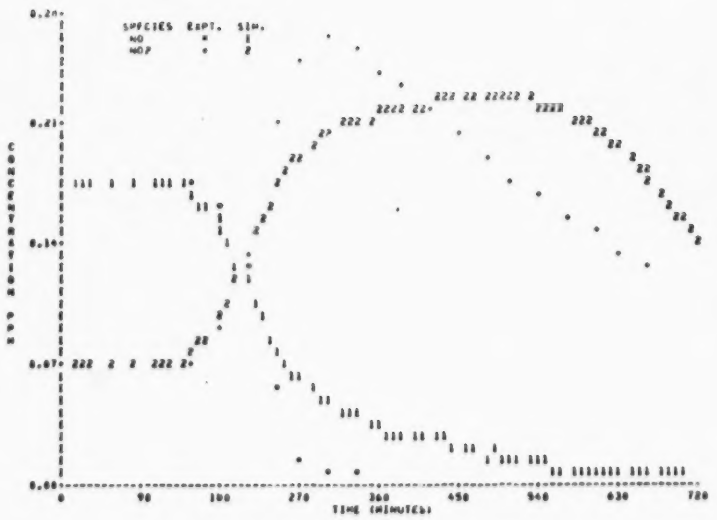

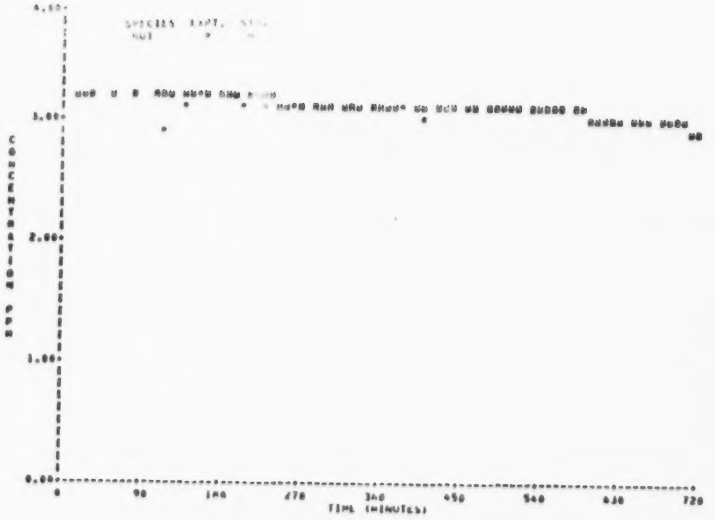

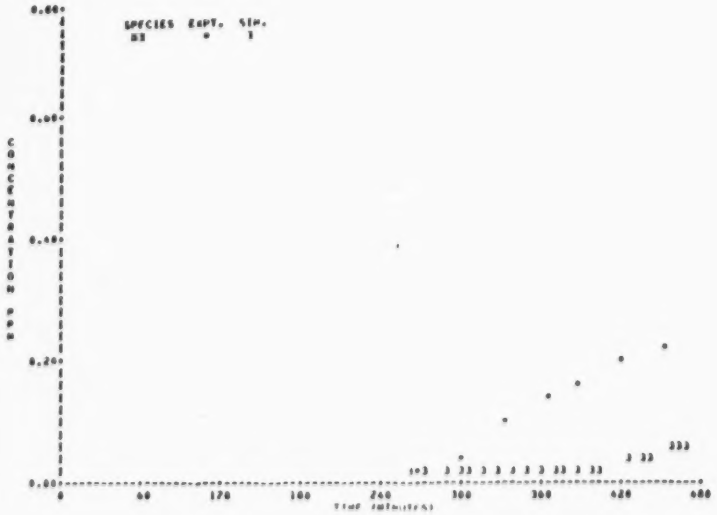

FIGURE C-9 UNC 2.27.78 Red

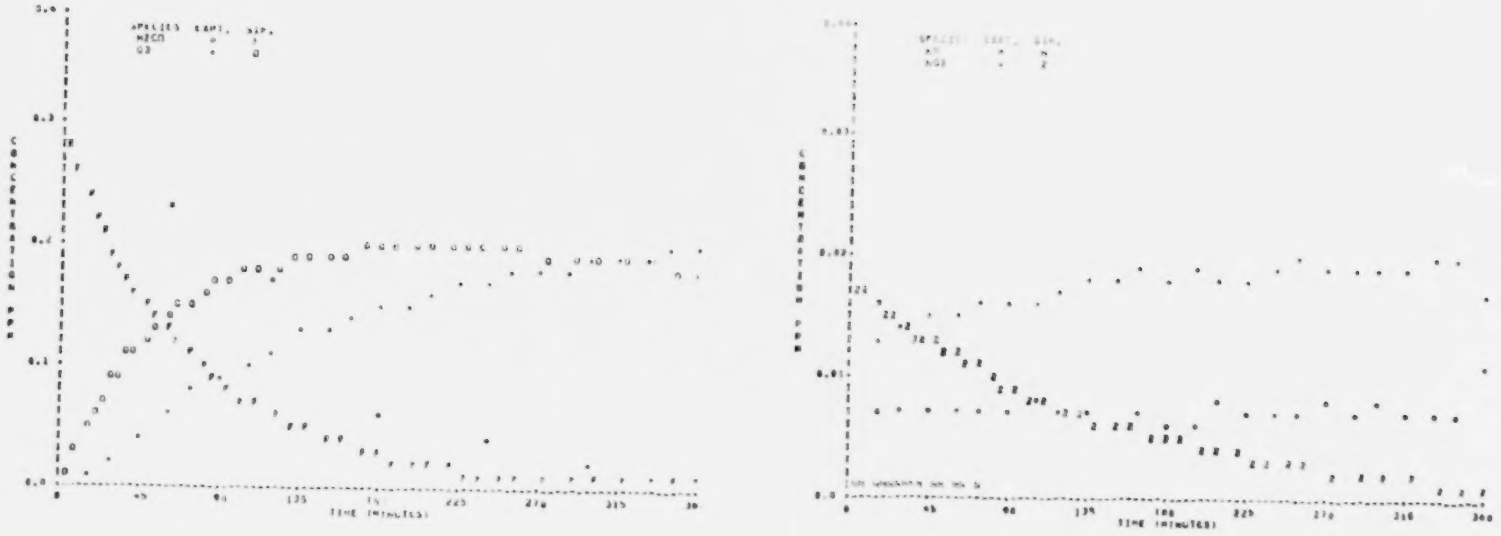

FIGURE C-10 SAPRC EC-250

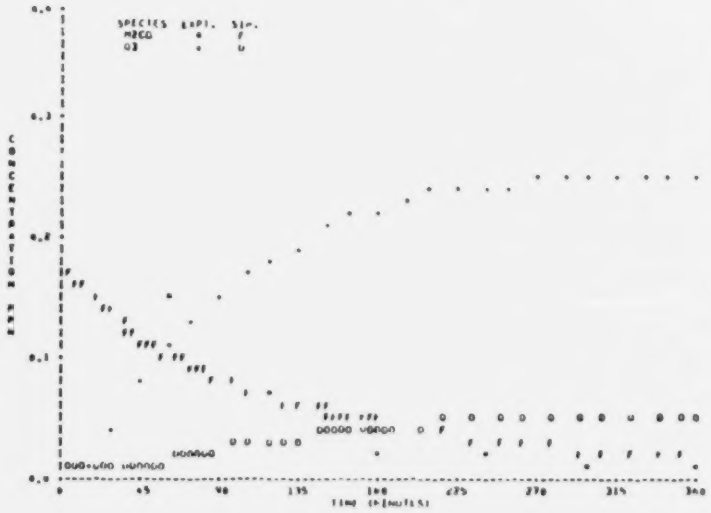

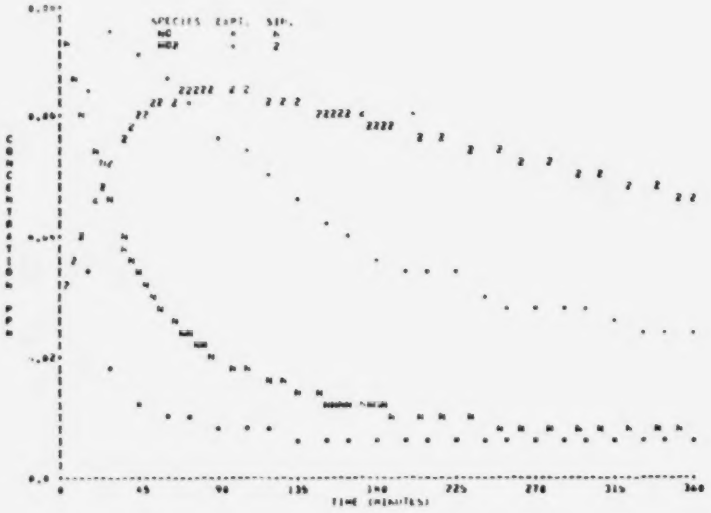

FIGURE C-11 SAPRC EC-251

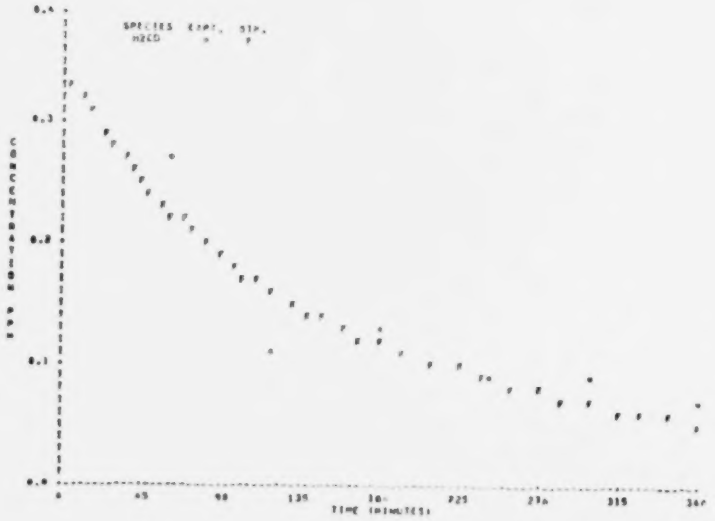

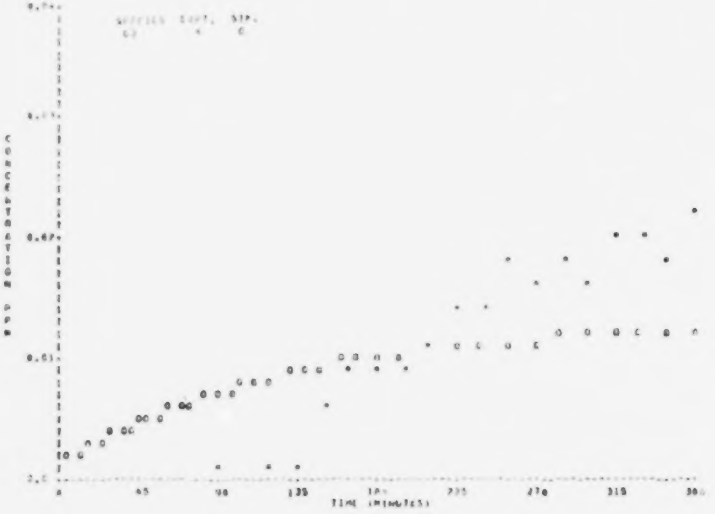

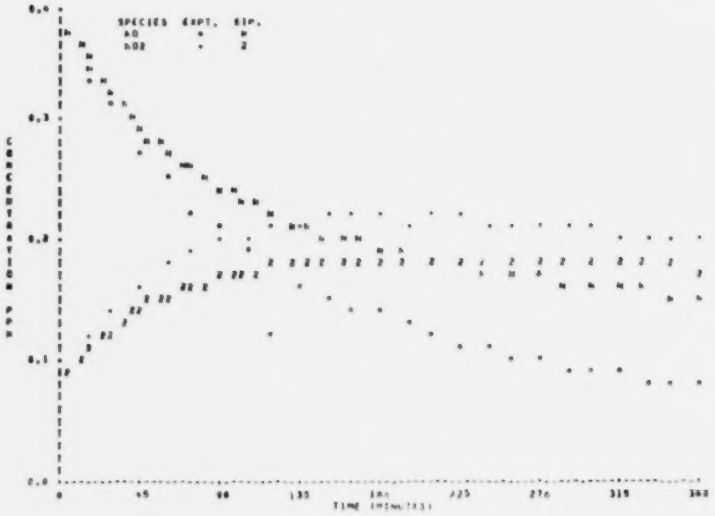

FIGURE C-12 SAPRC EC-252

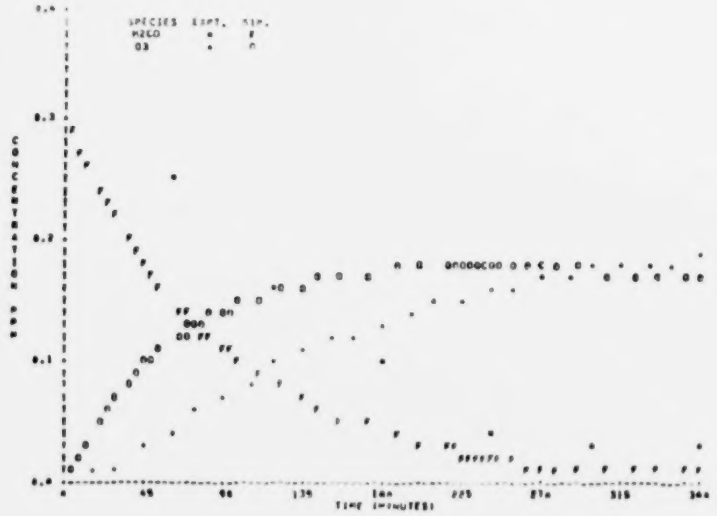

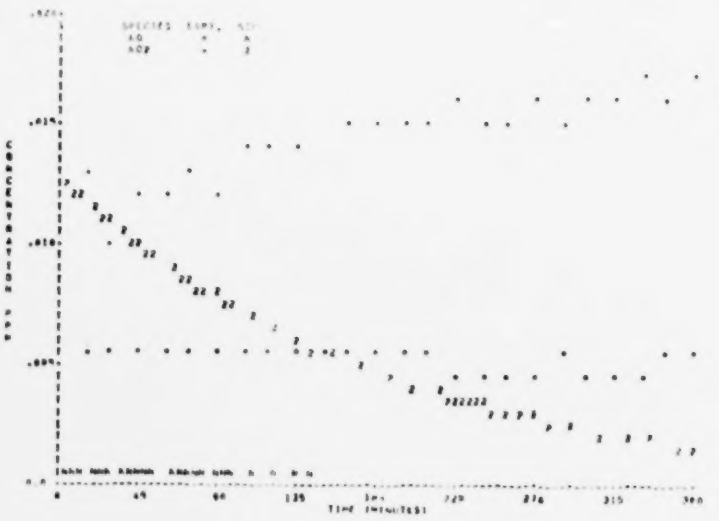

FIGURE C-13 SAPRC EC-255

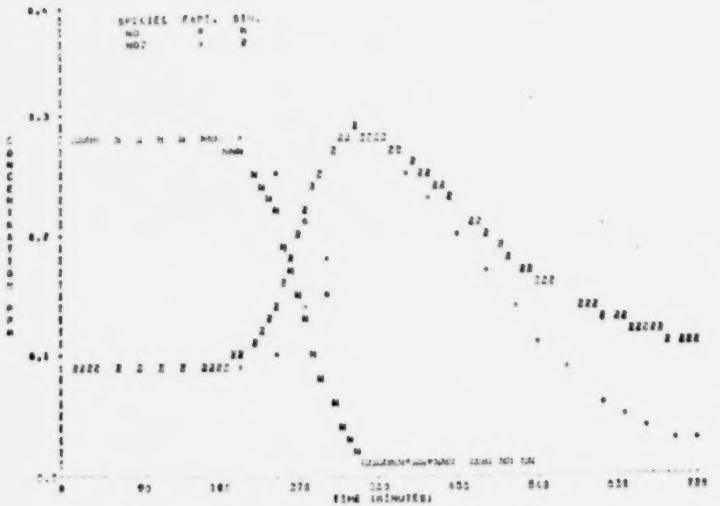

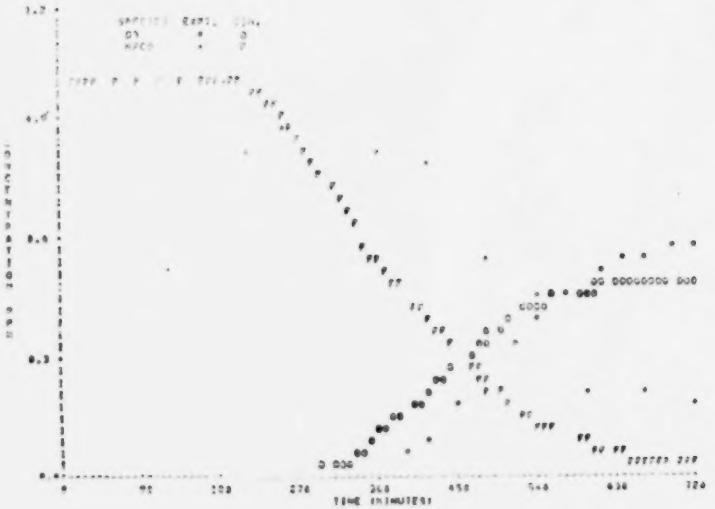

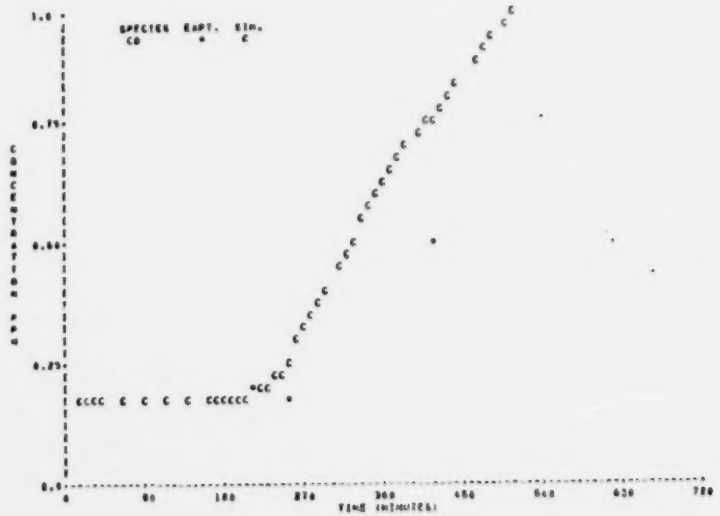

FIGURE C-14 UNC 9.14.77 Red

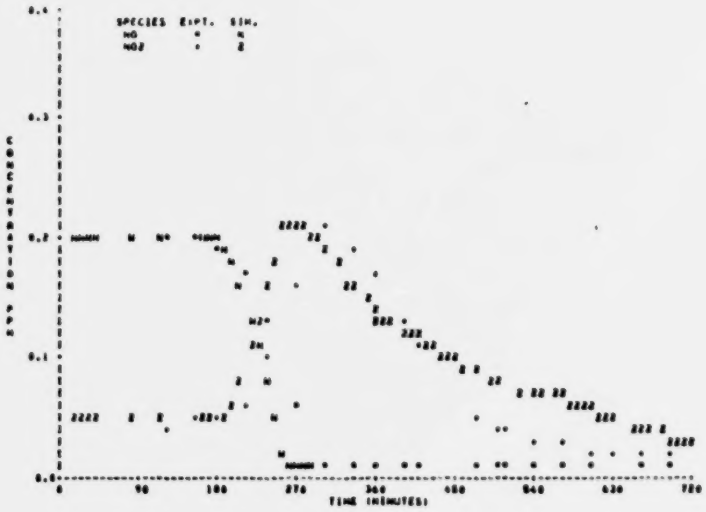

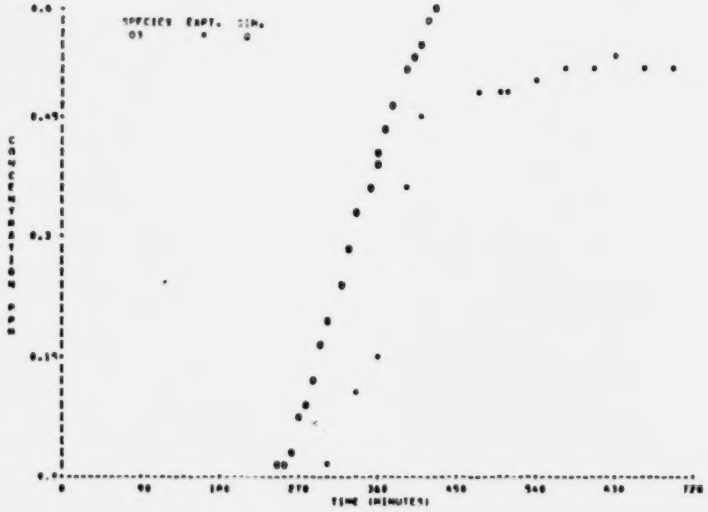

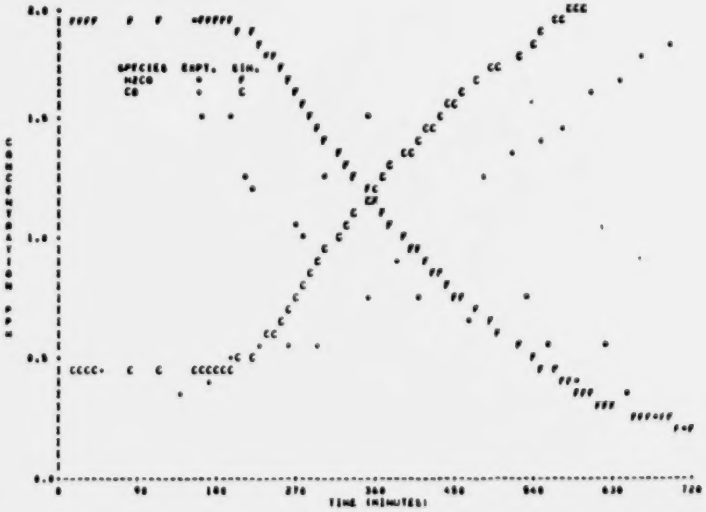

FIGURE C-15 UNC 9.15.78 Blue

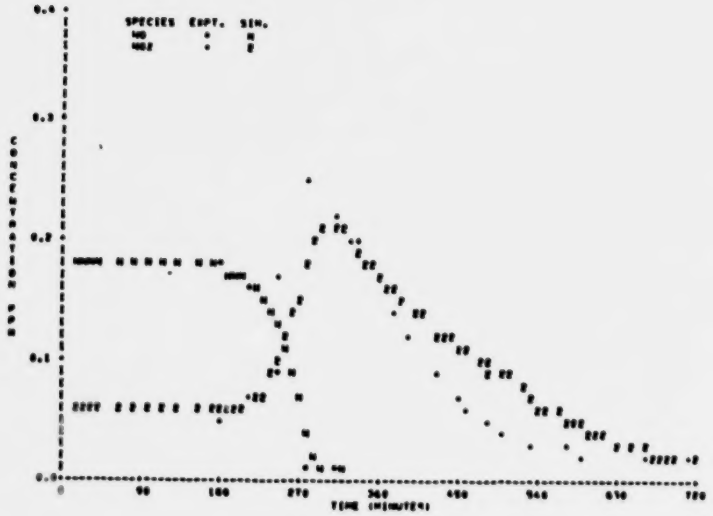

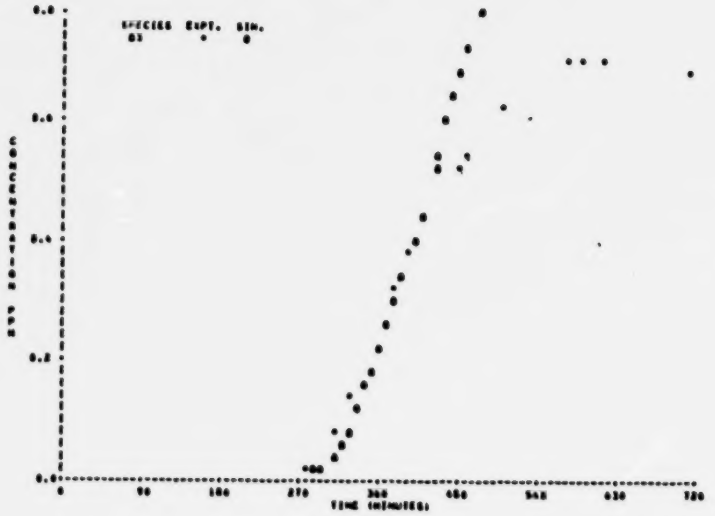

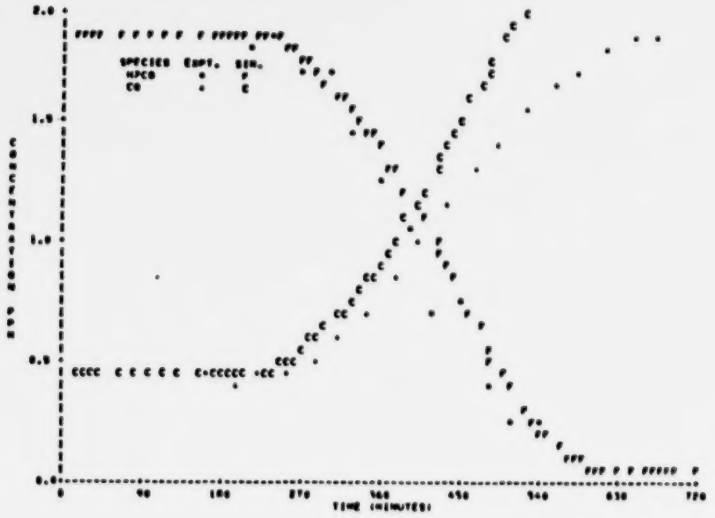

FIGURE C-16 UNC 9.21.78 Blue

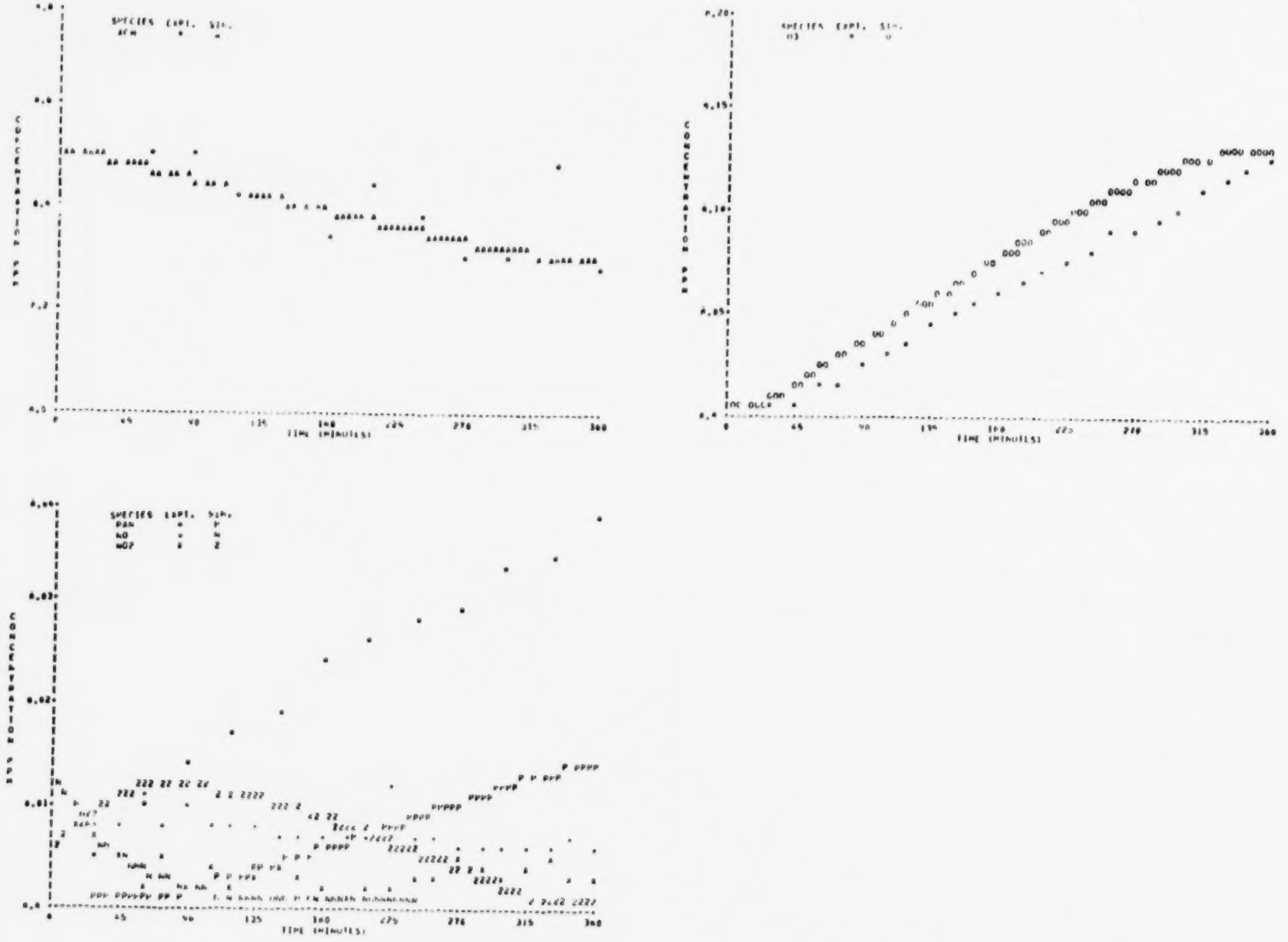

FIGURE C-17 SAPRC EC-253

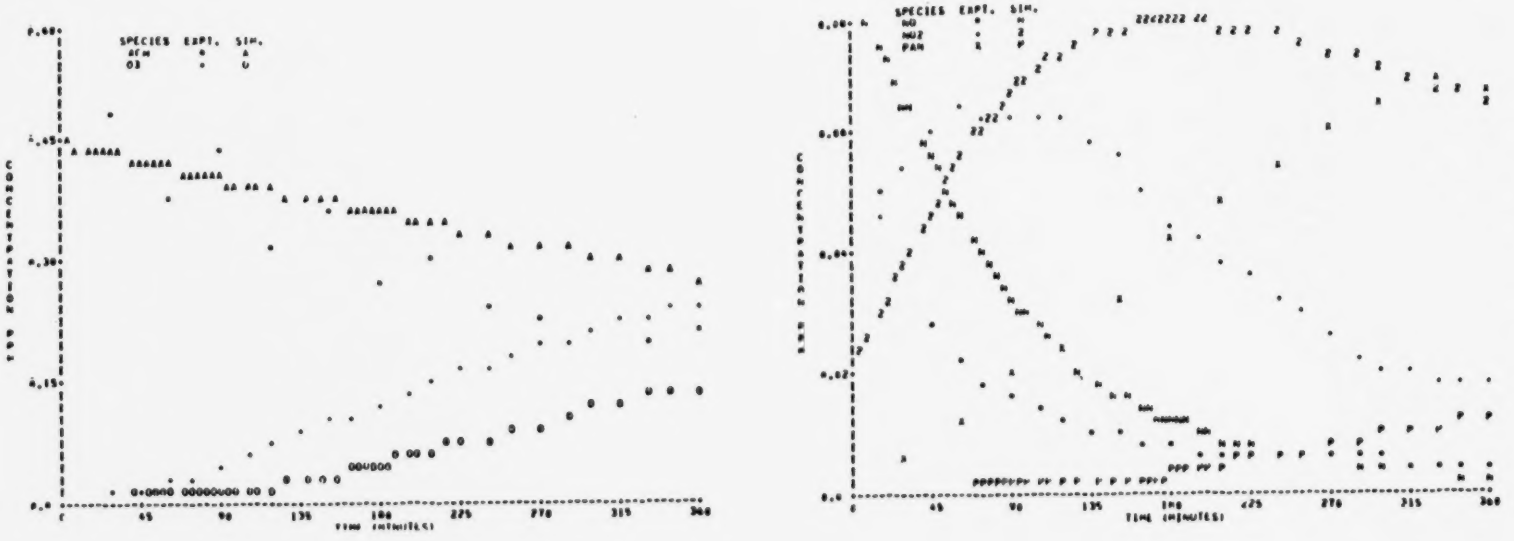

FIGURE C-18 SAPRC EC-253

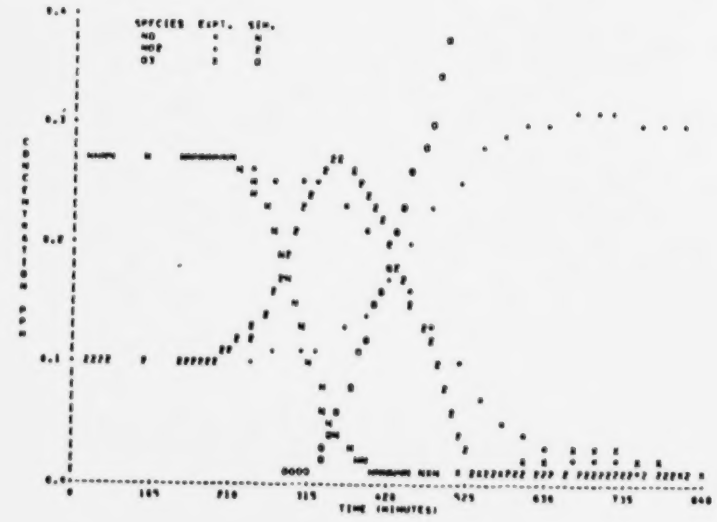

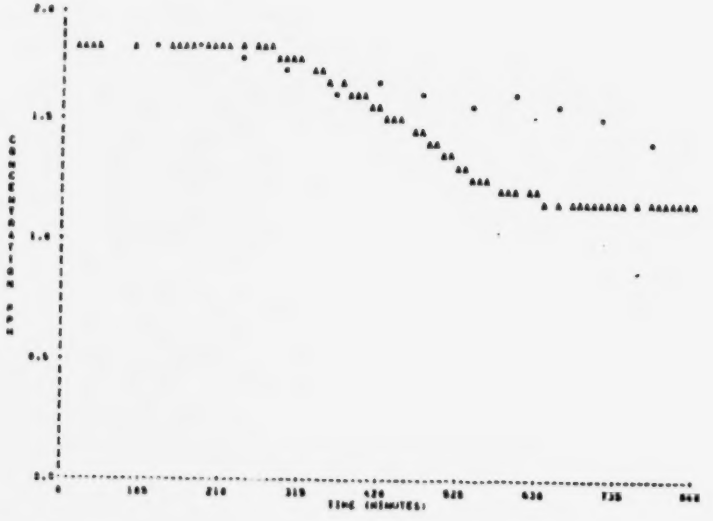

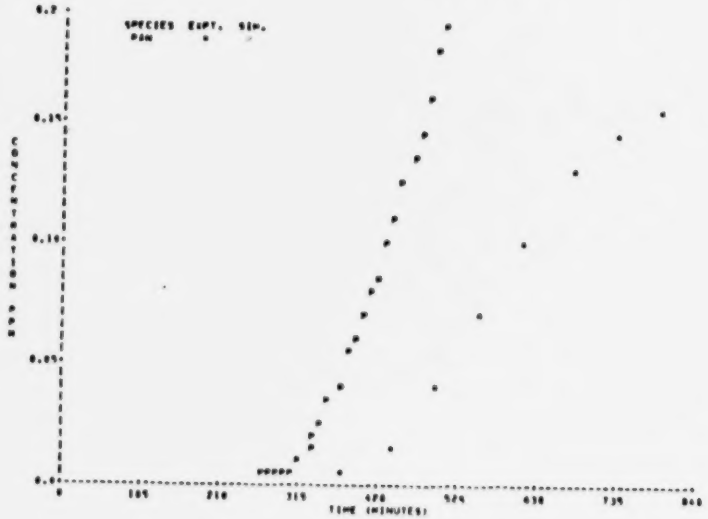

FIGURE C-19 UNC 12.26.77 Blue

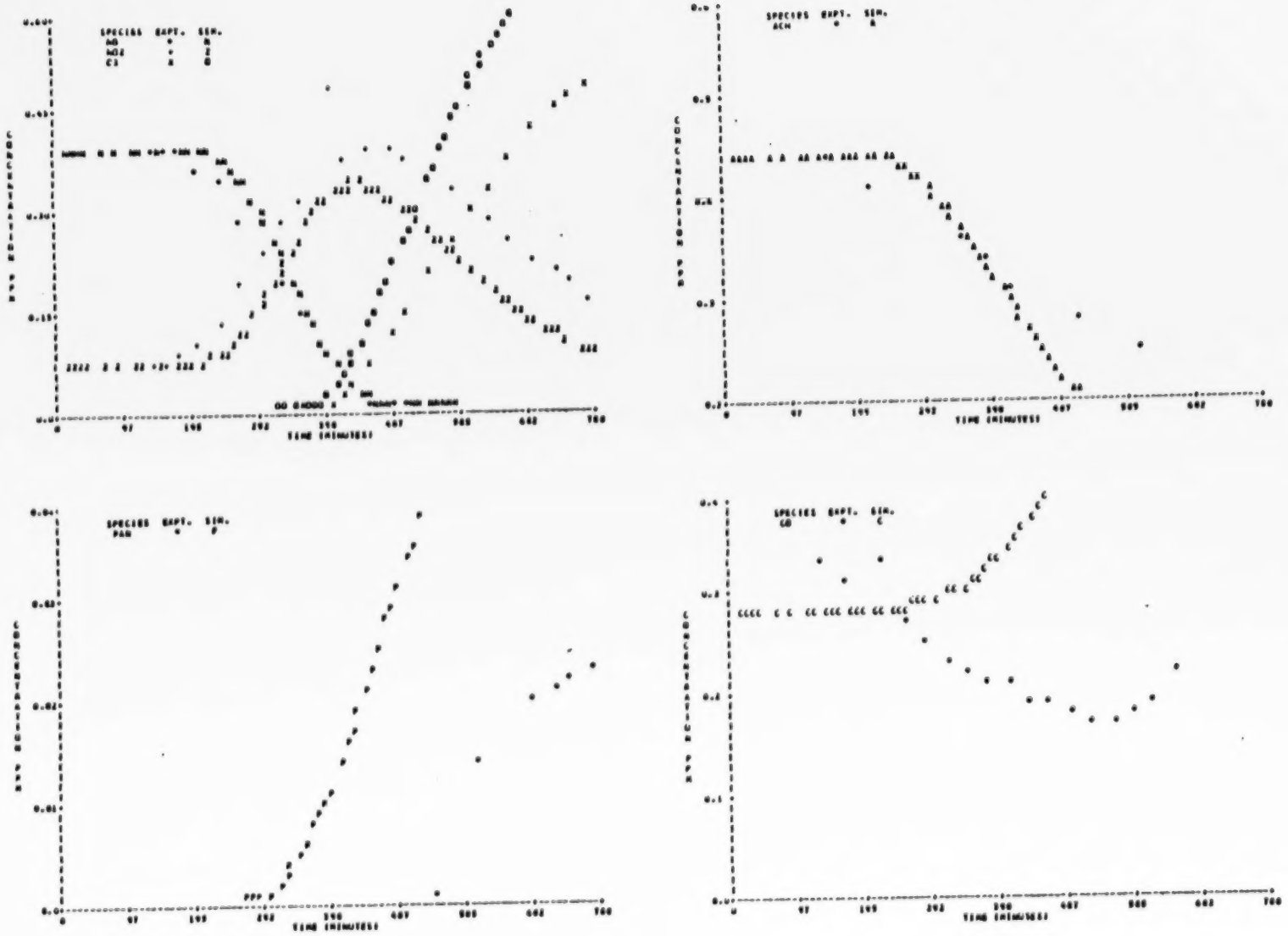

FIGURE C-20 UNC 8.08.78 Red